Experimental determination of the optimal means of combining topotecan and [^{131}I]MIBG therapies for the treatment of neuroblastoma

Anthony Gerald McCluskey

A thesis submitted for the degree of Doctor of Philosophy to the Faculty of Medicine, University of Glasgow

Targeted Therapy Group
Centre for Oncology & Applied Pharmacology
Cancer Research UK Beatson Laboratories
University of Glasgow

March 2005

Acknowledgements

There are many people whose help and guidance have been invaluable throughout the preparation of this thesis. First and foremost is my supervisor, Dr. Rob Mairs, who has provided more help and suggestions throughout the course of this work than I can remember. Likewise, Dr. Marie Boyd always lent a friendly ear, and provided a lot of assistance and encouragement.

I would also like to thank Dr. Sean Carlin, with whom I spent many scintillating hours wrestling with TaqMan RT-PCR, Dr. Shona Cunningham, who showed me the joy of clonogenic assays and [^{131}I]MIBG uptakes, Susan Ross and Anne Marie Clark for their work on tumour growth delay and CFU-A assays respectively, and Dr. Wilson Angerson, for his help with the statistical analyses in Chapter 7. Finally, I would like to thank all the staff (past and present) of the Targeted Therapy Group (Radiation Oncology as was). Cheers Guys!

Table of Contents

List of Figures

List of Tables

Abbreviations

[^{131}I]MIBG	^{131}Iodine-labelled meta-iodobenzylguanidine
[^{211}At]MABG	^{211}Astatine-labelled meta-astatobenzylguanidine
μg	Microgram
μl	Microlitre
μm	Micometre
μM	Micromole
ADEPT	Antibody-directed enzyme prodrug therapy
ADP	Adenosine diphosphate
AO	Antisense oligonuclide
au/AU	Arbitrary units
BER	Base excision repair
bNAT	Bovine noradrenaline transporter
bp	base pair
BSA	Bovine serum albumin
CCL	Coated cationic liposome
cDNA	DNA complementary to mRNA
CI	Combination index
cm	Centimetre
CO_2	Carbon dioxide
cpm/10^5c	Counts per minute per 10^5 cells
CPT	Camptothecin
C_t	Threshold cycle number
D	Dose
(*D*)	Dose of drug causing x% effect in combination
(*D*x)	Dose of drug causing x% effect as single agent
dATP	Deoxyadenosine-5'-triphosphate
DC	Dendritic cells
dCTP	Deoxycytidine-5'-triphosphate
dGTP	Deoxyguanosine-5'-triphosphate
Dm	IC_{50} dose
DMI	Desmethylimipramine

DNA	Deoxyribonucleic acid
dNTP	2 deoxynucleotide 5 tri-phophate
DS	Disulfiram
DSB	Double-strand DNA break
dsDNA	Double stranded DNA
dUTP	Deoxyuracil-5'-triphosphate
EDTA	Ethylene-diamine-tetra-acetic acid
fa	Fraction of cells affected by treatment
Fab	mAb fragment containing one antigen-binding site
FACS	Fluorescence-activated cell sorting
FAM	6-carboxyfluorescein
FCS	Foetal calf serum
fu	Fraction of cells unaffected by treatment
g	Force of terrestrial gravity
GAPDH	Glyceraldehyde-3-phosphate dehydrogenase
GD_2	Disialoganglioside
Gy	Gray
h	Hours
HCl	Hydrochloric acid
HEPES	4-(2-hydroxyethyl)-1-piperazineethanesulfonic acid
hNAT	Human noradrenaline transporter
HSV	Herpers simplex virus
hTERT	Telomerase protein subunit
hTR	Telomerase RNA subunit
i.p.	Intraperitioneal
IC_{10}	Inhibitory concentration (10%)
IC_{30}	Inhibitory concentration (30%)
IC_{50}	Inhibitory concentration (50%)
IC_{70}	Inhibitory concentration (70%)
IC_{90}	Inhibitory concentration (90%)
INSS	International Neuroblastoma Staging System
Kb	Kilobase
kBq	Kilobequerel

kDa	Kilodalton
KI	Potassium iodide
LET	Linear energy transfer
m	Coefficient of sigmoidicity of dose-effect curve
l	litre
mAb	Monoclonal antibody
MBq	Megabequerel
mCi	millicurie
MDR	Multidrug resistance
mg	milligram
Mg Cl_2	Magnesium Chloride
MIBG	Metaiodobenzylguanidine
mins	Minutes
ml	Millilitre
mM	millimole
mm	milimetre
mRNA	Messenger ribonucleic acid
n.c.a.	No-carrier added
Na Cl	Sodium Chloride
NAD+	Nicotinamide adenine dinucleotide
NAT	Noradrenaline transporter
Nb	Neuroblastoma
ng	nanogram
°C	Degrees centigrade
PARP-1	Poly(ADP-ribose)polymerase-1
PBS	Phosphate buffered saline
PBSC	Peripheral blood stem cell
PCR	Polymerase chain reaction
PMSF	Phenyl methyl sulfonyl fluoride
RIBBE	Radiation-induced biological bystander effect
Rn	Unbound fluorescent reporter
RNAi	Ribonucleic acid interference
RPM	Revolutions per minute

RSV	Rous sarcoma virus
RT	Reverse transcription
s.c.	subcutaneous
SCGE	Single cell gel electrophoresis
SCLC	Small cell lung carcinoma
SES	Standard error of skewness
SF	Surviving fraction
SSB	Single-strand DNA break
T_2	Time required for a doubling of tumour volume
T_{10}	Time required for a ten-fold increase of tumour volume
TAE	Tris-Acetate-EDTA
TAMRA	6-carboxytetramethylrhodamine
Taq	Thermus aquaticus
TBE	Tris-Borate-EDTA
Tdp 1	Tyrosyl DNA phosphodiesterase
TOP 1	Gene encoding topoisomerase 1
Topo I	Nuclear enzyme topoisomerase I
TPT	Topotecan
Tris	(Hydroxymethyl)aminomethane
TSA	Tumou specific antigen
V	Volt
VDEPT	Viral vector-directed enzyme prodrug therapy
XRCC-1	X-Ray Cross-Complementing group 1

Summary

Introduction: Neuroblastoma has a long-term survival rate of only 15%. While patients with early stage disease can usually be treated surgically, those with inoperable disease require intensive treatment. However, there has been no substantial improvement in the survival rates of patients with advanced disease. Targeted radiotherapy, using [^{131}I]meta-iodobenzylguanidine ([^{131}I]MIBG) has induced favourable remissions in some patients when used as a single agent. However, the full potential of this therapy may only be realised when it is combined with other agents. One class of agents with the potential to improve [^{131}I]MIBG therapy are the inhibitors of topoisomerase I, which have previously shown synergy when used in combination with radiotherapy. Furthermore [^{131}I]MIBG therapy could be improved by the rapid selection of patients who may derive benefit from this treatment.

Aims: The aims of this study were to develop a molecular assay for MIBG active uptake, and to determine the efficacy of [^{131}I]MIBG in combination with the topoisomerase I inhibitor topotecan *in vitro* and *in vivo*.

Results: RT-PCR analysis of NAT expression by neuroblastoma biopsies was predictive of tumour uptake of MIBG. However RT-PCR negativity failed to correctly determine MIBG uptake capacity with a frequency of 45%.

The combined effects of topotecan and [^{131}I]MIBG were assessed, in tumour cells expressing the noradrenaline transporter, using three treatment schedules: topotecan administered 24h before [i], after [ii] or simultaneously with [iii] [^{131}I]MIBG. Pre-treatment with TPT enhanced the intracellular concentration of [^{131}I]MIBG. However, analysis of TPT and [^{131}I]MIBG interactions *in vitro* and *in vivo* demonstrated that this was not the optimal order of administration for combination therapy. While supra-additive toxicity was observed *in vitro* by all combination schedules, schedule [i]

was less effective than schedules [ii] and [iii]. This was reflected in failure to repair DNA damage.

With respect to delay of growth of NAT-expressing xenografts in nude mice, combinations of topotecan and [^{131}I]MIBG were more effective than single agent treatments. Combination schedules [ii] and [iii] were superior to combination schedule [i]. Combination treatment caused negligible myelotoxicity according to platelet production, or stem cell clonogenic capacity.

Conclusions: Real-time PCR evaluation of primary neuroblastoma tumours has significant capability to reflect their capacity for the accumulation of MIBG, however PCR-based assessment of NAT gene expression cannot fully predict MIBG uptake. Inhibition of DNA repair and supra-additive toxicity to NAT expressing cells and xenografts were achieved using combinations of topotecan and [^{131}I]MIBG. Effectiveness was dependent on the order of administration of the two agents. If the synergy demonstrated in the model systems used in this study can be replicated in patients with neuroblastoma, there is potential for real therapeutic gain.

Chapter 1

Introduction:

[^{131}I]MIBG and topotecan: A rationale for combination therapy for neuroblastoma

1.1 Targeted radiotherapy as a treatment for cancer

1.1.1 Targeted therapy

The diagnosis and treatment of cancer has a very long history. Hippocrates considered the disease incurable, while Celsus and Galen both attempted surgical treatments. [1]. The 17th century clinicians Lusitanus and Sennert thought it was contagious [1, 2].

In the last century, great advances have been made in the understanding and therapy of cancer, and it has long been recognised that surgery alone is insufficient in the treatment of many types of disease [3]. Also, while the use of external beam radiation and chemotherapy have shown some success, the inability of these treatment modalities to discriminate between tumour cells and normal tissue has severely limited their effectiveness [3].

In recent years, advances in our knowledge of the molecular biology of cancer and human genetics have led to the identification of a number of strategies with the potential to actively target cancer cells, either in a tumour mass or in metastatic disease. One strategy involves selective disruption of tumour-specific genes through antisense oligonucleotide (AO) [4], or manipulation of the endogenous RNA interference (RNAi) pathway [5, 6].

Another approach involves the use of gene therapy, where a "suicide" gene, or an anti-oncogene is introduced into tumour cells [7], via immunoliposomes [8, 9], or tumour-targeting viral vectors [10]. Alternative gene therapy-derived strategies involve the introduction of a gene encoding a tumour specific antigen (TSA) into dendritic cells (DCs) to try to initiate an immune response [7, 11].

Other strategies currently under investigation involve the targeting of cytotoxic agents to malignant tissues. The efficacy of polyclonal or monoclonal antibodies, raised

against tumour specific antigens has been investigated. Antibodies used in this way can act as directly targeting cytotoxic agents (through conjugation to radio-isotopes [3, 12], or cytotoxic drugs [13]), or as a method of targeting delivery vehicles such as liposomes [8, 9].

More experimental methodologies are currently under investigation, such as ADEPT (antibody-directed enzyme prodrug therapy) [14] and VDEPT (viral vector-directed enzyme prodrug therapy) [15]. These multistep targeting systems seek to localise the activity of cytotoxic drugs to tumour cells by converting a previously administered nontoxic prodrug to an active cytotoxic agent. The enzyme responsible for this conversion is targeted to tumour cells, either by conjugation to an antibody specific for a tumour antigen (ADEPT), or by introduction via a viral vector, followed by activation of a tumour specific promoter to drive expression of the gene for the enzyme (VDEPT). While both of these approaches could prove beneficial in the future, trials involving these techniques have so far been disappointing [3].

1.1.2 Efficacy of targeted cancer therapy

Irrespective of the method of tumour targeting being utilised, it is important to ensure delivery of the treatment only to malignant sites, and not to normal tissues. Also, the targeting agent must be capable of maximal effectiveness at the site of the tumour mass [3].

In many cases the efficacy of targeted cancer therapy has been hampered by inefficient delivery of the therapeutic agent, non-optimal penetration of anti-tumour effects throughout the tumour mass and, in the case of antibody-directed strategies, anti-mouse immunoglobulin immune responses, which have resulted in administered doses that are significantly lower than the amount needed for eradication of the malignant deposits [3, 4, 12].

1.1.3 Targeted radiotherapy

After surgery, radiotherapy is the most commonly used form of cancer treatment, and it is estimated that 50% of all patients will require radiotherapy at some stage [16]. However, the main limitation in the use of radiotherapy is the potential damage to normal tissue, but, if the tumour is well defined, this can be circumvented by the use of eg. external beam conformal radiation, which can deliver a high dose to the tumour site, without extensively damaging nearby organs. Unfortunately, many tumours do not have well-defined margins, or are spread throughout the body, and cannot be treated in this fashion [17].

These problems can be overcome by targeted radiotherapy, where cytotoxic radionuclides are conjugated to tumour-seeking agents, leading to the selective irradiation of malignant areas while sparing normal tissues [18]. In theory, the use of monoclonal antibodies raised against tumour cellular structures should provide the specificity needed to target malignant sites. However, in practice, with the exception of antibody-directed therapy of lymphoma, this has been far from successful [3, 12].

An alternative to antibody-dependant methodologies is the use of small tumour-targeting molecules, which can be easily conjugated to radioisotopes. Due to their small size, these ligands do not evoke an immune response and have improved penetration [18].

1.1.4 Radiological bystander effect

An advantage of targeted radiation in the treatment of cancer is that the cytotoxic effects of radioisotopes are enhanced by the radiological bystander effect.

Heterogeneous uptake of the radioactive agent can result in only a fraction of tumour cells being successfully targeted. However, energy released by decay of the radioisotope emanates from the targeted portion of the tumour in three dimensions, causing damage to neighbouring cells that have not accumulated the radiolabelled drug [17]. Therefore, even if the success rate of transfer of the radiolabelled agent to tumour cells is less than 100%, underdosing of the tumour is circumvented (Figure 1-1).

Other targeting methodologies, such as ADEPT also employ bystander effects. However, these rely on the transport of activated cytotoxic drug through gap junctions, which often diminishes with tumour progression [19]. Toxicity due to radiation cross-fire does not rely on biological cellular functions, and energy emissions from a wide range of radio-nuclides have been evaluated, and their path lengths are well known. This raises the possibility of the utilisation of different radio-nuclides with different decay characteristics, to treat tumour masses of widely varying size [20].

The contribution of radioactive decay by particles emanating from targeted cells to kill of neighbouring, non-targeted cells is relatively well characterised [20]. Recently, it has been recognised that cellular processing of the radiation insult can translate the physical radiation insult into biological signals or toxins. This is known as the radiation-induced biological bystander effect (RIBBE). While investigations of RIBBE induced toxicity are outside the scope of this present study, these effects may have major implications on the course of future research, and this will be addressed in greater detail in Section 12.4.

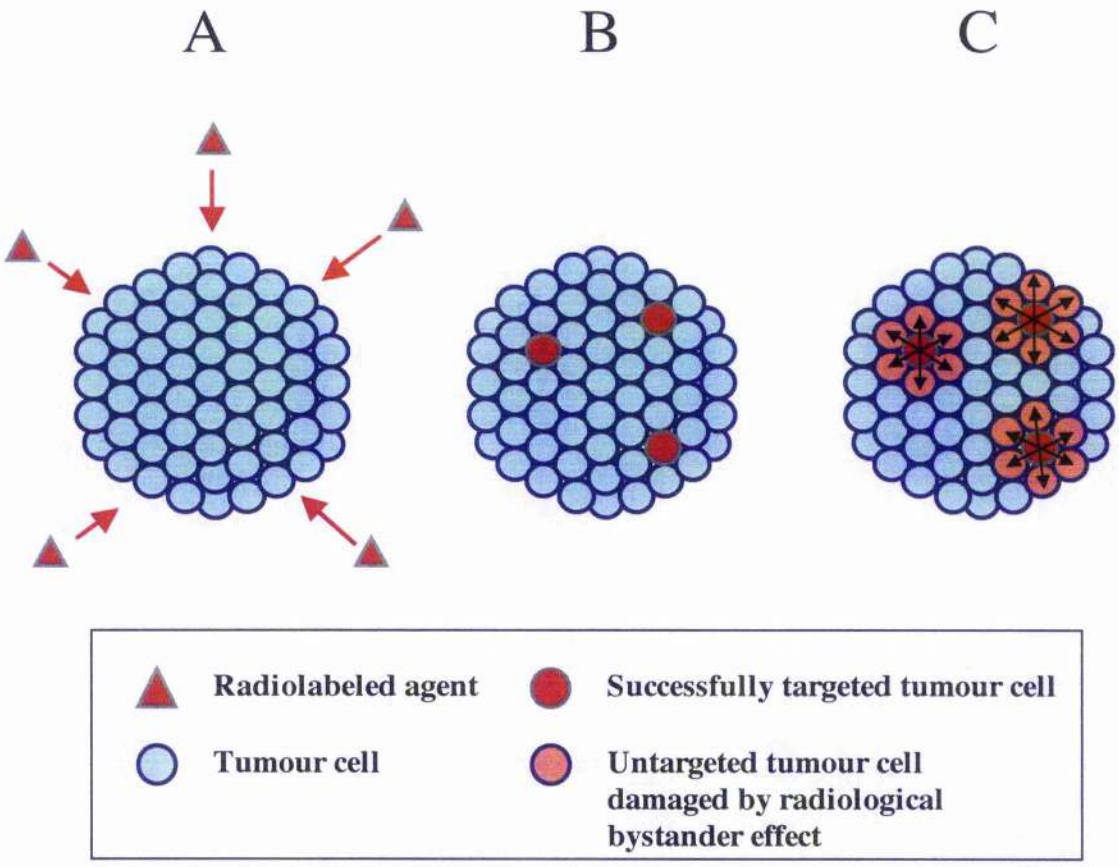

Figure 1-1: Radiological bystander effect

A Tumour cells are targeted by a radiolabelled agent.

B Only a fraction of the tumour is successfully targeted. The majority remains unaffected

C Energy released by decay of the radioisotope emanates from the targeted portions of the tumour in three dimensions, causing damage to neighbouring cells that have not been successfully targeted.

1.2 Neuroblastoma

1.2.1 Incidence / Survival

Neuroblastoma, an embryonal tumour of the sympathetic nervous system, is the most common extracranial solid tumour of childhood [21] and accounts for approximately 8% of all pediadtric malignancy [22, 23]. 96% of cases occur before the age of 10 years [24]. Neuroblastoma is responsible for approximately 15% of all childhood cancer deaths [25] and has a long-term survival rate of only 15% [20].

1.2.2 Molecular biology

Neuroblastoma cells show large genetic abnormalities. Both gain of, and loss of genetic material is typically seen. Amplification of the N-myc oncogene (located on chromosome 2) is seen in 25-33% of neuroblastoma patients [21], and is one of the most important prognostic indicators [26, 27]. Gain of 17q is a very common genetic abnormality in primary neuroblastoma, and is found in over 50% of cases [25]. Deletion of the short arm of chromosome 1 is also a common feature of advanced disease [28, 29], and loss of heterozygosity (LOH) is seen in 19-36% of primary tumours [30-37]. Deletions of chromosome 11 are seen in 15-20% of neuroblastoma karyotypes [38], and evidence suggests that a neuroblastoma suppressor gene may be located on 11q [25]. Other regions of the genome that show alterations, LOH and / or allelic abnormalities include 3p [39], 4p [40], 5q [41], 9p [42, 43], 14q [31, 33, 44, 45] and 18q [46]. Over-expression of multidrug resistance genes (MDR) is also commonly seen [21, 25], and may be associated with over-expression of N-myc [47].

1.2.3 Clinical features / Treatment regimes

At presentation, approximately 33% of neuroblastoma patients have localized disease, while the remaining 67% of patients have metastases [21]. However, neuroblastoma is an incredibly heterogeneous disease, and the likelihood of tumour progression varies widely depending on factors such as age of diagnosis and anatomic stage [25].

In general, children who are diagnosed before 1 year of age, and/or with localised disease can be cured by surgery, with little or no adjuvant therapy. Conversely, older children often show extensive metastases at diagnosis, and clinical prognosis is poor [25]. Patients are staged using the recognised International Neuroblastoma Staging System (Table 1-1).

Patients with stage 1 and stage 2A disease have localised tumours, and can usually be treated surgically, without the need for radiotherapy and / or chemotherapy [21]. Patients with stage 2B and stage 3 disease display lymph node involvement, and can also be treated by surgery [23], in conjunction with adjuvant chemotherapy [21, 48]. The effectiveness of radiotherapy to these patients remains inconclusive [27, 49]. In the case of patients with inoperable stage 3 and stage 4 (with the exception of patients with stage 4S, who generally display spontaneous regression without intensive intervention [21, 50]), intensive treatments, or "megatherapies" are utilised, involving combinations of high-dose myeloablative chemotherapy with total body irradiation and stem cell rescue [21, 51].

However, despite the use of such aggressive therapies, there has been no substantial improvement in the survival rates of patients with advanced disease [52].

Table 1-1: The International Neuroblastoma Staging System (INSS)

Stage 1:
Localized tumour* with complete gross excision, with or without microscopic residual disease; representative ipsilateral lymph nodes negative for tumour microscopically (nodes attached to and removed with the primary tumour may be positive).

Stage 2A:
Localized tumour with incomplete gross excision; representative ipsilateral nonadherent lymph nodes negative for tumour microscopically.

Stage 2B:
Localized tumour with or without complete gross excision, with ipsilateral nonadherent lymph nodes positive for tumour. Enlarged contralateral lymph nodes must be negative microscopically.

Stage 3:
Unresectable tumour infiltrating across the midline** with or without regional lymph node involvement; or localized unilateral tumour with contralateral regional lymph node involvement; or midline tumour with bilateral extension by infiltration (unresectable) or by lymph node involvement.

Stage 4:
Any primary tumour with dissemination to distant lymph nodes, bone, bone marrow, liver, skin and/or other organs (except as defined in Stage 4S).

Stage 4S:
Localized primary tumour (as defined for Stage 1, 2A, or 2B), with dissemination limited to skin, liver, and/or bone marrow***
(limited to infants less than one year of age).

* Multifocal primary tumours (e.g., bilateral adrenal primary tumours) should be staged according to the greatest extent of disease, as defined above, and followed by a subscript " M" (e.g., 3M).

** The midline is defined as the vertebral column. tumours originating on one side and " crossing the midline" must infiltrate to or beyond the opposite side of the vertebral column.

*** Marrow involvement in stage 4S should be minimal, i.e. less than 10% of total nucleated cells identified as malignant on bone marrow biopsy or on marrow aspirate. More extensive marrow involvement would be considered to be stage 4. The MIBG scan (if done) should be negative in the marrow.

1.2.4 Experimental treatment regimes

Attempts have been made to improve the outcome of patients with advanced neuroblastoma by utilising new techniques that can target the tumour directly. Pilot experiments have been carried out to evaluate the possibility of gene therapy using viral vectors for eg. prevention of angiogenesis [53]; generation of immune responses to neuroblastoma cells [54]; and purging residual neuroblastoma cells before stem cell rescue [55]. Other lines of research are concentrating on targeted liposomes [56-58] and immunotherapy using monoclonal antibodies [59, 60].

To date, however, the most promising use of a novel treatment for neuroblastoma is non-immunological targeting using radioiodinated meta-iodobenzylguanidine ([^{131}I]MIBG - Figure 1-2).

85-90% of neuroblastoma tumour cells express the noradrenaline transporter (NAT - Figure 1-3), a 12-spanning integral membrane protein responsible for the active intracellular accumulation of catecholamine neurotransmitters [61, 62].

Meta-iodobenzylguanidine (MIBG), a structural analogue of noradrenaline, is a derivative of the adrenergic neurone-blocking drugs bretylium and guanethidine, and is also selectively concentrated in neuroadrenergic tissue by this process [61, 62]. Tracer doses of radioiodinated MIBG have been used successfully for diagnostic scintigraphy of tumours derived from the neural crest [63], and it is expected that the ability of neural crest-derived tumours to accumulate and retain high concentrations of [^{131}I]MIBG will lead to more extensive therapeutic application of this drug [64].

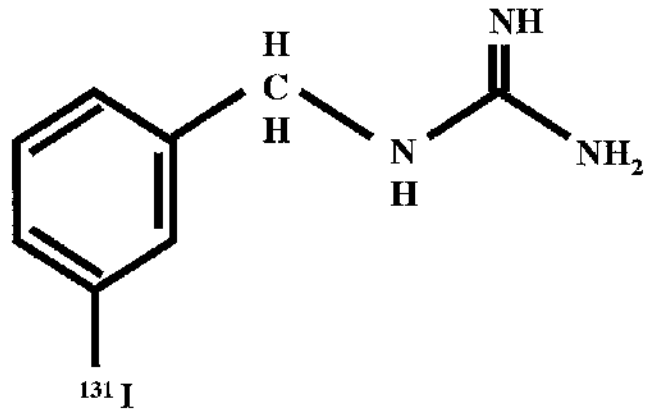

Figure 1-2: **[^{131}I] meta-iodobenzylguanidine ([^{131}I]MIBG)**

[^{131}I]MIBG is a structural analogue of adrenergic neurone blockers bretylium and guanethidine. It is selectively concentrated in neuroadrenergic tissue by the noradrenaline transporter (NAT). [^{131}I]MIBG causes favourable remissions in neuroblastoma patients when used as a single agent.

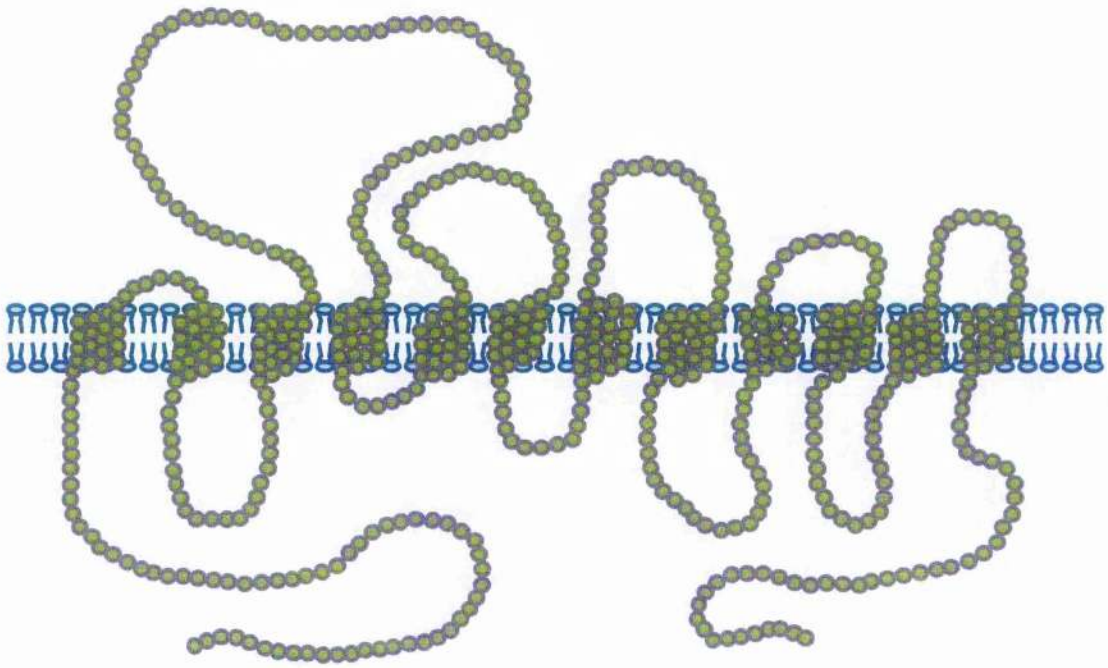

Figure 1-3: The noradrenaline transporter (NAT)

The noradrenaline transporter (NAT) is responsible for the active intracellular accumulation of catecholamine neurotransmitters in neuroadrenergic tissue by a process known as Uptake-1. It is expressed in 85-90% of neuroblastoma tumour cells.

The NAT protein consists of 617 amino acids and has 12 transmembrane domains. This conformation is similar to that of other membrane-associated proteins that are responsible for ion and solute transport. Note that the number of circles is not an accurate representation of the number of amino acid residues.

1.2.5 Combination therapy incorporating [^{131}I]MIBG

Targeted therapy using [^{131}I]MIBG has induced favourable remissions in some patients when used as a single agent [65-70]. However long-term cure remains elusive, and the full potential of this therapy may only be realised when it is combined with other agents [71].

In Ghent University Hospital, Gent, Belgium and Emma Children's Hospital, Amsterdam, The Netherlands, Potassium iodide (KI) was administered prior to [^{131}I]MIBG treatment, to prevent undesirable irradiation of the thyroid by free ^{131}I (caused by breakdown of [^{131}I]MIBG). One study found a large variation in radio-iodide uptake, both between different patients (absorbed thyroidal dose = 0.2-30.0 Gy) and, indeed, in individual patients at different timepoints (mean +/- sd = 24.1 +/- 19.2 Gy per patient) [72]. Another study found that 52.4% of patients exhibited thyroid damage after a mean period of 1.4 years (0.1-5.8yrs). In 25 survivors, tested after a mean period of 3.5 years, the percentage displaying thyroid damage rose to 64%, suggesting that ^{131}I induced thyroid disfunction could be a major difficulty long-term [73].

At the Netherlands Cancer Institute, [^{131}I]MIBG has been given in conjunction with hyperbaric oxygen [74], to try to overcome radioresistance in poorly oxygenated tumour regions. Improved survival rates, compared with [^{131}I]MIBG alone, were observed. This has also been tested in Faculty Hospital Motol, Prague, with favourable results [75].

In another study carried out in Emma Children's Hospital, Amsterdam, The Netherlands, [^{131}I]MIBG was administered to newly diagnosed patients before either surgery or chemotherapy [76]. This also gave encouraging results. Preoperative [^{131}I]MIBG was found to be less toxic than chemotherapy, but equally effective.

At the University of Michigan Medical Centre, Michigan, USA, in a pilot study patients were treated, following induction therapy, or after relapse, with a regimen which involved [^{131}I]MIBG treatment, followed 14 days later by a combination of carboplatin, etoposide and melphalan for 4 days, and ending in stem cell rescue 3 days later. The combined therapy was well tolerated, with 25% (2/8) patients exhibiting partial responses 100 days following transpantation and 37.5% (3/8) achieving complete response [77].

In the Gaslini Institute, Genova, Italy, patients with residual stage 4 neuroblastoma were treated with 4.1 - 11.1mCi/kg [^{131}I]MIBG 7-10 days before high-dose chemotherapy involving busulphan and melphalan followed by peripheral blood stem cell (PBSC) rescue. High gastrointestinal toxicity was seen in patients treated with [^{131}I]MIBG (76.5% or 13/17) and in control patients subjected to PBSC without [^{131}I]MIBG treatment (60% or 9/15). 12% (2/17) of patients treated with [^{131}I]MIBG developed pneumonia, suggesting that refinement of this treatment may be required to avoid lung complications [78].

In Hacettepe University, Ankara, Turkey, [^{131}I]MIBG was administered in conjunction with a combined chemotherapy regimen of vincristine, VP16, iphosphamide, carboplatin, epirubicin and cyclophosphamide. 5/8 patients with refactory neuroblastoma responded to [^{131}I]MIBG therapy, with 2/8 achieving complete responses and 3/8 exhibiting partial responses. In total, 5 patients relapsed and died of progressive disease, suggesting that although survival was improved by the inclusion of [^{131}I]MIBG into conventional therapy, overall prognosis was still poor [79].

At the Children's Hospital, University of Tubingen, Germany, patients were treated with [^{131}I]MIBG, followed by a combination of melphalan carboplatin and etoposide. They were then subjected to stem cell rescue supplemented with immunotherapy using anti-GD_2 antibodies. 3/11 experienced complete responses. 1/11 exhibited a partial

response, while 2/11 did not respond, and died. 19 months following treatment 9/11 were alive, with 8/11 showing no progression or relapse [80].

At Catholic University, Rome, Italy, [^{131}I]MIBG was administered as a part of two separate treatment regimes. In the first regimen, [^{131}I]MIBG was used along with cisplatin and cyclophosphamide. In the second regimen, VP16 and viscristine were added to the basic chemotherapy treatment. Favourable results have been reported for both of these regimens. [52]

In Middlesex Hospital, London, Britain, studies were undertaken to follow [^{131}I]MIBG treatment with multiagent chemotherapy (with high dose carboplatin and melphalan), and haemopoetic stem cell rescue. Patients with newly presenting, advanced stage disease were treated firstly with [^{131}I]MIBG and then with combinations of chemotherapy and radiotherapy five days later. Toxicity was assessed at an initial whole body dose of 1.5Gy, after which the [^{131}I]MIBG component was increased until peripheral stem cell rescue was required [81]. The results of this study were encouraging. Combined treatment was generally well tolerated, and there was no early mortality.

1.2.6 The potential of combination therapy incorporating [^{131}I]MIBG and topoisomerase I inhibitors

As described in the last section, targeted therapy using [^{131}I]MIBG in combination with complementary therapies has produced favourable responses. However, to realise its full potential, the most effective way to use this tumour-targeting drug has yet to be defined.

[^{131}I]MIBG-induced toxicity is due to ^{131}I decay. Therefore, it is expected that the effectiveness of this drug will be improved if used in combination with agents which potentiate radiation-induced damage. One such class of agents, with the potential to improve on existing regimes based on [^{131}I]MIBG therapy are inhibitors of the nuclear enzyme topoisomerase I (Topo I).

1.3 Topoisomerase I and its inhibitors

1.3.1 Topoisomerase I

Topoisomerase I (Topo I) is a nuclear enzyme that relaxes supercoiled DNA and plays a crucial role in DNA replication and in transcription [82-84]. It is a 100kDa protein encoded by the single-copy TOP1 gene, located on chromosome 20 [85-87]. The presence of up-regulated levels of Topo I in tumour cells compared to normal cells suggests a therapeutic advantage of utilising Topo I - targeting agents [85].

Topo I removes the topological tension in front of replication forks by inserting a nick on one of the DNA strands, allowing the other strand to pass through the cleavage site, before re-sealing the nick. During this process, an intermediatary state occurs by the formation of transient covalent bonds between the tyrosine-723 residue of the Topo I [82] and the 3' terminus of the nicked strand (the so-called "cleavable complex") [83, 84] (Figure 1-4).

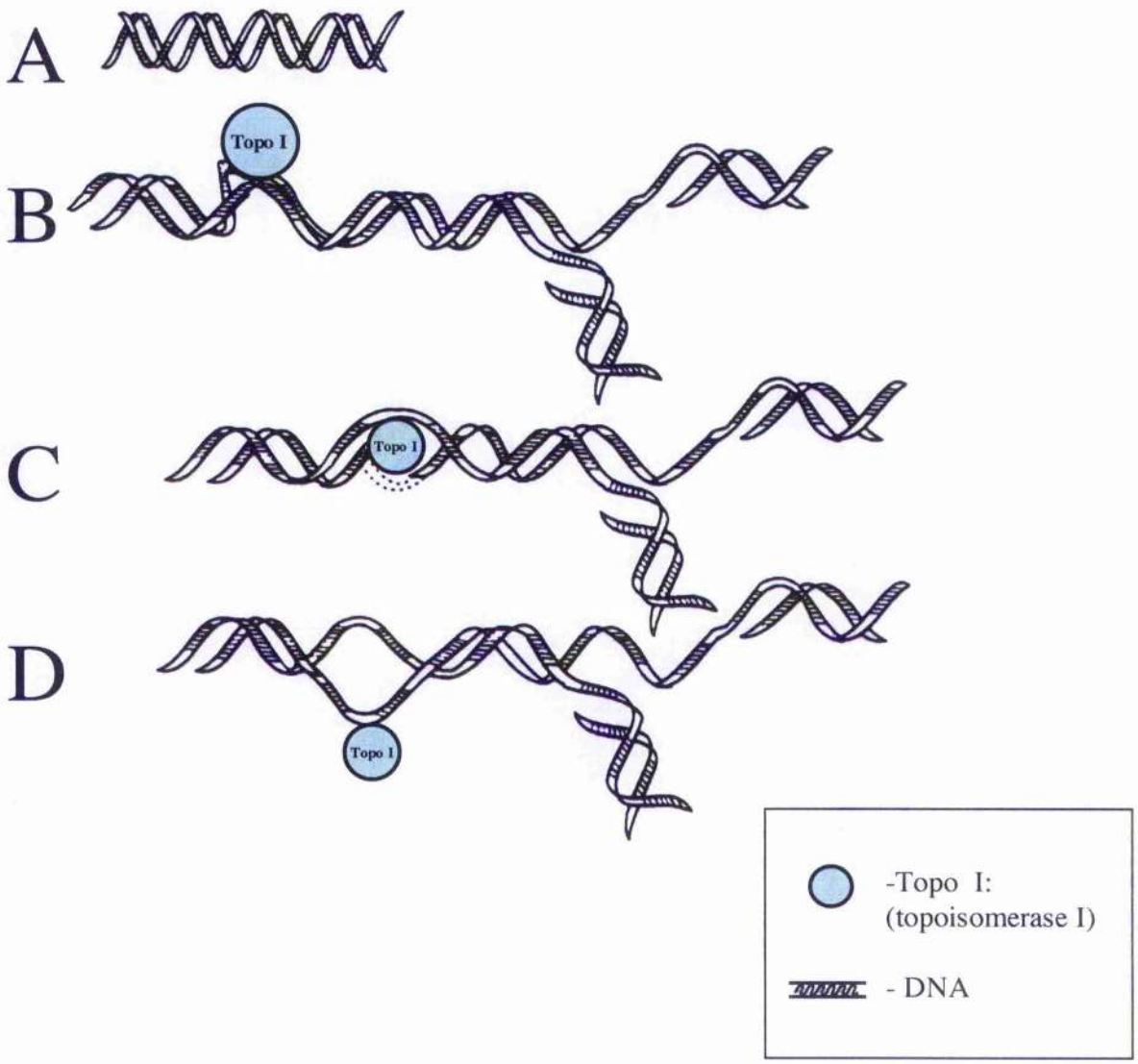

Figure 1-4: The mechanism of topoisomerase I action

Topoisomerase I (Topo I) is a nuclear enzyme that relaxes supercoiled DNA and plays a crucial role in DNA replication and in transcription. The mechanism of Topo I action is as follows:

A) Increasing tension and supercoiling of DNA occurs.
B) Topo I binds to one DNA strand and cuts it (cleavage reaction).
C) The intact strand of DNA passes through the neck, resulting in the relaxation of the torsional strain.
D) Topo I reseals the broken strand (religation step) and dissociates from the DNA molecule.

1.3.2 Inhibitors of topoisomerase I

Camptothecin (CPT - Figure 1-5), an alkaloid extract of the tree *Camptotheca acuminata*, was first identified in 1966 as exhibiting antitumour activity in murine leukemia models [86], although it was not until 1988 that the mode of action was identified as Topo I inhibition [88]. The hypothesised cytotoxic mechanism of camptothecin is known as the fork collision model. Briefly, CPT binds to, and stabilises the normally transient cleavable complex, inhibiting the Topo I-induced religation step. During the next round of DNA replication, collision of the stabilised Topo I - DNA complex with the replication fork results in an irreversible double strand break, leading to cell cycle arrest and cell death [83, 85] (Figure 1-6).

Clinical trials of CPT were carried out in the 1970s. However these were terminated due to excessive and unpredictable toxicity [83, 85]. Instead, researchers attempted to synthesise derivatives of camptothecin which would exhibit lower toxicity and greater solubility in water. This led to the identification of a new class of campotohecin analogues, including the semi-synthetic derivative topotecan (TPT - Figure 1-7).

Many studies have been carried out to ascertain the effectiveness of topotecan in the treatment of a variety of cancers.

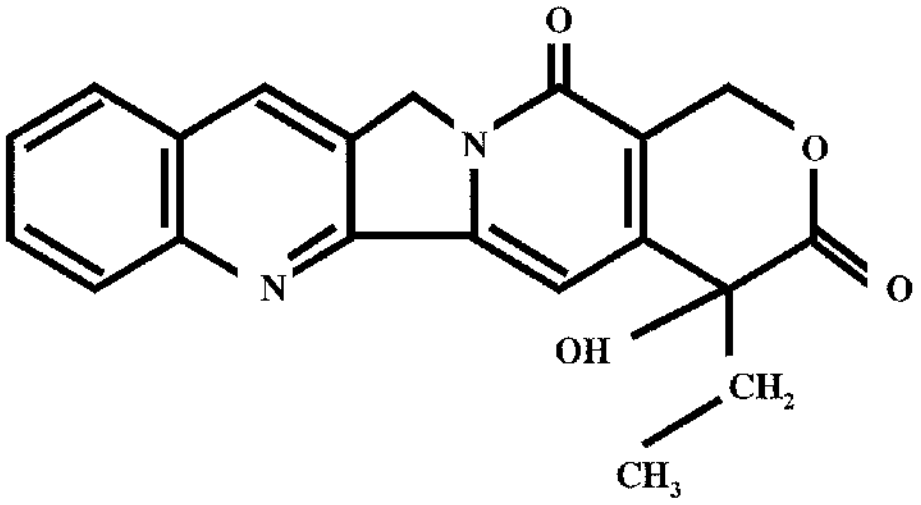

Figure 1-5: Camptothecin (CPT)

Camptothecin (CPT), is an alkaloid extract of the tree *camptotheca acuminata*. It is an inhibitor of topoisomerase I. Clinical trials of CPT were carried out in the 1970s. However these were terminated due to excessive and unpredictable toxicity.

In 1988 the mode of action of CPT was identified as inhibition of Topoisomerase I [88].

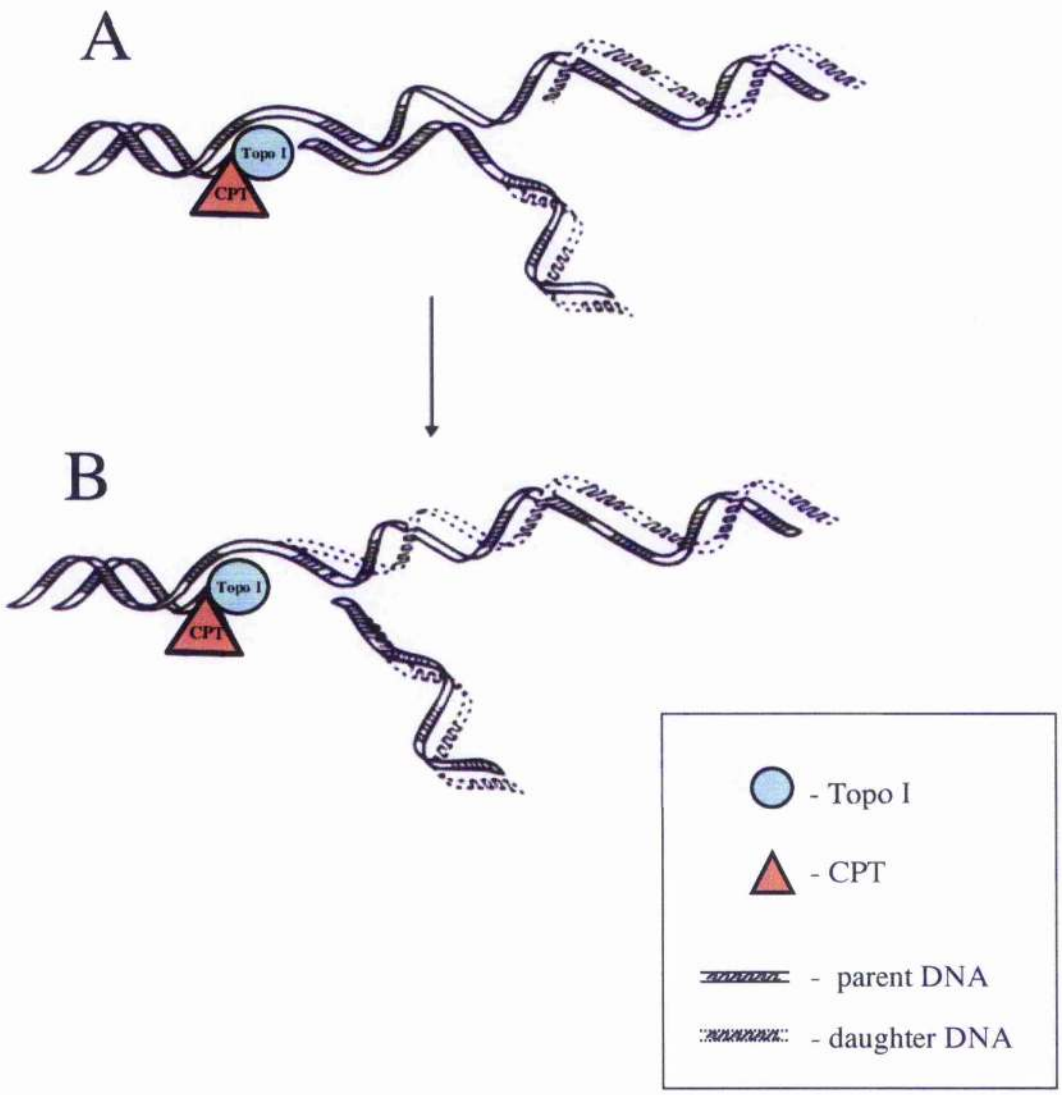

Figure 1-6: Interaction of topoisomerase I with camptothecin

Topoisomerase I interacts with the Topo I inhibitor camptothecin by the following mechanism:

A) Camptothecin binds to topo I and stabilises the normally transient cleavable complex, inhibiting the religation step.

B) Collision of the replication fork with the camptothecin-stabilized cleavable complex results in an irreversible double-strand break in the DNA.

1.3.3 Current status of topotecan used as a single agent

Topotecan has shown effectiveness as a single agent in phase I/II trials for the treatment of head-and-neck cancer [89], small cell lung carcinoma (SCLC), [90] and ovarian cancer [91-93]. Pilot studies of topotecan's effectivness against breast cancer also produced favourable results [94]. However in phase II trials, it showed only modest activity [95].

Also, phase II trials of TPT activity on esophageal carcinoma produced disappointing results [96], and topotecan had no effect on the management of hormone-refactory prostate cancer [97].

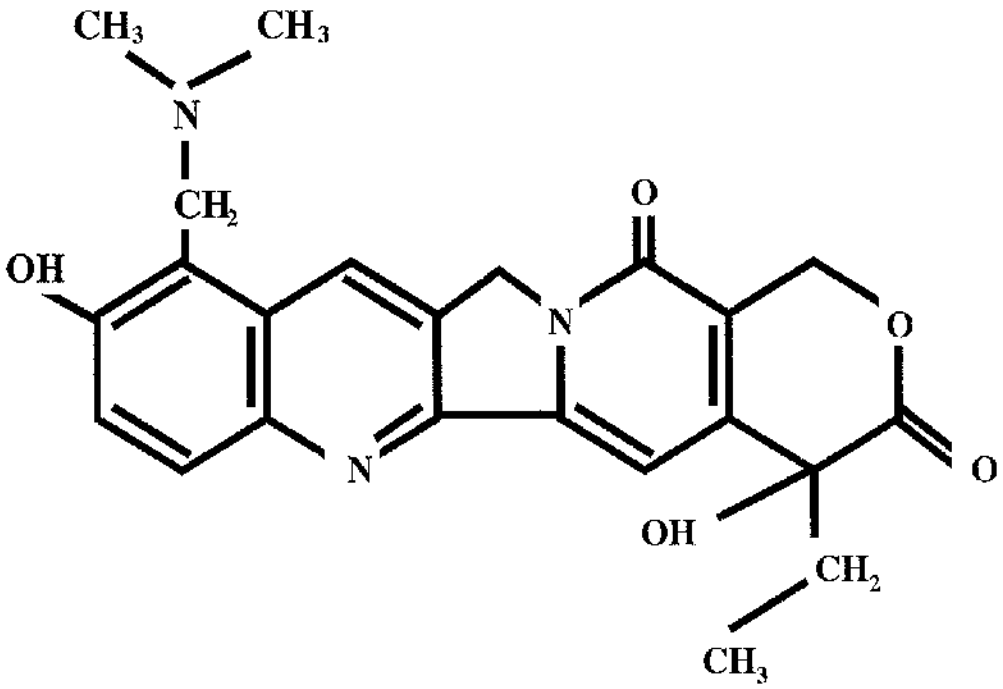

Figure 1-7: Topotecan (TPT)

Topotecan is a semi-synthetic derivative of camptothecin which has greater solubility. It inhibits the activity of Topo I in a similar fashion to CPT (see Figure 1-5).

Topotecan has been entered into a large number of clinical trials, to ascertain its effectiveness in the treatment of a wide range of cancers.

1.3.4 Topotecan in combination with other agents

Combinations of topotecan and cyclophosphamide produced encouraging results in phase II trials for the treatment of rhabdomyosarcoma, Ewing's sarcoma and osteosarcoma [98].

Topotecan has been used in phase I/II trials for the treatment of small cell lung carcinoma (SCLC), in combination with paclitaxel [99] gemcitabine [100, 101] cisplatin [101, 102] etoposide [103] cisplatin-etoposide [104], and doxorubicin [105]) and also in combination with irradiation for the treatment of SCLC metastases [106]. Phase II trials have also studied topotecan in combination with gemcitabine in the treatment of non-small cell lung carcinoma, [107], with favourable results. There have also been encouraging results when TPT was studied as a treatment of ovarian cancer in phase I/II trials, in combination with paclitaxel [108], paclitaxel-cisplatin [109], carboplatin [110], gemcitabine [111] and doxorubicin [112]).

Other phase I/II trials have studied the effect of topotecan on leukemia [113-115], and favourable results were seen when topotecan was used in combination with etoposide and mitoxantrone [113]. Phase I/II trials of topotecan in combination with cisplatin and/or radiation have been carried out for the treatment of advanced cervical cancer [116], with encouraging results [117].

However, a phase II study of sequential topotecan and etoposide in non-Hodgkin's lymphoma produced only modest effects [118]. Similarly, combinations of topotecan and radiation for the treatment of glioblastoma [119-121] produced no significant improvement on radiation alone [119], and no substantial activity in relapsed gliomas was observed [122].

1.3.5 Topotecan as a treatment for neuroblastoma

There have been tremendous advances in the treatment of childhood cancer during the past several decades with resultant improvement in survival of many children with cancer. However, this marked progress has not yet been realized for children with high-risk tumours such as neuroblastoma. Improvement of event-free and long-term survival of poor-prognosis paediatric tumours may depend on the identification of chemotherapeutic agents with novel mechanisms of action [123]. TPT has a distinctive mode of action, and its effectiveness is not compromised by tumour development of multi-drug resistance [124]. This characterisitic is particularly advantageous in therapy of neuroblastoma, which often involves multi-agent regimens.

Topotecan shows activity against neuroblastoma xenografts [125], regardless of their level of expression of the multidrug resistance gene MDR 1 [124]. It has been used as a palliative agent [126], and has been entered into clinical trials for the treatment of neuroblastoma, where it has shown effectiveness as a single agent in phase I/II trials [126-130].

Encouraging results have been obtained from combinations of topotecan and other chemotherapeutic agents, for example topotecan given in combination with cyclophosphamide in phase I/II trials [98, 131, 132]. Favourable results were also obtained for topotecan given in combination with myeloablative doses of thiotepa and carboplatin [128], and topotecan in combination with vincristine and doxorubicin [134]. Topotecan combined with cyclophosphamide, and vincristine was also found to be a good preparative regimen for monoclonal antibody-based therapy of neuroblastoma [135].

These studies suggest that topotecan-based therapies could prove to be beneficial in the treatment of neuroblastoma. It is expected that the effectiveness of TPT against

neuroblastoma could be greatly enhanced if this agent is given in combination with [^{131}I]MIBG, due to the ability of TPT to potentiate radiation-induced toxicity.

1.3.6 Interaction between topoisomerase I inhibition and radiation induced DNA damage in vitro and in vivo

In many previous studies, synergistic cell killing *in vitro* by ionising radiation and Topo I inhibitors has been reported in a wide range of tumour cell lines. Radiopotentiation has been observed in non-human cells such as murine leukemia (P388) [136], Chinese hamster ovary [136] Chinese hamster (V79) fibroblast [137] lines, and also from a wide range of human cell lines such as small-cell lung cancer (SBC3-CDDP) [138], glioblastoma (GBM) [139], HeLa [137], squamous carcinoma of the head and neck [133], breast cancer (MCF7) [85] and melanoma [141].

In vivo radiopotentiation by Topo I inhibitors has been seen in murine fibrosarcoma [140], and MCa-4 mammary carcinoma [142] and rhabdomyosarcoma [143].

However, no attempt has been made to investigate the potential of inhibitors of topoisomerase 1 to induce radiopotentiation *in vitro* and *in vivo* when combined with targeted radiotherapy.

1.4 Aim of this study

Clinical diagnosis of neuroblastoma involves histological examination of biopsy specimens and evaluation of scintigrams obtained following the administration of a tracer dose of either [^{123}I]- or [^{131}I]-labelled MIBG, and tumour uptake of MIBG at this stage also indicates suitability of the patient for a treatment regimen that includes [^{131}I]MIBG therapy. However, in many cases, radioiodinated MIBG is not immediately available, leading to possible delays of more than one week from the time of admission to gamma-camera scanning and reporting. A rapid and sensitive molecular assay for MIBG active uptake, which could be applied at initial biopsy, would be invaluable in selecting patients for therapeutic strategies which incorporate radiolabelled MIBG.

Experimental evidence has shown that the Camptothecins can act as radiosensitizers *in vitro* and *in vivo* when used in conjunction with ionising radiation delivered from an external source [85, 136-143]. However, to date, no attempt has been to demonstrate synergistic interactions between Topo I inhibitors and targeted radiotherapy.

The effectiveness of therapeutic applications of [^{131}I]MIBG will be improved if this drug is used in combination with agents which potentiate radiation-induced damage. TPT-induced radiosensitisation has the potential to improve on existing regimes based on [^{131}I]MIBG therapy for the treatment of neuroblastoma.

The aims of this study were:

i) To evaluate the potential of reverse transcription and polymerase chain reaction (RT-PCR) to accurately identify neuroblastoma patients who are most likely to benefit from [^{131}I]MIBG therapy. mRNA extracted from neuroblastoma biopsy samples, was analysed for NAT gene expression, quantified by real-time PCR and referenced against the expression of the housekeeping gene glyceraldehyde-3-phosphate dehydrogenase (GAPDH). The results of RT-PCR analyses were compared with scintigrams derived from the same patients.

ii) To investigate the efficacy of scheduled combinations of [^{131}I]MIBG and TPT *in vitro* and *in vivo*, to improve upon existing therapies for neuroblastoma. The interaction between the two drugs was investigated *in vitro* by two methods, namely isobologram and combination-index analyses. The interaction between [^{131}I]MIBG and TPT *in vivo* was investigated by delay of the growth of NAT-expressing tumour xenografts

iii) To assess the effect of TPT on [^{131}I]MIBG-induced DNA damage and cellular repair mechanisms using the single cell gel electrophoresis (SCGE), or comet assay.

Chapter 2

Development of a real-time RT-PCR assay for the prediction of [^{131}I]MIBG uptake

2.1 Introduction

2.1.1 MIBG and clinical diagnosis of neuroblastoma

85-90% of neuroblastoma tumours express the noradrenaline transporter (NAT), responsible for the active intracellular accumulation of catecholamines [61, 62]. MIBG is also selectively concentrated in neuroadrenergic tissue by this process, and previous studies have demonstrated that NAT gene expression correlates with [^{131}I]MIBG uptake *in vitro* [62]. [^{131}I]MIBG has been shown to be a useful agent for the diagnosis and treatment of neuroblastoma [144].

Clinical diagnosis of neuroblastoma involves histological examination of biopsy specimens and evaluation of scintigrams obtained following the administration of a tracer dose of either [^{123}I]MIBG or [^{131}I]MIBG. The ability of tumours to uptake [^{131}I]MIBG at this stage also indicates the suitability of the patient for a treatment regimen incorporating [^{131}I]MIBG therapy.

However, as radioiodinated MIBG is not available immediately to most hospitals, more than one week may elapse between the time of admission, to gamma-camera scanning and reporting. A rapid and sensitive molecular assay for the active uptake of [^{131}I]MIBG, which could be applied at initial biopsy, would be invaluable in selecting patients for therapeutic strategies, which incorporate this radiopharmaceutical.

Whilst quantitative PCR is feasible using serial dilution of cDNA followed by analysis of PCR reaction end-points, this procedure has proven both time-consuming and poorly reproducible [145]. The recent development of fluorescent TaqMan methodology shows great promise and may supersede existing methods. Accordingly, a TaqMan RT-PCR based assay was developed to determine the suitability of neuroblastoma patients for therapy using radiolabelled MIBG.

2.1.2 TaqMan PCR

Real-time, or TaqMan PCR is a system that enables quantitation of specific DNA sequences. The methodology employs a probe technology that exploits the 5'-3' nuclease activity of Amplitaq gold polymerase to allow the detection of PCR amplicon formation by the release of a fluorescent reporter during the amplification cycle [146] (Figure 2-1). This nuclease activity only occurs during polymerisation, therefore, probe that is not bound to target DNA remains uncleaved.

To facilitate TaqMan PCR analysis, it is necessary to design a primer / probe set, which hybridises specifically to the DNA sequence of interest. Three oligonucleotide sequences are utilised in TaqMan PCR. Two of these are forward and reverse primers, which are standard for PCR reactions. The third sequence, called the probe, is specific for a sequence which lies between the forward and reverse primers. A reporter dye such as FAM (6-carboxyfluorescein) is covalently liked to the 5' end, and a quencher, TAMRA (6-carboxytetramethylrhodamine) is covalently linked to the 3' end.

When the probe is intact, the proximity of the reporter to the quencher causes a suppression of reporter fluorescence by Förster-type energy transfer. During PCR, the probe anneals to its target sequence between the forward and reverse primers. The 5'-3' nuclease activity of amplitaq gold polymerase cleaves the probe, leading to an increase in free reporter dye after each amplification cycle. Subsequently, the absence of the fluorescent suppression caused by the quencher causes an increase in reporter fluorescence levels. This is quantified, and provides a direct measurement of amplicon formation (Figure 2-1)

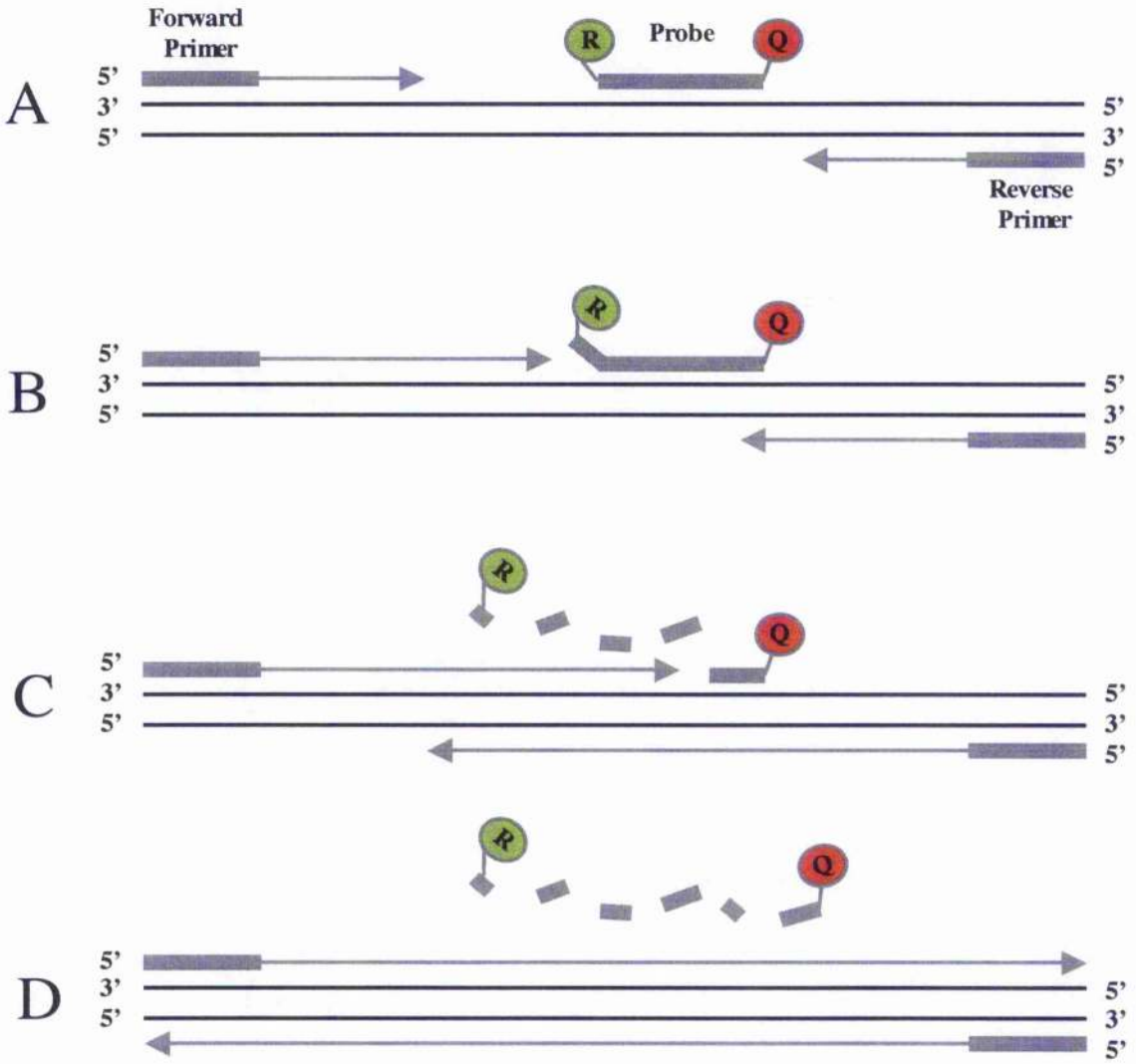

Figure 2-1: Summary of Taqman PCR amplification

A) Polymerisation: Forward and reverse primers anneal to specific sequences as in standard PCR. Probe binds to a specific sequence between the primers. Polymerisation commences.

B) Strand Displacement: Newly polymerised DNA reaches the probe, and begins to displace it from its target DNA as polymerisation continues.

C) Cleavage: 5'-3' nuclease activity of amplitaq gold polymerase cleaves the probe leading to an increase in free reporter molecules.

D) Polymerisation completed: Separation of reporter dye from quencher dye leads to an increase in reporter fluorescence after each round of replication.

Fluorescence emission by free reporter (Rn) is measured in real-time after every PCR cycle. At the completion of the last cycle of PCR, results are displayed as an amplification curve, where Rn (ΔRn) is plotted against cycle number (Figure 2-2). These results, which show a hypothetical TaqMan PCR reaction, allow the direct visualisation of product formation after each cycle. The threshold cycle (C_t) value of product detection, used for quantitation, is derived from the exponential phase of the PCR reaction, rather than the plateau phase where increasing cycle number has no effect on product formation.

This results in greater accuracy and sensitivity over alternative methods of nucleic acid quantitation. These features should facilitate progress toward the clinical application of PCR-based assays. Moreover, an RT-PCR analysis of tumoural expression of NAT-specific transcripts can be completed in one half of a working day. Therefore this procedure has the potential to allow the prompt identification of patients who may benefit from targeted therapy.

Using real-time PCR, the goal was to establish the relationship between the level of NAT gene transcription by cell lines and their capacity for active uptake of [^{131}I]MIBG, and to determine whether the detection of NAT cDNA sequences in neuroblastoma biopsy samples could predict the uptake by tumours of [^{131}I]MIBG.

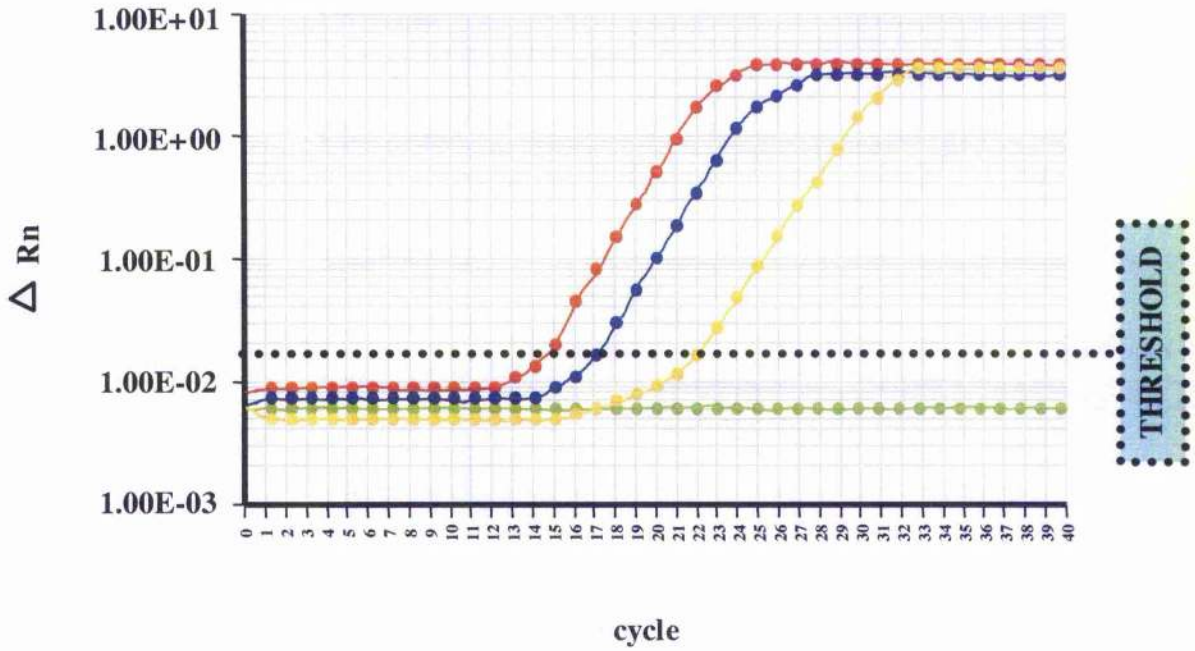

Figure 2-2: Example of TaqMan PCR results

In this experiment, four hypothetical samples were subjected to PCR to test for presence of a specific sequence. Increasing fluorescence is measured after each cycle. The threshold line denotes where each sample enters the exponential phase of amplification, known as the C_t.

from these results, the following conclusions can be reached:

Sample 1: (red line) had the lowest C_t (C_t = 15), denoting the highest starting number of target molecules.
Sample 2: (blue line) had the next lowest C_t (C_t = 17.5).
Sample 3: (yellow line) had a higher C_t (C_t = 22.5) denoting a low starting number of target molecules.
Sample 4: (green line) did not enter the exponential phase, denoting negativity.

2.2 Materials & methods

2.2.1 Cells and culture conditions.

Four human cell lines of neurogenic origin were cultured: SK-N-BE(2c), SHSY5Y, SK-N-MC [147] and IMR-32 [148]. In addition, three non-neural crest-derived cell lines were evaluated. These were the human breast adenocarcinoma line MCF-7 [149], the human glioblastoma cell line UVW [150, 151] and UVW/NAT, a NAT expressing cell line derived from UVW which was established in this laboratory [152] by transfection of UVW cells with a pREP9 episomal expression vector (Invitrogen) containing a copy of the bovine NAT (bNAT) cDNA. Utilisation of the bovine version of the NAT gene in the transfected cell line allowed differentiation between endogenous human NAT mRNA levels and transcription of the expression vector by TaqMan RT-PCR.

Cells were maintained in either MEM medium (IMR-32, SHSY5Y, SK-N-MC and UVW) or RPMI 1640 medium (SK-N-BE(2c) MCF-7, and UVW/NAT), containing 10% foetal calf serum (FCS) and glutamine (2mM) at 37°C in a 5% CO_2 atmosphere. UVW/NAT media contained 500ng/ml Geneticin, which is toxic to cells not expressing the pREP9 vector. All media and supplements were purchased from Invitrogen (Paisley, UK).

2.2.2 Tumour samples.

Samples of 54 neuroblastoma tumours, frozen in liquid nitrogen immediately after excision, were obtained retrospectively from the Academical Medical Center, Amsterdam, Netherlands, the G. Gaslini Institute, Genova, Italy and from ten UK Children's Cancer Study Group hospitals. Histological examination revealed that all samples contained greater than 20% neuroblastoma cellularity [153]. Biopsy material was obtained from the primary tumour in each case.

2.2.3 RNA extraction

Total RNA was extracted from cell lines and patient biopsy material using the RNAzol method according to manufacturer's instructions (Biogenesis, Poole, UK). The RNA samples were assessed for expression of NAT and the reference gene GAPDH by reverse transcription and real-time PCR. This study was approved by the Research Ethics Committees of the participating institutions.

2.2.4 Accumulation of [^{131}I]MIBG in cell lines

Cells were seeded in six-well plates at 0.25 x 10^5 cells per well, and incubated at 37°C, in 5% CO_2 in RPMI 1640 medium containing 10% FCS. After 48h cells were washed once with PBS, and incubated in media containing 7kBq [^{131}I]MIBG per well for 2h, after which time uptake of [^{131}I]MIBG is maximal [154]. After incubation, cells were washed twice in PBS, and the radioactivity was extracted with two 0.5ml aliquots of 10% trichloroacetic acid at 4°C.

Non-specific uptake was measured in the presence of 1.5μM desmethylimipramine (DMI), a tricyclic antidepressant which inhibits the re-uptake of neurotransmitters by adrenergic neurones. Activity was measured in a Cobra II auto-γ counting system (Canberra Packard, Berkshire, UK). Specific uptake was calculated by subtracting values obtained from DMI inhibited extracts from total uptake, and expressed as counts per minute per 10^5 cells (cpm/10^5c).

2.2.5 Evaluation of scintigrams.

Evaluation of scintigrams was coordinated by Dr. Alan Sprigg (Department of Radiology, Sheffield Children's Hospital). Radioiodinated-MIBG scintigrams were obtained from the referral centres, and the hard-copy images were appraised independently by two assessors. The activity pattern was compared with the known site of the primary tumour (as biopsied) and correlated with other cross sectional imaging as necessary (e.g. where liver uptake was superimposed on a primary upper abdominal tumour mass).

Review of the MIBG scintigrams and cross-sectional imaging was performed blind, without prior knowledge of the abundance of NAT-specific mRNA. Only samples from patients with evaluable MIBG scans were included in the study. The uptake of [^{123}I]MIBG into the primary mass was recorded as negative or positive.

2.2.6 Primers and probes

The primer and probe sequences chosen for hNAT and bNAT RT-PCR were species specific, in order to differentiate between endogenous transcripts, and those generated from pREP9 plasmid gene expression. Primer and probe sequences were designed from the published sequence for the human noradrenaline transporter (hNAT) (accession No. M65105) using the ABI prism PrimerExpress™ v1.0 software. Both primers and probe were custom synthesised (MWG-Biotech, Milton Keynes, UK). The sense primer corresponded to bases 241-260 of the hNAT sequence (5'-CGCTTCCCCTACCTCTGCTA-3'). The antisense primer was complementary to bases 372-391 of the hNAT sequence (5'-AGATTTTCCAAACGGTGGCA-3'). These primers generated a PCR product of 151 base pairs. The internal probe corresponded to bases 273-299 of the hNAT sequence (5'-CGGTGCCTTCTTGATCCCGTACACACT-3'). The probe was labelled with the fluorescent reporter dye 6-carboxyfluoroscein (FAM) at the 5' end, and the quencher molecule 6-carboxytetramethylrhodamine (TAMRA) at the 3' end.

Similarly, primer and probe sequences were designed from the published sequence for the bovine noradrenaline transporter (bNAT) (accession No. U09198), and custom synthesised as above (MWG-Biotech). The sense primer corresponded to bases 1583-1602 of the bNAT sequence (5'-TCAGCAACGACATCCAGCAG-3'). The antisense primer was complementary to bases 1637-1657 of the bNAT sequence (5'-GGCTGACAAACTTCCAGCAGA-3'). These primers generated a PCR product of 75 base pairs. The internal probe corresponded to bases 1612-1635 of the bNAT sequence (5'-TTCAAGCCCGGCCTGTACTGGAGA-3'). This probe was also labelled with the fluorescent reporter dye FAM at the 5' end, and the quencher molecule TAMRA at the 3' end.

The housekeeping gene glyceraldehyde-3-phosphate dehydrogenase (GAPDH) was used as an internal standard for all real-time PCR reactions. GAPDH PCR was carried out using the specifically designed primers and probe kit, TaqMan GAPDH control reagents. This was obtained from Perkin-Elmer Applied Biosystems (Cheshire, UK), P/N 402869.

2.2.7 Standard curve generation and quantitation of test samples

A standard curve was constructed, which was used to produce an exact quantitation of starting number of copies of the target sequence. To construct the standard curve, firstly a PCR reaction was carried out using TaqMan-generated PCR primers, but using standard (ie. non-TaqMan) PCR reagents. The resulting PCR products were then purified. The PCR product was quantified spectrophotometrically at A_{260}, and converted to number of molecules/μl, using the equation in Figure 2-3 [155, 156]. TaqMan PCR of standards and unknown samples was then carried out, and the ABI 7700 sequence detection software determined the initial amounts of unknown samples by direct comparison of their C_t value with the C_t values of known standards. An example of a standard curve is shown in Figure 2-4.

hNAT-specific, and GAPDH-specific PCR products were obtained by reverse transcribing and PCR amplifying 1 g of total RNA obtained from the human neuroblastoma cell line SK-N-BE(2c) using the same primer pairs employed later in the quantitative real-time PCR. The resulting PCR products were then purified using an S-400 spin column (Pharmacia Biotech, Uppsala, Sweden) and quality-assessed by agarose gel electrophoresis and ethidium bromide staining. The PCR product was quantified spectrophotometrically and then serially diluted in mouse genomic DNA (Clontech, CA, USA) to maintain a constant total DNA concentration. The standard curve used for quantitation of the real-time PCR reaction was constructed using 10^1 to 10^8 copies of the SK-N-BE(2c) PCR products obtained from the reaction described above.

Similarly, bNAT specific PCR products were obtained by reverse transcribing and PCR amplifying 1 g of total RNA obtained from the transfected glioblastoma cell line line UVW/NAT. The resulting PCR product was purified and assessed as above, and a standard

curve used for quantitation of the real-time PCR reaction was constructed using 10^1 to 10^8 copies of the bNAT sequence.

$$\text{No. of molecules / } \mu\text{l} = \left(\frac{A_{260}}{13.2 \times S} \right) \times \frac{NA}{10^{12}}$$

Where:

A_{260} = absorbance at 260nm,
S = size of DNA in kilobases
NA = Avogadro's number: 6.022×10^{23}

Figure 2-3: Calculation of initial number of molecules for generation of a standard curve

This calculation is used to determine the number of molecules in a sample of known DNA concentration. It is based on the determination of concentration of double stranded DNA [155], which establishes the molarity (in pmol/μl) of a DNA sample from its absorbance at 260nm.

1 mole contains 6.022×10^{23} molecules (Avogadro's number [156]), allowing calculation of the initial number of molecules in a DNA sample.

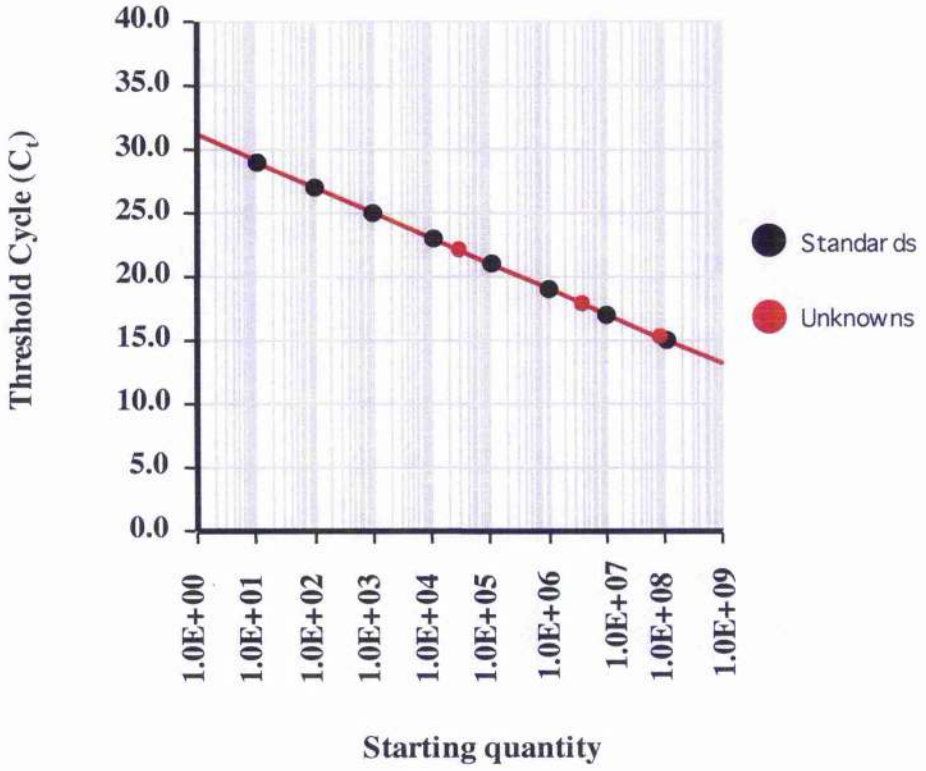

Figure 2-4: Standard curve construction

8 standards of known initial copy number (10^1 to 10^8 copies of target DNA) were subjected to TaqMan PCR.

ABI 7700 sequence detection software plotted the C_t value for each standard against starting quantity, and automatically plots unknown test reactions onto this line.

It is therefore possible to determine the starting quantity of your test sample by comparing its C_t to the C_t values of the standards.

In this example, the samples previously shown in Figure 2-2 are plotted along with the standards. The results are as follows:

Sample 1 (C_t = 15): 1 x 10^8 copies of target
Sample 2 (C_t = 17.5): 4 x 10^6 copies of target
Sample 3 (C_t = 22.5): 3 x 10^4 copies of target

2.2.8 Real-time RT-PCR amplification.

Real-time RT-PCR was carried out using the commercially available TaqMan Gold RNA PCR kit (Perkin-Elmer Applied Biosystems, Warrington UK: P/N N808-0232).

Briefly, 1μg of total RNA was reverse transcribed in a 50μl reaction volume, containing 5.5 mM $MgCl_2$, 5μl 10x TaqMan RT buffer, 2mM dNTP mix (500uM each nucleotide), 20 units of RNAse Inhibitor, 2.5μM oligo $d(T)_{16}$ and 62.5 units of MultiScribe Reverse Transcriptase. 2.5μl of the resulting solution, containing cDNA template, was added to an amplification reaction mixture of total volume 25μl consisting of 5.5 mM $MgCl_2$, 2.5μl 10x TaqMan buffer, 200 M dATP, dCTP, dGTP and 400 M dUTP, 0.625 units of AmpliTaq Gold, 0.25 units of AmpErase uracil N-glycosylase (UNG) and 100 nM each of both primers and probe.

The thermal cycling conditions consisted of an initial incubation for 2min at 50°C, followed by 10 min at 95°C. Thermal cycling was then carried out at 95°C for 15 sec, followed by 60°C for 1 min, for 40 cycles.

Each assay included a standard curve (10^1 to 10^8 copies) and a no-template control, along with the unknown cDNA templates obtained from the reverse-transcription step. PCR reactions were performed using an ABI prism 7700 Sequence Detection System (Perkin-Elmer Applied Biosystems, Foster City, USA), which measured the fluorescent signal generated by the PCR reaction.

2.2.9 Statistical analysis.

The relationship between expression of the noradrenaline transporter and specific uptake of [^{131}I]MIBG by NAT expressing cells was determined by linear regression. The relationship between tumour uptake of MIBG and NAT gene expression was examined by Fisher's exact test (two-sided) using GraphPad Prism software, version 3.0, 1999 (CA).

2.3 Results

2.3.1 Real-time PCR.

A range of quantities of NAT- and GAPDH-specific PCR products were amplified using the real-time PCR method to establish corresponding C_t values (Figure 2-5A). These were plotted against the initial quantity of substrate to produce standard curves (Figure 2-5B). This exemplifies the high sensitivity and accuracy of amplification over a large concentration range ($r = 0.985$).

RNA obtained from cell lines and patient biopsy material was reverse transcribed and PCR-amplified using the real-time methodology. Samples were assayed three times in duplicate for both NAT and GAPDH expression.

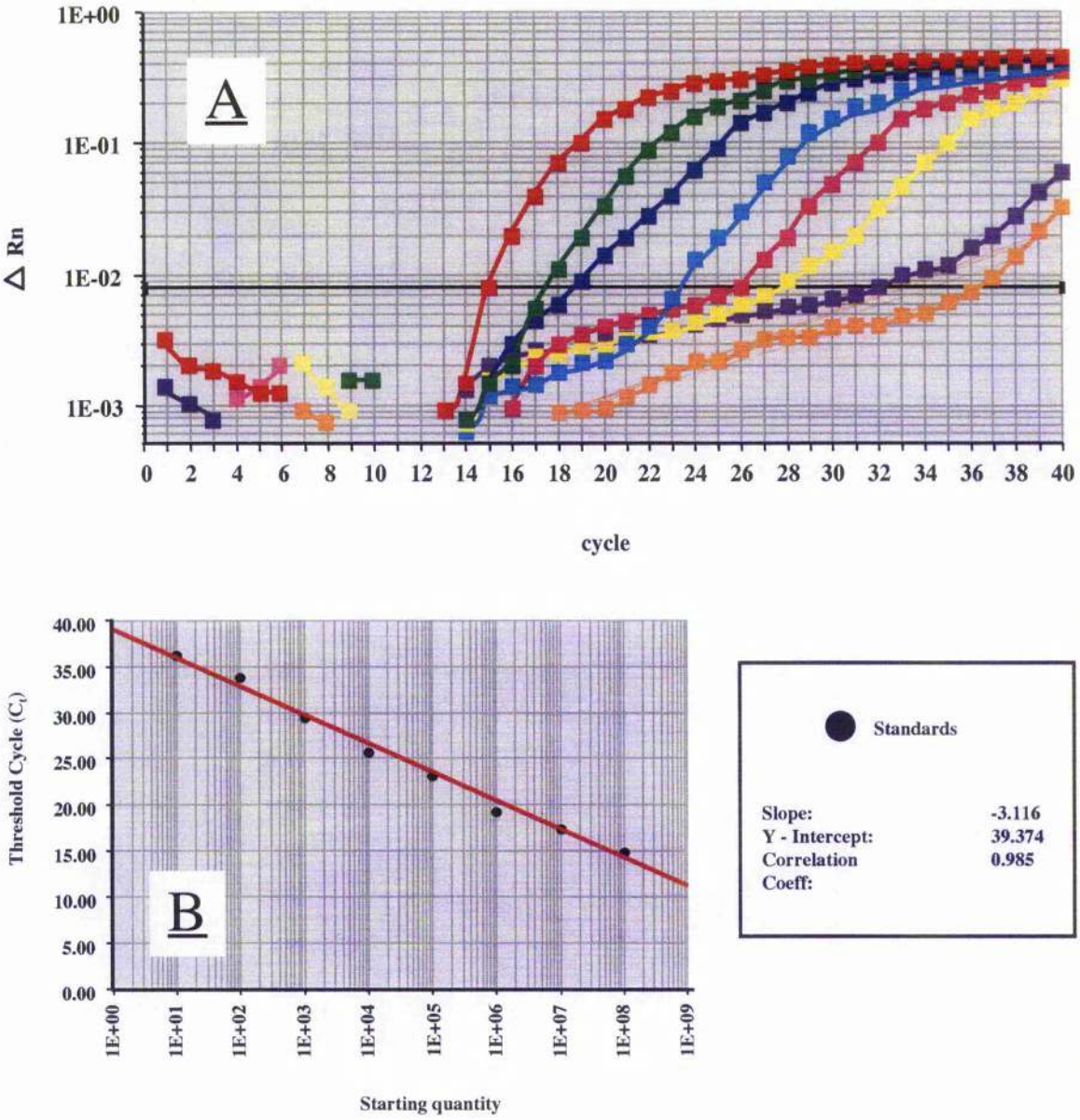

Figure 2-5: Amplification plot and standard curve of the NAT sequence

Standards were obtained by PCR amplification of cDNA from the cell line SK-N-BE(2c). The NAT-specific PCR product was then quantified spectrophotometrically, serially diluted and amplified using the real-time PCR method.

A: The plots, from left to right, correspond to 10^8 to 10^1 NAT sequence copies.

B: The C_t values obtained were plotted against the initial quantity of substrate to produce a standard curve.

A similar procedure was used to quantify the reference GAPDH sequence.

2.3.2 [^{131}I]MIBG uptake compared with NAT gene expression in cell lines.

Three out of four neuroblastoma cell lines, demonstrated active uptake of [^{131}I]MIBG. In non-neural crest-derived cell lines, [^{131}I]MIBG uptake was observed only in UVW/NAT, which was transfected with a plasmid containing bNAT. Real-time RT-PCR, with specificity for NAT and GAPDH sequences, indicated transcription of the NAT gene only in those cell lines which actively accumulated [^{131}I]MIBG (Table 2-1). The coefficients of variation of the C_t values of the NAT-positive cell lines, obtained from three separate determinations in duplicate, were 2.9% (SK-N-BE(2c)), 2.5% (SHSY5Y), 2.0% (IMR-32) and 3.0% (UVW/NAT). These indices of reproducibility are superior to those previously obtained by means of conventional RT-PCR methodology [62]. The level of expression of the hNAT gene by the panel of five neuroblastoma cell lines correlated significantly ($p < 0.05$) with the capacity for active uptake of [^{131}I]MIBG.

Cell line	Active MIBG uptake (cpm x 10^3 per 10^5 cells)	NAT copies per 10 GAPDH copies
SK-N-BE(2c)	**112 ± 11**	**3.550 ± 0.103***
SHSY5Y	**46 ± 5**	**1.117 ± 0.028***
IMR-32	**8 ± 2**	**0.402 ± 0.008***
SK-N-MC	**0**	**0**
MCF-7	**0**	**0**
UVW	**0**	**0**
UVW/NAT	**132 ± 13**	**35.34 ± 1.07+**

<u>Table 2-1:</u> NAT gene expression and MIBG uptake by neuroblastoma cell lines

Using the RNA obtained from seven human tumour cell lines, NAT and GAPDH expression were assessed by reverse transcription and real-time PCR amplification. The results are means ± s.d. of three separate determinations in duplicate. Active uptake of [^{131}I]MIBG was determined by subtraction of non-specific uptake (assessed in the presence of desmethylimipramine) from total [^{131}I]MIBG uptake.

* Expression of the human noradrenaline transporter (hNAT)
+ Expression of the bovine noradrenaline transporter (bNAT)

2.3.3 NAT gene expression in biopsy specimens.

The real-time PCR procedure revealed a wide range of NAT gene expression levels in neuroblastoma biopsy samples (Figure 2-6). Most tumours (63%) expressed fewer than 2 NAT copies per 10 reference gene (GAPDH) transcripts. A minority (37%) of the tumours exhibited higher NAT transcription. The highest expression of the cohort (two tumours, or 3.7%) was greater than 9 NAT transcripts per 10 GAPDH transcripts.

[^{131}I]MIBG uptake by neuroblastoma tumours was compared with NAT gene expression in biopsies. NAT and GAPDH copy numbers of neuroblastoma biopsy samples were obtained in the same manner as described for cell lines. RNA isolates from biopsy specimens were assayed three times in duplicate. Table 2-2 illustrates the disease stage and MIBG scintigraphic and RT-PCR results from the specimens collected from patients. Of the 54 patients' samples with evaluable MIBG scans, 48 (89%) accumulated MIBG into the primary tumour. 43/54 (80%) tumour samples were positive for NAT mRNA.

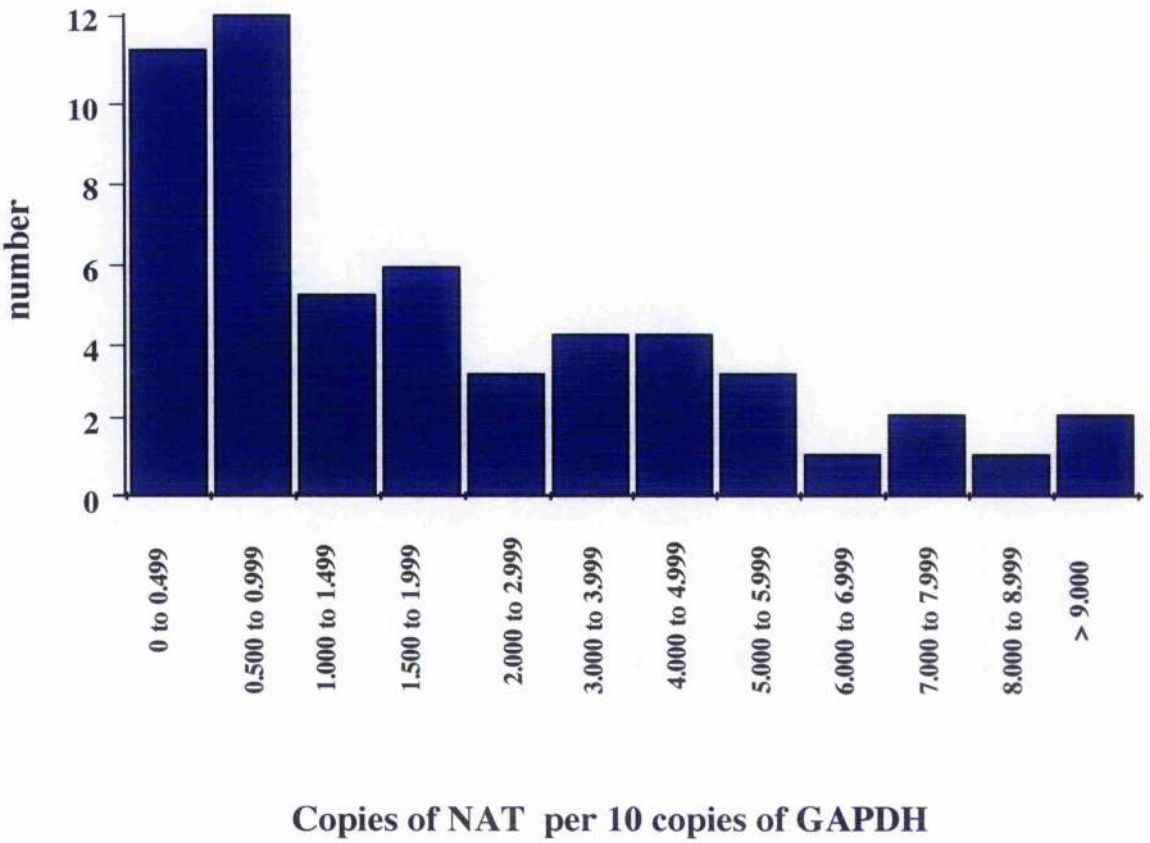

Figure 2-6: Distribution of NAT mRNA expression levels in neuroblastoma biopsy samples

The real-time PCR procedure revealed a wide range of NAT gene expression levels in neuroblastoma biopsy samples. Most tumours (63%) expressed fewer than 2 NAT copies per 10 reference gene (GAPDH) transcripts.

A minority (37%) of the tumours showed higher NAT transcription levels. The highest expression observed (two tumours) was greater than 9 NAT transcripts per 10 GAPDH transcripts.

Of the 11/54 (20%) tumour specimens in which NAT-specific sequences were undetectable, 6/54 (11%) were derived from tumours which did not accumulate MIBG whereas 5/54 (9%) originated from MIBG scan-positive primary tumours. Samples derived from tumours which failed to accumulate MIBG did not display NAT gene expression (Table 2-3).

There was a significant association between tumour MIBG uptake, evaluated by scintigraphy, and PCR-determined NAT expression ($P < 0.0001$, Fisher's exact test). The prognostic value of a NAT-specific, positive PCR test was 1 (100%). However the predictive merit of a negative test was only 0.55 (55 %).

Patient No.	Stage	Scan	RT-PCR	Patient No.	Stage	Scan	RT-PCR
1	4	+	+	28	2	+	+
2	4s	+	+	29	2	+	+
3	2	+	-	30	4	+	+
4	2	+	+	31	4	-	-
5	4	+	+	32	4	+	-
6	4	-	-	33	3	+	+
7	4s	+	-	34	1	+	+
8	4	+	+	35	4	+	+
9	3	+	+	36	2	+	+
10	4	+	+	37	1	-	-
11	4	+	+	38	1	+	+
12	2	+	+	39	3	+	+
13	4	+	+	40	4	+	+
14	2	+	+	41	4	+	+
15	4	+	+	42	4	+	+
16	4	+	+	43	3	+	+
17	2	+	+	44	2	-	-
18	3	-	-	45	4	+	+
19	4s	+	+	46	3	+	+
20	4	+	+	47	4	+	+
21	4	+	+	48	4	+	-
22	4s	+	+	49	3	-	-
23	2	+	+	50	4	+	+
24	4	+	+	51	3	+	+
25	3	+	-	52	3	+	+
26	4s	+	+	53	4	+	+
27	4	+	+	54	1	+	+

Table 2-2: Comparison of tumour uptake of [^{131}I]MIBG with NAT mRNA expression in biopsy samples

[^{131}I]MIBG uptake and NAT mRNA levels were determined by gamma camera scanning of the patients and Taqman RT-PCR of biopsy-derived RNA respectively. Tumours were classified according to the International Neuroblastoma Staging System (Table 1-1).

	MIBG scan + ve	MIBG scan – ve	Total
PCR + ve	**43**	**0**	**43**
PCR – ve	**5**	**6**	**11**
Total	**48**	**6**	**54**

Fisher's exact test, 2 sided,	$p < 0.0001$
Sensitivity	**= 90%**
Specificity	**= 100%**
Positive predictive value	**= 100%**
Negative predictive value	**= 55%**

Table 2-3: MIBG uptake by neuroblastoma tumours compared with NAT expression

The accumulation of MIBG by tumour was determined by gamma camera scanning after the administration to patients of [^{123}I]MIBG. NAT expression in neuroblastoma biopsy specimens was assessed by real-time RT-PCR analysis.

There was a significant association between tumour MIBG uptake, evaluated by scintigraphy, and RT-PCR-determined NAT expression ($p < 0.0001$, Fisher's exact test).

2.4 Summary of results

The assay, based on real-time PCR analysis, showed substantial power to predict MIBG uptake capacity and has the potential to select patients for [^{131}I]MIBG therapy. The real-time PCR technique allowed the simultaneous evaluation of a large number of individual samples as well as internal controls. This assay involves the use of industry-standardised reagents and requires less manipulation of sample than traditional PCR techniques, resulting in increased reliability and accuracy.

Of the 54 patients' samples with evaluable MIBG scans, 48 (89%) showed MIBG uptake into the primary tumour, while 43 (80%) of the tumour samples were positive for the expression of NAT mRNA. This is equivalent to 90% concordance with respect to positive outcome of the two tests. All 6 tumours (11%) that failed to accumulate MIBG had undetectable NAT mRNA expression. However, biopsies from 5 patients (10.4%) with positive MIBG scans did not express detectable NAT mRNA.

Therefore, while a positive PCR test always predicted tumour uptake of MIBG, a negative PCR test failed to correctly determine MIBG uptake capacity with a frequency of 45%. This may be due to heterogeneous uptake of radioidinated MIBG in different areas of a tumour mass, leading to a negative PCR result from biopsy material obtained from a NAT-negative area, and a positive MIBG scan from a NAT-positive area of the same tumour mass. It is also possible that the quality of biopsy material used for analysis was not optimal.

Furthermore, the possible presence of alternatively spliced NAT gene transcripts, mutant forms of the NAT protein, or alternative MIBG uptake pathways, which could be undetectable by the PCR primers employed in this study, cannot be discounted.

Finally, in this study the house-keeping gene GAPDH was used as a reference to assess NAT gene expression. However, to predict tumour cell concentration of MIBG more accurately, it may be necessary to use alternative internal standards with specificity for neuroblastoma cells. The limitations of TaqMan PCR, and other avenues of research arising from this study will be further discussed in Chapter 10.

These results indicate that NAT-specific, real-time PCR evaluation of primary neuroblastoma tumours has significant capability to reflect their capacity for the accumulation of MIBG. However, PCR-based assessment of NAT gene expression cannot be regarded as fully predictive of MIBG uptake. The results of this study were recently published in Clinical cancer research [153].

Chapter 3

The effect of topotecan pre-treatment on intracellular uptake of [^{131}I]MIBG

3.1 Introduction

3.1.1 Effect of DNA-interacting agents on active uptake of [^{131}I]MIBG

It has previously been reported that a wide range of DNA-interacting agents cause an increase in the ability of neuroblastoma cells to actively accumulate radiolabelled MIBG [154, 157-159]. This suggests that the efficacy of [^{131}I]MIBG-induced cytotoxicity can be improved by the prior administration of an agent which enhances cellular uptake of the radiopharmaceutical, and clinical evaluation of therapy involving drugs which increase accumulation of the [^{131}I]MIBG are currently underway [71].

3.1.2 Topotecan and [^{131}I]MIBG uptake

To date, no attempt has been made to investigate the potential of inhibitors of topoisomerase I to induce radiopotentiation *in vitro* and *in vivo* when combined with targeted radiotherapy. However, it is necessary to determine this potential effect of TPT, because of its possible influence on the optimal scheduling of the two agents.

The effect on NAT expressing cells of TPT pre-treatment was examined in two ways. Firstly, TPT treated cells were tested for their ability to accumulate [^{131}I]MIBG (functional assay). Secondly, RNA was extracted from TPT treated cells, and expression of the noradrenaline transporter (NAT) gene was evaluated by real time RT-PCR as previously described (Chapter 2).

3.2 Materials & methods

3.2.1 Cell Lines

Three NAT expressing cell lines were examined for the effect of TPT pre-treatment on their accumulation of [^{131}I]MIBG. These were the neuroblastoma cell lines SK-N-BE(2c) and SHSY5Y [62, 160], and the glioblastoma-derived UVW/NAT line [152] which had previously demonstrated uptake of [^{131}I]MIBG and NAT gene expression (Chapter 2).

3.2.2 The effect of topotecan on [^{131}I]MIBG uptake

The ability of TPT to affect [^{131}I]MIBG uptake was studied using the protocol previously described (Section 2.2.4). Briefly, cells were seeded in six-well plates at 0.25 x 10^5 cells per well, and incubated for 48h at 37^{0}C, in 5% CO_2, TPT was added at the appropriate concentration and the plates were incubated for a further 24h. The concentration of TPT assessed for each cell line corresponded to the dose of the drug which was required for 50% clonogenic cell kill, which will be discussed in greater detail in Chapter 4. For SK-N-BE(2c) treatments, TPT dose was 2ng/ml. For UVW/NAT cells, TPT concentration was 4.2ng/ml. For SHSY5Y cells TPT dose was 0.67ng/ml.

To assess the extent, and longevity of TPT-induced enhancement of [^{131}I]MIBG uptake, cells were either assayed immediately following 24h TPT incubation, or left in fresh media, and tested at 24h intervals for 72h. Specific [^{131}I]MIBG uptake was measured as previously described (Section 2.2.4) and expressed as counts per minute per 10^5 cells (cpm/10^5c). Results were analysed for enhancement of [^{131}I]MIBG accumulation in treated cells compared to untreated controls by Student's t-test (Excel 2001, ®Microsoft Corporation).

3.2.3 The effect of topotecan on expression of the noradrenaline transporter gene

The effect of TPT exposure on expression of the noradrenaline transporter gene was investigated by real time RT-PCR [153] (see Chapter 2). Cells were treated with TPT for 24h, and then either subjected to RNA extraction immediately following removal of the drug, or incubated in drug-free media. Further RNA extractions were carried out at 24h intervals up to 72h after removal of TPT.

3.2.4 RNA extractions

Total RNA was extracted from SK-N-BE(2c) cells using the RNeasy method (Qiagen, UK). 1mg of total RNA was reverse transcribed, and the resulting cDNA was analysed for NAT-specific sequence by real-time PCR, using an ABI Prism™ 7700 sequence detector. PCR conditions were as previously described in Chapter 2 (Section 2.2.8), as were hNAT, bNAT and GAPDH primer and probe sequences (Section 2.2.6).

3.3 Results

3.3.1 The effect of topotecan on [^{131}I]MIBG uptake in NAT expressing cells

SK-N-BE(2c), UVW/NAT and SHSY5Y cells assayed immediately following TPT treatment exhibited a small, but insignificant enhancement of [^{131}I]MIBG uptake compared to untreated controls. Cells assayed following a 24h incubation in fresh media consistently exhibited an significant increase in [^{131}I]MIBG incorporatation ($p < 0.05$), approximately 2-2.5 times that of untreated controls. Cells assayed 24h after this (ie. 48h after removal of the drug) retained an increased ability to uptake [^{131}I]MIBG ($p < 0.05$), but at a reduced level compared with the 24h time point. 72h after removal of TPT [^{131}I]MIBG uptake capacity had returned to the level of untreated cells. See Figure 3-1.

Previous studies have reported that a wide range of DNA-interacting drugs cause an increase in uptake of radio-labelled MIBG by neuroblastoma cells. The enhancement factor of TPT pretreatment was similar to that caused by, IFN-γ + retinoic acid [66], IFN-γ + IFN-α [157], cisplatin [154, 158], adriamycin [158] and γ-rays [159] (Table 3-1). This suggests that a common mechanism may be involved.

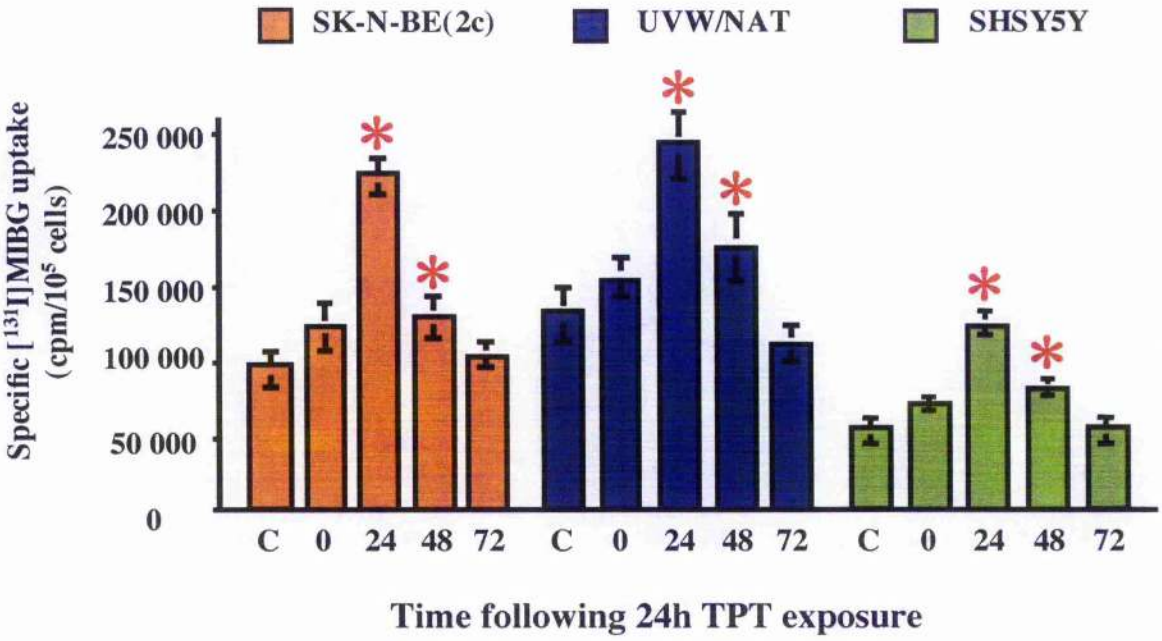

Figure 3-1: The effect of topotecan on [^{131}I]MIBG uptake

This figure shows the effect of TPT pretreatment on the ability of SK-N-BE(2c), UVW/NAT and SHSY5Y cells to accumulate [^{131}I]MIBG.

Cells were treated with TPT for 24h, and then either assayed immediately, or left in fresh media, and tested at 24h intervals for 72h. Results were analysed by Student's t-test. Results showing significant enhancement of uptake ($p < 0.05$) compared to untreated controls (C) are highlighted (*).

Cells assayed immediately following TPT treatment showed a small, but insignificant increase in [^{131}I]MIBG uptake compared to untreated controls (C). However, significantly enhanced uptake was observed after 24h incubation in fresh media; cells consistently exhibited an enhanced ability to incorporate [^{131}I]MIBG, approximately 2-2.5 times that of untreated controls.

Cells assayed 24h after this (ie. 48h following removal of TPT) retained a significantly increased ability to uptake [^{131}I]MIBG. Cells tested 72h after removal of TPT exhibited no increase in [^{131}I]MIBG uptake. This pattern was observed in all cell lines tested.

Treatment	[^{131}I]MIBG Uptake Enhancement Factor
5 Gy γ-rays	1.8
IFN-γ + retinoic acid	3.0
IFN-γ + IFN-α	2.5
Cisplatin	2.8
Adriamycin	3.0
Topotecan	**2-2.5**

Table 3-1: Effect of topotecan pretreatment on [^{131}I]MIBG uptake: Comparison with other DNA interacting agents

Previous studies have shown that a wide range of agents which interact with DNA cause an enhancement in the ability of neuroblastoma cell lines to actively uptake radio-labelled MIBG *in vitro*.

The enhancement factor of topotecan pretreatment seen in [^{131}I]MIBG uptake studies (Figure 3-1) is similar to that which is caused by these other agents. This suggests that a common mechanism may be involved.

3.3.2 TaqMan RT-PCR analysis of NAT gene expression

Previous studies have reported that increased [^{131}I]MIBG uptake correlated with an increase in NAT gene expression [154, 157, 158].

The results of real time RT-PCR of RNA derived from untreated SK-N-BE(2c) and SHSY5Y cells revealed expression of the human NAT (hNAT) gene (2.81 ± 1.59 and 1.02 ± 0.32 hNAT copies per 10 GAPDH copies respectively). SK-N-BE(2c) and SHSY5Y are human neuroblastoma cell lines, and therefore displayed no expression of the bovine NAT (bNAT) gene.

The UVW/NAT cell line is a human glioblastoma line that has been tranfected with an expression vector incorporating the bNAT gene under the control of a strong viral (RSV) promoter [152]. Real time RT-PCR revealed high expression of the bNAT gene (38.3 ± 5.9 bNAT copies per 10 GAPDH copies). However, UVW/NAT cells displayed negligible expression of the hNAT gene.

Following TPT incubation, SK-N-BE(2c) UVW/NAT and SHSY5Y cells were assayed by RT-PCR at 0h, 24h, 48h and 72h after removal of the drug. While similarly treated cells consistently exhibited an increase in [^{131}I]MIBG uptake, this did not correlate with an increase of NAT gene product. SK-N-BE(2c) and SHSY5Y cells displayed little, or no stimulation of expression of the hNAT gene, compared to untreated controls at any of the time points (0h, 24h, 48h) which gave rise to increased accumulation of [^{131}I]MIBG. Likewise, UVW/NAT cells displayed no stimulation of bNAT or hNAT gene expression at any of the time points assessed (Figure 3-2).

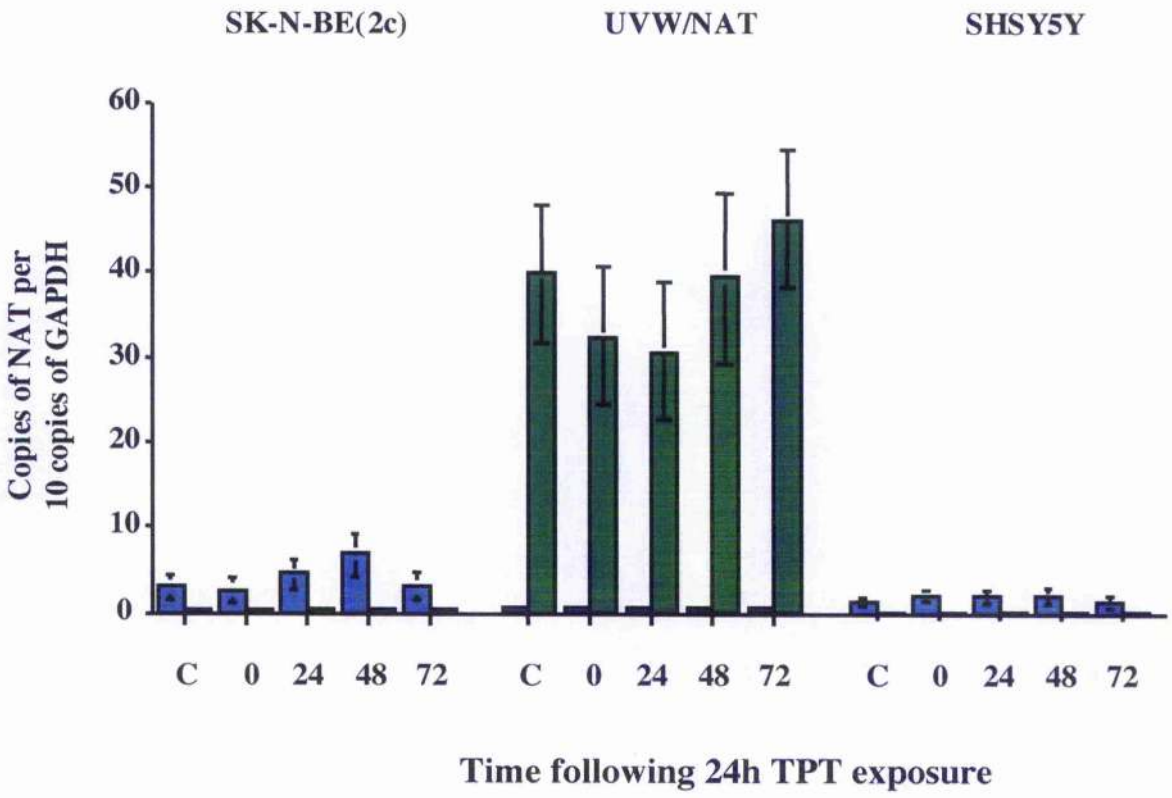

Figure 3-2: Real-time RT-PCR analysis of NAT gene expression

TPT treated SK-N-BE(2c) and UVW/NAT cells were assayed by RT-PCR at 0h, 24h, 48h and 72h after removal of TPT.

There was no increase in hNAT or bNAT gene expression in SK-N-BE(2c) or UVW/NAT cells, compared to untreated controls (C), at any of the time points assessed.

3.4 Summary of results

Significant enhancement of [^{131}I]MIBG uptake, approximately 2-2.5 times the level in untreated controls, was observed in two neuroblastoma cell lines; SK-N-BE(2c) and SHSY5Y. This effect was optimal 24h after removal of the drug. At time points later than 24h, there was a lower, but still significant accumulation of the radiopharmaceutical, and uptake capacity returned to the levels observed in untreated cells 72h after removal of TPT.

Interestingly, increased uptake of [^{131}I]MIBG was also observed *in vitro* in TPT pretreated UVW/NAT cells, which contain an expression vector incorporating the bNAT gene under the control of a viral (RSV) promoter.

However, while previous studies have found an upregulation of mRNA signal (by Northern blotting or semi-quantitative RT-PCR) following administration of DNA interacting agents (Table 3-1), in this study, pre-treatment with TPT did not induce significant upregulation of hNAT gene expression in SK-N-BE(2c) or SHSY5Y cells. Likewise, TPT pre-treatmentment did not induce increased hNAT or bNAT gene expression in UVW/NAT cells, as measured by real time RT-PCR. It is possible that alternatively spliced forms of NAT mRNA, which allow production of functional NAT protein, but are undetectable by the PCR primers employed in this study, could be responsible for enhanced [^{131}I]MIBG uptake.

It may be necessary to design a new primer / probe set, which hybridises to another region of the NAT cDNA sequence. If NAT protein levels are entirely due to transcription of a single version of NAT mRNA, then identical results should be obtained by analysis of the copy numbers of different regions of the NAT mRNA sequence. However, any differences in the starting copy numbers detected by primers which anneal to different

regions of the published NAT cDNA sequence would suggest the presence of alternative versions of NAT mRNA.

Alternatively, expression of the NAT gene product may be partially controlled at the post-transcriptional or post-translational stages, by an as yet undiscovered pathway. This could lead to some alteration in the cellular concentration of functional NAT protein, without affecting gene transcription. Development of assay for NAT protein concentration (eg. Western blot) would help to resolve this issue.

These points will be discussed further in Chapter 10.

Chapter 4

Cytotoxic effects of topotecan and [^{131}I]MIBG *in vitro*

4.1 Introduction

The toxic effects of [^{131}I]MIBG are due to its potential to generate DNA damage by radioactive decay of ^{131}I. Combining [^{131}I]MIBG with an agent which enhances radiation-induced DNA breaks, will improve the effectiveness of [^{131}I]MIBG as a therapeutic agent for the treatment of neuroblastoma [71].

Many previous studies have reported synergistic cell killing *in vitro* by ionising radiation and Topo I inhibitors in non-human cell lines [136, 137] and in human cancer-derived cell lines [85, 137-141]. *In vivo* radiopotentiation by Topo I inhibitors has also been observed [140, 142, 143]. This effect is associated with the creation of double-strand breaks [136, 139, 151]. However, to date, no attempt has been made to investigate the potential of inhibitors of topoisomerase I to induce radiopotentiation *in vitro* and *in vivo* when combined with targeted radiotherapy.

In order to assess the toxic effects of combinations of [^{131}I]MIBG and TPT, it was first necessary to understand how each agent affects the clonogenic potential of treated cells. Therefore, initial experiments were carried out to characterise the toxic effects of [^{131}I]MIBG and TPT as single agents.

4.2 Materials & methods

4.2.1 Topoisomerase I relaxation assays

Topoisomerase I levels were determined using the Topoisomerase I Assay Kit (Topogen Inc, Columbus, Ohio, USA), which allows determination of Topo I activity through measurement of the amount of relaxation of a supercoiled DNA template.

Nuclear extracts were collected, using a protocol recommended by the manufacturers, from the neuroblastoma cell lines SK-N-BE(2c) and SHSY5Y [147], and the transfected glioblastoma line UVW/NAT [152].

Briefly, cells were centrifuged (800 x g for 5mins at 4°C) and the pellets washed once in TEMP buffer (10mM Tris-HCl, 1mM EDTA, 4mM $MgCl_2$, 0.5mM PMSF). Cells were then centrifuged (800 x g for 5mins at 4°C), resuspended in TEMP buffer and homogenised. Nuclei were pelleted (1,500 x g for 10mins at 4°C), washed in TEMP, recentrifuged (1,500 x g for 10mins at 4°C) and resuspended in 4 pellet volumes of TEP buffer (10mMTris-HCl, 1mM EDTA, 0.5mM PMSF). An equal volume of 1M Na Cl was added to the extracts, followed by centrifugation (15,000 x g for 1mins at 4°C). Topoisomerase I was contained in the resulting supernatant.

Topoisomerase I activity in each cell line was determined by serial two-fold dilutions of nuclear extracts. These solutions were incubated with 0.25μg of supercoiled pHOT-1 plasmid for 15mins at 37°C, in 1 x assay buffer (10mM Tris-HCl pH7.9, 1mM EDTA, 0.15M NaCl, 0.1% BSA, 0.1mM Spermidine and 5% Glycerol). The reaction was stopped using stop/loading dye (1% sarkosyl, 0.025% bromophenol blue, 5% glycerol) and loaded onto an agarose gel (2% agarose in 4 x TAE buffer: 0.16M Tris-Acetate, 0.004 M EDTA, pH 8.3), electrophoresed for 16 hours at 1.4 V/cm, then stained with ethidium bromide (0.5μg/ml) for one hour. Gels were visualised using the GeneGenius bioimaging

system, incorporating GeneSnap v6.03 software (SynGene Division, Synoptics Group, Cambridge UK). Band intensities were quantified densitometrically, using ImageJ v1.34i software (National Institutes of Health, USA).

Results were plotted as a percentage of a relaxed plasmid control and expressed in arbritary units (AU), where 1AU is described as the amount of topoisomerase I needed to unwind 0.25μg supercoiled (form 1) pHOT 1 plasmid in 15 mins at 37°C.

4.2.2 Clonogenic assay

The clonogenic assay [154] was used to assess the capacity of each cytotoxic agent to affect the ability of cultured cells to form viable colonies of daughter cells (Figure 4-1). This assay is based on the principal that, while clonogenic cells are capable of unlimited proliferation, viable, but damaged cells will only undergo a limited number of cell divisions and are incapable of forming colonies.

The neuroblastoma cell lines SK-N-BE(2c) and SHSY5Y [147], and the transfected glioblastoma line UVW/NAT were assessed for their ability to form colonies. While SK-N-BE(2c) and UVW/NAT cells readily formed clonogens, the results of initial experiments on SHSY5Y were disappointing Therefore, subsequent *in vitro* assessments of the toxic effects of TPT and [^{131}I]MIBG were conducted using SK-N-BE(2c) and UVW/NAT, but not SHSY5Y cells.

Monolayers of cells were cultured in 25cm^2 flasks (Nunclon Plastics, Denmark) at 2.5 x 10^5 cells per flask in RPMI 1640 medium containing 10% FCS. After two days, medium was removed and replaced with fresh medium containing the appropriate concentration of test drug. After experimental therapy, medium was removed, the cells were washed twice in phosphate buffered saline (PBS), and allowed to grow in fresh medium for a further 24 hours. The cells were detached by addition of 1 x trypsin (Invitrogen, Paisley, UK) counted and seeded, in triplicate, in 25cm^2 flasks at 1 x 10^3 cells per flask, for each test concentration. Flasks were incubated at 37°C in 5% CO_2 for 14 days. Colonies were fixed in 100% methanol, stained with Giemsa's stain solution (BDH Laboratory Supplies) and counted.

Results were expressed as a percentage of the initial concentration of cells plated, known as the plating efficiency. The cytotoxic potency of the drug was determined by

comparing the number of colonies formed by treated cells to the number of colonies formed by untreated controls (the surviving fraction, or SF).

TPT incubation time was 24h, which has previously been shown to result in maximal supra-additive cell killing in cells treated with TPT and external beam irradiation [139]. TPT concentrations ranged from 0ng/ml to 50ng/ml

The incubation time for [^{131}I]MIBG was 2h, after which uptake is maximal [154]. Concentrations of [^{131}I]MIBG ranged from 0MBq/ml to 10MBq/ml.

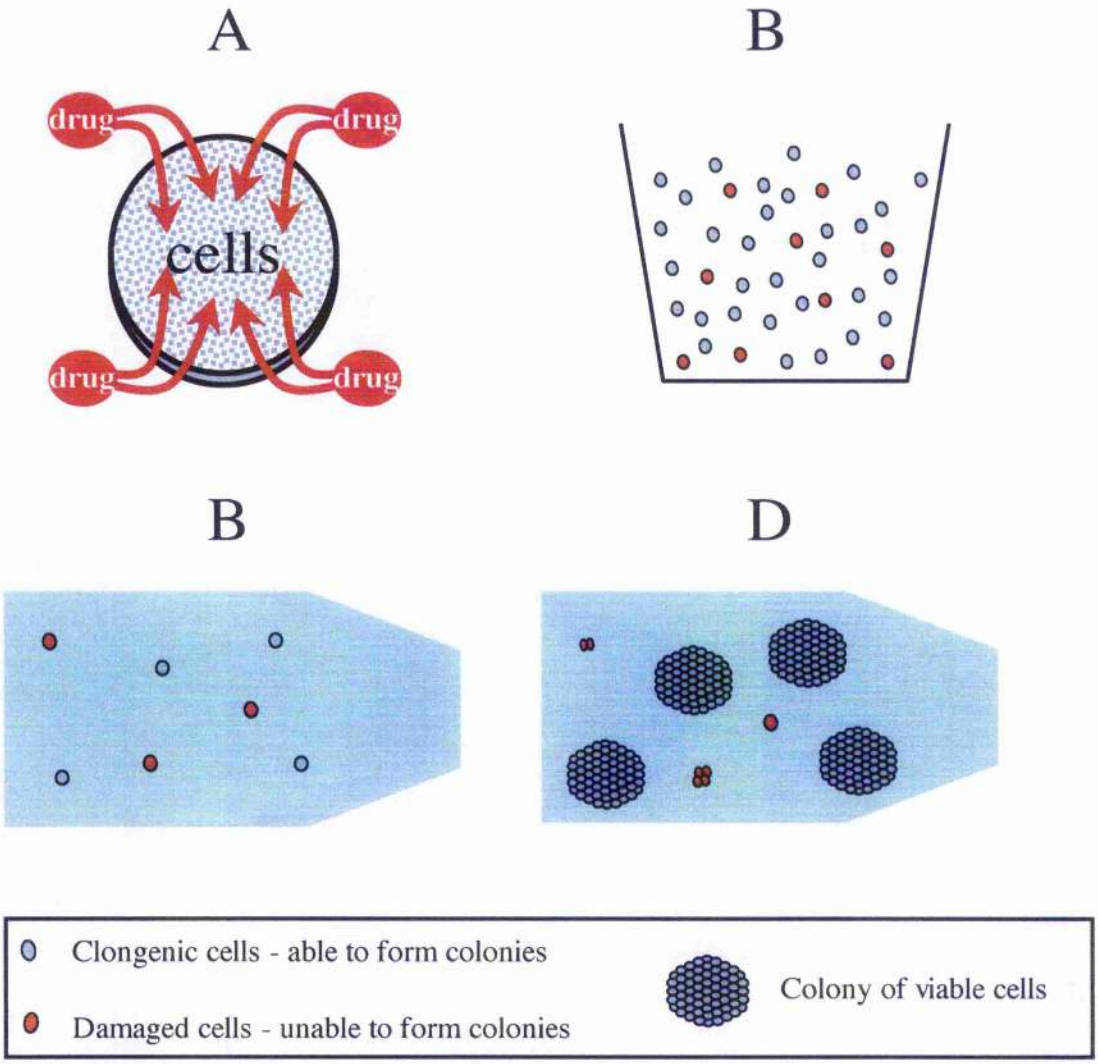

Figure 4-1: Clonogenic assay of cell viability

This test is used to assess the capacity of a cytotoxic agent to affect the ability of cultured cells to form viable colonies of daughter cells. The experimental procedure is as follows:

A) Plated cells are dosed with cytotoxic agent.
B) Cells are trypsinised, placed in single cell suspension, and counted.
C) Single cells are plated in flasks and grown at 37°C in 5% CO_2 for at least 6 doubling times, to allow colony formation. A colony contains ≥ 50 cells).
D) Clonogenic cells will grow into colonies. Damaged cells may still be viable for several cell divisions. However, they are unable to form colonies.

4.3 Results

4.3.1 Topoisomerase I assays

The results of Topo I unwinding assays are shown in Figure 4-2, and the resultant Topo I levels for SK-N-BE(2c), UVW/NAT and SHSY5Y cells are shown in Table 4-1.

UVW/NAT had the highest level of Topo I activity, with 100% unwinding in undiluted extract and 10% unwinding at 1:8 dilution. This gave a Topo I level of 1.99AU/μl. This was almost double the activity exhibited by SK-N-BE(2c) cells, which exhibited 100% unwinding in undiluted extract and 10% at approximately 1:3.5 dilution, corresponding to a Topo I level of 1.01AU/μl. SHSY5Y had the lowest levels of Topo I activity, with 100% unwinding in undiluted extract and 10% unwinding at 1:2, corresponding to a Topo I level of 0.34AU/μl.

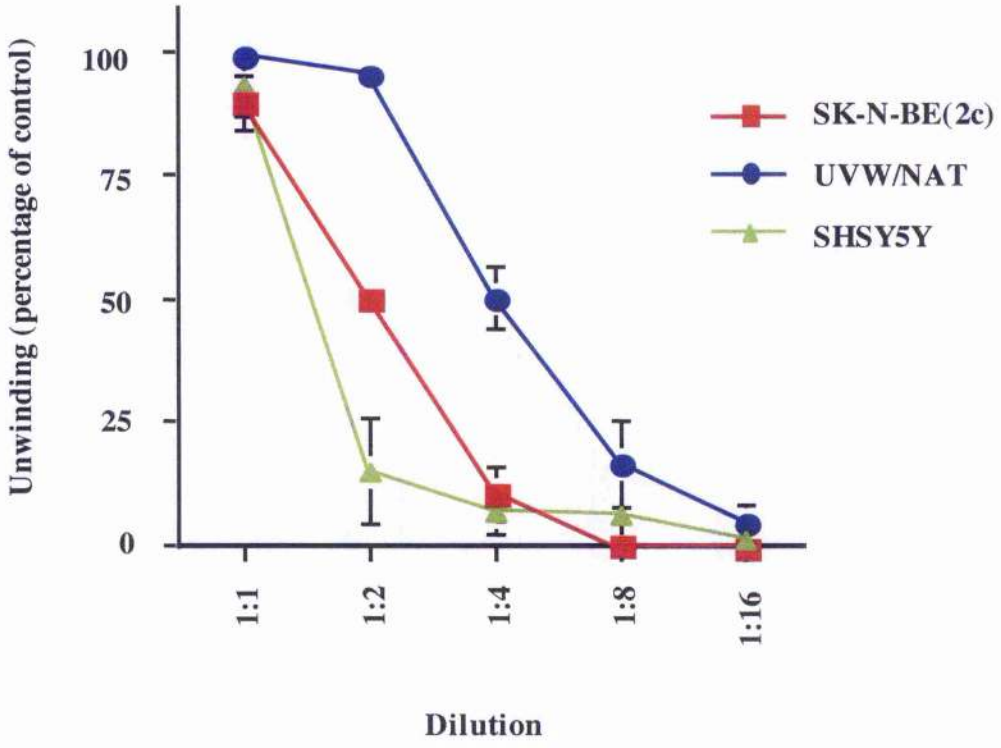

Figure 4-2: Topoisomerase I activity in NAT expressing cell lines

Endogenous topoisomerase I levels were elucidated by Topo I relaxation assay. Topo I was extracted from each cell line, and serial 2-fold dilutions were incubated with 0.25ug supercoiled (form 1) pHOT 1 plasmid for 15min at 37°C.

After electrophoresis, band intensities were quantified using densitometric analyses and plotted as a percentage of a relaxed plasmid control. Data values are means and standard deviations of two determinations. Each assay was carried out three times.

UVW/NAT: Highest level of Topo I - 100% unwinding in undiluted extract, falling to 10% unwinding at 1:8 dilution.
SK-N-BE(2c): Intermediate level of Topo I - 100% unwinding in undiluted extract falling to 10% at approx.1:3.5 dilution.
SHSY5Y: Lowest level of Topo I - 100% unwinding in undiluted extract falling to 10% unwinding at 1:2.

Topo I levels were expressed in arbitrary units (U), where 1U is described as the amount of topoisomerase I needed to unwind 0.25ug supercoiled pHOT 1 plasmid in 15 mins at 37°C. These values are shown in Table 4-1.

Cell Line	Topoisomerase I level (Units/ul)
SK-N-BE(2c)	1.01
UVW/NAT	1.99
SHSY5Y	0.34

Table 4-1: Topoisomerase I levels in NAT expressing cell lines

This table shows the endogenous Topo I levels in each cell line, found by Topo I relaxation assay (Figure 4-2).
UVW/NAT had the highest level of Topo I activity, almost double the activity exhibited by SK-N-BE(2c). SHSY5Y had the lowest levels of Topo I activity.
1 Unit = the amount of topoisomerase I needed to unwind 0.25ug supercoiled (form 1) plasmid in 15 mins at 37°C

4.3.2 Clonogenic assays: The toxic effects of topotecan

The toxic effects of TPT as a single agent were determined for each cell line:

4.3.2-1 SK-N-BE(2c)

Cell survival fell sharply in the 1-5ng/ml TPT dose range, from 90% survival (IC_{10}) at a concentration of 1ng/ml, to 10% survival (IC_{90}) at 5ng/ml. Thereafter a plateau, with respect to clonogenic survival, was observed. That is, concentrations of TPT greater than 5ng/ml did not result in greater toxicity than that achieved by 5ng/ml. This observation is in agreement, with previously reported effects of TPT [139] and of other Topo I inhibitors [137, 162]. The concentration of topotecan which caused 50% reduction in colony number (IC_{50}) in SK-N-BE(2c) cells was 2ng/ml (Figure 4-3A).

4.3.2-2 UVW/NAT

Cell survival fell sharply, in the 1-8ng/ml TPT dose range. 90% survival (IC_{10}) was observed at a concentration of 1ng/ml, falling to 5% survival (IC_{95}) at 8ng/ml. Again, a plateau effect was observed. The concentration of topotecan which caused 50% reduction in colony number (IC_{50}) in UVW/NAT cells was 4.2ng/ml (Figure 4-4A).

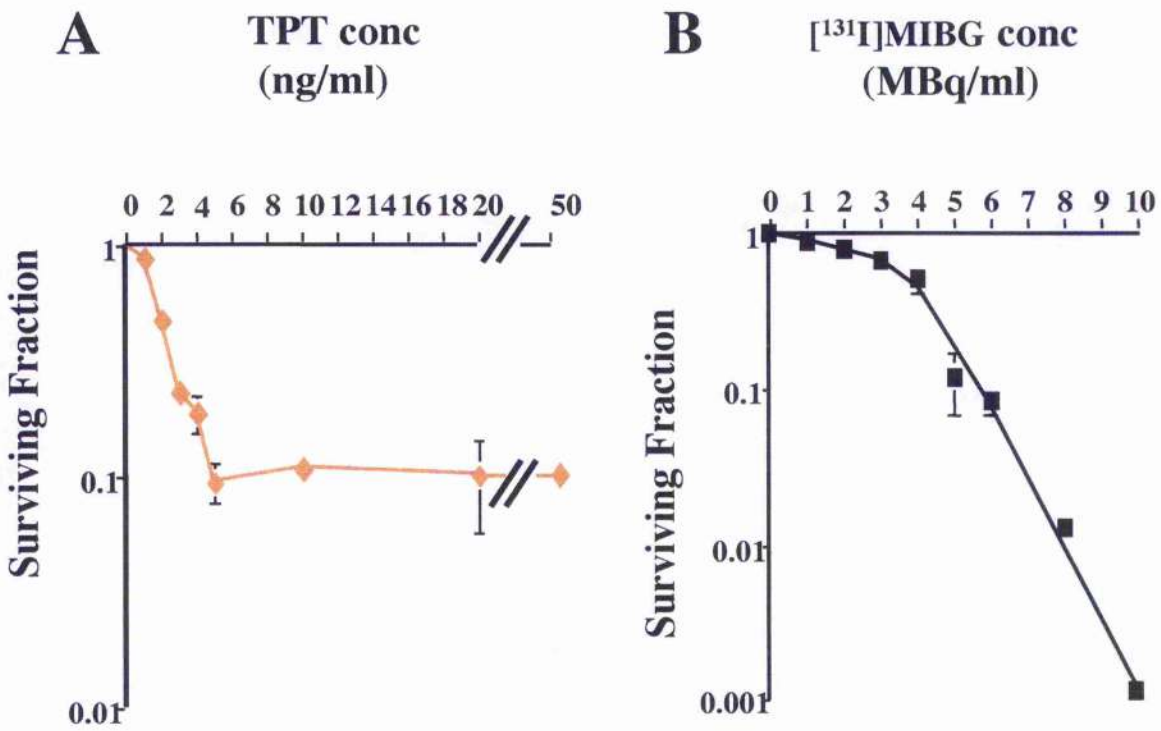

Figure 4-3: The toxic effects of [^{131}I]MIBG and TPT on SK-N-BE(2c) cells

The toxicity of (A) TPT and (B) [^{131}I]MIBG as single agents to SK-N-BE(2c) cells was studied by clonogenic assay. The effects of each agent were determined by comparing the ability of treated cells to form colonies compared to untreated controls.

A) TPT:
Cell survival fell sharply in the 1-5ng/ml TPT dose range, from 90% survival (IC_{10}) at a concentration of 1ng/ml, to 5% survival (IC_{90}) at 5ng/ml. Thereafter a plateau effect was observed, with no added toxicity seen. This effect tallies with previously reported effects of TPT and of other Topo I inhibitors. The concentration of topotecan which caused 50% reduction in colony number (IC_{50}) was 2ng/ml.

B) [^{131}I]MIBG :
Cell survival fell from 70% survival (IC_{30}) at 1MBq, to 10% survival (IC_{90}) at 8MBq. The concentration of [^{131}I]MIBG which caused 50% reduction in colony number (IC_{50}) was 4MBq/ml.

4.3.3 Clonogenic assays: The toxic effects of [^{131}I]MIBG

The toxic effects of [^{131}I]MIBG as a single agent were determined for each cell line.

4.3.3-1 SK-N-BE(2c):

Cell survival fell from 70% survival (IC_{30}) at 1MBq, to 10% survival (IC_{90}) at 8MBq. The concentration of [^{131}I]MIBG which caused 50% reduction in colony number (IC_{50}) was 4MBq/ml (Figure 4-3B).

4.3.3-2 UVW/NAT:

In the case of UVW/NAT, survival fell from 70% survival (IC_{30}) at 1MBq, to 10% survival (IC_{90}) at 10MBq. The concentration of [^{131}I]MIBG which caused 50% reduction in colony number (IC_{50}) was 4.1MBq/ml (Figure 4-4B).

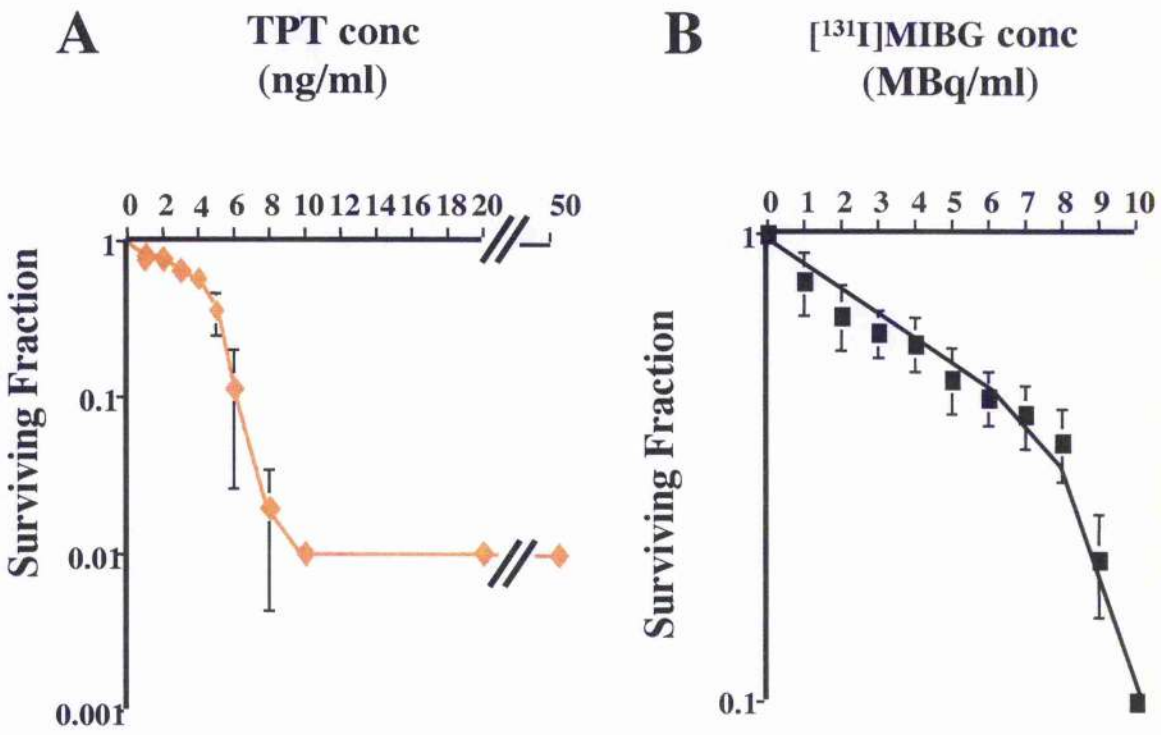

Figure 4-4: The toxic effects of [^{131}I]MIBG and TPT on UVW/NAT cells

The toxicity of (A) TPT and (B) [^{131}I]MIBG as single agents to UVW/NAT cells was studied by clonogenic assay. The effects of each agent were determined by comparing the ability of treated cells to form colonies compared to untreated controls.

A) TPT:
As with SK-N-BE(2c), cell survival fell sharply, this time in the 1-8ng/ml TPT dose range. 90% survival (IC_{10}) was seen at a concentration of 1ng/ml, falling to 5% survival (IC_{95}) at 8ng/ml. Again, a plateau effect was observed, with no added toxicity seen. The concentration of topotecan which caused 50% reduction in colony number (IC_{50}) in UVW/NAT cells was 4.2ng/ml.

B) [^{131}I]MIBG :
In the case of UVW/NAT, survival fell from 70% survival (IC_{30}) at 1MBq, to 10% survival (IC_{90}) at 10MBq. The concentration of [^{131}I]MIBG which caused 50% reduction in colony number (IC_{50}) was 4.1MBq/ml.

4.4 Summary of results

Both SK-N-BE(2c) and UVW/NAT cells were sensitive to [^{131}I]MIBG, and similar doses of the radiopharmaceutical produced 50% reduction in clonogenic survival (4MBq/ml for SK-N-BE(2c), 4.1MBq/ml for UVW/NAT).

SK-N-BE(2c) cells were highly sensitive to low doses of TPT (90% survival at 1ng/ml; 10% survival at 5ng/ml (Figure 4-3)). Thereafter a plateau, with respect to clonogenic survival, was observed (ie. concentrations of TPT greater than 5ng/ml did not result in greater levels of toxicity). UVW/NAT were not as sensitive to low doses of the drug (90% survival at 1ng/ml; 45% survival at 5ng/ml (Figure 4-4)), however a greater proportion of UVW/NAT were susceptible to treatment (ie. the plateau observed in UVW/NAT cells corresponded to approximately 2% clonogenic survival, compared to ≈10% in SK-N-BE(2c) cells).

This plateau is in agreement, with previously reported effects of TPT [139] and of other Topo I inhibitors [137, 162], and is attributed to the S-phase specificity of topotecan-induced toxicity. In any population of cells, different sub-populations will be at different stages of the cell cycle. Cells in G_1 during treatment will be unaffected by topotecan exposure. The results of this study suggest that a higher proportion of SK-N-BE(2c) cells were in G_1, and were resistant to TPT, while a lower percentage of UVW/NAT cells were in G_1, and consequently a higher subpopulation was affected by topotecan treatment. The cell cycle distribution of SK-N-BE(2c) and UVW/NAT cells will be assessed in Chapter 8, and the results of this chapter will be further discussed in Chapter 10.

Characterisation of the toxic effects of [^{131}I]MIBG and TPT as single agents as described in this chapter was necessary to allow subsequent assessment of the toxic effects of combinations of these two agents. Two different methods were used to assess the

interactions between TPT and [^{131}I]MIBG. Chapter 5 describes the results of isobologram analyses of TPT / [^{131}I]MIBG combinations. In this method, variable doses of each agent are administered, and the resultant level of toxicity is compared to a hypothetical combination which should theoretically produce an purely additive level of clonogenic cell kill.

Chapter 6 describes how the relative toxicities of TPT and [^{131}I]MIBG used as single agents to each cell line described in this chapter, were used to determine the concentrations of these drugs which were administered to SK-N-BE(2c) and UVW/NAT cells, to investigate the interactions between TPT and [^{131}I]MIBG by median-effect analysis. In this method, a range of concentrations of each drug in a fixed ratio is assessed, so that the proportional contribution of each drug is similar at all treatment intensities for each cell line.

Chapter 5

Analysis of the cytotoxic interaction between topotecan and [^{131}I]MIBG *in vitro*

I: The isobologram method

5.1 Introduction

5.1.1 Analysing the interaction between topotecan and [^{131}I]MIBG

Whenever the efficacy of combining different cytotoxic agents is investigated, the most important question which must be answered is whether the combination of the agents results in cell kill which is greater or less than would be expected by the action of each treatment modality individually. If the combination has an effect that is greater than the individual treatments, then this combination can be said to be "supra-additive", or more effective than each agent alone. Conversely, combinations that are less effective than each agent alone can be said to be "infra-additive", and convey no therapeutic benefit [163].

However, the choice of methodology used to assess the nature and intensity of agent interaction has historically proven to be controversial, and many competing models have been reported [156]. Examination of scientific literature suggests that the two most commonly reported models of drug interacton analysis are the isobologram method of Steel and Peckham [163-165], and the median-effect / combination-index method of Chou and Talalay [163, 166-167].

Therefore, in analysing the *in vitro* interaction between topotecan and [^{131}I]MIBG, both of these methodologies were utilised. This chapter describes the results of isobologram analyses of TPT / [^{131}I]MIBG combinations, while Chapter 6 describes the results of median-effect / combination-index analyses of TPT / [^{131}I]MIBG interactions.

5.1.2 Isobologram analysis of the interaction between two toxic agents

The isobologram method [164, 165] is used to examine the interaction between two drugs, regardless of the mechanism of action of the individual agents. Cells are treated with combinations of the two drugs in various concentrations, and two dose-response curves are generated from the results. An example of this, using hypothetical data, is shown in Figure 5-1. The first plot (Figure 5-1A) shows the effect of increasing the concentration of Drug A on cells treated with a specific dose of Drug B; the second plot (Figure 5-1B) shows the effect of increasing Drug B concentration on cells treated with a specific dose of Drug A. From these curves, the doses of Drug A and Drug B which, as single agents, cause a certain level of toxicity are determined (eg. the IC_{50} dose: the dose which inhibits 50% colony formation). Likewise, the combinations of Drug A and Drug B which cause 50% effect are determined. These are known as the isoeffect points.

A graph is drawn, with the IC_{50} value for Drug A alone plotted on the horizontal axis, and the IC_{50} result for Drug B alone plotted on the vertical axis. A line is drawn connecting these two points. This line denotes the alignment of values of each agent, which would, in theory, give rise to an additive effect. The isoeffect points for combinations of Drug A and Drug B are then plotted on this graph (Figure 5-1C).

The different possible outcomes of isobologram analyses are shown in Figure 5-2. When the experimental isoeffect points lie directly on the line, the two agents are interacting in a purely additive way. For example, in Figure 5-1, IC_{50} dose for Drug A is 4mg/ml, and for Drug B the IC_{50} dose is 4mg/ml. An isoeffect point is generated by a combination of 2mg/ml Drug A + 2mg/ml Drug B. This plots directly onto the hypothetical line of additivity, suggesting that in this hypothetical example, the drugs are combining in a purely additive way (Figure 5-1C; Figure 5-2A).

However, if the isoeffect points plot below the hypothetical line of additivity, a supra-additive, or synergistic effect is indicated. For example, in the hypothetical example the IC_{50} doses are 4mg/ml for Drug A alone, and 4mg/ml for Drug B alone. If these agents had combined in a supra-additive fashion, then the combination required to produce 50% cell kill would have been < 2mg/ml of Drug A + < 2mg/ml of Drug B (Figure 5-2B).

If the isoeffect points plot above the hypothetical line of additivity, an infra-additive, or antagonistic effect is indicated. In the hypothetical example, the IC_{50} doses are 4mg/ml for Drug A alone, and 4mg/ml for Drug B alone. If these agents had combined in an infra-additive fashion, then the combination required to produce 50% cell kill would have been > 2mg/ml of Drug A + > 2mg/ml of Drug B (Figure 5-2C).

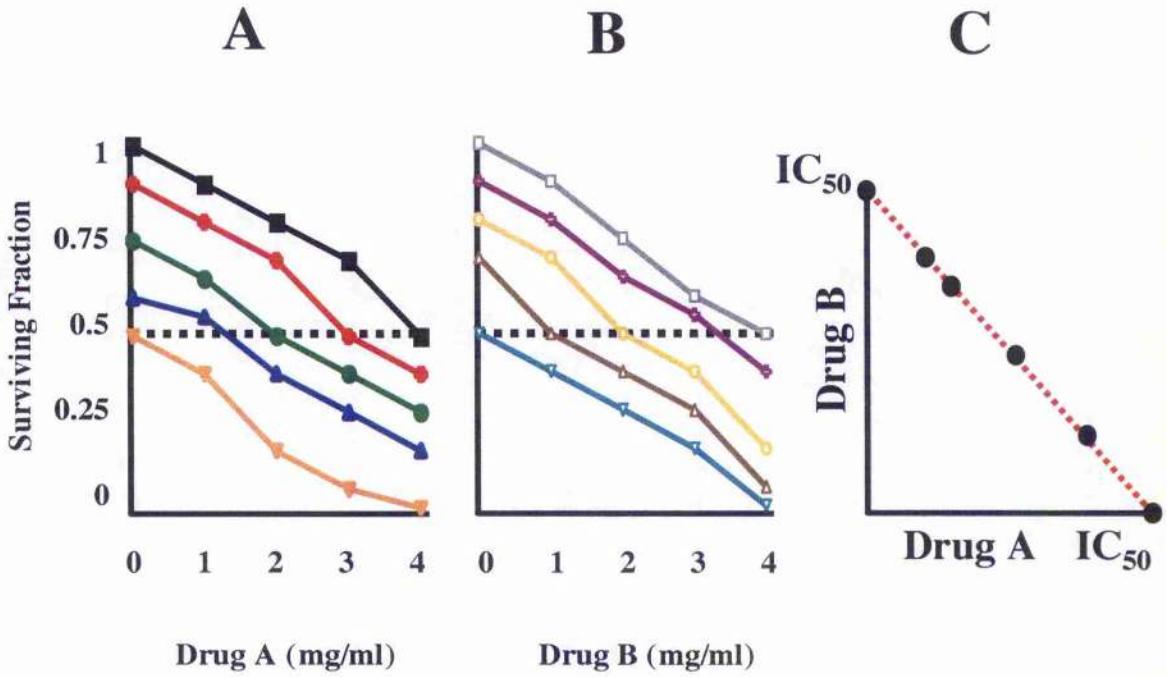

Figure 5-1: Toxic effects of two hypothetical drugs alone and in combination

Drug B (mg/ml)	Drug A (mg/ml)
-0-	□
-1-	✣
-2-	○
-3-	△
-4-	▽

Both of the survival curves represent the same data plotted in two ways:

(**A**) The effect of increasing the concentration of Drug A on cells treated with a specific dose of Drug B.

(**B**) The effect of increasing the concentration of Drug B on cells treated with a specific dose of Drug A.

(**C**) IC_{50} isobologram constructed from the isoeffect points generated from (A) & (B) above (ie. the combinations of Drug A and Drug B which cause 50% effect when combined). These are found where each survival curve crosses the dotted line.

All of these isoeffect points plot directly onto the line of additivity. This suggests that in this example, the hypothetical drugs are combining in a purely additive way. See Figure 5-2.

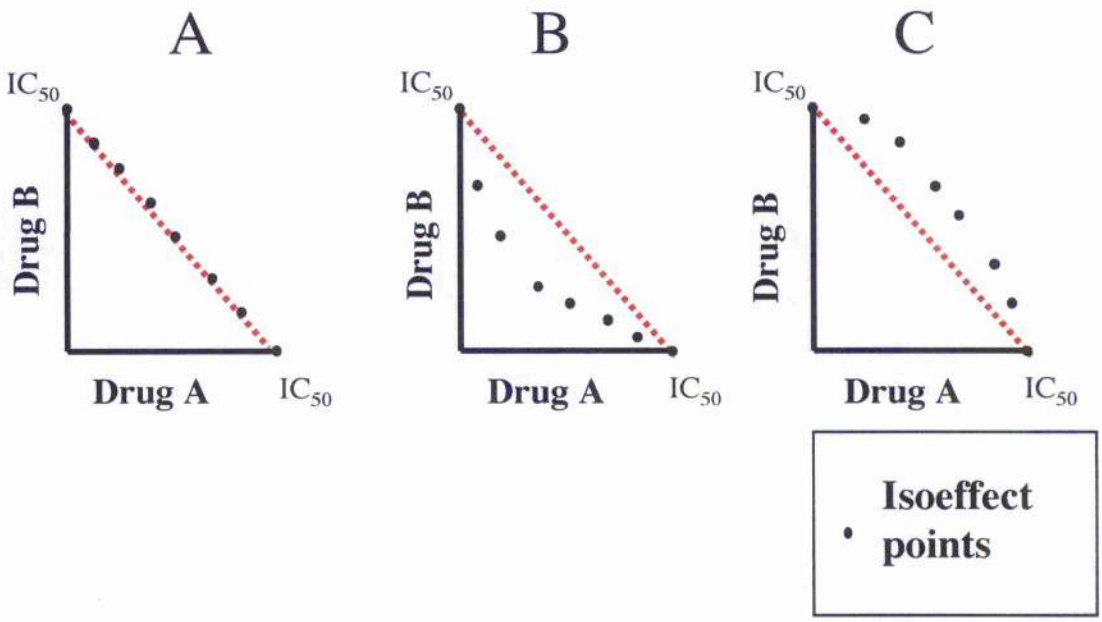

Figure 5-2: Isobologram analyses of the hypothetical relationship between two agents

The above figures provide examples of the different outcomes of isobologram analyses. The IC_{50} value for Drug A is plotted on the horizontal axis, and the IC_{50} result for Drug B is plotted on the vertical axis. A line is drawn connecting these two points, denoting the alignment of values of each agent, which, in theory, give rise to an additive effect. For combinations of Drug A and Drug B, the isoeffect points (being the concentrations, which cause 50% reduction in colony number when combined), are then plotted on this graph.

(**A**) The results obtained when Drug A and Drug B combine in a purely additive way. In this case, the isoeffect points all lie on the line.

(**B**) The results obtained when Drug A and Drug B combine in a synergistic way. In this case, the isoeffect points all lie below the line.

(**C**) The results obtained when Drug A and Drug B combine in an antagonistic way. In this case, the isoeffect points all lie above the line.

5.1.3 Scheduling of topotecan and [^{131}I]MIBG in combination treatment

Synergistic cell killing *in vitro* and *in vivo* by ionising radiation and Topo I inhibitors have been widely reported. However, there is no consensus with respect to the optimum order of delivery of these therapeutic agents. While some studies state that radiosensitisation is observed when Topo I inhibitors are administered prior to irradiation [85, 140], others claim that radiopotentiation is only achieved when exposure to ionising radiation precedes, or is concurrent with administration of Topo I inhibitors [136, 141] (Table 5-1).

To date, no attempt has been made to investigate combinations of topotecan and [^{131}I]MIBG. Therefore, it was not known if a synergistic interaction would occur. Likewise, it was unclear whether possible synergistic effects resulting from a combination of these drugs would be affected by the order of delivery, and possibly the greatest cytotoxicity would occur only when one agent was administered prior to exposure to the second.

Three treatment modalities were investigated. In schedule [i] topotecan was administered 24 hours before [^{131}I]MIBG treatment. In schedule [ii] topotecan was administered 24 hours after [^{131}I]MIBG treatment. In schedule [iii] topotecan and [^{131}I]MIBG were administered simultaneously. See Figure 5-3.

In vitro: Non-human cell lines	Treatment schedule examined	[Ref]
Murine leukemia (P388)	*(iii), (iv), (v)*	**[136]**
Chinese hamster ovary (CHO)	*(iii), (iv), (v)*	**[136]**
Chinese hamster fibroblast (V79)	*(iii)*	**[137]**
***In vitro:* Human cancer cell lines**		
Breast cancer (MCF7)	*(i), (iii), (v)*	**[85]**
Cervical cancer (HeLa)	*(iii)*	**[137]**
Small-cell lung cancer (SBC3-CDDP)	*(ii), (iii)*	**[138]**
Glioblastoma (GBM)	*(ii), (iii), (iv)*	**[139]**
Squamous carcinoma of the head and neck (SCC-25)	*(i)*	**[140]**
Melanoma (U1-Mel)	*(ii), (iii), (iv)*	**[141]**
***In vivo* models**		
Murine fibrosarcoma	*(i), (iii)*	**[140]**
Murine mammary carcinoma	*(i), (iii)*	**[142]**
Human rhabdomyosarcoma	*(ii), (iii)*	**[143]**

Table 5-1: Scheduled combinations of ionising radiation and Topo I inhibitors reported to cause synergistic cell killing

Synergistic cell killing by ionising radiation and Topo I inhibitors have been widely reported, as shown above. However, there is no consensus on the order of delivery:

(i) Synergy observed when Topo I inhibitors were administered prior to irradiation;
(ii) Synergy observed when Topo I inhibitors were administered following irradiation;
(iii) Synergy observed when Topo I inhibitors and radiation were administered concurrently;
(iv) Administration of Topo I inhibitors prior to irradiation did not induce synergy;
(v) Administration of Topo I inhibitors following irradiation did not induce synergy.

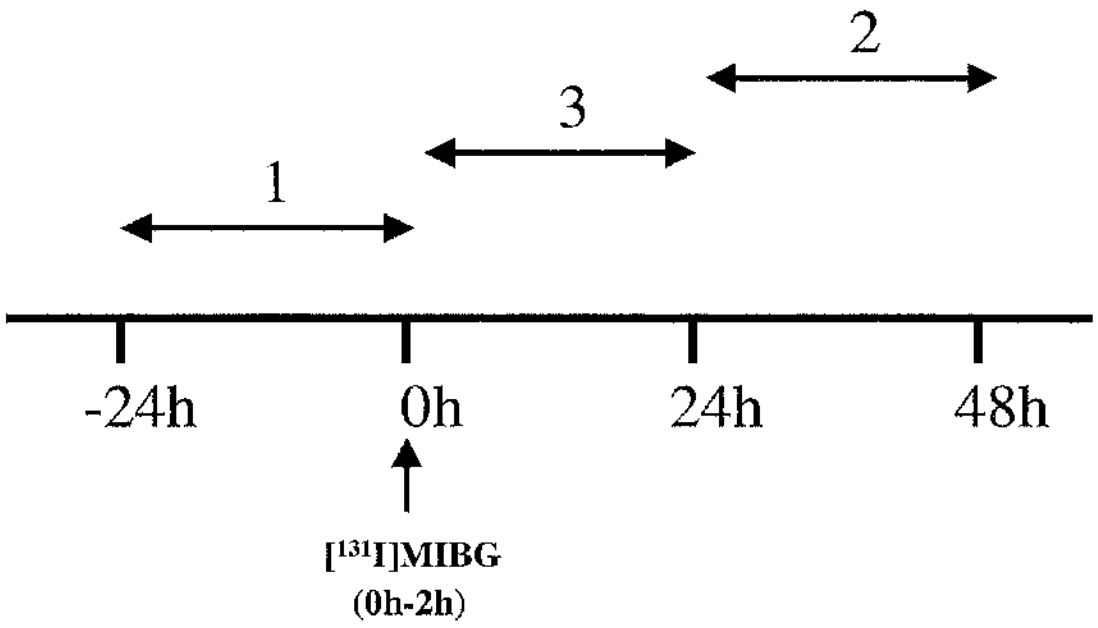

Figure 5-3: Scheduling of TPT and [^{131}I]MIBG combinations

Three different scheduled combinations of topotecan and [^{131}I]MIBG were tested :

Schedule [i]: Topotecan administered 24 hours before [^{131}I]MIBG treatment

Schedule [ii]: Topotecan administered 24 hours after [^{131}I]MIBG treatment

Schedule [iii]: Topotecan and [^{131}I]MIBG administered simultaneously

5.2 Materials & methods

5.2.1 Clonogenic assays

Monolayers of SK-N-BE(2c) and UVW/NAT of cells were cultured in 25cm^2 flasks (Nunclon Plastics, Denmark), at 2.5 x 10^5 cells per flask. After two days, medium was removed and replaced with fresh medium containing a dose of TPT and/or [^{131}I]MIBG. Following treatments, the cytotoxic effects of each combination schedule were assessed by clonogenic assay, as previously described in Chapter 4. For each schedule, every treatment group was assessed three times, in triplicate.

5.2.2 Concentrations of TPT and [^{131}I]MIBG

For SK-N-BE(2c) cells, TPT concentration ranged from 0-2ng/ml, and [^{131}I]MIBG concentration ranged from 0-4MBq/ml. For UVW/NAT cells, TPT concentration ranged from 0-5ng/ml, and [^{131}I]MIBG concentration ranged from 0-5MBq/ml.

These concentrations were based on the relative effectiveness of each agent to each cell line, as described in Chapter 4. Again, the incubation time for [^{131}I]MIBG was 2h, and incubation time for TPT was 24h.

5.3 Results

5.3.1 Isobologram analysis of the interaction between [^{131}I]MIBG and topotecan

The results of clonogenic assays of toxicity to combined treatments were plotted as dose-response curves. These results were presented in two ways for each data set. In the first, data was plotted as the effect of increasing TPT concentration on colony formation in cells treated with [^{131}I]MIBG (SK-N-BE(2c): Figure 5-4; UVW/NAT: Figure 5-9). In the second, the data was plotted as the effect of increasing [^{131}I]MIBG concentration on TPT treated cells (SK-N-BE(2c): Figure 5-5; UVW/NAT: Figure 5-10).

From these dose-response curves, IC_{30}, IC_{50} and IC_{70} isoeffect points were generated. These were TPT/MIBG combinations which produced a certain level of colony inhibition (ie. 30%, 50% and 70% of the maximum effect). From these data, the interaction between TPT and [^{131}I]MIBG was evaluated at each toxicity level using the isobologram method.

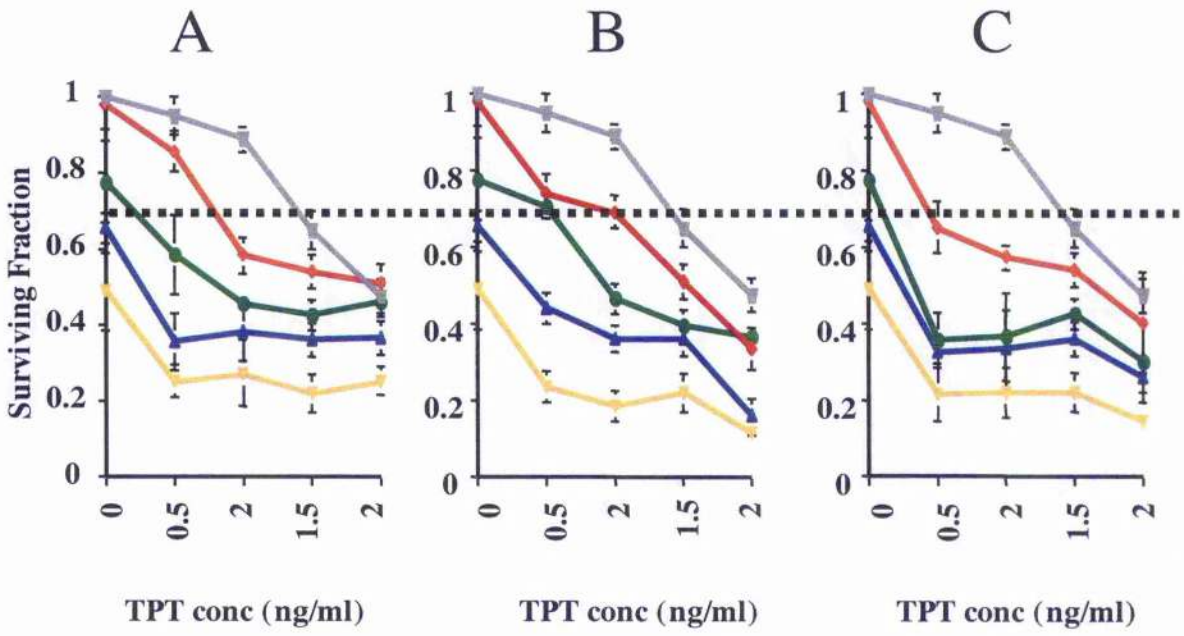

Figure 5-4: The effect of increasing TPT concentration on [^{131}I]MIBG treated SK-N-BE(2c) cells

In this figure, survival data are plotted against TPT concentration for a range of doses of [^{131}I]MIBG. Figure 5-5 shows the same data, plotted as the effect of increasing [^{131}I]MIBG concentration on TPT treated cells.

The concentration of TPT which gives an IC_{30} (ie. the dose which causes 30% effect) when combined with each concentration of [^{131}I]MIBG occurs at the point where the appropriate MIBG line crosses the dotted line. These isoeffect points were used along with the isoeffect points from Figure 5-5 to generate the isobolograms shown in Figure 5-6. Isoeffect points were derived in a similar fashion for the IC_{50} and the IC_{70} doses. These were used to generate the isobologram analyses in Figures 5-7 and 5-8 respectively.

Survival curves A, B and C were generated by the administration of combination schedules [i], [ii] and [iii] respectively.

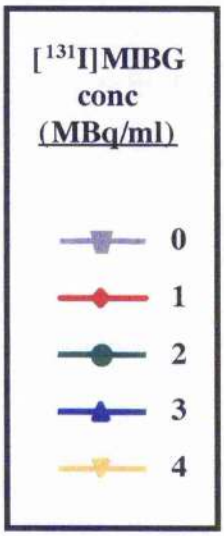

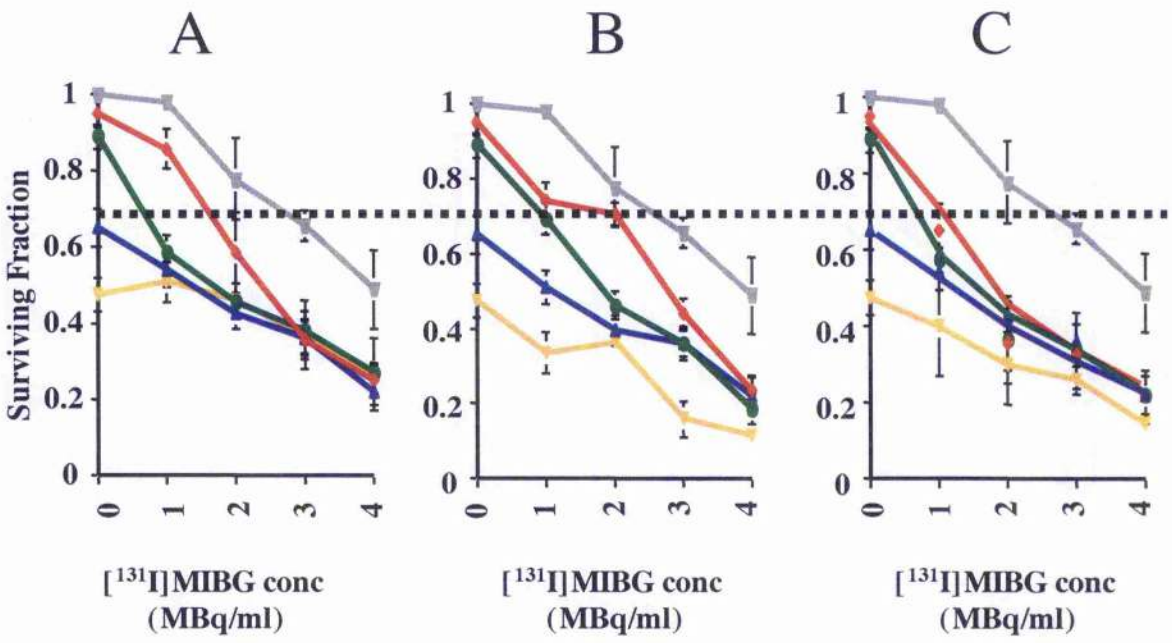

Figure 5-5: The effect of increasing [^{131}I]MIBG concentration on TPT treated SK-N-BE(2c) cells

In this figure, survival data are plotted against [^{131}I]MIBG concentration for a range of doses of topotecan. Figure 5-4 shows the same data, plotted as the effect of increasing TPT concentration on [^{131}I]MIBG treated cells.

As with Figure 5-4, the concentration of [^{131}I]MIBG which gives an IC_{30} (ie. the dose which causes 30% effect) when combined with each concentration of TPT occurs at the point where the appropriate TPT line crosses the dotted line. These isoeffect points were used along with the isoeffect points from Figure 5-4 to generate the isobologram analyses in Figure 5-6. Isoeffect points were derived in a similar fashion for the IC_{50} and the IC_{70} doses. These were used to generate the isobologram analyses in Figures 5-7 and 5-8 respectively.

Again, survival curves A, B and C were generated by the administration of combination schedules [i], [ii] and [iii] respectively.

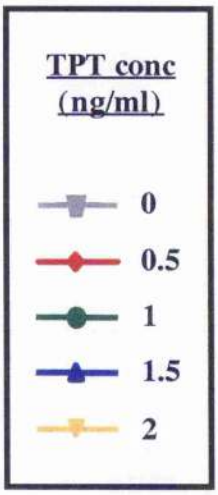

5.3.2 SK-N-BE(2c)

Isoeffect points generated at the IC_{30} and the IC_{50} by all three combination schedules examined plotted below the hypothetical line of additivity (Figures 5-6 & 5-7). This suggested that all of the scheduled combinations of TPT and [^{131}I]MIBG produced supra-additive effects at these levels of toxicity. However, at the IC_{50}, cells treated by combination schedules [i] and [iii] displayed some isoeffect points which plotted above the hypothetical line of additivity. These were generated by combinations of a relatively low dose of [^{131}I]MIBG and a relatively high dose of TPT, suggesting that combinations involving relatively high dose of [^{131}I]MIBG and a relatively low dose of TPT may be more effective.

At the IC_{70} (Figure 5-8), the majority of isoeffect points generated by administration of TPT and [^{131}I]MIBG plotted above the hypothetical line of additivity. This was observed in cells treated with all three scheduled combinations. This suggests that combinations of TPT and [^{131}I]MIBG were not as effective at this level of toxicity, although as with the results obtained by isobologram analyses at the IC_{50}, combinations involving relatively high doses of [^{131}I]MIBG and relatively low doses of TPT appeared to be more effective.

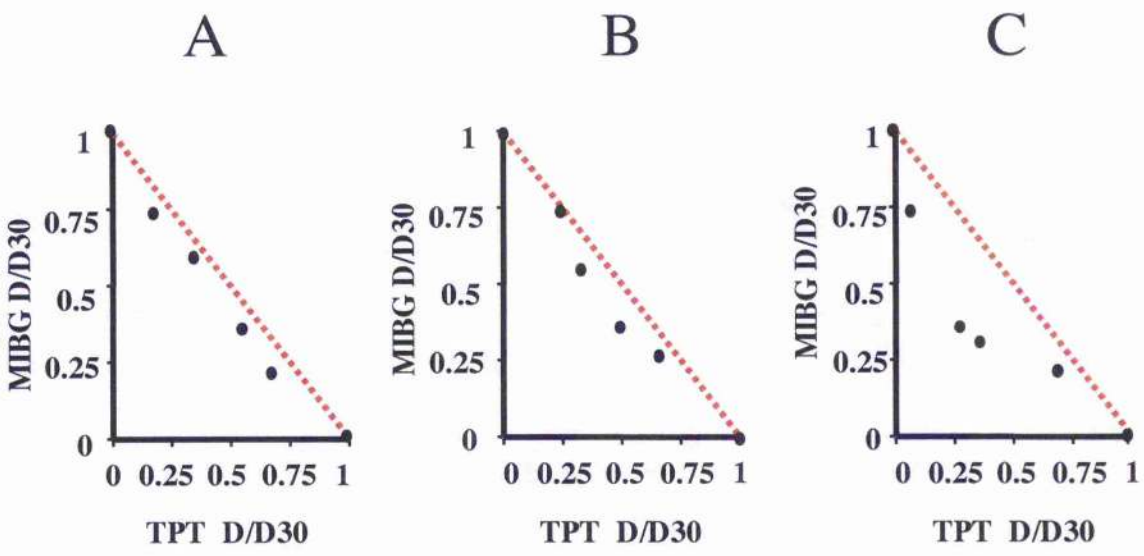

Figure 5-6: IC_{30} Isobologram analyses of SK-N-BE(2c) cells treated with different [^{131}I]MIBG and topotecan schedules

The interaction between TPT and [^{131}I]MIBG was analysed at the IC_{30} toxicity level by isobologram analysis. These diagrams were generated using the isoeffect points generated by Figures 5-4 and 5-5. The doses of each agent (D) are expressed as a fraction of the IC_{30} dose (D30).

Isobolograms A, B and C show the effect of administration of combination schedules [i], [ii] and [iii] respectively.

This data suggested that administration of TPT and[^{131}I]MIBG, in any scheduled combination, produced a supra-additive effect in SK-N-BE(2c) cells.

.

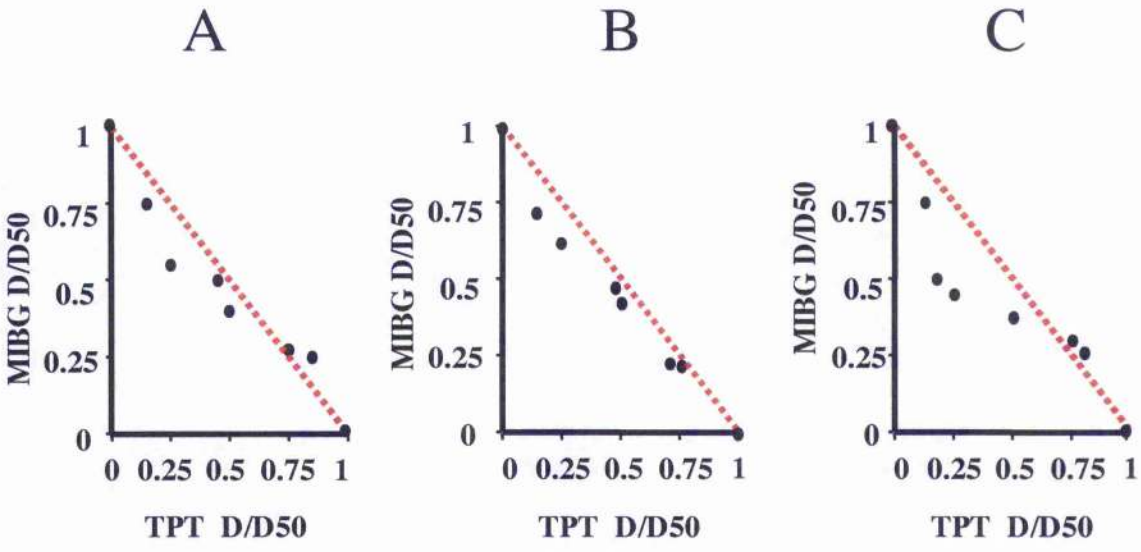

Figure 5-7: IC_{50} Isobologram analyses of SK-N-BE(2c) cells treated with different [^{131}I]MIBG and topotecan schedules

The interaction between TPT and [^{131}I]MIBG was also analysed at the IC_{50} toxicity level by isobologram analysis. These diagrams were generated using the isoeffect points generated by Figures 5-4 and 5-5. The doses of each agent (D) are expressed as a fraction of the IC_{50} dose (D50).

Again, isobolograms A, B and C show the effect of administration of combination schedules [i], [ii] and [iii] respectively.

This data suggested that administering TPT and[^{131}I]MIBG, in any scheduled combination, produced a supra-additive effect in SK-N-BE(2c) cells, although combinations involving a relatively low dose of [^{131}I]MIBG and a relatively high dose of TPT were less effective.

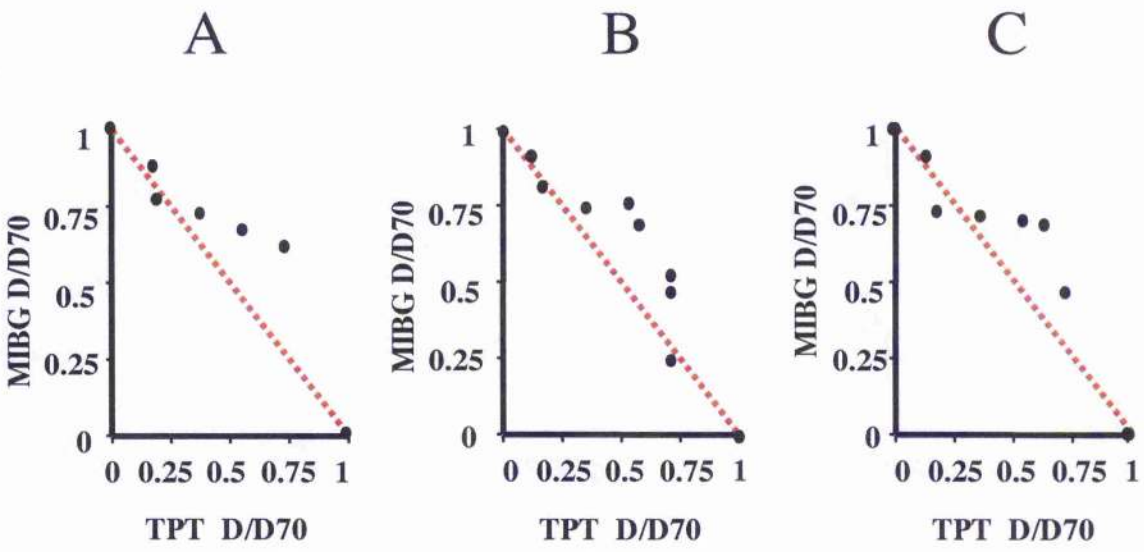

Figure 5-8: IC_{70} Isobologram analyses of SK-N-BE(2c) cells treated with different [^{131}I]MIBG and topotecan schedules

The interaction between TPT and [^{131}I]MIBG was also analysed at the IC_{70} toxicity level by isobologram analysis. These diagrams were generated using the isoeffect points generated by Figures 5-4 and 5-5. The doses of each agent (D) are expressed as a fraction of the IC_{70} dose (D70).

Again, isobolograms A, B and C show the effect of administration of combination schedules [i], [ii] and [iii] respectively.

This data suggested that, at this toxicity level, administration of TPT and[^{131}I]MIBG, in any scheduled combination, produced a predominantly infra-additive effect in SK-N-BE(2c) cells. As with the results obtained by isobologram analyses at the IC_{50}, combinations involving relatively high doses of [^{131}I]MIBG and relatively low doses of TPT appeared to be more effective.

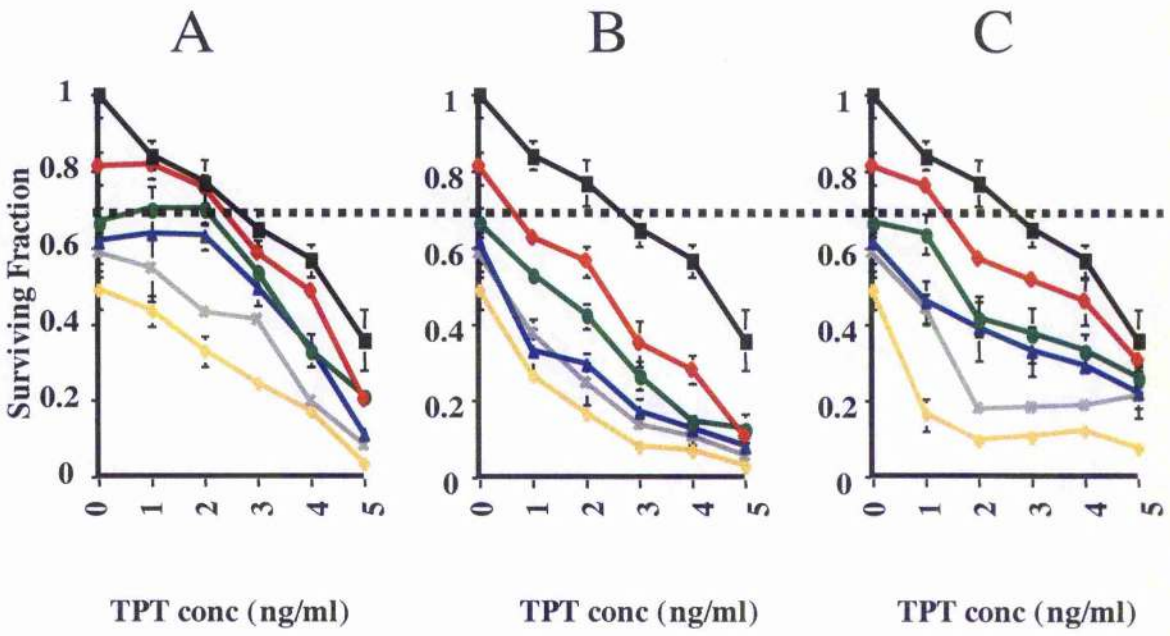

Figure 5-9: The effect of increasing TPT concentration on [^{131}I]MIBG treated UVW/NAT cells

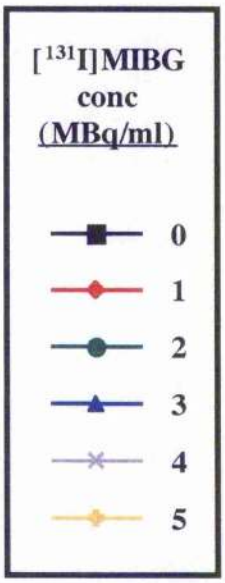

These survival curves show the combined effects of TPT and [^{131}I]MIBG on UVW/NAT cells. In this figure, survival data are plotted against topotecan concentration for a range of doses of [^{131}I]MIBG. Figure 5-10 shows the same data, plotted as the effect of increasing [^{131}I]MIBG concentration on TPT treated cells.

Again, the concentration of TPT which gives an IC_{30} (ie. the dose which causes 30% effect) when combined with each concentration of [^{131}I]MIBG occurs at the point where the appropriate MIBG line crosses the dotted line. These are the isoeffect points used along with the isoeffect points from Figure 5-10 to generate the isobolograms shown in Figure 5-11. Isoeffect points were derived in a similar fashion for the IC_{50} and the IC_{70} doses. These were used to generate the isobologram analyses in Figures 5-12 and 5-13 respectively.

Again, survival curves A, B and C were generated by the administration of combination schedules [i], [ii] and [iii] respectively.

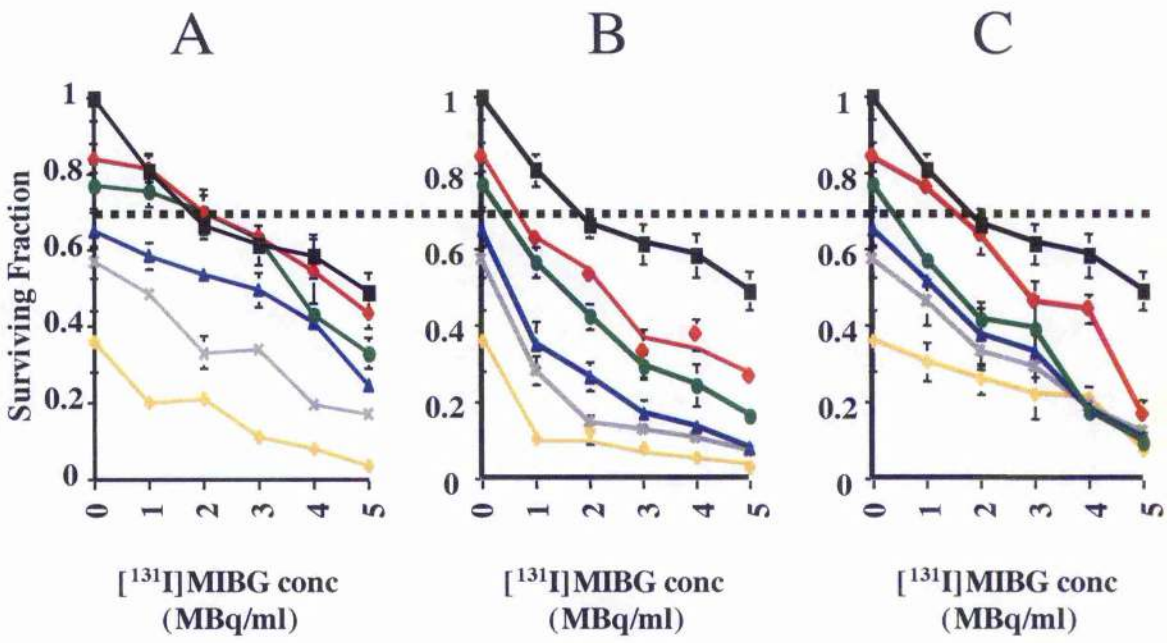

Figure 5-10: The effect of increasing [^{131}I]MIBG concentration on TPT treated UVW/NAT cells

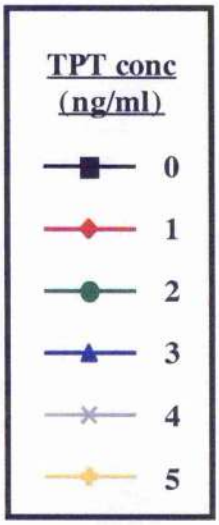

These survival curves show the combined effects of topotecan and [^{131}I]MIBG on UVW/NAT cells. In this figure, survival data are plotted against [^{131}I]MIBG concentration for a range of doses of topotecan. Figure 5-9 shows the same data, plotted as the effect of increasing TPT concentration on [^{131}I]MIBG treated cells.

Again, the concentration of [^{131}I]MIBG which gives an IC_{30} (ie. the dose which causes 30% effect) when combined with each concentration of TPT occurs at the point where the appropriate TPT line crosses the dotted line. These isoeffect points were used along with the isoeffect points from Figure 5-9 to generate the isobologram analyses in Figure 5-11. Isoeffect points were derived in a similar fashion for the IC_{50} and the IC_{70} doses. These were used to generate the isobologram analyses in Figures 5-12 and 5-13 respectively.

Again, survival curves A, B and C were generated by the administration of combination schedules [i], [ii] and [iii] respectively.

5.3.3 UVW/NAT

At the IC_{30} dose, administration of TPT before, or simultaneously with [^{131}I]MIBG (schedules [i] & [iii]) produced isoeffect points which plotted above the hypothetical line of additivity (Figure 5-11A, 5-11C). Administration of TPT after [^{131}I]MIBG (schedule [ii]) produced isoeffect points which plotted below the hypothetical line of additivity (Figure 5-11B). This suggested that supra-additive effects at the IC_{30} level of toxicity by combinations TPT and [^{131}I]MIBG were only achieved by combination schedule [ii] at this toxicity level.

At the IC_{50} dose, administration of TPT before [^{131}I]MIBG (schedule [i]) produced isoeffect points which plotted above the hypothetical line of additivity (Figure 5-12A). This suggested that, as with the results at IC_{30}, administering TPT before [^{131}I]MIBG produced an antagonistic effect. Again, as with the results at IC_{30}, administration of TPT after [^{131}I]MIBG (schedule [ii]) produced isoeffect points which plotted below the hypothetical line of additivity (Figure 5-12B). However, unlike the results observed at IC_{30}, isoeffect points generated at the IC_{50} by administration of TPT and [^{131}I]MIBG simultaneously (schedule [iii]) plotted below the hypothetical line of additivity (Figure 5-12C). As with the results observed in UVW/NAT cells treated with schedule [ii], this suggested that administering TPT and [^{131}I]MIBG simultaneously also produces a supra-additive effect.

As with the results obtained at the IC_{50} dose, at the IC_{70} toxicity level, the majority of isoeffect points generated by administration of TPT either after, or simultaneously with [^{131}I]MIBG (schedules [ii] & [iii]) plotted below the line of additivity (Figures 5-13B & 5-13C), suggesting supra-additive interactions. However, some isoffect points, generated by combinations of a relatively low dose of TPT and a relatively higher dose of [^{131}I]MIBG

plotted above the hypothetical line of additivity. Also, unlike the results obtained at the IC_{30} and IC_{50} levels of toxicity, at the IC_{70}, administration of TPT before [^{131}I]MIBG (schedule [i]) generated some isoeffect points which plotted below the hypothetical line of additivity. This response was obtained by combinations of a relatively low dose of [^{131}I]MIBG and a relatively high dose of TPT (Figure 5-13A).

However, as with the effects of combination schedules [ii] and [iii], isoffect points generated by combinations of a relatively low dose of TPT and a relatively higher dose of [^{131}I]MIBG plotted above the hypothetical line of additivity. This suggests that combinations involving relatively high doses of [^{131}I]MIBG and relatively low doses of TPT may be less effective than administration of combinations involving relatively high doses of TPT and relatively low doses of [^{131}I]MIBG, which resulted in supra-additivity at the IC_{70} toxicity level in cells treated by all three combination schedules, although schedule [i] was not as effective as schedules [ii] or [iii].

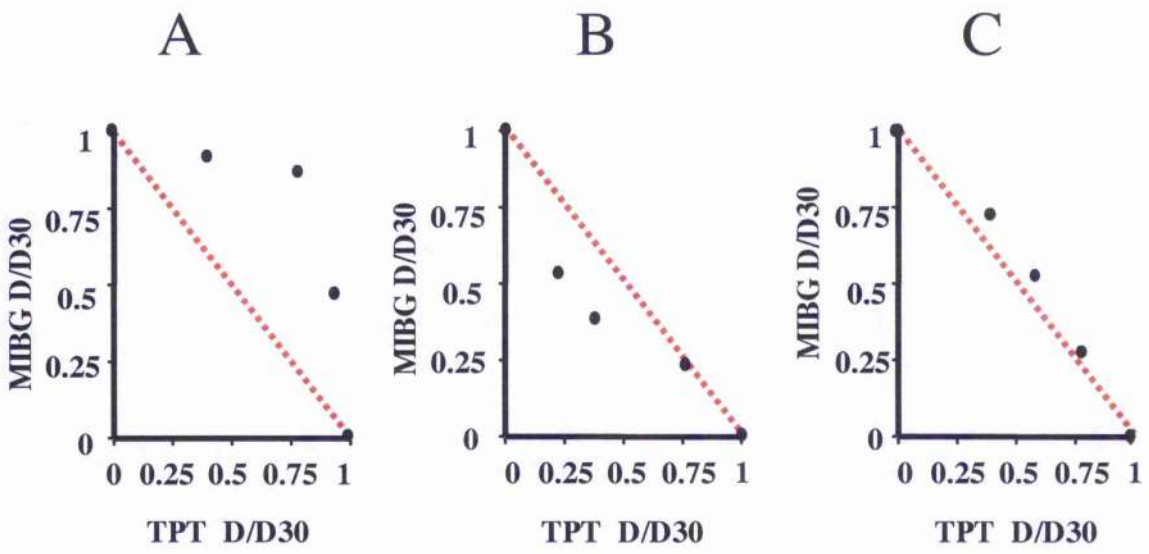

Figure 5-11: IC_{30} Isobologram analyses of UVW/NAT cells treated with different [^{131}I]MIBG and topotecan schedules

The interaction between TPT and [^{131}I]MIBG was analysed at the IC_{30} toxicity level by isobologram analysis. These diagrams were generated using the isoeffect points generated by Figures 5-9 and 5-10. The doses of each agent (D) are expressed as a fraction of the IC_{30} dose (D30).

Again, isobolograms A, B and C show the effect of administration of combination schedules [i], [ii] and [iii] respectively.

This data suggested that combination schedule [ii] was inducing supra-additive responses at this toxicity level. However, schedules [i] and [iii] were not as effective, as isoeffect points plotted above the theoretical line of additivity, suggesting infra-additive responses.

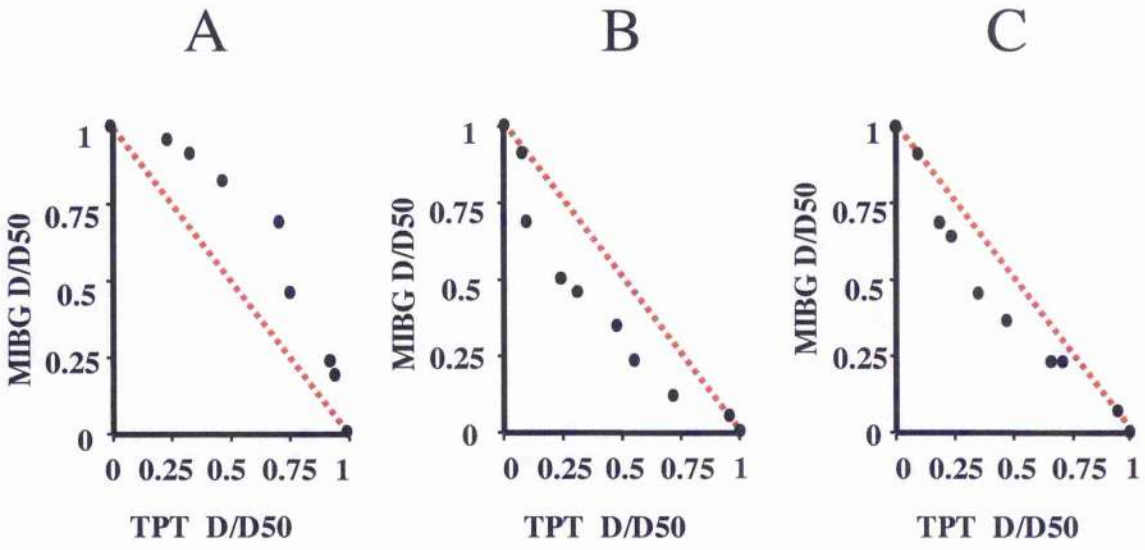

Figure 5-12: IC_{50} Isobologram analyses of UVW/NAT cells treated with different [^{131}I]MIBG and topotecan schedules

The interaction between TPT and [^{131}I]MIBG was also analysed at the IC_{50} toxicity level by isobologram analysis. These diagrams were generated using the isoeffect points generated by Figures 5-9 and 5-10. The doses of each agent (D) are expressed as a fraction of the IC_{50} dose (D50).

Again, isobolograms A, B and C show the effect of administration of combination schedules [i], [ii] and [iii] respectively.

This data suggested that combination schedules [ii] and [iii] induced supra-additive responses at this toxicity level. However, schedules [i] was not as effective, as isoeffect points plotted above the theoretical line of additivity, suggesting an infra-additive response.

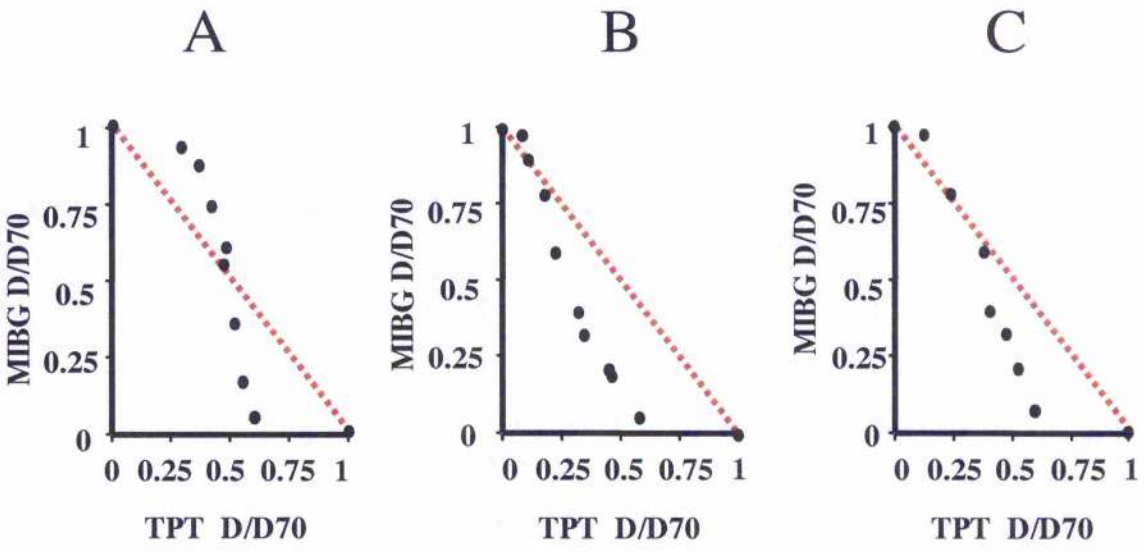

Figure 5-13: IC_{70} Isobologram analyses of UVW/NAT cells treated with different [^{131}I]MIBG and topotecan schedules

The interaction between TPT and [^{131}I]MIBG was also analysed at the IC_{70} toxicity level by isobologram analysis. These diagrams were generated using the isoeffect points generated by Figures 5-9 and 5-10. The doses of each agent (D) are expressed as a fraction of the IC_{70} dose (D70).

Again, isobolograms A, B and C show the effect of administration of combination schedules [i], [ii] and [iii] respectively.

Combinations involving relatively low doses of [^{131}I]MIBG and relatively high doses of TPT resulted in supra-additivity at the IC_{70} toxicity level in cells treated by all three combination schedules.

However, isoffect points generated by combinations of a relatively low dose of TPT and a relatively high dose of [^{131}I]MIBG plotted above the hypothetical line of additivity, suggesting that combinations involving relatively high doses of [^{131}I]MIBG and relatively low doses of TPT may be less effective.

Schedule [i] was not as effective as schedules [ii] or [iii].

5.4 Summary of results

In SK-N-BE(2c) cells, while isoeffect points generated at the IC_{30} by all three combination schedules examined plotted below the hypothetical line of additivity (Figures 5-6 & 5-7), at the IC_{50}, cells treated by combination schedules [i] and [iii] displayed some isoeffect points which plotted above the hypothetical line of additivity. These were generated by combinations of a relatively low dose of [^{131}I]MIBG and a relatively high dose of TPT, suggesting that combinations involving relatively high dose of [^{131}I]MIBG and a relatively low dose of TPT may be more effective. Combinations of TPT and [^{131}I]MIBG were not as effective at the IC_{70} level of toxicity, and most of the isoeffect points generated by the three scheduled combinations plotted above the line of additivity. Again, relatively high doses of [^{131}I]MIBG and relatively low doses of TPT were more effective.

In UVW/NAT cells, at the IC_{30} level of toxicity, administration of schedule [ii] produced isoeffect points which plotted below the theoretical line of additivity, suggesting a supra-additive interaction. Combination schedules [i] and [iii] were less effective at this toxicity level. At the IC_{50} toxicity level, supra-additive interactions were obtained following administration of combination schedules [ii] and [iii], but not following administration of combination schedule [i]. All three combination schedules produced supra-additive responses at the IC_{70} level of toxicity. Again, combination schedule [i] was less effective than the other two schedules. However, unlike SK-N-BE(2c) cells, combinations involving relatively high doses of [^{131}I]MIBG and relatively low doses of TPT were not as effective against UVW/NAT cells than combinations involving relatively low doses of [^{131}I]MIBG and relatively high doses of TPT.

These results indicate that supra-additive levels of killing may be achieved in NAT expressing cells treated with a combination of TPT and [^{131}I]MIBG, suggesting that combined therapies involving these two agents for the treatment of neuroblastoma could improve upon existing modalities.

In this study, the cytotoxic interaction between topotecan and [^{131}I]MIBG was assessed by isobologram analysis. However, the choice of methodology used to assess the nature and intensity of agent interaction has historically proven to be controversial, and many competing models have been used to assess the nature and intensity of agent interactions [156]. While the isobologram method has been utilised by many previous studies, this technique is not universally applied. Indeed, several different versions of isobologram analyses have been reported [164, 165, 168, 169].

For this reason, the cytotoxic interaction between TPT and [^{131}I]MIBG was further assessed using another model of drug interacton analysis, in order to confirm the results of isobologram analyses described in this chapter. This second model is the median-effect / combination-index method, and is described in Chapter 6.

Chapter 6

Analysis of the cytotoxic interaction between topotecan and [^{131}I]MIBG *in vitro*

II: Median-effect / combination index analysis

6.1 Introduction

6.1.1 Analysing the interaction between topotecan and [^{131}I]MIBG

As previously discussed in Chapter 5, many competing models have been used to assess the nature and intensity of agent interactions. While the isobologram method described in the previous chapter has been utilised by many previous studies, this technique is not universally applied.

Therefore, in order to accurately assess the interaction between TPT and [^{131}I]MIBG, another commonly reported model of multiple drug interaction, the median-effect / combination-index method of Chou and Talalay [163, 166, 167] was also used to examine the *in vitro* effects of these agents. Unlike isobologram analysis, where a range of concentrations of drug A are combined with each dose of drug B (and vice versa), in this model the agents are combined using a fixed dose ratio of drug A to drug B based on the effectiveness of each drug as single agents, so that the proportional contribution of the effect of each drug in the mixtures should be the same at all treatment intensities.

6.1.2 Multiple drug effect analysis of the interaction between two toxic agents

The multiple drug effect analysis of Chou and Talalay [166, 167] is based on the median-effect principle. Dose-effect curves were constructed using the equations described in Figure 6-1. In equations (1) and (2), *D* is the dose, *Dm* is the IC_{50} dose, *fa* is the fraction of cell affected, *fu* is the unaffected fraction and *m* is the coefficient of the sigmoidicity of the dose-effect curve. The logarithmic form of equation (2) converts the equation into the form of "y=mx+c", where the value *m* becomes the slope of the line, and the log IC_{50} value becomes the x-intercept.

Therefore, from the plot of log (*D*) against log (*fa/fu*), the x-intercept (log IC_{50}) and slope *m* were calculated for each drug and for combinations by the method of least squares. These parameters were then used to calculate doses of the component agents and combinations required to produce various cytotoxicity levels according to the non-logarithmic form of equation (2).

For each level of toxicity, the combination index (CI) was calculated according to equation (3), where $(D)_1$ and $(D)_2$ are the doses of each agent which sterilise x% of clonogens when used in combination, and $(Dx)_1$ and $(Dx)_2$ are the doses of each drug which sterilise x% of clonogens when used as single agents.

If the agents have similar, or dependent modes of action, then $\alpha = 0$ and the CI value is equivalent to the sum of the first two terms. If the agents have independent modes of action, then $\alpha = 1$ and the CI value is equivalent to the sum of all three terms. If the manner of the interaction between the agents is uncertain, then the formula is solved in both ways.

$CI < 1$, $CI = 1$ and $CI > 1$ indicate synergism, additivity and antagonism respectively.

Equation (1): $fa/fu = (D/Dm)^m$

Equation (2): $D = Dm[fa/fu]^{1/m}$

Equation (3): $CI = (D)_1/(Dx)_1 + (D)_2/(Dx)_2 + \alpha(D)_1(D)_2/(Dx)_1(Dx)_2$

Figure 6-1: Equations used to study the interaction between two agents by median-effect and combination index analysis

The cytotoxic interaction between two agents can be further evaluated using multiple drug effect analysis, based on the median-effect principle of Chou & Talalay, which allows the analysis of drug effect using the median-effect equation (equation (1)), which can be rearranged to give equation (2).

In equations (1) & (2), D is the dose, Dm is the dose required for 50% effect (ie. the IC_{50} dose), fa is the fraction of cell affected, fu is the unaffected fraction and m is a coefficient of the sigmoidicity of the dose-effect curve.

In equation (3), $(D)_1$ and $(D)_2$ are the doses of each agent which inhibit x% of cell growth when used in combination, and $(Dx)_1$ and $(Dx)_2$ are the doses of each drug which inhibit x% of colonies when used as single agents. If the agents have similar, or dependent modes of action, then $\alpha = 0$ (ie the CI value = the sum of the first two terms). If the agents have independent modes of action (eg independent modes of action) then $\alpha = 1$ (ie the CI value = the sum of all three terms).

$CI < 1$, $CI = 1$ and $CI > 1$ indicate synergism, additivity and antagonism respectively.

6.2 Materials & methods

6.2.1 Clonogenic assays

As with isobologram analyses of drug interactions (Chapter 5), three scheduled combinations of TPT and [^{131}I]MIBG were investigated. In schedule [i] topotecan was administered 24 hours before [^{131}I]MIBG treatment. In schedule [ii] topotecan was administered 24 hours after [^{131}I]MIBG treatment. In schedule [iii] topotecan and [^{131}I]MIBG were administered simultaneously (Figure 5-3).

Monolayers of SK-N-BE(2c) and UVW/NAT of cells were cultured in 25cm^2 flasks (Nunclon Plastics, Denmark) at 2.5 x 10^5 cells per flask. After two days, medium was removed and replaced with fresh medium containing a dose of TPT and/or [^{131}I]MIBG. Following treatments, the cytotoxic effects were assessed in triplicate by clonogenic assay, as previously described (Section 4.2.2). Every treatment group was assessed three times.

6.2.2 Fixed ratios of TPT and [^{131}I]MIBG

For combination treatments the fixed ratio of TPT (ng/ml) to [^{131}I]MIBG (MBq/ml) employed was 1:2 (i.e 1ng/ml:2MBq/ml) for SK-N-BE (2c) cells.

For analyses of drug interactions in UVW/NAT cells the fixed ratio of TPT:[^{131}I]MIBG employed was 1:1. These ratios were determined from the relative toxicities to each cell line of the drugs used as single agents, described in Chapter 4. This meant that the proportional contribution of each drug was the same at all treatment intensities for each cell line.

6.3 Results

6.3.1 Median-effect/combination-index analysis of the interaction between [^{131}I]MIBG and topotecan

The effects of TPT and [^{131}I]MIBG on SK-N-BE(2c) as single agents or in combination are shown in Figure 6-2. From the survival curves from Figure 6-2, median-effect plots were constructed, to enable the calculation of various levels of toxicity. These are shown in Figure 6-3.

Similarly, the effects of TPT and [^{131}I]MIBG on UVW/NAT cells as single agents or in combination are shown in Figure 6-4. Median-effect plots were constructed from this data, and these are shown in Figure 6-5.

CI values were determined using equation (3) from Figure 6-1. The formula was solved in two different ways, as the manner of the interaction between the agents was uncertain. TPT has an effect which is independent of [^{131}I]MIBG activity (S-phase specific toxicity [83, 85]) and an effect which is dependent on [^{131}I]MIBG activity (due to Topo I's involvement in the response to [^{131}I]MIBG-initiated DNA damage [170-175]).

In Figure 6-6 (SK-N-BE(2c)), and in Figure 6-7 (UVW/NAT) the data (CI values) corresponding to the modes of action of the two agents which are dependent or distinct, are presented graphically as (a) solid lines, or (b) dashed lines, respectively. These modes of action therefore represent the extreme values that can be generated by the interaction between these agents, and the "true" CI value is likely to lie somewhere in between. Data corresponding to similar modes of action are presented in bold type. Data corresponding to distinct modes of action are presented in italics. CI < 1, CI = 1 and CI > 1 indicated synergism, additivity and antagonism respectively.

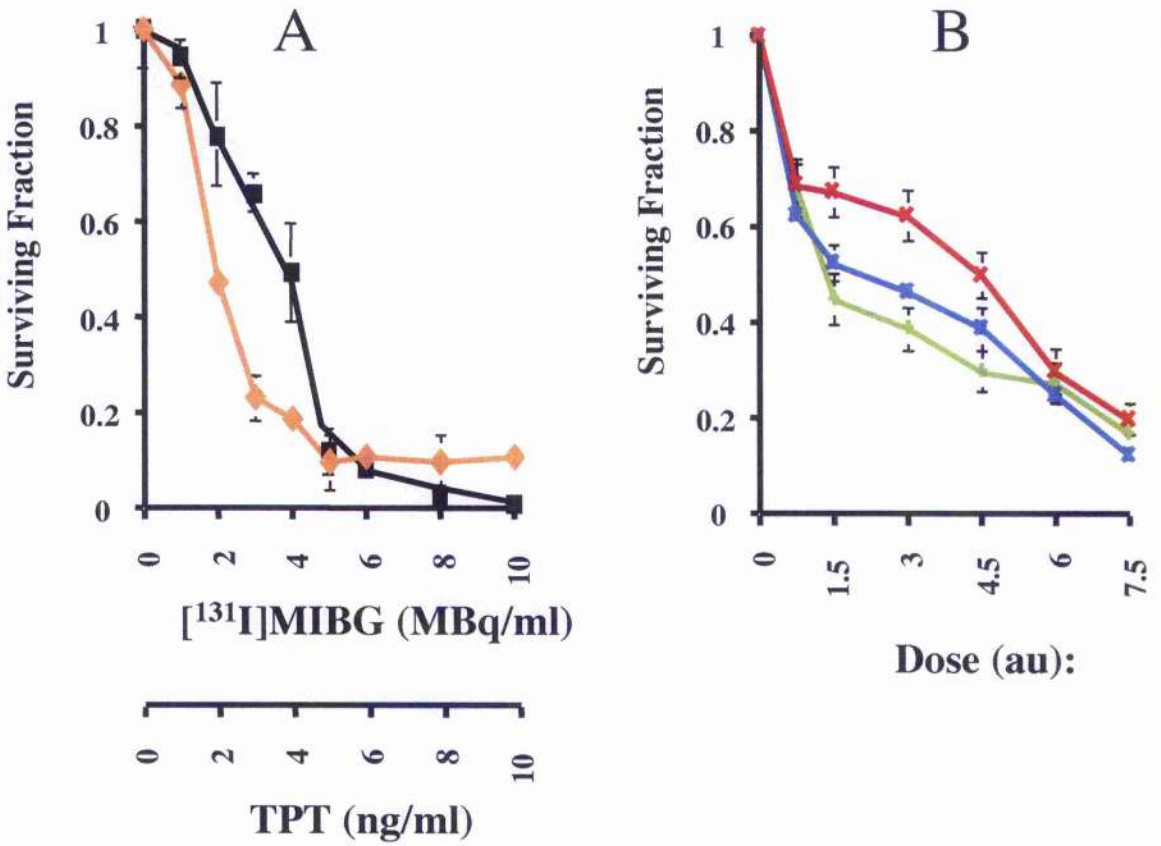

Figure 6-2: Effect of [^{131}I]MIBG and TPT alone and in combination on clonogenic survival of SK-N-BE(2c) cells

A) The effects of TPT and [^{131}I]MIBG on SK-N-BE(2c) cells as single agents. These survival curves were plotted using the same data shown in Figure 4-3.

B) The effects of TPT and [^{131}I]MIBG on SK-N-BE(2c) cells in combination. Based on data from (A), SK-N-BE(2c) cells were dosed with TPT and [^{131}I]MIBG in a fixed 1:2 ratio (TPT:MIBG.
1au = 0.333..ng/ml of TPT + 0.666...MBq/ml of [^{131}I]MIBG .

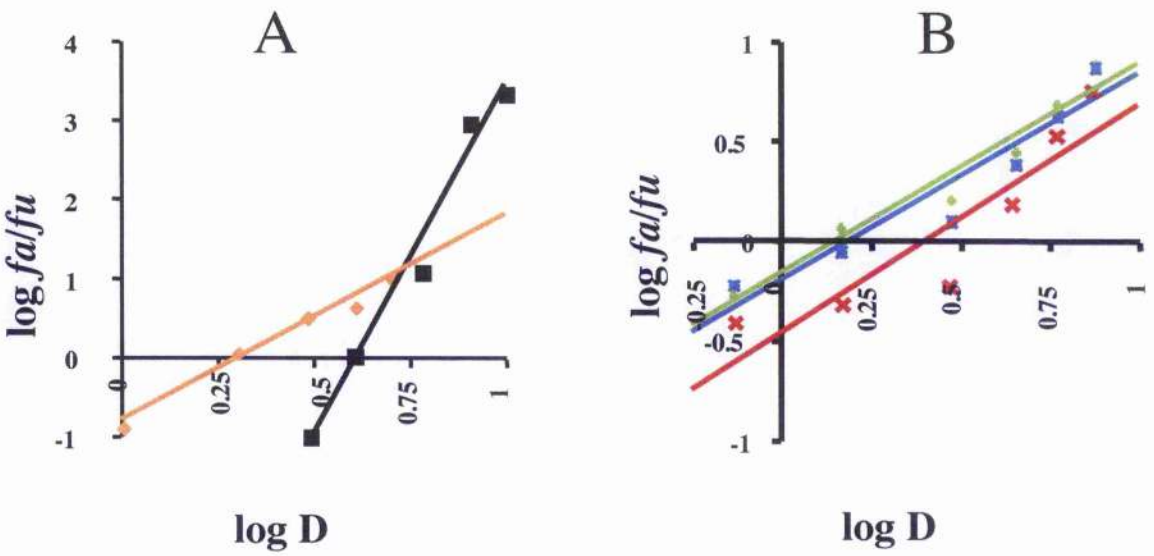

Figure 6-3: Median-effect plots for TPT and [^{131}I]MIBG treated SK-N-BE(2c) cells

The cytotoxic interaction between TPT and [^{131}I]MIBG was further assessed using the median-effect principle.

The dose response curves from Figure 6-2 were replotted using the logarithmic form of equation (1): log[*fa/fu*] = *m*log*D* - *m*log*Dm*. This converts the relationship between effect *(fa/fu)* and dose *(D)* into a linear form (ie. y = mx + c).

From the resulting median-effect lines, x-intercept (log IC_{50}) and slope *m* were calculated for each agent alone (A) and for each agent in combination (B).

These parameters were used to calculate *D*, the doses of component agents (and combinations) required to produce various levels of toxicity, using equation (2): $D = Dm[fa/fu]^{1/m}$.

The resultant toxicity data were used to calculate the CI values shown in Figure 6-6.

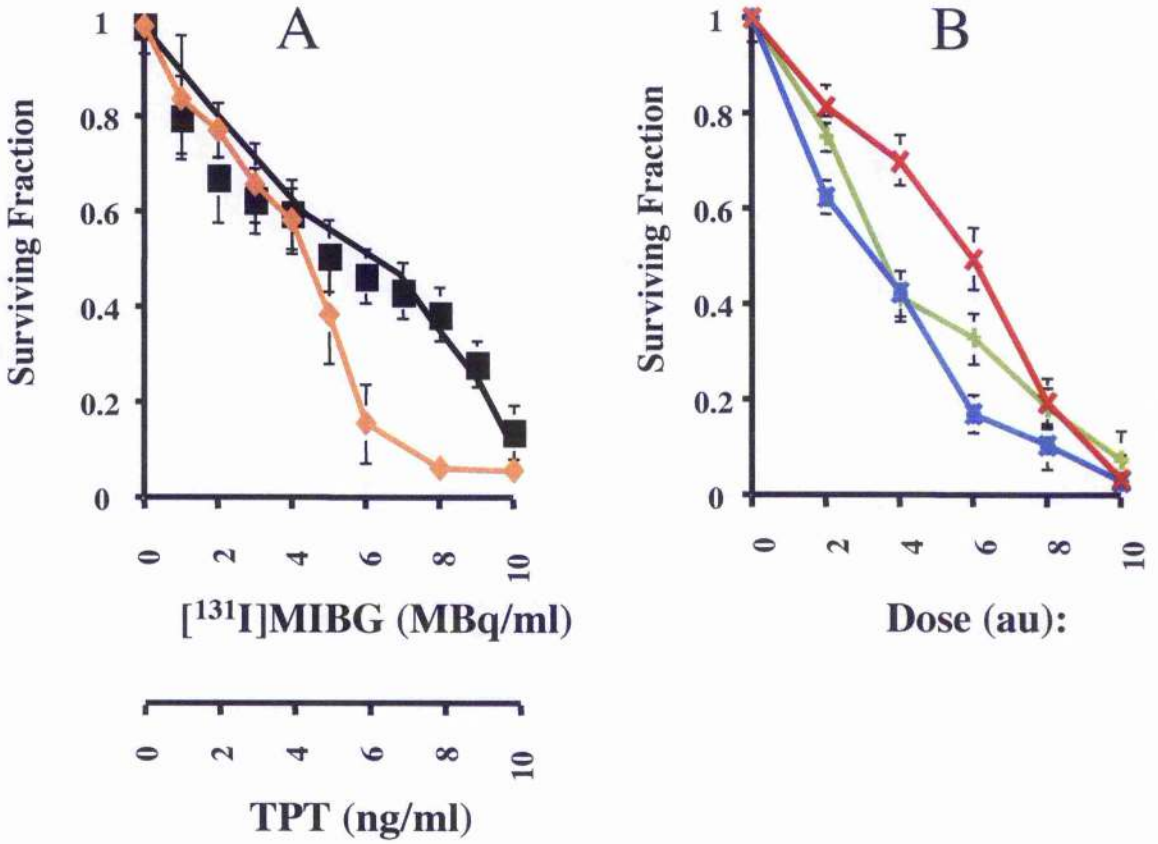

Figure 6-4: Effect of [^{131}I]MIBG and TPT alone and in combination on clonogenic survival of UVW/NAT cells

A) The effects of TPT and [^{131}I]MIBG on UVW/NAT cells as single agents. These survival curves were plotted using the same data shown in Figure 4-4.

B) The effects of TPT and [^{131}I]MIBG on SK-N-BE(2c) cells in combination. Based on data from (A), UVW/NAT cells were dosed with TPT and [^{131}I]MIBG in a fixed 1:1 ratio (TPT:MIBG).
1au = 0.5ng/ml of TPT + 0.5MBq/ml of [^{131}I]MIBG .

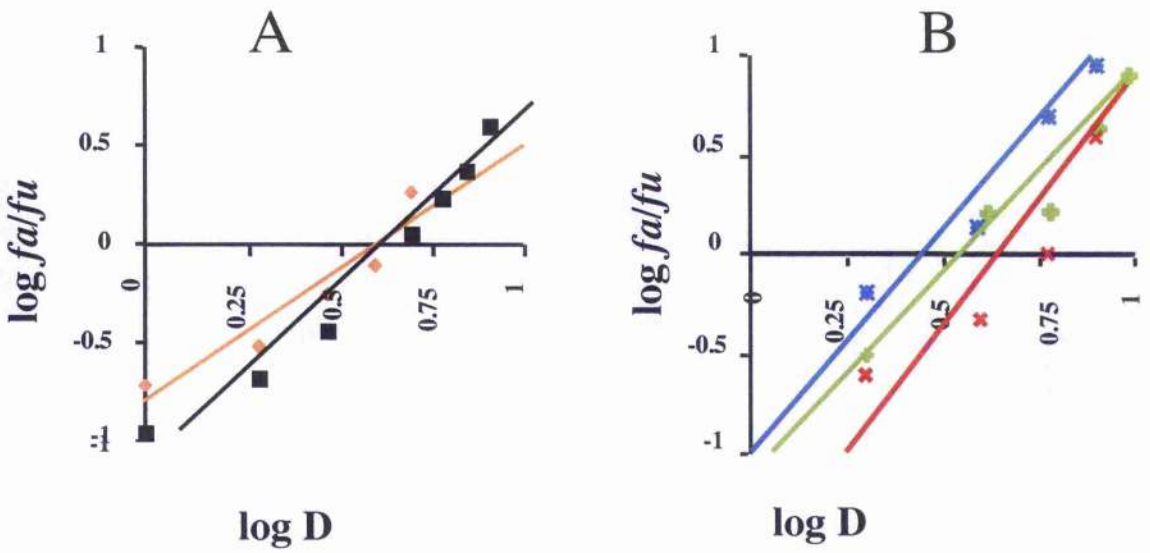

Figure 6-5: Median-effect plots for TPT and [^{131}I]MIBG treated UVW/NAT cells

As with SK-N-BE(2c) cells, the cytotoxic interaction between TPT and [^{131}I]MIBG was further assessed using the median-effect principle.

Again, the dose response curves from Figure 6-4 were replotted using the logarithmic form of equation (1) $\log[fa/fu] = m\log D - m\log Dm$, and from the resulting median-effect lines, x-intercept (log IC_{50}) and slope m were calculated for each agent alone (A) and for each agent in combination (B).

These parameters were used to calculate D, the doses of component agents (and combinations) required to produce various levels of toxicity, using equation (2): $D = Dm[fa/fu]^{1/m}$).

The resultant toxicity data were used to calculate the CI values shown in Figure 6-7.

6.3.2 SK-N-BE(2c)

The results of combination analyses of different scheduled combinations of TPT and [^{131}I]MIBG are shown in Figure 6-6. The data (CI values) corresponding to the modes of action of the two agents which are dependent or distinct, are presented below in bold type and italics respectively. Supra-additive kill of SK-N-BE(2c) cells after treatment with all combination schedules resulted in CI values < 1 at the IC_{10}, and IC_{30}, (eg. at IC_{30}: schedule [i] = **0.501 ± 0.117** / *0.566 ± 0.147;* schedule [ii] = **0.282 ± 0.037** / *0.302 ± 0.043;* schedule [iii] = **0.260 ± 0.018** / *0.277 ± 0.020).*

However, after combination therapy involving levels of cytotoxicity greater than IC_{50}, the combined treatments were less effective than the individual drugs and CI values > 1 were obtained at the IC_{70} and IC_{90}.

At the IC_{50}, in the case of schedule [i], the CI value calculated assuming a dependent interaction was slightly less than 1 (**0.922 ± 0.027**) whereas the CI value which was calculated, assuming independent modes of action of the two agents, was slightly greater than 1 (*1.134 ± 0.039).* In contrast, the effects of combination schedules [ii] and [iii] were synergistic at the IC_{50} regardless of the method of derivation of CI (schedule [ii] = **0.562 ± 0.015** / *0.641 ± 0.019*; schedule [iii] = **0.507 ± 0.043** / *0.572 ± 0.054).*

Likewise, at every level of toxicity analysed, administration of TPT before [^{131}I]MIBG (schedule [i]) was not as effective as administration of TPT either after, or simultaneously with [^{131}I]MIBG (schedules [ii] and [iii] respectively).

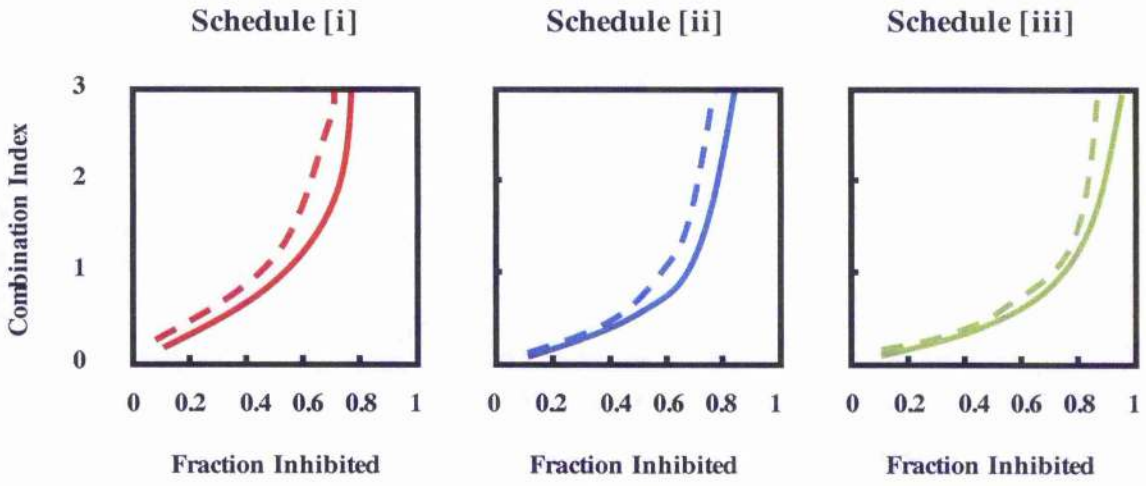

Figure 6-6: Combination-index (CI) *versus* cytotoxicity: Interaction between TPT and [^{131}I]MIBG in SK-N-BE(2c) cells

The data (CI values) corresponding to modes of action of the two agents which are similar, are presented as **bold** text, and graphically as solid lines. The CI values corresponding to modes of action of the two agents which are distinct, are presented as *italics*, and graphically as dashed lines.

CI < 1, CI = 1 and CI > 1 indicated synergism, additivity and antagonism respectively.

Supra-additive levels of kill were achieved at low toxicity levels. This was observed in each scheduled combination of the two agents. However, at each level of toxicity analysed, administration of TPT before exposure to [^{131}I]MIBG was not as effective as administration of TPT either after, or simultaneously with [^{131}I]MIBG; eg. at IC_{50}:

Schedule [i] = **0.922 ± 0.027** *(1.134 ± 0.039);*
Schedule [ii] = **0.562 ± 0.015** *(0.641 ± 0.019);*
Schedule [iii] = **0.507 ± 0.043** *(0.572 ± 0.054).*

6.3.3 UVW/NAT

The results of combination analyses of different scheduled combinations of TPT and [^{131}I]MIBG are shown in Figure 6-7. The data (CI values) corresponding to the modes of action of the two agents which are dependent or distinct, are presented below in bold type and italics respectively. Unlike SK-N-BE(2c) cells, administration of all combination schedules resulted in CI values > 1 at the IC_{10}. At the IC_{30} however, while cells treated by schedule [i] and schedule [iii] continued to exhibit infra-additive interactions (schedule [i] = **1.564 ± 0.140** / *2.176 ± 0.250;* schedule [iii] = **1.204 ± 0.076** / *1.565 ± 0.121),* in the case of schedule [ii], the CI value calculated assuming a dependent interaction was slightly less than 1 (**0.973 ± 0.022**) whereas the CI value which was calculated, assuming independent modes of action of the two agents, was slightly greater than 1 (*1.208 ± 0.033).*

At the IC_{50} level of toxicity, treatment by schedule [ii] and schedule [iii] resulted in CI values < 1 (schedule [ii] = **0.662 ± 0.043** / *0.772 ± 0.057;* schedule [iii] = **0.856 ± 0.094** / *1.041 ± 0.135).* Treatment by schedule [i] continued to result in an infra-additive interaction CI = **1.021 ± 0.128** / *1.284 ± 0.193).*

UVW/NAT cells exposed to combinations of TPT and [^{131}I]MIBG at levels of colony inhibition > IC_{50} exhibited supra-additive sterilisation of clonogens with all three schedules of administration (eg. at IC_{70}: schedule [i] = **0.672 ± 0.108** / *0.785 ± 0.144;* schedule [ii] = **0.455 ± 0.057** / *0.507 ± 0.070;* schedule [iii] = **0.615 ± 0.097** / *0.710 ± 0.126).*

As in the case of SK-N-BE(2c) cells, at every level of toxicity analysed, treatment with TPT before exposure to [^{131}I]MIBG (schedule [i]) was less effective than administration of TPT either after, or simultaneously with [^{131}I]MIBG (schedules [ii] and [iii] respectively).

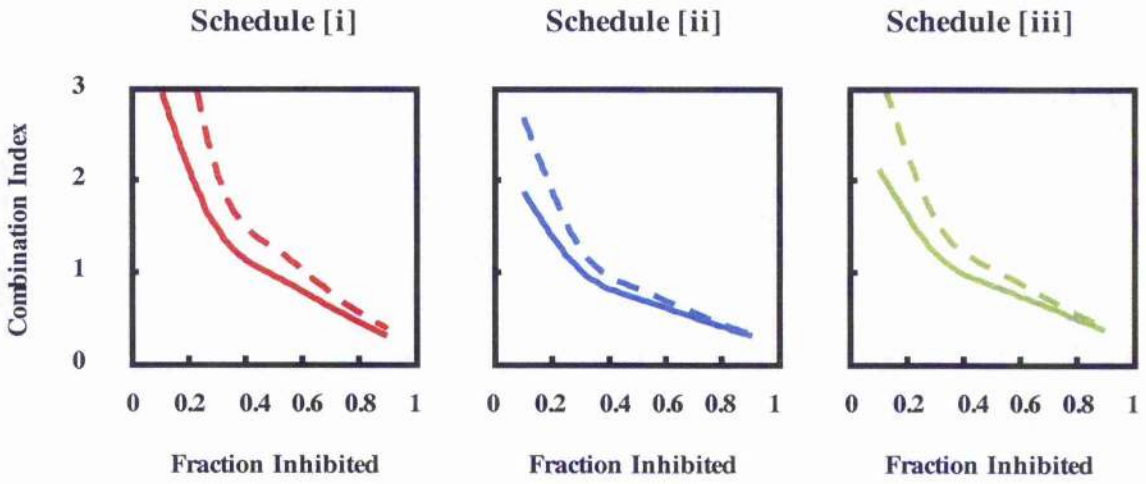

Figure 6-7: Combination-index (CI) *versus* cytotoxicity: Interaction between TPT and [^{131}I]MIBG in UVW/NAT cells

Again, the data (CI values) corresponding to modes of action of the two agents which are similar, are presented as **bold** text, and graphically as solid lines. The CI values corresponding to modes of action of the two agents which are distinct, are presented as *italics*, and graphically as dashed lines.

CI < 1, CI = 1 and CI > 1 indicated synergism, additivity and antagonism respectively.

Supra-additive levels of kill were achieved by combinations of TPT and [^{131}I]MIBG at high toxicity levels. This was observed in each scheduled combination of the two agents. However, as with SK-N-BE, at each level of toxicity analysed, administration of TPT before exposure to [^{131}I]MIBG was not as effective as administration of TPT either after, or simultaneously with [^{131}I]MIBG; eg. at IC_{50}:

Schedule [i] = **1.021 ± 0.128** *(1.284 ± 0.193);*
Schedule [ii] = **0.662 ± 0.043** *(0.772 ± 0.057);*
Schedule [iii] = **0.856 ± 0.094** *(1.041 ± 0.135).*

6.4 Summary of results

In SK-N-BE(2c) cells, administration of combinations of TPT and [^{131}I]MIBG at low levels of toxicity (ie. < IC_{50}) resulted in supra-additive levels of clonogenic sterilisation. However, following the administration of doses which resulted in higher levels of cytotoxicity (ie. > IC_{50}), the combined treatments were less effective than the individual drugs and CI values > 1 were obtained at the IC_{70} and IC_{90}. At every level of toxicity analysed, administration of TPT before [^{131}I]MIBG (schedule [i]) was less effective than administration of TPT either after, or simultaneously with [^{131}I]MIBG (schedules [ii] and [iii] respectively).

UVW/NAT cells were more resistant than SK-N-BE(2c) cells to combination therapy, and CI values < 1 were obtained following doses of TPT and [^{131}I]MIBG which resulted in low levels of toxicity (ie. ≤ IC_{30}). UVW/NAT cells were more sensitive to higher doses of TPT/MIBG combinations, and all three schedules induced supra-additive responses at high levels of toxicity (ie. ≥ IC_{70}). However, as was observed in SK-N-BE(2c) cells, administration of combination schedule [i] was less effective than combination schedules [ii] or [iii], and at the IC_{50} level of toxicity, while administration of schedules [ii] and [iii] resulted in supra-additive responses, treatment by schedule [i] resulted in an infra-additive interaction.

The results of combination-index analyses described in this chapter were in agreement with the results of isobologram analyses previously reported in Chapter 5, which found that supra-additive levels of killing were achieved in NAT expressing cells treated with combinations of TPT and [^{131}I]MIBG. Furthermore, combination-index analyses suggested that schedule [i] was less effective than schedules [ii] and [iii] at every toxicity level evaluated.

The isobologram method described in Chapter 5 involved the administration of variable doses of each agent. The use of fixed TPT:MIBG ratios in median-effect / combination-index analysis meant that this model did not provide as much information on the specific interactions between, for example, combinations involving low doses of TPT and high doses of [^{131}I]MIBG. However, while different versions of isobologram analyses have been reported [164, 165, 168, 169], the same mathematical equations are applied in all examples of combination-index analyses [163, 166, 167]. Furthermore, median-effect / combination-index analysis is less laborious than isobologram analysis [166], and its versatility is demonstrated by its wide-spread use in reported analyses of drug-drug interactions [163, 176].

While the results of *in vitro* experiments to assess the cytotoxic interactions between TPT and [^{131}I]MIBG described in Chapters 5 & 6 are valuable, it is desirable to examine TPT/[^{131}I]MIBG combination therapy *in vivo*, before progressing to clinical evaluation. This will be the topic of Chapter 7.

Chapter 7

Analysis of the cytotoxic interaction between topotecan and [^{131}I]MIBG *in vivo*

7.1 Introduction

7.1.1 Anti-tumour effects of topotecan and [^{131}I]MIBG

The results of *in vitro* experiments to assess the cytotoxicity of TPT and [^{131}I]MIBG as single agents and in combination, previously described in Chapters 4-6 provide valuable information about the interaction between these drugs. However, it is desirable to examine the efficacy and optimal order of delivery of TPT/[^{131}I]MIBG combination therapy *in vivo*, before progressing to clinical evaluation. This was accomplished using SK-N-BE(2c) and UVW/NAT nude mice tumour xenograft models, previously described [177, 178].

7.1.2 Effect of TPT and [^{131}I]MIBG on marrow toxicity

The dose limiting tissue in neuroblastoma patients treated with [^{131}I]MIBG is bone marrow and toxicity is manifest by prolonged thrombocytopenia [179]. Furthermore, topotecan is also myelotoxic [126].

It was therefore important to investigate the effects of combinations of these agents on platelet production and proliferative capacity of haemopoietic stem cells in experimental animals. See Figure 7-1.

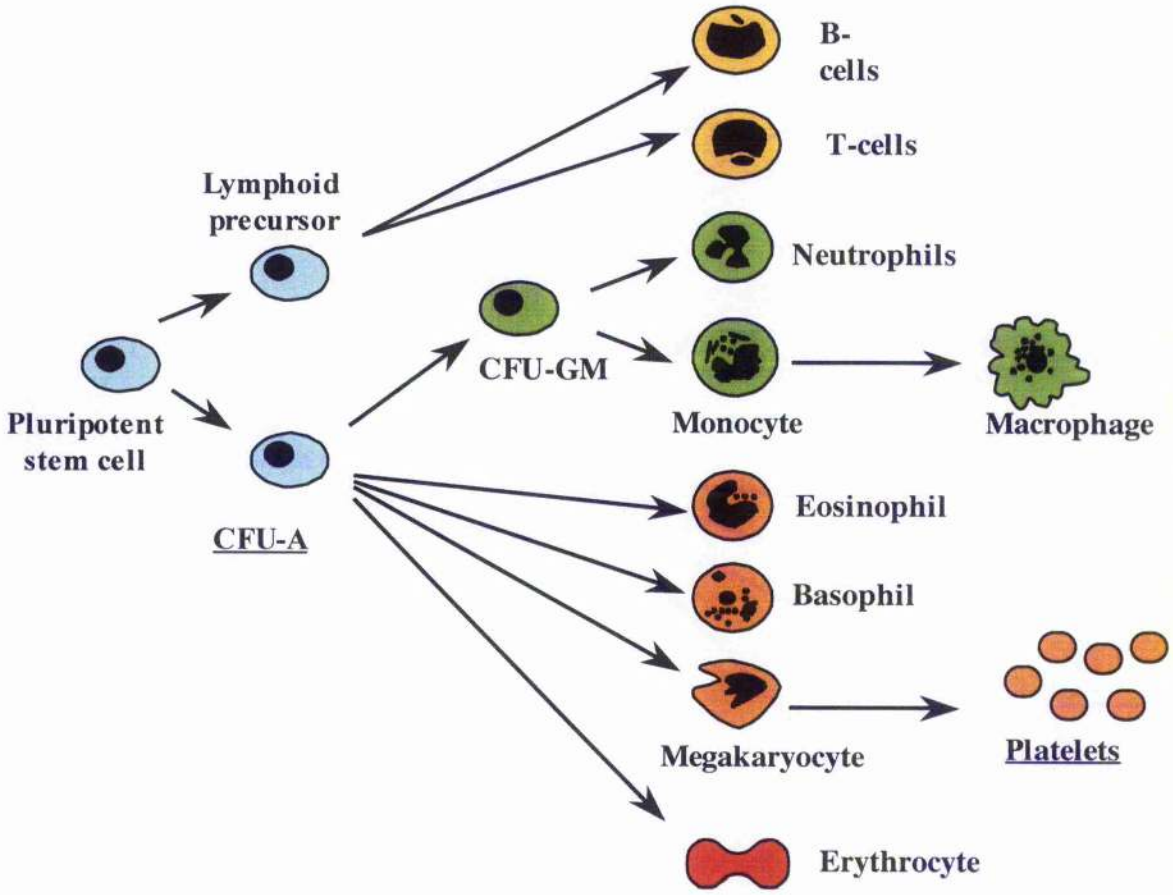

Figure 7-1: Haemopoiesis

CFU-A cells are progenitors of the myeloid lineage, and are one division removed from the pluripotent stem cells. These are more abundant than the pluripotent stem cell and are radiosensitive.

7.2 Materials & methods

7.2.1 Experimental animals.

Six-week-old male and female, congenitally athymic nude mice of strain MF1 nu/nu were obtained from Harlan Olac, Bicester, UK. *In vivo* experiments were carried out in accordance with the UK Coordinating Committee for Cancer Research guidelines on experimental neoplasia in animals [180].

7.2.2 Xenografts.

Two tumour models were employed. SK-N-BE(2c) xenografts, initiated by subcutaneous insertion of tumour fragments, were appropriate for the evaluation of experimental therapy of large tumours whereas UVW/NAT xenografts, established by the injection of a single cell suspension, were used for investigation of combination treatment of smaller tumours.

7.2.3 SK-N-BE(2c)

Tumour growth was established by intrasplenic injection of 3 x 10^6 exponentially growing SK-N-BE(2c) cells as previously described [177]. Following the growth of tumours in the spleen and liver, animals were euthanized and tumour fragments 2-3mm in diameter were then implanted subcutaneously in the subcostal flanks of other nude mice. Mice were used for experimental therapy 17 days after tumour implantation when the subcutaneous tumours had reached approximately 10mm diameter (500mm^3).

7.2.4 UVW/NAT

Xenografts were established in nude mice by subcutaneous (s.c.) injection of 3 x 10^6 UVW/NAT cells, freshly harvested at 60 to 70% confluence to ensure that their growth was in the logarithmic phase. [^{131}I]MIBG therapy experiments were initiated nine days later, at which time tumour volume was approximately 60mm^3. To monitor potential toxicity, body weight was measured daily and experimental animals were scored for signs of distress using standard guidelines [178].

7.2.5 Effect of topotecan pretreatment on the biodistribution of [^{131}I]MIBG

Twenty four hours before administration of [^{131}I]MIBG, the mice received, by intraperitoneal (i.p.) injection, 1.75 mg/kg of topotecan or the equivalent volume of saline. At least one hour before [^{131}I]MIBG injection, tumour-bearing mice were weighed and injected i.p. with 1 ml of a 0.1% potassium iodide solution to diminish thyroid uptake of radioiodine. The animals then received, by i.p. injection, 2MBq of [^{131}I]MIBG. The precise activity administered to each mouse was measured using a Curiemonitor-2

ionization chamber (Radiation Components, Bracknell, UK). After 24 hours mice were euthanized. Samples of femur contents, tumour, heart, lung, adrenal glands, muscle, kidney, thyroid and liver were excised and weighed and the associated radioactivity was measured in an automated gamma counter (Packard Biosciences Ltd, Berkshire, UK). Comparison of tissue activity levels was performed by Student's t-test.

7.2.6 Therapy experiments.

Groups of twelve mice with SK-N-BE(2c) or UVW/NAT tumours were used for each treatment regimen. The mice were randomized into six treatment groups which received, by i.p. injection, saline (control), 18 MBq of [^{131}I]MIBG alone (SK-N-BE(2c) tumours) or 10 MBq of [^{131}I]MIBG alone (UVW/NAT tumours), 1.75 mg/kg of topotecan alone or combinations of the two agents.

As with the *in vitro* analysis of the interactions between TPT and [^{131}I]MIBG (Chapters 5 & 6), three treatment schedules were assessed: topotecan administered 24h before [i], after [ii] or simultaneously with [iii] [^{131}I]MIBG. The dose of [^{131}I]MIBG administered to the mice was previously shown to induce significant delay of the growth, but incomplete sterilisation of SK-N-BE(2c) [181] or UVW/NAT xenografts [182]. The injected dose of topotecan was equivalent to 88% of the maximal tolerated dose contained in one administration of a fractionated dose [183].

Subcutaneous tumours were measured with callipers immediately prior to treatment and every two or three days thereafter. On the assumption of ellipsoidal geometry, diameter measurements were converted to an approximate volume by multiplying half the longest diameter by the square of the mean of the two shorter diameters. Mice whose xenograft volume reached 1900mm^3 were euthanized. The tumour volumes, against time,

were plotted for each animal. In the growth/regrowth phase, these profiles were log-linear. Separate log-linear regressions were fitted to each animal's data.

For each treatment group, the mean time taken to reach two times (SK-N-BE(2c) xenografts) or ten times (UVW/NAT xenografts) the tumour volume at the initiation of treatment was calculated to allow comparison among treatment groups. Cure was defined as the failure of tumours to increase in size over a period of 30 days. The comparison of antitumour efficacies of the various treatment combinations was performed by the Mann-Whitney U-test. $p < 0.05$ was considered statistically significant. All statistical tests used GraphPad Prism software, version 3.0, 1999 (CA).

7.2.7 Assessment of marrow toxicity

Separate groups of six mice were used for the determination of possible adverse effects on bone marrow of the various combinations of [^{131}I]MIBG and topotecan. One, two, three and six weeks following treatment, mice were killed and samples of blood (0.5ml) were collected using 1.5mg/ml dipotassium EDTA as anticoagulant. The numbers of thrombocytes per ml were determined by an automated analyser (STK-S Coulter, Miami, Fl, USA).

As a further indicator of myelotoxicity, the clonogenic potential of CFU-A cells in the same groups of mice was determined. These are transiently engrafting haemopoietic stem/progenitor cells whose proliferative capacity is indicative of the status of the haemopoietic stem cell compartment in general [184] (Figure 7-1). After separating surrounding muscle and epiphyses from femurs under sterile conditions, marrow was obtained by flushing out femur contents with PBS using a 25-guage syringe. Clonogenic haemopoietic stem/progenitor cells were numerically assessed using the *in vitro* CFU-A assay as described previously [185].

Briefly, a feeder layer consisting of 0.6% agar in -MEM with 25% donor horse serum was prepared. Prior to plating, and after equilibrating to 37°C, growth factors (R & D Systems, Abingdon, UK) were added to the feeder layer. Specifically, murine GM-CSF was added to 0.2ng/ml; recombinant human CSF-1 to 6ng/ml and recombinant murine CSF to 12 ng/ml. One milliliter of this feeder layer mixture was plated out per standard 3cm tissue culture dish and allowed to set.

The upper agar layer consisted of 0.3% agar in -MEM and 25% donor horse serum to which normal murine bone marrow cells were added to a concentration of 5 x 10^3 per ml. One milliliter of this upper layer agar mix was then placed on top of the feeder

layer and allowed to set. The plates were incubated at 37°C in an atmosphere of 10% CO_2 and 5% O_2. The assays were allowed to develop for 11 days and the CFU-A colonies, defined as having a diameter greater than 2mm, were scored. Platelet and CFU-A colony counts of the various treatment groups were compared by Student's t-test.

7.3 Results

7.3.1 Effect of topotecan on the biodistribution of [^{131}I]MIBG.

The influence of prior administration of topotecan on the distribution of [^{131}I]MIBG in tumour-bearing nude mice was determined by measurement of radioactivity in excised tissues (Figure 7-2). Concentration of [^{131}I]MIBG in SK-N-BE(2c) or UVW/NAT tumours was second only to that in adrenals. Previous exposure to topotecan had no effect on [^{131}I]MIBG accumulation by UVW/NAT tumours but induced a modest though insignificant increase in uptake by SK-N-BE(2c) tumours. Similarly, while topotecan treatment induced greater accumulation of [^{131}I]MIBG in adrenals and heart in both groups of tumour-bearing mice, these increases were not significant.

In contrast, the concentration of [^{131}I]MIBG was low in muscle, kidney, lung, thyroid and marrow. In none of these non-sympathetically innervated tissues was there a significant difference in radiopharmaceutical uptake after topotecan administration. Topotecan had no effect on the concentration of activity in bone marrow.

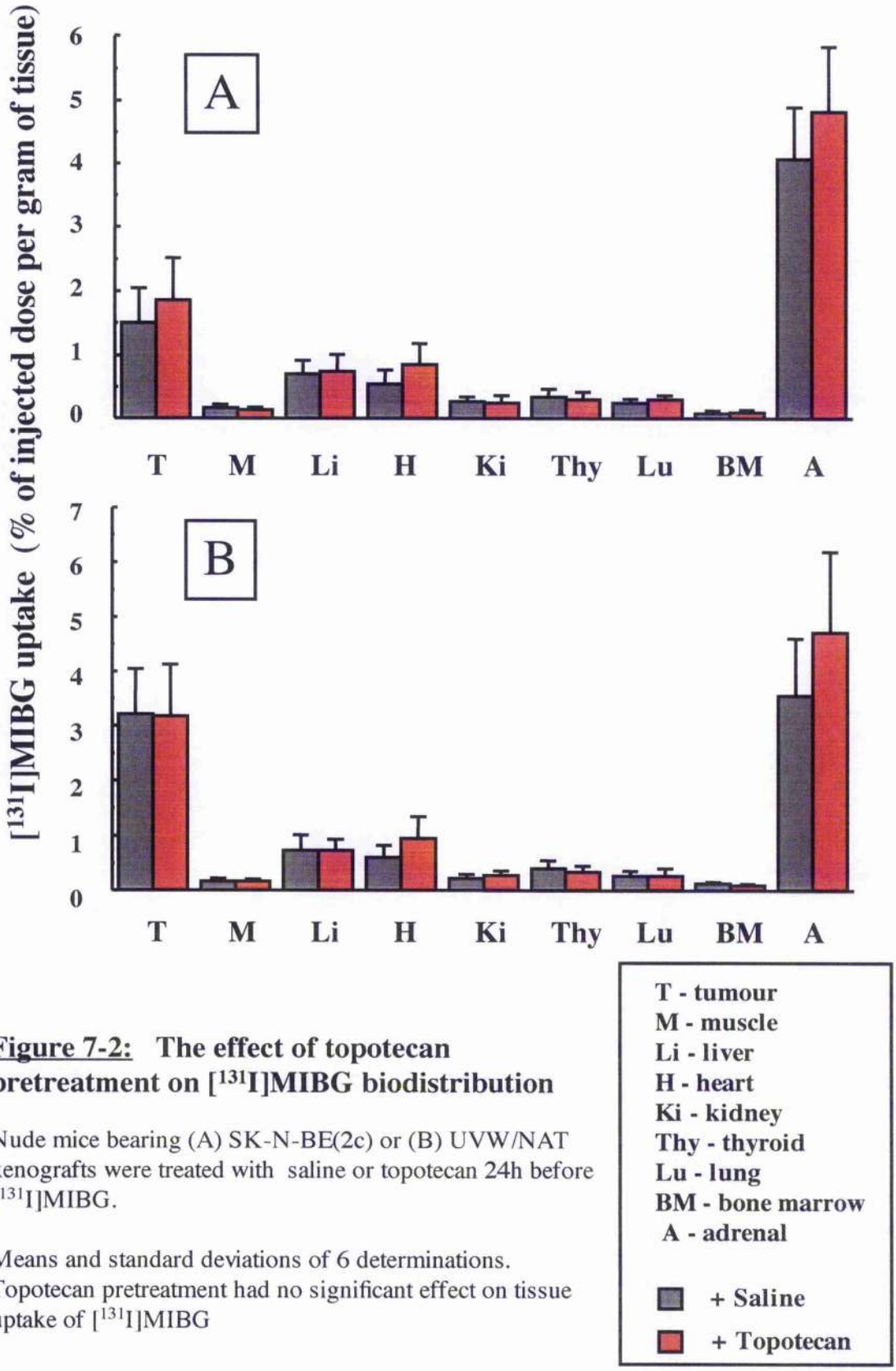

Figure 7-2: The effect of topotecan pretreatment on [^{131}I]MIBG biodistribution

Nude mice bearing (A) SK-N-BE(2c) or (B) UVW/NAT xenografts were treated with saline or topotecan 24h before [^{131}I]MIBG.

Means and standard deviations of 6 determinations. Topotecan pretreatment had no significant effect on tissue uptake of [^{131}I]MIBG

7.3.2 In vivo effects of [^{131}I]MIBG and topotecan alone or combined

None of the animals in this study suffered weight loss. Figure 7-3 shows the effect on the growth of SK-N-BE(2c) tumour xenografts of the administration of topotecan or [^{131}I]MIBG either alone or in combination. Figure 7-4 shows the effects of these same treatment regimens on UVW/NAT tumours. Tumour cure rates are presented in Table 7-1.

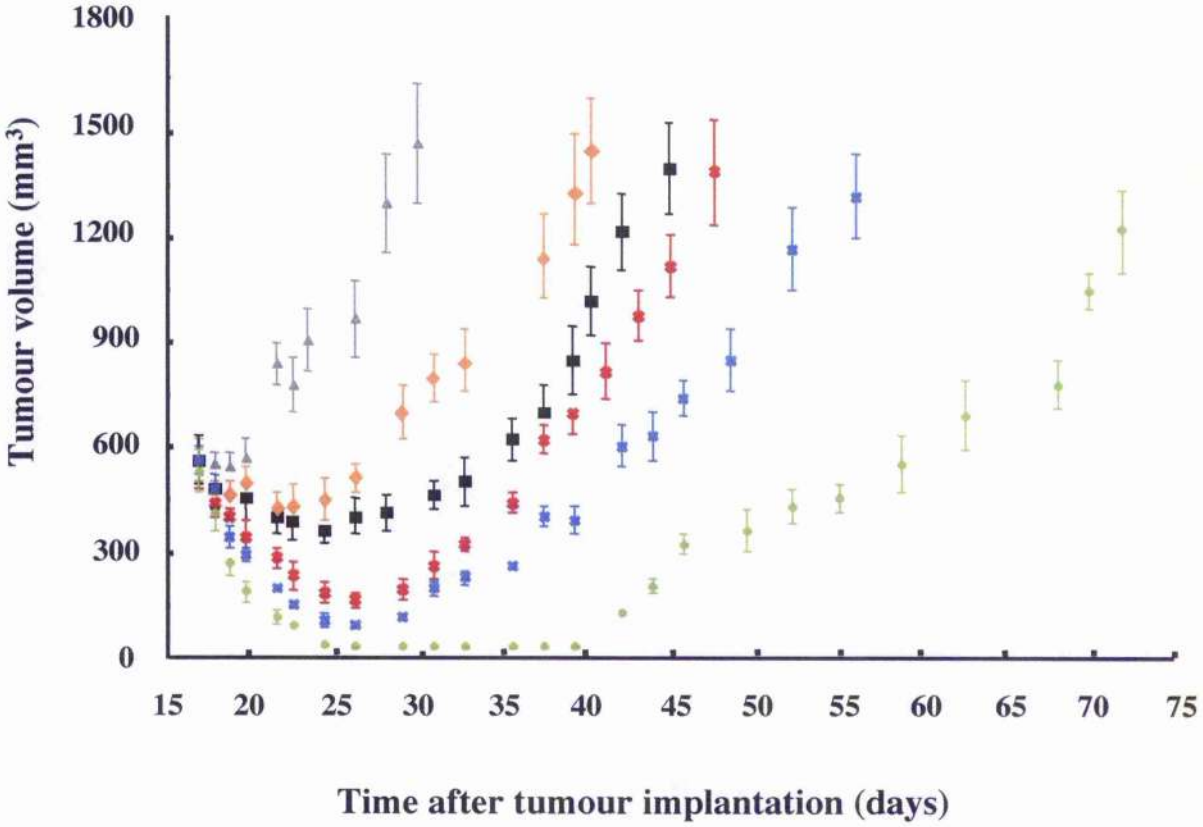

Figure 7-3: Effect of [^{131}I]MIBG and TPT alone and in combination on the growth of SK-N-BE(2c) tumours in nude mice

Treatment was administered 17 days after s.c. implantation of 2-3mm tumour fragments. Each treatment group consisted of 12 animals. Results are mean ± s.d.

no-carrier-added [^{131}I]MIBG concentration was 18MBq, TPT concentration was 1.75mg/kg

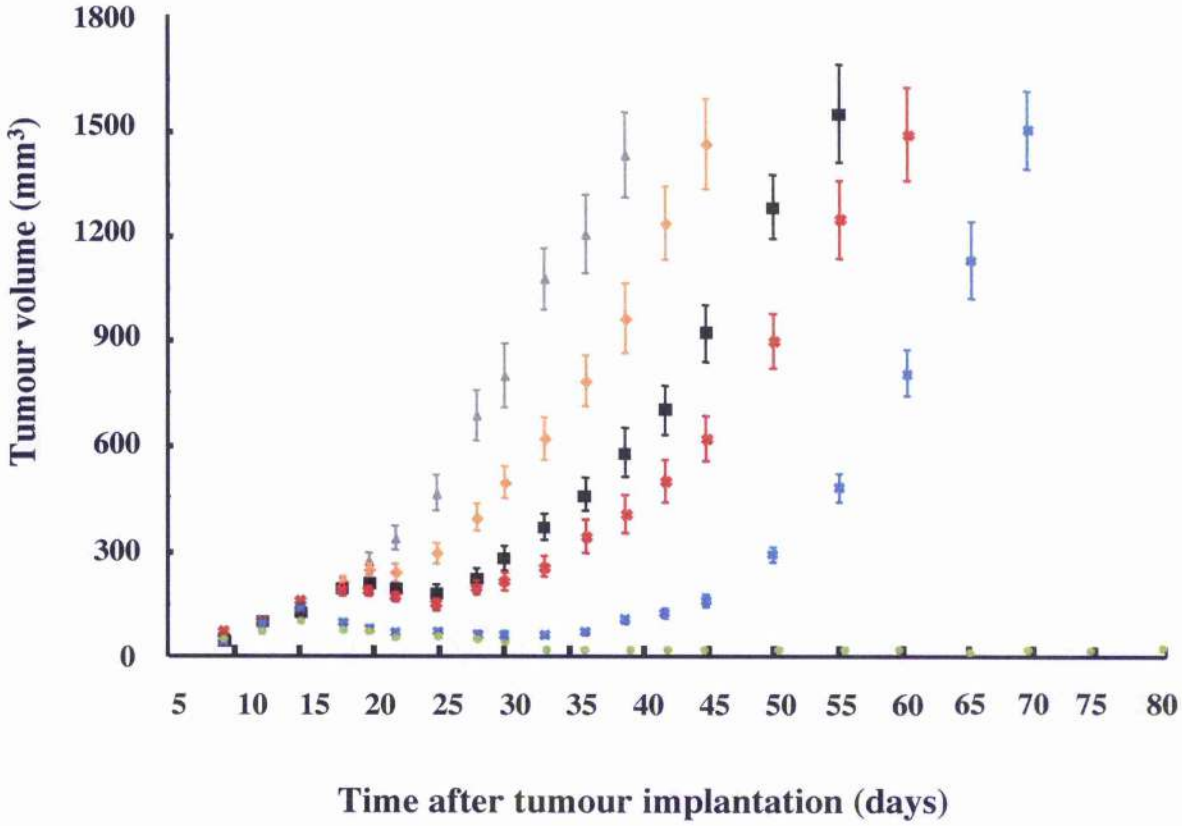

Figure 7-4: Effect of [^{131}I]MIBG and TPT alone and in combination on the growth of UVW/NAT tumours in nude mice

Treatment was administered 9 days after s.c. injection of 1 x10^6 UVW/NAT cells. Each treatment group consisted of 12 animals. Results are mean ± s.d.

no-carrier-added [^{131}I]MIBG concentration was 10MBq, TPT concentration was 1.75mg/kg

7.3.3 SK-N-BE(2c) tumours

The tumours of mice which received i.p. injection of saline (controls) had a volume doubling time (T_2) of 10.4 ± 2.0 days (mean ± s.d.). Single treatments with topotecan or [^{131}I]MIBG significantly increased the T_2 to 19.7 ± 6.6 days ($p < 0.001$) or 22.8 ± 10.1 days ($p < 0.001$) respectively. No complete tumour regression resulted from either single agent therapy.

Combination schedule [i] produced a greater tumour growth delay (T_2 = 26.3 ± 10.3 days) than either drug alone but the difference was not statistically significant. Administration of the two agents by combination schedule [ii] produced a greater T_2 (34.3 ± 8.3 days) than schedule [i] and sterilised 8% of tumours. This schedule was significantly more effective than either topotecan ($p < 0.001$) or [^{131}I]MIBG ($p < 0.01$) given alone.

The most effective tumour control was obtained when the two agents were given simultaneously (combination schedule [iii]). The resulting T_2 (53.2 ± 7.5 days) was significantly greater than those of the other two combination treatments ($p < 0.001$). Schedule [iii] treatment also cured 42% of tumours.

	SK-N-BE(2c)		UVW/NAT	
Treatment	**T_2 (days)**	**cure rate (%)**	**T_{10} (days)**	**cure rate (%)**
saline control	**10.4 ± 2.0**	**0**	**18.6 ± 4.2**	**0**
TPT alone	**19.7 ± 6.6**	**0**	**25.3 ± 6.1**	**17**
[^{131}I]MIBG alone	**22.8 ± 10.1**	**0**	**31.9 ± 7.4**	**50**
Schedule [i]	**26.3 ± 10.3**	**0**	**37.1 ± 12.8**	**50**
Schedule [ii]	**34.3 ± 8.3**	**8**	**49.7 ± 12.0**	**67**
Schedule [iii]	**53.2 ± 7.5**	**42**	**71**	**100**

Table 7-1: Tumour cure and delayed tumour growth resulting from the administration of topotecan or [^{131}I]MIBG alone or in combination

Cure rates are expressed as percentages of animals in each treatment group.

SK-N-BE(2c): T_2 values are the mean number of days ± s.d. required for a doubling of volume of SK-N-BE(2c) tumours.

UVW/NAT: T_{10} values are the mean number of days ± s.d. required for a ten-fold increase in volume of UVW/NAT tumours. All tumours treated simultaneously with topotecan and [^{131}I]MIBG failed to regrow. These were assigned a T_{10} value > 71 corresponding to the day of termination of the experiment.

7.3.4 UVW/NAT tumours

In the saline-treated group of mice, tumours reached a ten-fold increase in volume (T_{10}) in 18.6 ± 4.2 days (mean ± s.d.). None of the tumours in this control group spontaneously regressed.

Tumours treated with topotecan alone had significantly greater T_{10} values than the saline group: 25.3 ± 6.1 days, and two tumours were cured (17%). In mice which received [^{131}I]MIBG alone, a T_{10} of 31.9 ± 7.4 days, and a cure rate of 50% was achieved. Both single agent treatments were significantly more effective than saline (topotecan $p < 0.01$, [^{131}I]MIBG $p < 0.001$).

The T_{10} value (37.1 ± 12.8 days) corresponding to the delivery of [^{131}I]MIBG 24h after injection of topotecan (combination schedule [i]) was greater than those of the groups which received either drug as a single agent, and the cure rate was 50%. However, this improvement was not statistically significant.

When topotecan was administered 24h after [^{131}I]MIBG (combination schedule [ii]), rather than in the reverse order (schedule [i]), an increased T_{10} (49.7 ± 12.0 days) was observed, and 67% of tumours were cured. This represented a significant improvement in efficacy relative to topotecan alone ($p < 0.001$), but not relative to [^{131}I]MIBG alone or relative to schedule [i].

A more dramatic effect was noted when the two agents were given simultaneously (combination schedule [iii]). Unlike combination schedules [i] and [ii], concurrent delivery of [^{131}I]MIBG and topotecan cured all UVW/NAT tumours.

This constituted a significant improvement in efficacy relative to combination schedule [i] as well as both single agent treatments ($p < 0.014$) although not relative to schedule [ii].

7.3.5 Assessment of marrow toxicity of [^{131}I]MIBG alone, and combinations of topotecan and [^{131}I]MIBG

Table 7-2 depicts the bone marrow toxicity associated with combined [^{131}I]MIBG and topotecan treatment in mice hosting SK-N-BE(2c) tumours. Table 7-3 presents the responses of similarly treated UVW/NAT xenografts.

In SK-N-BE(2c) treated with 18MBq of [^{131}I]MIBG, there was a significant decline in colony-forming units and thrombocytes at one week after [^{131}I]MIBG treatment with or without topotecan ($p < 0.01$). No difference in bone marrow toxicity was observed between topotecan and non-topotecan-treated animals. Recovery to normal values was observed at two weeks.

In mice bearing UVW/NAT tumours and treated with 10MBq of [^{131}I]MIBG, no evidence of thrombocytopenia was observed up to 6 weeks after treatment with any of the 3 combination schedules (Table 7-3). There was no significant difference in platelet count between any of the treatment groups. Likewise, the clonogenic potential of pluripotent stem cells was not adversely affected by any of the treatment regimes. While CFU-A colony counts were, in most saline-treated animals, higher than those of the combination treatment groups, these differences did not reach statistical significance.

	Saline control	[^{131}I]MIBG alone	Schedule [i]	Schedule [ii]	Schedule [iii]
Week 1	**7.7 ± 1.7** *976 ± 186*	**3.2 ± 0.9*** *438 ± 107**	**2.4 ± 0.6*** *503 ± 134**	**2.2 ± 0.7*** *475 ± 119**	**2.4 ± 0.7*** *524 ± 172**
Week 2	**9.1 ± 2.2** *1107 ± 262*	**8.1 ± 2.5** *848 ± 288*	**6.8 ± 1.6** *971 ± 218*	**7.0 ± 1.9** *922 ± 204*	**6.4 ± 2.0** *907 ± 293*
Week 3	**8.8 ± 2.1** *1133 ± 304*	**7.3 ± 2.6** *922 ± 154*	**7.7 ± 2.0** *857 ± 202*	**6.8 ± 1.6** *900 ± 139*	**6.6 ± 1.8** *824 ± 173*
Week 6	**7.6 ± 2.5** *1150 ± 249*	**8.3 ± 2.3** *1004 ± 167*	**7.8 ± 1.9** *1036 ± 167*	**8.9 ± 2.7** *902 ± 213*	**6.9 ± 1.9** *855 ± 197*

Table 7-2: CFU-A colony formation and platelet production in SK-N-BE(2c) tumours in nude mice

The effect of combined [^{131}I]MIBG and TPT administration on CFU-A progenitor cells was examined by colony forming assays and were expressed as colonies / 5 x 10^3 cells. Platelet counts were taken from blood collected by heart puncture, and were expressed as counts x 10^9 /l.

Results of CFU-A colony forming assays are stated in **bold type**. Platelet counts are stated in *italics*. All results were analysed by Student's t-test, and are means ± s.d. of 6 determinations. All were not significant except *, where $p < 0.01$.

no-carrier-added [^{131}I]MIBG concentration was 18MBq, TPT concentration was 1.75mg/kg.

	Saline control	[^{131}I]MIBG alone	Schedule [i]	Schedule [ii]	Schedule [iii]
Week 1	**8.8 ± 3.0** *1044 ± 349*	**9.3 ± 2.5** *1108 ± 185*	**7.9 ± 2.6** *1242 ± 317**	**8.2 ± 2.8** *1139 ± 320*	**6.8 ± 1.8** *1087 ± 318*
Week 2	**10.0 ± 4.0** *1255 ± 291*	**8.3 ± 2.0** *1060 ± 235*	**9.4 ± 2.9** *1238 ± 303*	**6.5 ± 2.2** *951 ± 226*	**8.2 ± 1.9** *966 ± 193*
Week 3	**9.7 ± 3.3** *984 ± 240*	**9.0 ± 2.8** *1010 ± 195*	**7.1 ± 1.8** *943 ± 211*	**5.9 ± 2.6** *986 ± 165*	**7.6 ± 2.2** *942 ± 189*
Week 6	**8.5 ± 2.7** *1127 ± 212*	**7.7 ± 1.9** *976 ± 178*	**6.8 ± 1.6** *995 ± 283*	**7.6 ± 2.4** *937 ± 208*	**8.2 ± 2.5** *1220 ± 256*

Table 7-3: CFU-A colony formation and platelet production in UVW/NAT tumours in nude mice

The effect of combined [^{131}I]MIBG and TPT administration on CFU-A progenitor cells was examined by colony forming assays and were expressed as colonies / 5 x 10^3 cells. Platelet counts were taken from blood collected by heart puncture, and were expressed as counts x 10^9 /l.

Results of CFU-A colony forming assays are stated in **bold type**. Platelet counts are stated in *italics*. All results were analysed by Student's t-test, and are means ± s.d. of 6 determinations. All were not significant.

no-carrier-added [^{131}I]MIBG concentration was 10MBq, TPT concentration was 1.75mg/kg.

7.4 Summary of results

In this study, topotecan induced radiosensitisation, resulting in enhanced effectiveness of [^{131}I]MIBG in SK-N-BE(2c) and UVW/NAT xenograft models. However, as with the investigations of combined treatments *in vitro* (Chapters 5 & 6), the effectiveness of combinations of TPT and [^{131}I]MIBG was dependent on scheduling. Schedule [iii] was most effective, while schedule [i] was the least effective scheduled combination.

The dose limiting tissue in neuroblastoma patients treated with [^{131}I]MIBG is bone marrow and toxicity is manifest by prolonged thrombocytopenia [179]. Furthermore, topotecan is also myelotoxic [126]. In this study, combinations of topotecan and [^{131}I]MIBG induced a reduction of platelet numbers and a decrease in the clonogenic capacity of CFU-A stem cells in SK-N-BE(2c) tumour-bearing mice at one week after treatment. However, these indices of marrow integrity returned to normal levels two weeks after treatment. This suggests that, while SK-N-BE(2c) tumour-bearing mice were adversely affected by combination treatments, this effect was transient, and the animals did not exhibit long-term damage to marrow integrity.

These results indicate that it may be possible to increase the efficacy of [^{131}I]MIBG by concomitant or subsequent administration of TPT, without increased toxicity to the bone marrow.

Chapter 8

The effects of topotecan and [^{131}I]MIBG on cellular mechanisms

8.1 Introduction

8.1.1 The effect of topotecan and [^{131}I]MIBG on cell cycle distribution

The established model of TPT action predominantly involves collision of the replication fork with TPT-stabilized Topo I – DNA complexes, resulting in irreversible dsDNA breaks [83, 85]. This suggests that the effectiveness of this drug will be most evident in cells undergoing S-phase [83, 85].

It has previously been reported that cells in late G_1, G_2 and M are more sensitive to ionising radiation than cells in early G_1 and S-phase, possibly due to cell cycle checkpoints leading to repair or apoptosis [186]. However the effect of [^{131}I]MIBG on the cell cycle distribution of NAT expressing cells remains unresolved.

Likewise, the effects of combinations of TPT and [^{131}I]MIBG have not been investigated. A role for Topo I has been postulated in cellular pathways involved in the response to DNA damage, and several studies have suggested Topo I involvement in DNA damage repair [170-175]. This would suggest that administration of DNA damaging agents in conjunction with TPT may induce effects beyond the traditional transcription- and S-phase-related models previously reported, and these additional effects may be reflected in the distribution of cells at different stages of the cell cycle.

In this study, the effects of TPT and [^{131}I]MIBG, either alone or in combination, on the cell cycle distribution of treated cells was assessed using fluorescence-activated cell sorting, or FACS analysis.

8.1.2 The effect of topotecan and [^{131}I]MIBG on topoisomerase I-induced unwinding

Topo I activity during replication prevents torsional stress to the DNA molecule [82, 83]. During transcription, transient unwinding of the DNA helix prevents RNA polymerase generating supercoiled tension in template DNA [187]. Furthermore, a role for Topo I has been postulated in cellular pathways involved in the response to DNA damage. Several studies have suggested Topo I involvement in DNA damage repair and have reported a decrease in Topo I - mediated unwinding of supercoiled DNA following irradiation [161, 170-175, 188]. However, the effect of [^{131}I]MIBG on Topo I activity is unresolved. Likewise, the effects of [^{131}I]MIBG in combination with TPT on the efficiency of Topo I-induced unwinding is, to date, unknown. In this study, the effects of TPT and [^{131}I]MIBG, either alone or in combination, on topoisomerase I activity was assessed by Topo I relaxation assay (see Section 4.2.1).

8.2 Materials & methods

8.2.1 Cell Lines

SK-N-BE(2c) and UVW/NAT cells were seeded at a density of 4 x 10^3 cells/cm^2 in 75cm^2 flasks (Iwaki® products, Bibby Sterilin Ltd. Staffordshire, UK) and grown in RPMI 1640 medium containing 200mM L-glutamine, 25mM HEPES and 10% FCS at 37°C and 5% CO_2. All media and supplements were obtained from Invitrogen (Paisley, UK). After 48h, fresh media was added to the cells, containing either topotecan, [^{131}I]MIBG or a scheduled combination of both agents. Following treatment, cells were analysed by flow cytometry and Topo I relaxation assay.

8.2.2 Concentrations and incubation times of TPT and [^{131}I]MIBG

The doses of TPT and [^{131}I]MIBG employed in studies of DNA damage and repair were the doses of each agent required to reduce clonogenic survival to 50% of control cultures, as determined by clonogenic assay (see Chapter 4). For the treatment of SK-N-BE(2c) cells, [^{131}I]MIBG concentration was 4 MBq/ml, and topotecan concentration was 2ng/ml. For UVW/NAT cells, [^{131}I]MIBG concentration was 4.1MBq/ml and TPT concentration was 4.2ng/ml.

The incubation times of TPT and [^{131}I]MIBG used in this study were the same as those used for investigations of *in vitro* cytotoxicity, as described in Section 4.2.2. Briefly, [^{131}I]MIBG incubation time was 2h, after which uptake is maximal [154], followed by a further 24h in fresh media to allow for the accumulation of damage due to the radiological bystander effect [17].

TPT incubation time was 24h, which has previously produced optimal supra-additive killing of cells treated with TPT and external beam irradiation [139].

8.2.3 Scheduled combinations of TPT and [^{131}I]MIBG

As with investigations of the toxic effects of these agents (see Chapters 5, 6 &7), three treatment modalities were investigated. In schedule [i] topotecan was administered 24 hours before [^{131}I]MIBG treatment. In schedule [ii] topotecan was administered 24 hours after [^{131}I]MIBG treatment. In schedule [iii] topotecan and [^{131}I]MIBG were administered simultaneously. See Figure 5-3.

8.2.4 FACS analysis

Following treatment, cells were trypsinised and counted. Cells were washed twice with PBS (centrifugation was 4mins at 1500RPM) and resuspended in PBS at a concentration of 1 x 10^6 cells/ml. Cells were fixed by addition of 100% ethanol at 4°C (3ml per 1 x 10^6 cells), so that the final concentration of ethanol was 75%. Cells were incubated for 1h at 4°C.

Fixed cells were centrifuged at 1750RPM for 7mins, and washed twice with PBS. Cell pellets were resuspended in 1ml PBS containing 50ug/ml Propidium Iodide (Sigma chemicals, Dorset UK). RNase A (Qiagen Ltd. W. Sussex, UK) was added to a final concentration of 5ug/ml, and cells were stained for 3h at 4°C before analysis by flow cytometry. Analysis was carried out using a BD FACScan analyser (Becton Dickinson Systems, Cowley, UK), and results were analysed using BD CellQuest™ Pro software, version 5.1.1.

8.2.5 Topoisomerase I relaxation assays

Following treatment, topoisomerase I was extracted from SK-N-BE(2c) and UVW/NAT cells, and Topo I activity was determined using the Topoisomerase I Assay Kit (Topogen Inc, Columbus, Ohio, USA) as described in Section 4.2.1.

8.3 Results

8.3.1 Cell cycle distribution of SK-N-BE(2c) and UVW/NAT cells

The proportions of SK-N-BE(2c) and UVW/NAT cells in different phases of the cell cycle, assessed by flow cytometry are shown in Figure 8-1. Of the two cell lines, a higher percentage of SK-N-BE(2c) than UVW/NAT cells were in G_1 (75.13 ± 0.29%, compared to 62.56 ± 0.53% of UVW/NAT cells). Conversely, a higher proportion of UVW/NAT cells were undergoing DNA replication and mitosis. 10.47 ± 0.25% of SK-N-BE(2c) cells were in S-phase, compared to 12.26 ± 0.24% of UVW/NAT cells. 11.79 ± 0.45% of SK-N-BE(2c) cells were in G_2/M, compared to 21.22 ± 0.64% of UVW/NAT cells.

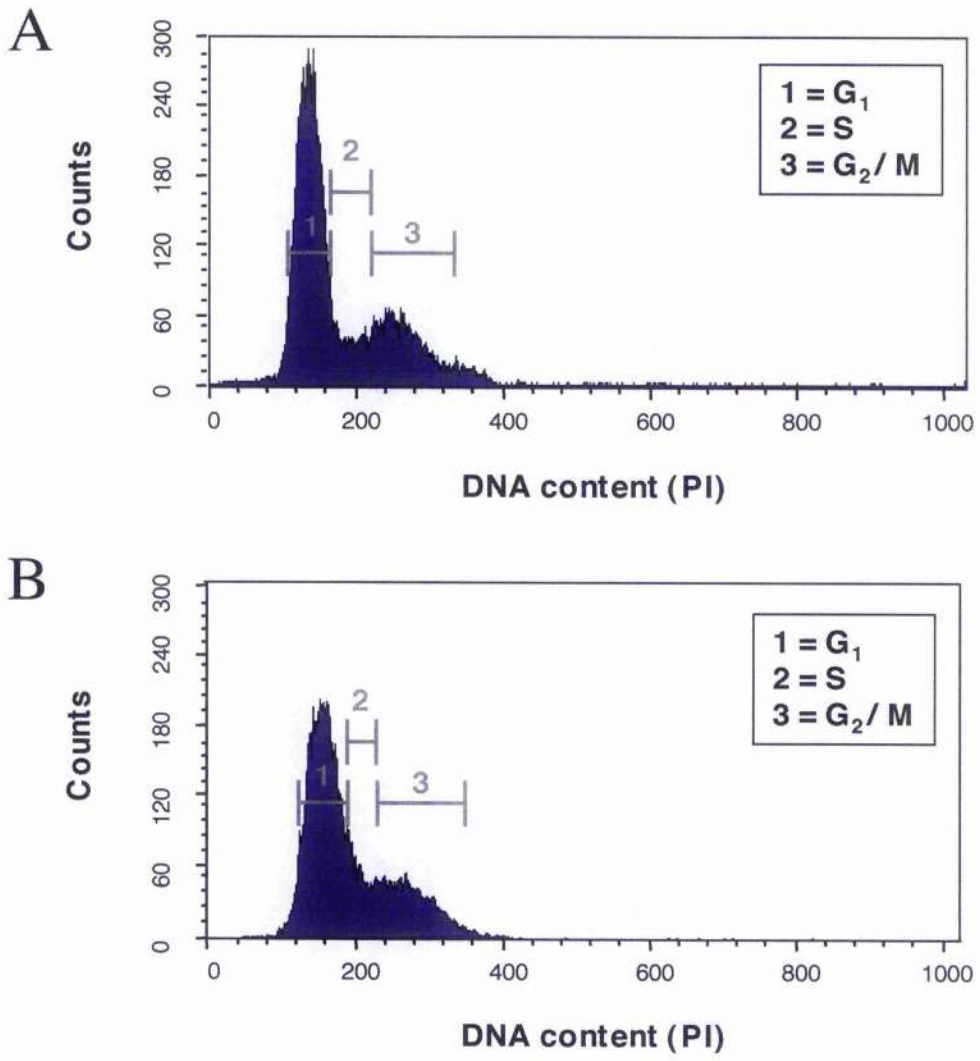

Figure 8-1: The cell cycle distribution of SK-N-BE(2c) and UVW/NAT cells

The proportions of (**A**) SK-N-BE(2c) and (**B**) UVW/NAT cells in different phases of the cell cycle, assessed by flow cytometry. Each determination was carried out in triplicate. Results are mean ± sd of 15000 cells and are presented as the percentage of total cells counted. Proportions are shown as G_1:S:G_2/M:

(**A**) 75.13 ± 0.29 : 10.47 ± 0.25 : 11.79 ± 0.45
(**B**) 62.56 ± 0.53 : 12.26 ± 0.24 : 21.22 ± 0.64

Of the two cell lines, a higher percentage of SK-N-BE(2c) cells were in G_1, whereas a higher proportion of UVW/NAT cells were undergoing cell division and mitosis.

8.3.2 The effects on cell cycle distribution of topotecan and [^{131}I]MIBG as single agents

8.3.2-1 SK-N-BE(2c)

The effects of TPT and [^{131}I]MIBG as single agents on the cell cycle distribution of SK-N-BE(2c) cells are shown in Figure 8-2. Treatment by TPT alone induced a reduction in the percentage of cells in G_1, from 75.13 ± 0.29% to 43.65 ± 2.15%. A contemporaneous increase in the percentage of cells in S-phase was observed following TPT treatment, from 10.47 ± 0.25% to 19.92 ± 0.46%, as was an increase in the proportion of cells in G_2/M, from 11.79 ± 0.45% to 33.27 ± 1.46%.

Administration of [^{131}I]MIBG alone also reduced the percentage of cells in G_1, from 75.13 ± 0.29% to 56.07 ± 0.38%. Therefore, [^{131}I]MIBG was less effective than TPT at reducing the distribution of cells in G_1. Similarly, while administration of [^{131}I]MIBG alone induced an increase in the proportion of cells in both S-phase (from 10.47 ± 0.25 to 17.45 ± 0.43%), and G_2/M (from 11.79 ± 0.45% to 22.69 ± 0.27%), this was less effective than TPT alone.

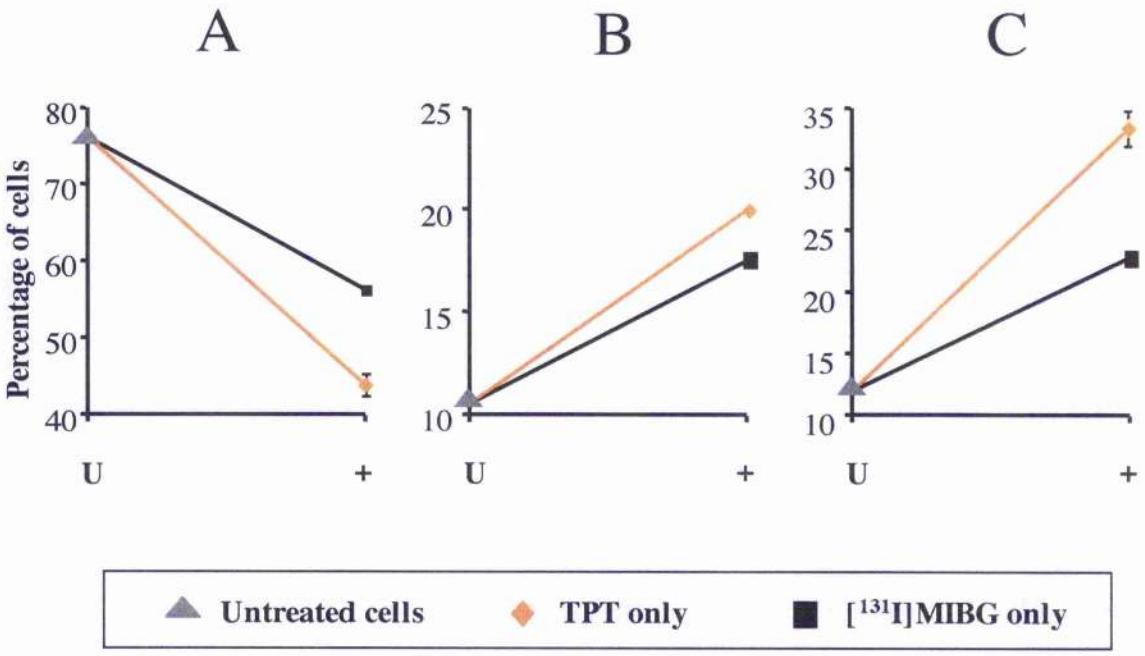

Figure 8-2: The effect of TPT and [^{131}I]MIBG administration on the cell cycle distribution of SK-N-BE(2c) cells

This figure shows the cell cycle distribution of untreated SK-N-BE(2c) cells (**U**) and the effect on the distribution of treatment with TPT or [^{131}I]MIBG (**+**).

In the above figures, the percentage of cells in G_1, S and G_2/M are shown in (A), (B) and (C) respectively.

Treatment by either agent alone induced a reduction in the percentage of cells in G_1, and an increase in the percentage in S-phase and in G_2/M. TPT reduced a higher percentage of cells in G_1 than [^{131}I]MIBG, and increased the proportion of cells in both S-phase and G_2/M:

Topotecan treated cells (G_1:S:G_2/M) - 43.65 ± 2.15 : 19.92 ± 0.46 : 33.27 ± 1.46)
[^{131}I]MIBG treated cells (G_1:S:G_2/M) - 56.07 ± 0.38 : 17.45 ± 0.43 : 22.69 ± 0.27)

8.3.2-2 UVW/NAT

The effects of TPT and [^{131}I]MIBG as single agents on the cell cycle distribution of UVW/NAT cells are shown in Figure 8-3. Results obtained following administration of TPT or [^{131}I]MIBG as single agents were similar to those observed in SK-N-BE(2c) cells. Treatment by TPT reduced the proportion of UVW/NAT cells in G_1-phase from 62.56 ± 0.53% to 24.15 ± 0.50%, and increased the percentage of cells in S-phase and G_2/M from 12.26 ± 0.24% and 21.22 ± 0.64% to 16.32 ± 0.12% and 57.86 ± 0.25% respectively.

Furthermore, while administration of [^{131}I]MIBG alone also reduced the percentage of cells in G_1 (from 62.56 ± 0.53% to 50.65 ± 0.16), and increased the proportions in S-phase (from 12.26 ± 0.24% to 15.06 ± 0.49%) and G_2/M (from 21.22 ± 0.64% to 31.81 ± 0.53%), the changes induced by administration of [^{131}I]MIBG were not as pronounced as the cell cycle distribution changes induced by TPT.

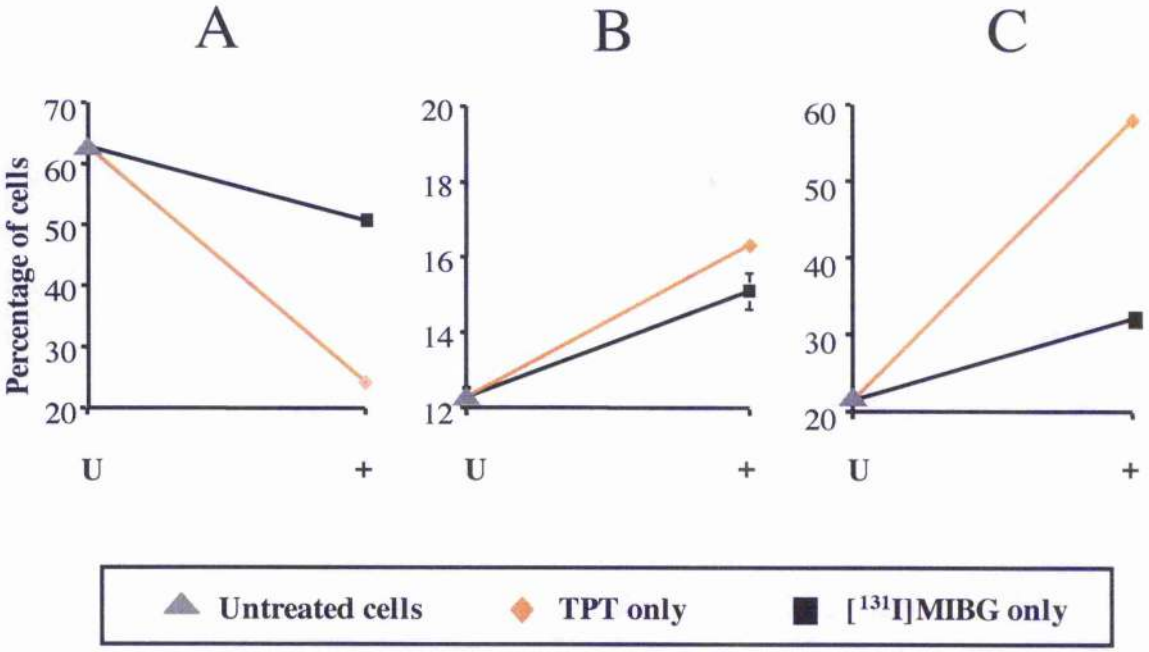

Figure 8-3: The effect of TPT and [^{131}I]MIBG administration on the cell cycle distribution of UVW/NAT cells

This figure shows the cell cycle distribution of untreated UVW/NAT cells (**U**) and the effect on the distribution of treatment with TPT or [^{131}I]MIBG (**+**).

As in Figure 8-2, in the above figures, the percentage of cells in G_1, S and G_2/M are shown in (A), (B) and (C) respectively.

Results were similar to those observed in SK-N-BE(2c) cells. Treatment by either agent alone induced a reduction in the percentage of cells in G_1, and an increase in the percentage in S-phase and in G_2/M. Again, in UVW/NAT cells, TPT reduced a higher percentage of cells in G_1 than [^{131}I]MIBG, and increased the proportion of cells in both S-phase and G_2/M:

Topotecan treated cells (G_1:S:G_2/M) - 24.15 ± 0.50 : 16.32 ± 0.12 : 57.86 ± 0.25)
[^{131}I]MIBG treated cells (G_1:S:G_2/M) - 50.65 ± 0.16 : 15.06 ± 0.49 : 31.81 ± 0.53)

8.3.3 The effect of combinations of TPT and [^{131}I]MIBG on cell cycle distribution

8.3.3.1 SK-N-BE(2c)

The effects of combinations of TPT and [^{131}I]MIBG on the cell cycle distribution of SK-N-BE(2c) cells are shown in Figure 8-4. As with the effects of either agent alone, administration of all three combination schedules induced a similar reduction in the percentage of cells in G_1, and an increase in the percentage in both S-phase and in G_2/M. Schedule [i] induced a greater accumulation of cells in S-phase than either agent alone, or schedules [ii] or [iii].

No combination schedule was as effective as TPT as a single agent at increasing accumulation of cells in G_2/M. However, all three combination schedules were more effective than [^{131}I]MIBG alone at increasing accumulation of cells in G_2/M. Interestingly, while administration of combination schedules [ii] and [iii] induced identical changes in S- and G_2/M-phase distribution, schedule [i] administration was more effective at inducing S-phase arrest, and less effective at increasing G_2/M accumulation.

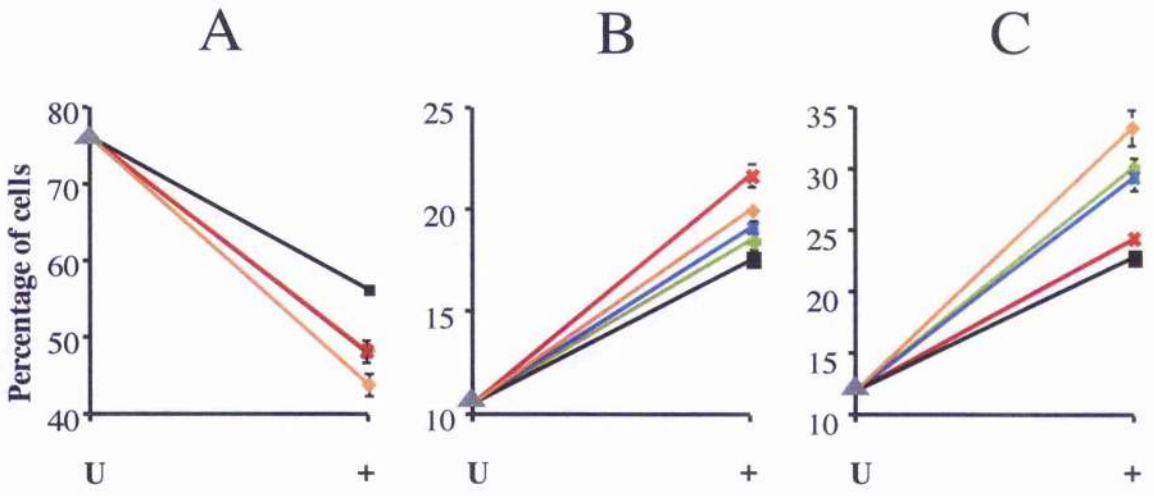

Figure 8-4: The effect of combinations of TPT and [^{131}I]MIBG on the cell cycle distribution of SK-N-BE(2c) cells

This figure shows the results from Figure 8-2, along with the results obtained by the three scheduled combinations of TPT and [^{131}I]MIBG.

Again, the percentage of cells in G_1, S and G_2/M are shown in (A), (B) and (C) respectively.

As with the effects of either agent alone, administration of all three combination schedules induced a reduction in the percentage of cells in G_1, and an increase in the percentage in both S-phase and in G_2/M. Schedule [i] induced a greater accumulation of cells in S-phase than either agent alone, or schedules [ii] or [iii]. However, no combination schedule was as effective as TPT as a single agent at increasing accumulation of cells in G_2/M.

Interestingly, while administration of schedules [ii] and [iii] resulted in similar alterations in cell cycle distribution, schedule [i] administration did not alter the percentage of cells in each phase in the same way, suggesting that cells may be responding to schedule [i] treatment differently.

Schedule [i] (G_1:S:G_2/M) - 47.75 ± 0.80 : 21.64 ± 0.58 : 24.17 ± 0.38
Schedule [ii] (G_1:S:G_2/M) - 47.62 ± 0.33 : 19.06 ± 0.70 : 29.20 ± 0.51
Schedule [iii] (G_1:S:G_2/M) - 47.99 ± 0.23 : 18.42 ± 0.48 : 30.06 ± 0.65

8.3.3-2 UVW/NAT

The effects of combinations of TPT and [^{131}I]MIBG on the cell cycle distribution of UVW/NAT cells are shown in Figure 8-5. Again, administration of all three combination schedules induced a reduction in the percentage of cells in G_1, and an increased cell distribution in S-phase and in G_2/M. Unlike SK-N-BE(2c) cells, in UVW/NAT cells, all three combination schedules induced a greater accumulation of cells in S-phase than either agent alone. Again, no combination schedule was as effective as TPT as a single agent at increasing accumulation of cells in G_2/M. However, all three combination schedules were more effective than [^{131}I]MIBG alone at increasing the proportion of cells in the G_2/M compartment.

Administration of combination schedules [ii] and [iii] induced identical changes in S-phase and G_2/M distribution in UVW/NAT cells, whereas schedule [i] administration was more effective than schedules [ii] and [iii] at inducing S-phase accumulation, and less effective at inducing G_2/M accumulation.

8.3.4 The effects of TPT and [^{131}I]MIBG on topoisomerase I activity

Topo I extracted from SK-N-BE(2c) and UVW/NAT cells treated with of TPT or [^{131}I]MIBG as single agents, exhibited a reduced ability to induce relaxation of the supercoiled pHOT-1 plasmid. Likewise, Topo I isolated from cells treated with all three combination schedules had a reduced unwinding efficiency (Table 8-1).

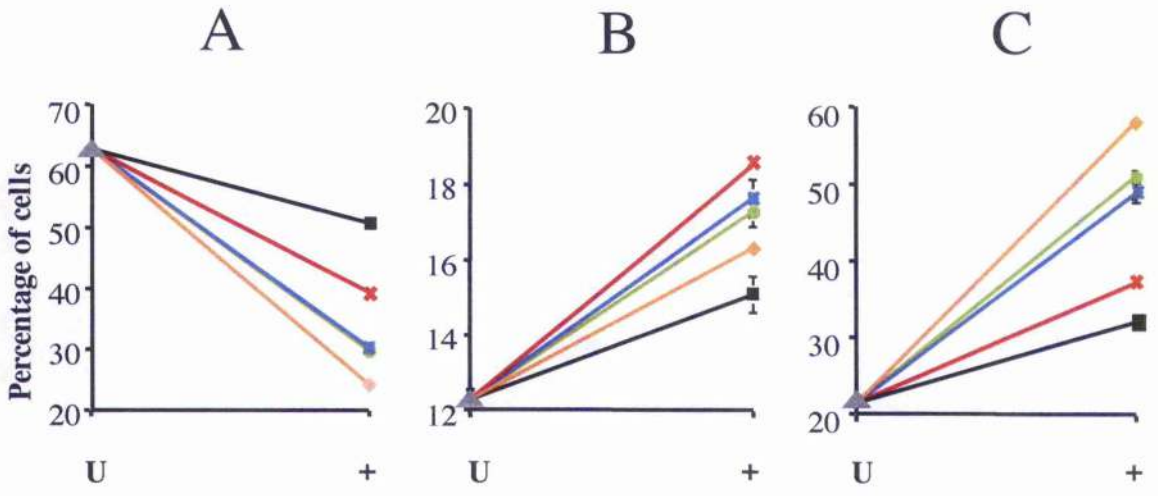

Figure 8-5: The effect of combinations of TPT and [^{131}I]MIBG on the cell cycle distribution of UVW/NAT cells

This figure shows the results from Figure 8-3, along with the results obtained by the three scheduled combinations of TPT and [^{131}I]MIBG.

Again, the percentage of cells in G_1, S and G_2/M are shown in (A), (B) and (C) respectively.

Administration of all three combination schedules induced a reduction in the percentage of cells in G_1, and an increase in the percentage in both S-phase and in G_2/M. Again, schedule [i] induced a greater accumulation of cells in S-phase than either agent alone, or schedules [ii] or [iii]. However, unlike SK-N-BE(2c) cells, in UVW/NAT cells, schedules [ii] and [iii] were also more effective than TPT alone at increasing accumulation in S-phase. Again, no combination schedule was as effective as TPT as a single agent at increasing accumulation of cells in G_2/M.

Also, as with SK-N-BE(2c) cells, administration of schedule [i] altered cell cycle distribution of UVW/NAT cells in a different way to schedules [ii] and [iii], suggesting that cells treated by schedules [ii] and [iii] may be responding differently to cells treated by schedule [i].

Schedule [i] (G_1:S:G_2/M) - 39.35 ± 0.36 : 18.49 ± 0.05 : 37.05 ± 0.27
Schedule [ii] (G_1:S:G_2/M) - 30.06 ± 0.59 : 17.61 ± 0.49 : 49.78 ± 1.01
Schedule [iii] (G_1:S:G_2/M) - 29.72 ± 0.35 : 17.25 ± 0.40 : 50.97 ± 0.47

	SK-N-BE(2c)	UVW/NAT
Untreated control	**1.01**	**1.99**
TPT only	**0.56**	**1.11**
[^{131}I]MIBG only	**0.49**	**1.21**
Schedule [i]	**0.46**	**1.55**
Schedule [ii]	**0.63**	**1.86**
Schedule [iii]	**0.48**	**1.64**

Table 8-1: Effect of TPT and [^{131}I]MIBG on topoisomerase I levels in SK-N-BE(2c) and UVW/NAT cells

This table shows the effects of TPT and [^{131}I]MIBG on Topo I levels in SK-N-BE(2c) and UVW/NAT cells, found by Topo I relaxation assay.

TPT and [^{131}I]MIBG, either alone or in combination, induced a reduction in the ability of Topo I isolated from treated SK-N-BE(2c) and UVW/NAT cells to unwind supercoiled DNA.

8.4 Summary of results

Of the two cell lines, a higher percentage of SK-N-BE(2c) than UVW/NAT cells were in G_1 (75.13 ± 0.29%, compared to 62.56 ± 0.53%), while a higher proportion of UVW/NAT cells were undergoing DNA replication and mitosis (for SK-N-BE(2c) cells, S-phase and G_2/M proportions were 10.47 ± 0.25% and 11.79 ± 0.45% respectively; for UVW/NAT S-phase and G_2/M proportions were 12.26 ± 0.24% and 21.22 ± 0.64% respectively).

In both cell lines, administration of TPT as a single agent resulted in a reduction in the proportion of cells in G_1, and a concurrent increase in accumulation of cells in S- and G_2/M-phases. The effects of TPT are consistent with reduced progression through S-phase, and G_2 arrest that has previously been reported following administration of topisomerase I inhibitors [189-191].

To date, there has been no investigation into the effects of [^{131}I]MIBG on cell cycle distribution. This study confirmed that [^{131}I]MIBG also reduced the percentage of cells in G_1-phase and increased the proportion of cells in the remaining cell cycle compartments. The ability of [^{131}I]MIBG to induce reduction in the proportion of cells in G_1, and increase accumulation in G_2/M observed in SK-N-BE(2c) and UVW/NAT cells is consistent with previously reported effects of ionising radiation, which is most effective against cells in late G_1-, G_2- and M-phase [186].

Following administration of schedule [ii], the percentage of SK-N-BE(2c) cells in different cell cycle compartments (G_1-, S- and G_2/M-phases) were 47.62 ± 0.33%, 19.06 ± 0.70% and 29.20 ± 0.51% respectively. A similar distribution was observed following schedule [iii] treatment (G_1-, S- and G_2/M-phase proportions were 47.99 ± 0.23%, 18.42 ± 0.48%, and 30.06 ± 0.65% respectively). However, schedule [i] administration did not

alter the percentage of SK-N-BE(2c) cells in each phase in the same way (G_1-, S- and G_2/M-phase proportions were 47.75 ± 0.80%, 21.64 ± 0.58% and 24.17 ± 0.38% respectively). This suggests that there may be a qualitative difference between the cellular response to schedule [i] treatment and the response to administration of schedules [ii] and [iii].

Similar results were obtained from the treatment of UVW/NAT cells. Administration of schedule [ii] and schedule [iii] induced comparable alterations in the percentages of cells in different cell cycle compartments (schedule [ii] ratios were 30.06 ± 0.59%, 17.61 ± 0.49% and 49.78 ± 1.01% for G_1-, S- and G_2/M-phases respectively, and schedule [iii] ratios were 29.72 ± 0.35%, 17.25 ± 0.40% and 50.97 ± 0.47% respectively). However, as with SK-N-BE(2c) cells, schedule [i] administration did not alter the percentage of UVW/NAT cells in each phase in the same way (G_1-, S- and G_2/M-phase proportions were 39.35 ± 0.36%, 18.49 ± 0.05% and 37.05 ± 0.27% respectively), again suggesting a qualitative difference to the effects caused by schedule [i] administration.

Administration of TPT and [^{131}I]MIBG, either as single agents, or in any scheduled combination, induced a reduction in Topo I-mediated unwinding of supercoiled DNA. TPT-induced reduction in unwinding efficiency is in agreement with previously reported effects of camptothecin analogues, and it is hypothesised that this is caused by stabilisation of the Topo I - DNA cleavable complex, which keeps Topo I molecules irreversibly bound to DNA [85]. This reduces the amount of free Topo I in these cells, and therefore the amount of free enzyme in nuclear extracts used to assess Topo I activity.

[^{131}I]MIBG also caused a reduction in Topo I-induced relaxation. This is in agreement with previously reported effects of ionising radiation, which induced a down-regulation in Topo I catalytic activity in cells attempting DNA repair [161, 188].

Chapter 9

The effects of topotecan and [^{131}I]MIBG on DNA damage and repair

9.1 Introduction

9.1.1 The effect of topotecan on DNA damage

Previous studies have reported synergistic cell killing *in vitro* by ionising radiation and Topo I inhibitors [85, 137-141], associated with increases in topoisomerase I binding to DNA, and formation of double strand breaks (DSBs) [85, 136, 170-172]. To date, no attempt has been made to study whether topotecan can affect the number of DNA lesions caused by targeted radionuclide therapy using [^{131}I]MIBG.

To assess the effect of topotecan on [^{131}I]MIBG-induced DNA strand breaks, two NAT expressing cell lines, the neuroblastoma cell line SK-N-BE(2c) and the NAT gene-transfected glioblastoma cell line UVW/NAT, were dosed with [^{131}I]MIBG and/or TPT to cause DNA damage. Cells were then assayed for DNA strand breaks either immediately after treatment, or following a 24h incubation, to allow for DNA repair.

9.1.2 Single cell gel electrophoresis (SCGE) assay

Cells were assayed for DNA strand breaks using the single cell gel electrophoresis (SCGE), or the comet assay. In this method, individual damaged cells are embedded in agarose on a microscope slide. The cells are lysed and the cellular contents removed, with the exception of nuclear material, which is subjected to mild alkaline conditions. This causes partial DNA unwinding from DNA strand break points.

The cells are then electrophoresed. The electrical current causes DNA to migrate towards the anode. Therefore cells with increased DNA damage display increased DNA migration, leading to the distinctive "comet tail" which gives the assay its name [192] (see Figure 9-1).

A

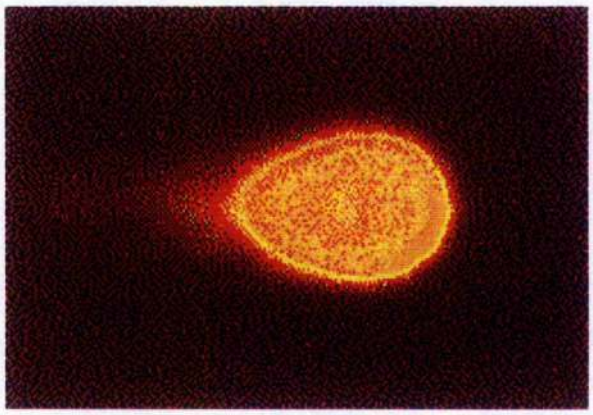

B

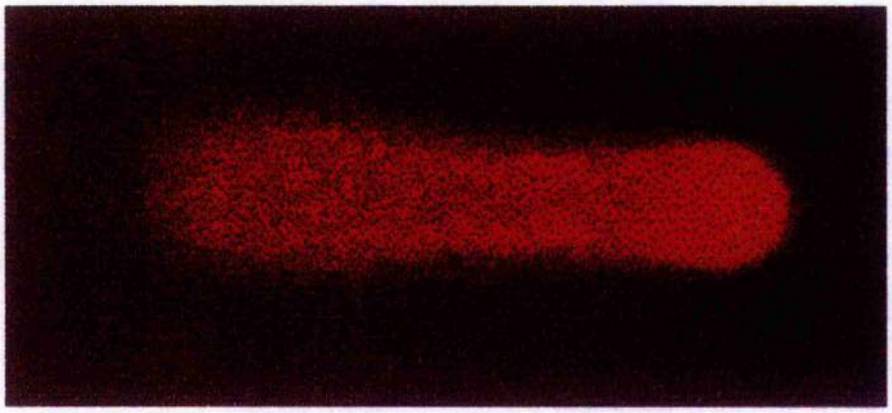

Figure 9-1: Single cell gel electrophoresis assay (comet assay)

This figure shows examples of cells that have been subjected to single cell gel electrophoresis, also known as the comet assay.

In this method, individual damaged cells are embedded in agarose on microscope slides. After lysis and DNA unwinding, cells are electrophoresed, causing DNA to migrate towards the anode.

Cells with larger amounts of DNA damage display increased DNA migration, leading to the distinctive "comet tail" which gives the assay its name.

In the examples below, (A) shows a cell with minimal DNA damage, while (B) shows a cell with extensive DNA damage.

9.2 Materials & methods

9.2.1 Cell lines

SK-N-BE(2c) and UVW/NAT cells were seeded at a density of 1 x 10^3 cells/cm^2 in 25cm^2 flasks (Nunclon Plastics, Denmark) and grown in RPMI 1640 medium containing 200mM L-glutamine, 25mM HEPES and 10% FCS at 37°C and 5% CO_2. All media and supplements were obtained from Invitrogen (Paisley, UK). After 48 hours, fresh media was added to the cells, containing either topotecan, [^{131}I]MIBG or a scheduled combination of both agents.

9.2.2 Concentrations and incubation times of TPT and [^{131}I]MIBG

The doses of TPT and [^{131}I]MIBG employed in studies of DNA damage and repair were the doses of each agent required to reduce clonogenic survival to 50% of control cultures, as determined by clonogenic assay (see Chapter 4). For the treatment of SK-N-BE(2c) cells, [^{131}I]MIBG concentration was 4 MBq/ml, and topotecan concentration was 2ng/ml. For UVW/NAT cells, [^{131}I]MIBG concentration was 4.1MBq/ml and TPT concentration was 4.2ng/ml.

The incubation time was 2h for [^{131}I]MIBG, after which uptake is maximal [154]. For TPT, incubation time was 24h, which has previously produced optimal supra-additive killing of cells treated with TPT and external beam irradiation [139]. Adopting a similar drug exposure procedure allowed comparison of published data with the results of combined TPT and [^{131}I]MIBG–induced cytotoxicity reported in Chapters 5 & 6.

9.2.3 Scheduling of topotecan and [^{131}I]MIBG treatments

As previously discussed, although synergistic cell killing *in vitro* and *in vivo* by ionising radiation and Topo I inhibitors have been widely reported, there is no consensus with respect to the order of delivery of these therapeutic agents (see Table 5-1).

Therefore, the three combination treatment schedules utilised in *in vitro* and *in vivo* analyses of the cytotoxic interaction between topotecan and [^{131}I]MIBG were assessed for their potential to induce DNA framentation and inhibit DNA damage repair. Again, in schedule [i] topotecan was administered 24 hours before [^{131}I]MIBG treatment. In schedule [ii] topotecan was administered 24 hours after [^{131}I]MIBG treatment. In schedule [iii] topotecan and [^{131}I]MIBG were administered simultaneously. See Figure 5-3.

Following treatment, cells were either assayed by single cell electrophoresis immediately, or incubated in fresh medium for a further 24h to allow for possible repair of DNA damage before assaying.

9.2.4 SCGE assay

SCGE assays were carried out using the Trevigen CometAssay™ Single Cell Electrophoresis Assay kit (Trevigen Inc. Gaithersburg, Maryland, USA), according to the manufacturer's instructions. Briefly, cells at a concentration of 5 x 10^5 cells/ml were combined at a ratio of 1:10 with low melting point agarose (LMAgarose). 75μl of this LMAgarose/cell mixture was pipetted onto a Trevigen Cometslide™, and stored at 4°C to set. Slides were immersed in lysis solution (2.5M Na Cl, 100mM EDTA pH 10, 10mM Tris base, 1% sodium lauryl sarcosinate, 1% Triton X-100), then immersed in alkaline solution (300mM Na OH, 1mM EDTA) followed by electrophoresis in 1 x TBE buffer (0.089M Tris base 0.089M Boric acid, 0.02M EDTA, pH 8.0) for 10 mins at 1 volt/cm.

Slides were stained with 1 x SYBR® Green solution (Trevigen Inc) and examined by fluorescence microscopy (435-500nm) using a Zeiss Axiovert inverted microscope (Carl Zeiss Ltd, Welwyn Garden City, Hertfordshire UK). Images were captured by a Zeiss MC 100 SPOT camera, and saved by Axiovision 3.0.6.1 software. Comets were measured by NIH Image 1.57 software, using the methodology described previously by Geller et al. [193].

Statistical analyses of results were carried out using software freely available online at the SISA (Simple Interactive Statistical Analysis) website [194], and the VassarStats: Statistical computation website [195]. The mean number of comets analysed in each treatment group was 120 and 110 for SK-N-BE(2c) and UVW/NAT cells respectively.

9.3 Results

9.3.1 Analysis of DNA fragmentation

The amount of cellular DNA damage present in each comet was measured by tail moment (originally defined as the median distance migrated by the DNA multiplied by the fraction of DNA in the comet tail), as described by Olive, et al. [196, 197].

The results of combination treatments of SK-N-BE(2c) and UVW/NAT cells are shown in Figures 9-2 and 9-3 respectively. Each spike represents an individual comet moment, expressed as arbitrary units (au), where 1au equals one percent of the median tail moment in untreated controls.

The mean number of SK-N-BE(2c) comets analysed per treatment group was 120. The mean number of UVW/NAT comets analysed per treatment group was 110.

A wide variation in tail moment values was observed for both cell lines. For example, untreated SK-N-BE(2c) cells tested at 0h exhibited tail moments ranging from 2.985au to 450.03au. Untreated UVW/NAT cells tested at 0h exhibited tail moments ranging from 4.68au to 1737.58au.

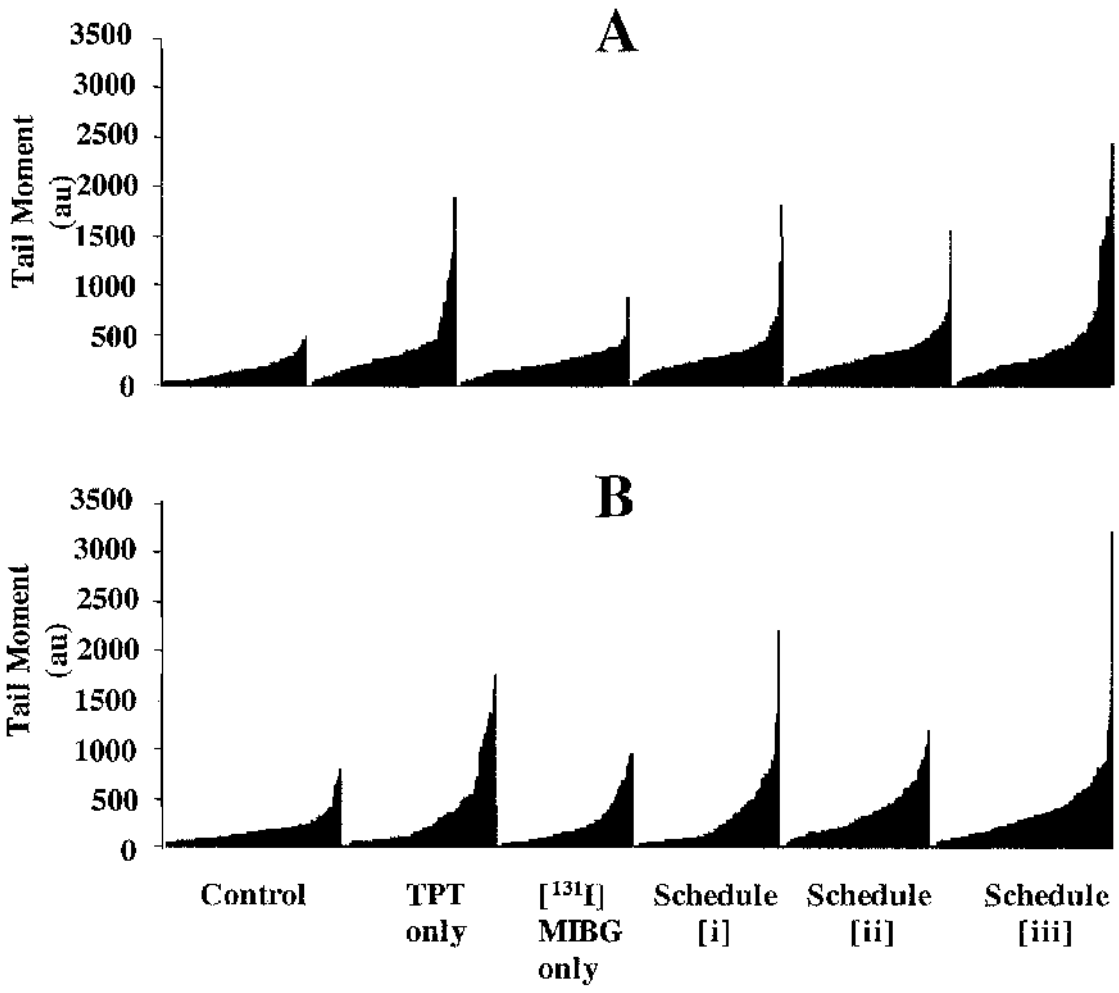

Figure 9-2: Total DNA fragmentation in SK-N-BE(2c) cells

DNA damage in treated SK-N-BE(2c) cells as measured by SCGE assay. Cells were treated with topotecan alone, [^{131}I]MIBG alone, or with one of the scheduled combinations shown in Figure 5-3.

Results were calculated using the tail moment method devised by Olive et al [196, 197]. Tail moment is defined as the average distance migrated by the DNA multiplied by the fraction of DNA in the comet tail. Measurements were plotted as arbitrary units, where 1au was equal to 1 percent of the median tail moment in untreated controls. Mean number of comets analysed per treatment group was 120.

A) The size of each individual comet moment observed when SK-N-BE(2c) cells are assayed immediately following treatment.
B) The size of each comet moment 24h after treatment.

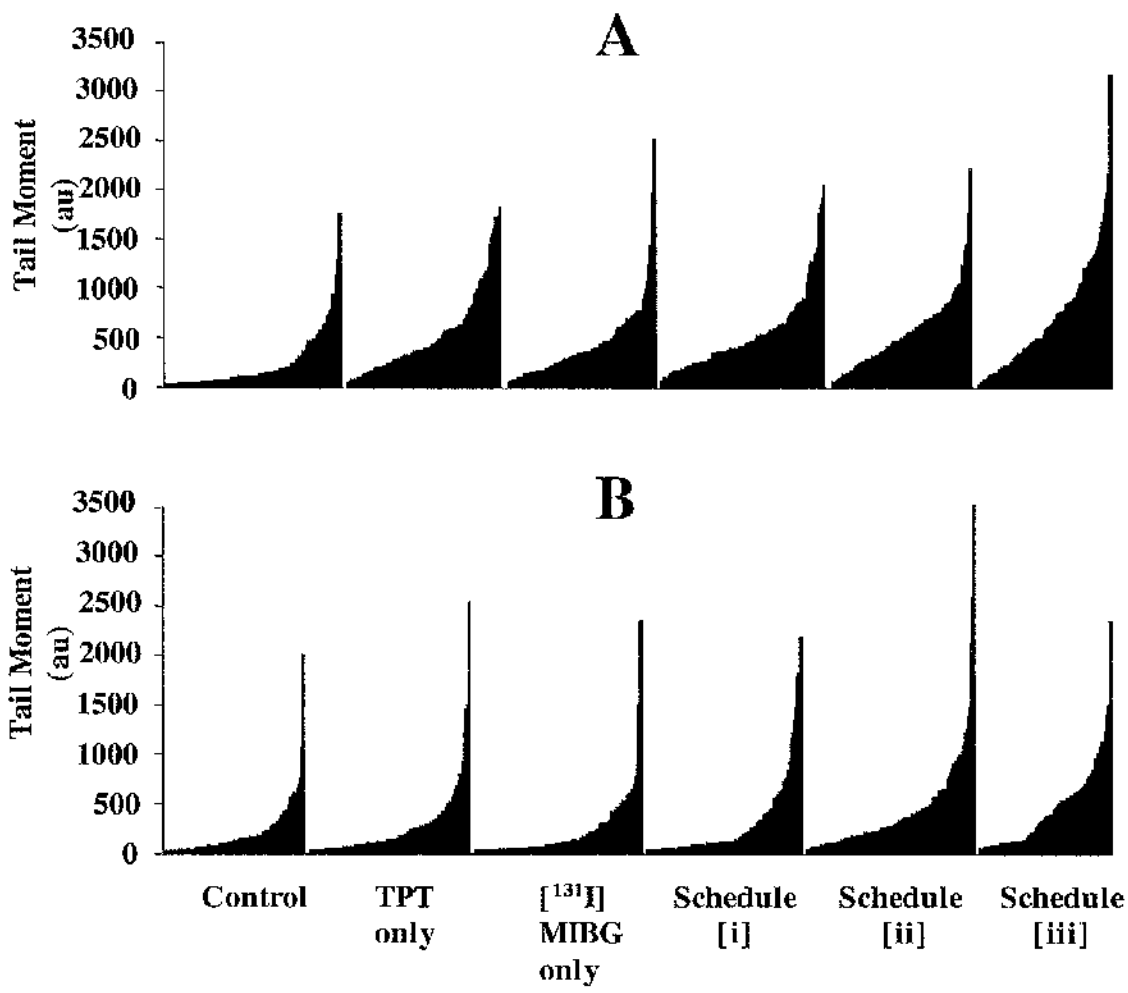

Figure 9-3: Total DNA fragmentation in UVW/NAT cells

DNA damage in treated UVW/NAT cells as measured by SCGE assay. As with SK-N-BE(2c), cells were treated with topotecan alone, [^{131}I]MIBG alone, or with one of the scheduled combinations shown in Figure 5-3.

Again, results were calculated using the tail moment method and measurements were plotted as arbitrary units. Mean number. of comets analysed per treatment group was 110.

A) The size of each individual comet moment when UVW/NAT cells were assayed immediately following treatment.
B) The size of each comet moment 24h after treatment.

9.3.2 Distribution of results

The comet moments obtained immediately after treatment (ie. Fig 9-2A and Fig 9-3A) were plotted as histograms to show the distribution of the data (Figure 9-4 for SK-N-BE(2c) results; Figure 9-5 for UVW/NAT results). The results for each cell line were evaluated for conformity to a normal distibution.

In a normal distribution, the mean and the median are identical, and the skew value is 0. For data that is significantly skewed, the mean and median are distinctly different, and the z-value, (which is the skew value divided by the standard error of skewness), is significantly high [198]. The equations used to calculate the skew value, the standard error of skewness (SES) and the z-value are shown in Figure 9-6. Statistical significance can be established by using the z-*p* calculator found on the VassarStats website [195].

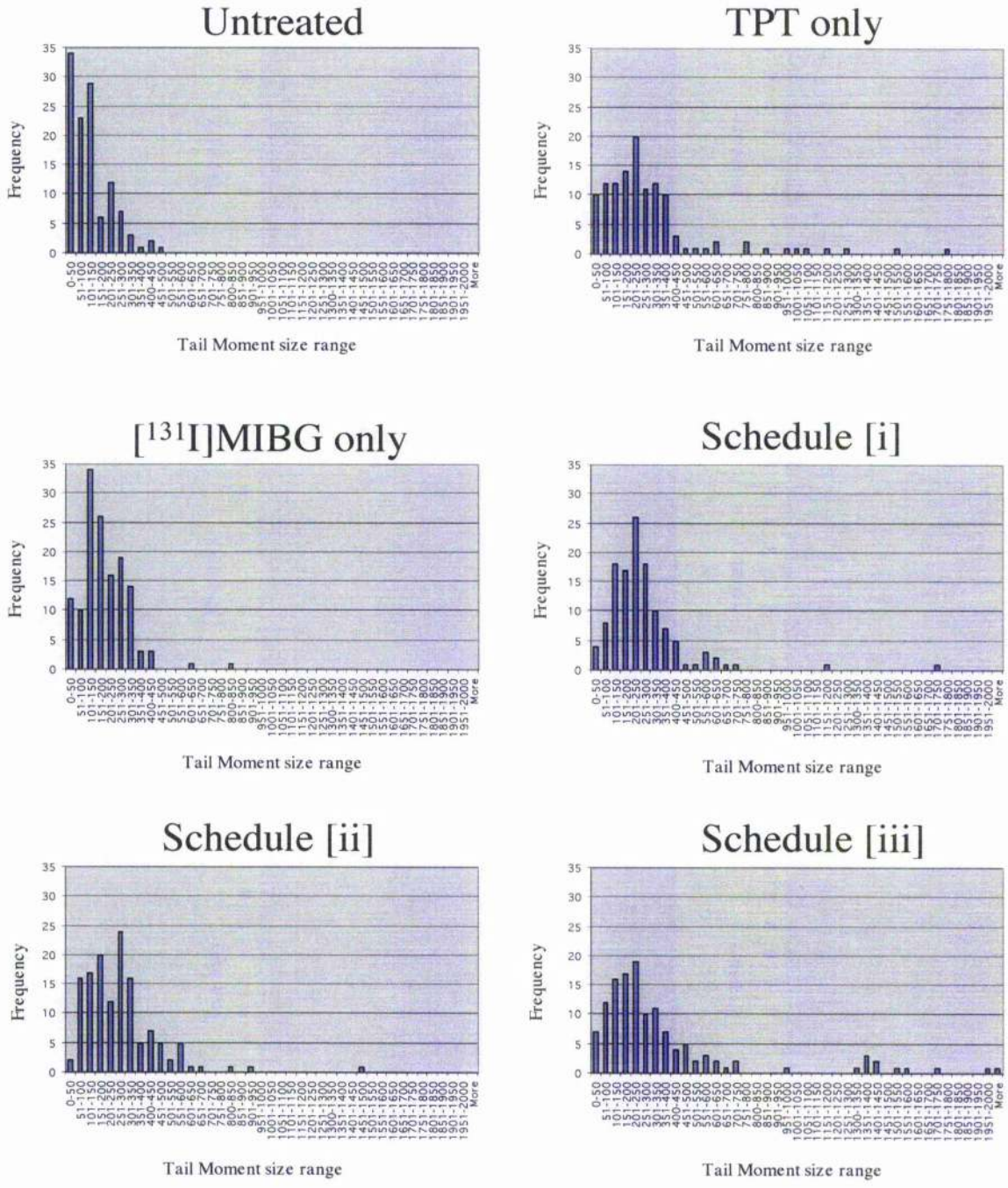

Figure 9-4: Distribution of results in SK-N-BE(2c) cells

Distribution of comet measurements. This figure shows the distribution of comet sizes (see Figure 9-2A), for untreated SK-N-BE(2c) cells and SK-N-BE(2c) cells treated with TPT and [^{131}I]MIBG, either alone or in combination.

Analysis of skewness of tail moments data is presented in Table 9-1.

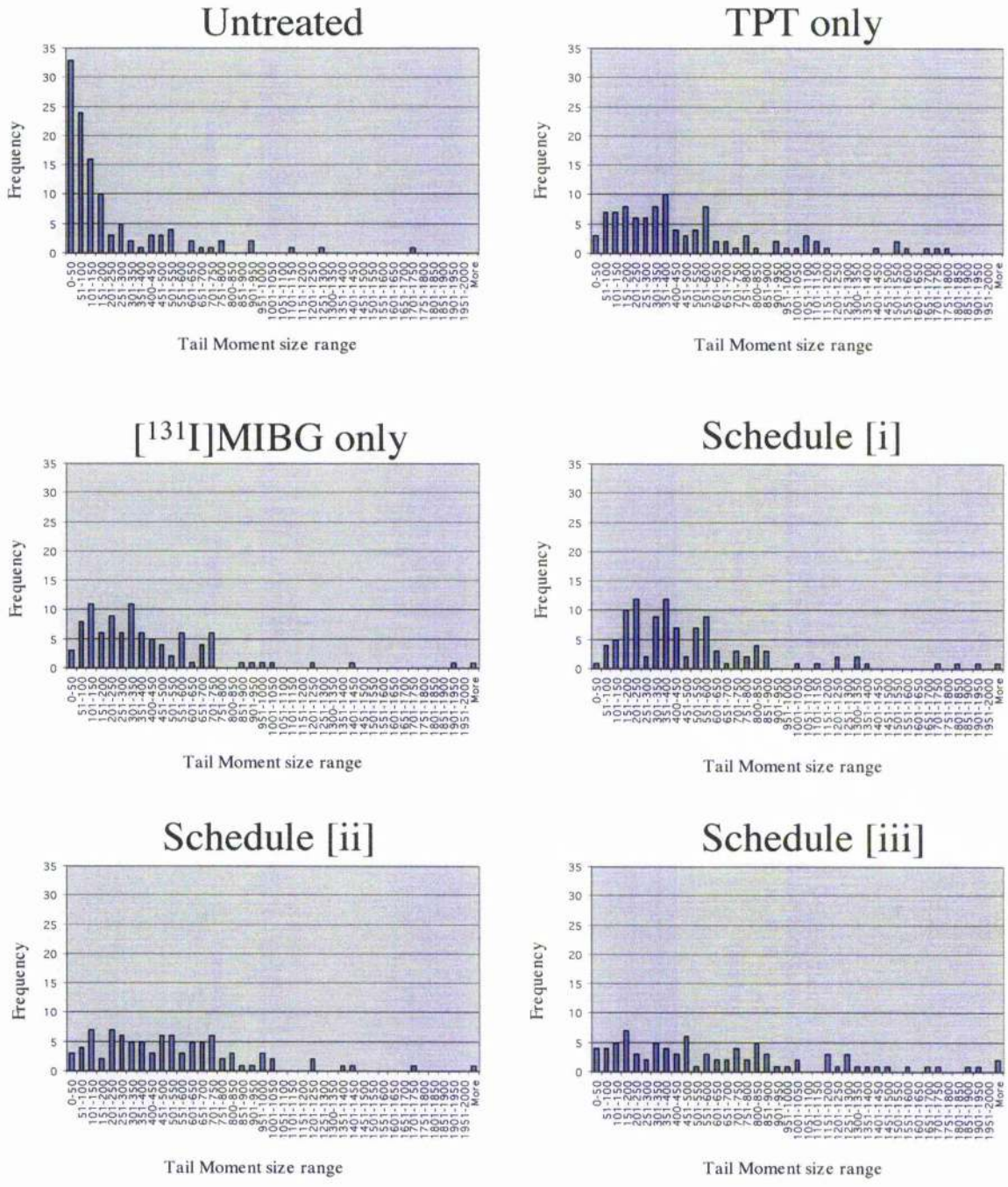

Figure 9-5: Distribution of results in UVW/NAT cells

Distribution of comet measurements. This figure shows the distribution of comet sizes (see Figure 9-3A), for untreated UVW/NAT cells and UVW/NAT cells treated with TPT and [^{131}I]MIBG, either alone or in combination.

Analysis of skewness of tail moments data is presented in Table 9-2.

For univariate data Y_1, Y_2.....Y_N,
the formula for skewness is:

A $$\mathbf{S} = \frac{\sum_{i=1}^{N}(Y_i - \bar{Y})^3}{(N-1)s^3}$$

B $$SES = \sqrt{\frac{6}{N}}$$

C $$\mathbf{z} = \frac{\mathbf{S} - 0}{SES}$$

where

$\mathbf{S}$ - Skewness value
$\bar{Y}$ is the mean
s is the standard deviation
N is the number of data points
SES - standard error of skewness

Figure 9-6: Statistical analysis of skewness

This figure shows the equations used to test whether data derive from a normal distribution.

A) The equation used to test data for skew. Skewness was calculated using *Excel*™ statistical software.

B) The equation used to calculate the standard error of skewness (Tabachnick & Fidell [198]).

C) The equation used to calculate the z-value, which describes deviation from the mean in a distribution. 1unit of z is equal to one standard deviation. This equation is described by Tabachnick & Fidell [198].

From the z-value, the *p*-value of statistical significance was calculated using the *z-p* calculator freely available online [195].

9.3.2-1 SK-N-BE(2c):

Tail moments data derived from untreated controls, and from cells treated with TPT and [^{131}I]MIBG, exhibited a significant level of positive skewness, suggesting that these results are not normally distributed. See Table 9-1.

9.3.2-2 UVW/NAT:

As with SK-N-BE(2c), tail moments derived from untreated controls, and from cells treated with TPT and [^{131}I]MIBG, were significantly skewed. Again, this suggests that these results are not normally distributed. See Table 9-2.

	control	TPT only	[^{131}I]MIBG only	Schedule [i]	Schedule [ii]	Schedule [iii]
Mean	122.16	297.04	193.17	266.66	272.33	365.46
Median	100.00	227.64	172.56	232.30	255.46	218.79
Skew	0.952	1.677	1.251	2.170	1.581	1.923
S.E.S	0.225	0.225	0.208	0.220	0.210	0.215
z value	4.224	7.468	6.021	9.864	7.528	8.952
***p* value**	<0.005	<0.005	<0.005	<0.005	<0.005	<0.005

Table 9-1: Analysis of skewness of tail moment data derived from SK-N-BE(2c) cells treated with TPT and [^{131}I]MIBG

This data is derived from the histograms displayed in Figure 9-4

For every treatment group, there was a distinct difference between the mean and the median. Significance of skewness was calculated using the method of Tabachnick & Fidell [198]. Briefly, z-values were calculated by dividing the Skew score by the S.E.S (standard error of skewness), from this, the appropriate p-value was assigned.

In SK-N-BE(2c) cells, all of the data curves displayed a significant positive skew.

This suggests that the comet size of SK-N-BE(2c) cells are not normally distributed, necessitating the use of a non-parametric analysis.

	control	TPT only	[^{131}I]MIBG only	Schedule [i]	Schedule [ii]	Schedule [iii]
Mean	211.48	502.19	414.59	511.51	530.12	679.02
Median	100.00	367.01	323.20	395.50	461.96	542.68
Skew	3.158	1.079	1.380	1.561	0.706	0.854
S.E.S	0.228	0.245	0.250	0.237	0.257	0.263
z value	13.824	4.404	5.522	6.592	2.750	3.252
***p* value**	<0.005	<0.005	<0.005	<0.005	<0.005	<0.005

Table 9-2: Analysis of skewness of tail moment data derived from UVW/NAT cells treated with TPT and [^{131}I]MIBG

This data is derived from the histograms displayed in Figure 9-5

UVW/NAT cells, like SK-N-BE(2c) cells, displayed a distinct difference between the mean and the median. Significance of skewness was calculated using the method of Tabachnick & Fidell [198].

In UVW/NAT cells, all of the data curves were significantly skewed.

As in the case of tail moments produced in SK-N-BE(2c) cells (Table 9-1), this analysis also suggests that the comet size data were not normally distributed, necessitating the use of a non-parametric analysis.

9.3.3 Analysis of Results

As the results obtained from both cell lines did not conform to a normal distribution, it was necessary to use a non-parametric statistical test to analyse the data. Results were analysed using the Mann-Whitney U test (from the SISA website [194]). In this method, the results of two groups are combined, ranked in order of size, and a rank number assigned. The U test then compares of the sum of the rank values for each group to determine if they are similar enough to come from the same population, or significantly different (ie. from different populations).

9.3.4 Comparison of DNA Fragmentation in treated cells at 0h and 24h – Analysis of DNA damage repair

Following treatment with TPT and [^{131}I]MIBG as single agents or in combination, SK-N-BE(2c) and UVW/NAT cells were assayed immediately after treatment. Similarly treated cells were assayed 24 hours after treatment. The extra incubation time allowed DNA repair to occur, and this was analysed by comparing the amount of DNA fragmentation in each treatment group at 0h to the amount of DNA fragmentation in similarly treated cells at 24h.

9.3.4-1 SK-N-BE(2c)

SK-N-BE(2c) cells assayed 24h after treatment exhibited significantly lower levels of DNA fragmentation than similarly treated cells assayed at 0h, following administration of TPT or [^{131}I]MIBG as single agents, or following combination schedule [i]. However, cells treated with combination schedule [ii] or schedule [iii] did not display significant reduction in DNA fragmentation after 24h compared to similarly treated cells assayed at 0h (Figure 9-7).

9.3.4-2 UVW/NAT

As with SK-N-BE(2c), treated UVW/NAT cells assayed 24h after treatment exhibited significantly lower levels of DNA fragmentation than similarly treated cells assayed at 0h, following administration of TPT or [^{131}I]MIBG as single agents, or following combination schedule [i]. However, unlike SK-N-BE(2c), where the reduction in DNA fragmentation observed in cells treated by combinations of TPT and [^{131}I]MIBG was dependent on scheduling, in UVW/NAT cells a significant decrease in DNA damage was also observed in cells treated with combination schedules [ii], and [iii] (Figure 9-8).

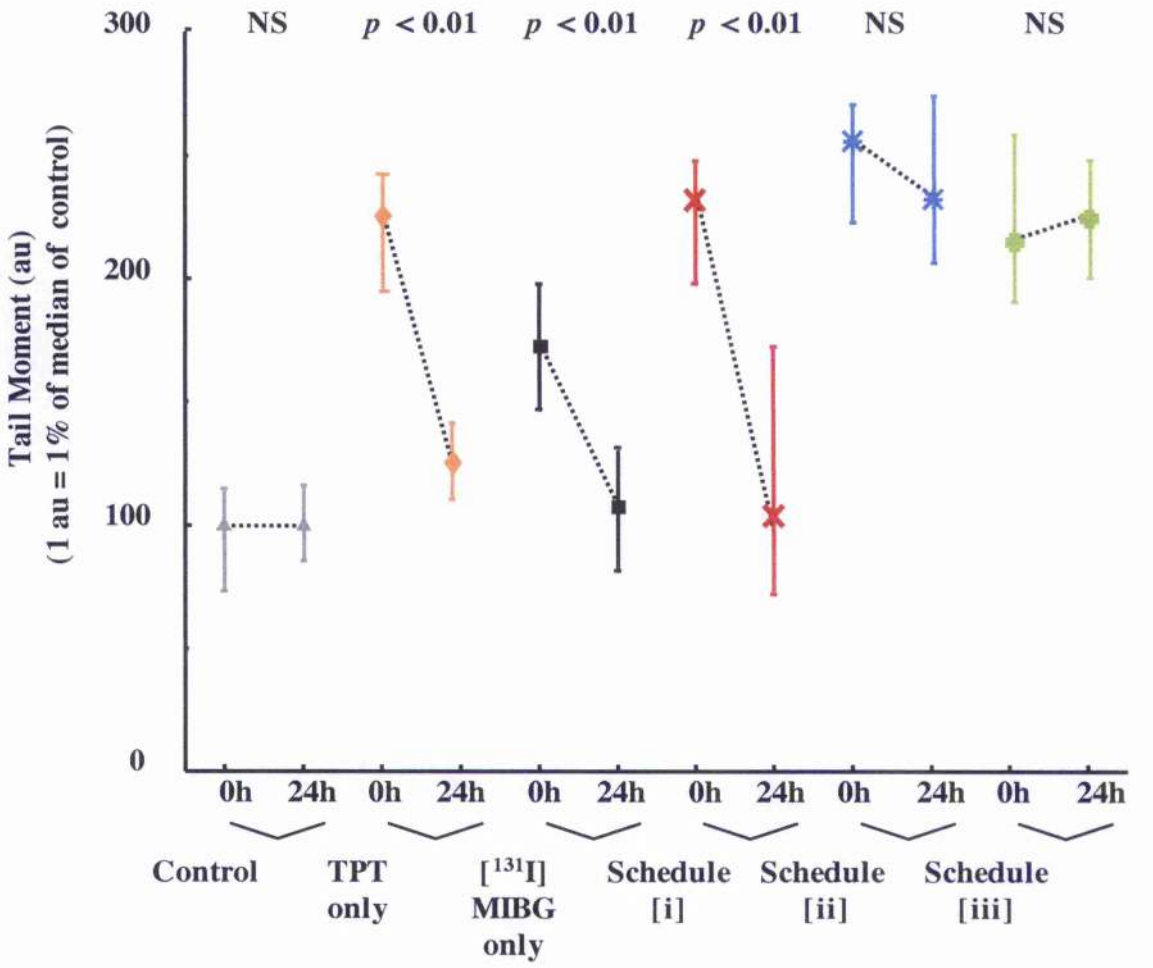

Figure 9-7: Repair of DNA fragmentation in SK-N-BE(2c) cells

The amount of DNA fragmentation observed immediately after treatment was compared to similarly treated cells left in fresh medium for 24h to allow DNA repair. Data is presented as medians of data range and 95% confidence intervals.

SK-N-BE(2c) cells treated with TPT alone, [^{131}I]MIBG alone, or with TPT scheduled before [^{131}I]MIBG, (schedule[i]) exhibited a significant reduction in DNA damage when assayed 24h after treatment, compared to similarly treated cells assayed at 0h. However, cells treated with TPT scheduled either after [^{131}I]MIBG (schedule[ii]), or simultaneously with [^{131}I]MIBG (schedule[iii]), and assayed 24h after treatment exhibited no significant change in DNA fragmentation, compared to treated cells assayed at 0h.

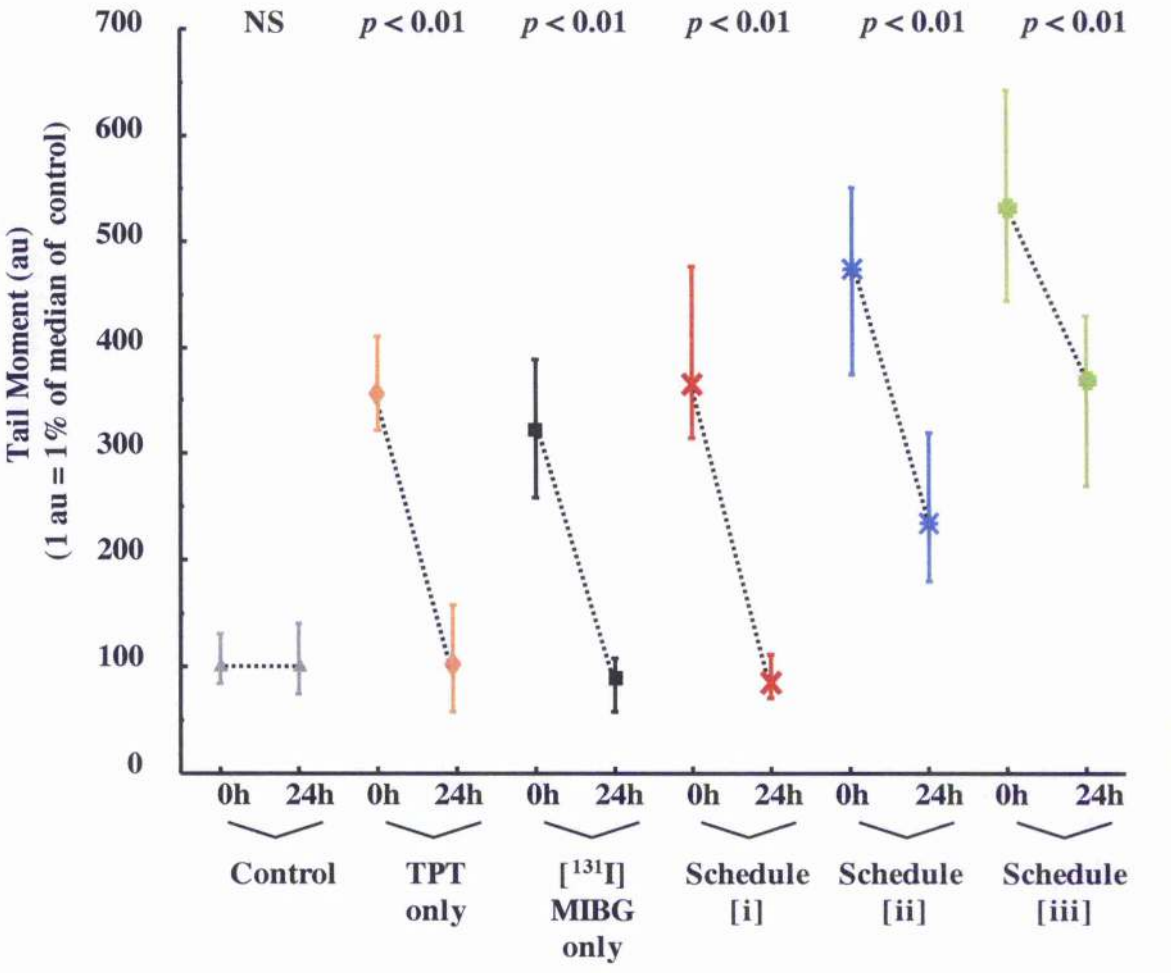

Figure 9-8: Repair of DNA fragmentation in UVW/NAT cells

Again, the amount of DNA fragmentation observed immediately after treatment was compared to similarly treated UVW/NAT cells left in fresh medium for 24h to allow DNA repair.

Treated UVW/NAT cells assayed at 24h displayed a significant decrease in DNA fragmentation, compared to similarly treated cells assayed at 0h. Unlike SK-N-BE(2c) cells, in UVW/NAT cells, reduction of DNA damage was not affected by the order of administration.

9.3.5 DNA fragmentation in treated compared to untreated cells at 0h and 24h - Analysis of the duration of DNA damage

DNA fragmentation in treated and untreated SK-N-BE(2c) and UVW/NAT was assessed at 0h and 24h to examine the amount and duration of DNA damage caused by single agent and combination regimens.

Compared to untreated controls, SK-N-BE(2c) and UVW/NAT cells dosed with topotecan and [^{131}I]MIBG, either alone or in combination and assayed immediately after treatment displayed statistically significant levels of DNA fragmentation (Table 9-3). When assayed 24h after treatment, cells treated with either agent alone or with combination schedule [i], no longer exhibited significant amounts of DNA damage, compared to untreated controls, suggesting that efficient DNA repair has occurred.

However, SK-N-BE(2c) and UVW/NAT cells treated with combination schedule [ii] and schedule [iii] and assayed at 24h continued to exhibit significant levels of DNA fragmentation, suggesting that cells treated with either of these regimens are not as efficient at DNA damage repair than cells treated by schedule [i], or by either agent alone.

		control	TPT only	[^{131}I]MIBG only	Schedule [i]	Schedule [ii]	Schedule [iii]
SK-N-BE(2c)	0h	NS	$p < 0.05$	$p < 0.05$	$p < 0.05$	$p < 0.05$	$p < 0.05$
	24h	NS	NS	NS	NS	$p < 0.05$	$p < 0.05$
UVW/NAT	0h	NS	$p < 0.05$	$p < 0.05$	$p < 0.05$	$p < 0.05$	$p < 0.05$
	24h	NS	NS	NS	NS	$p < 0.05$	$p < 0.05$

Table 9-3: Significance of cellular DNA damage caused by TPT and [^{131}I]MIBG treatment

All of the treatment regimens (ie. administration of each agent either alone, or in combination) resulted in significant levels of DNA fragmentation in cells assayed immediately, compared to untreated controls.

However, in cells left for 24h to allow for DNA damage repair there was no significant difference between untreated controls, and cells treated with either agent alone, or when TPT was scheduled before [^{131}I]MIBG in combination therapy. DNA fragmentation remained significantly high only when TPT was scheduled simultaneously with, or after [^{131}I]MIBG.

This suggests that administration of topotecan concurrently with, or following [^{131}I]MIBG results in a reduced ability to efficiently repair DNA damage in SK-N-BE(2c) and UVW/NAT cells. However, administration of topotecan prior to [^{131}I]MIBG has no effect on DNA damage repair pathways.

2.4 Summary of results

The treatment of SK-N-BE(2c) and UVW/NAT cells with topotecan or [^{131}I]MIBG, either as single agents, or in combination resulted in significant levels of DNA fragmentation immediately after administration. This effect was independent of the scheduling of the two agents.

NAT expressing cells treated with a combination of topotecan and [^{131}I]MIBG displayed a reduced capacity for DNA repair compared to cells treated with either agent alone. However this effect was dependent on the order of delivery of the two agents. Only when topotecan was administered following [^{131}I]MIBG (schedule [ii]), or concurrently with [^{131}I]MIBG (schedule [iii]) was DNA damage repair significantly impaired.

This corresponds to the order of effectiveness of different combination schedules to induce clonogenic cell kill and delay of tumour growth (Chapters 5, 6 &7). However, while less effective than schedules [ii] and [iii], administration of combination schedule [i] produced supra-additive levels of cytotoxicity *in vitro* (Chapters 5 & 6), and increased the growth delay of experimental tumours *in vivo* (Chapter 7). This suggests that the time points examined in this study of DNA fragmentation and repair were not sufficient to adequately correlate long-term disruption of DNA repair, and TPT/MIBG-induced toxicity. These issues will be discussed further in Chapter 10.

The effects of TPT administration on [^{131}I]MIBG-induced DNA damage described in this chapter could be due to inhibition of DNA repair mechanisms [170-172], or TPT-induced Topo I cleavage activity [161]. These theories will be discussed in greater detail in Chapter 11.

Chapter 10

Discussion

I:

The results of this study,

and proposals for future work

10.1 Development of a real-time RT-PCR assay for prediction of the uptake of [^{131}I]MIBG by neuroblastoma tumours

10.1.1 Clinical diagnosis of neuroblastoma

Chapter 2 described the development of a rapid and specific assay for NAT expression in biopsy samples obtained from neuroblastoma patients. The assay, based on real-time PCR analysis, showed substantial power to predict MIBG uptake capacity and has the potential to select patients for [^{131}I]MIBG therapy.

The clinical diagnosis of neuroblastoma currently involves histological examination of biopsy specimens and diagnostic MIBG scintigraphy [21], which involves the administration of a tracer dose of radioiodinated MIBG. In addition to providing an indication of the suitability of patients for [^{131}I]MIBG therapy, scintigraphy allows the localisation of metastatic deposits and (if supplemented by information allowing the estimation of tumour size) also enables dosimetric calculation. The assay detailed in this report could support the data obtained by MIBG scintigraphy by identifying those patients most suitable for [^{131}I]MIBG therapy as a front line treatment.

10.1.2 Comparison of TaqMan RT-PCR to existing methodologies

TaqMan RT-PCR analysis of NAT expression was superior, in terms of speed and reproducibility, to previously published methods of NAT mRNA quantitation [62]. The real-time PCR technique allowed the simultaneous evaluation of a large number of individual samples as well as internal controls. This assay involves the use of industry-standardised reagents and requires less manipulation of sample than traditional PCR techniques, resulting in increased reliability and accuracy.

10.1.3 Limitations of TaqMan RT-PCR

Of the 54 patients' samples with evaluable MIBG scans, 48 (89%) showed MIBG uptake into the primary tumour, while 43 (80%) of the tumour samples were positive for the expression of NAT mRNA. This is equivalent to 90% concordance with respect to positive outcome of the two tests. All 6 tumours (11%) that failed to accumulate MIBG had undetectable NAT mRNA expression. However, biopsies from 5 patients (10.4%) with positive MIBG scans did not express detectable NAT mRNA.

Therefore, while a positive PCR test always predicted tumour uptake of MIBG, a negative PCR test failed to correctly determine MIBG uptake capacity with a frequency of 45%.

This suggests that PCR-based assessment of NAT gene expression cannot be regarded as fully predictive of MIBG uptake.

10.1.4 Heterogeneity of uptake

There are plausible explanations for the occasional coincidence of a negative PCR test with a positive MIBG scan. It is possible that heterogeneous uptake of radioidinated MIBG is occurring. In this scenario, while one area of a tumour mass is expressing the NAT gene and can be imaged successfully, another area of the same tumour mass may not express the NAT gene and will not take up radiolabelled MIBG. A biopsy taken from the NAT-negative area would therefore give a negative PCR result. However, radioiodinated MIBG would still accumulate in the NAT-positive area of the tumour mass, leading to a positive MIBG scan.

10.1.5 Quality of biopsy material

It is also possible that the quality of biopsy material used for analysis was not optimal. In the present study, specimens were subjectively assessed for neuroblastoma content and those with less than 20% neuroblastic component were rejected. It would be preferable to establish an objective assessment of the proportion of malignant cells in biopsy material.

10.1.6 Alternative internal references

To predict tumour cell concentration of MIBG more accurately, it may be necessary to use alternative internal standards with specificity for neuroblastoma cells. Possibilities include the transcript of the tyrosine hydroxylase gene [199], which is expressed only in catecholamine-synthesising cells, or mRNA specific for neural crest cell proteins such as PGP9.5 [200] or GD_2 synthase [201].

10.1.7 Involvement of an alternative MIBG uptake pathway?

Monoamine transporters other than NAT may be partly responsible for the accumulation of MIBG by tumour cells. Although the principal mechanism of cellular uptake of MIBG involves the NAT, the possibility of tumour concentration via vesicular or cell-membrane-associated monoamine transporters cannot be discounted [202, 203]. Alternatively, mutant forms of NAT could be involved. These may be undetectable by the PCR primers employed in this study.

It may be necessary to design a new primer / probe set, which hybridises to another region of the NAT cDNA sequence. If [^{131}I]MIBG uptake is entirely due to transcription of a single version of NAT mRNA, then identical results should be obtained by analysis of the copy numbers of different regions of the NAT mRNA sequence. However, any differences in the starting copy numbers detected by primers which anneal to different regions of the published NAT cDNA sequence would suggest the presence of alternative versions of NAT mRNA.

10.2 Future work arising from the development of a real-time RT-PCR assay

10.2.1 Tumour heterogeneity and sensitivity of scintigraphy and RT-PCR

A major obstacle to the application of molecular tests on real tumours rather than cultured cells is tumour heterogeneity with respect to expression of specific markers. In order to assess the sensitivity of the RT-PCR assay *in vivo*, it is necessary to compare MIBG concentration with real-time PCR data derived from tumours which contain known percentages of NAT-positive cells.

10.2.2 The use of multicellular mosaic spheroids

This can be achieved by the use of a tumour model, which incorporates cell population heterogeneity. Multicellular mosaic spheroids are composed of variable percentages of two cell populations with different characteristics [204]. This model would address the limitation to detectability imposed by heterogencity of NAT expression.

In this case, one of the cell populations would display no expression of the NAT gene, while the other would be positive for NAT gene expression. In order to assess the sensitivity of the assay, mosaic xenografts composed of a range of proportions of NAT-expressing cells would be established. Scintigraphic analyses of these xenografts would be compared to the results of analyses of NAT gene expression by TaqMan RT-PCR to assess the respective sensitivities of the two procedures. See Figure 10-1

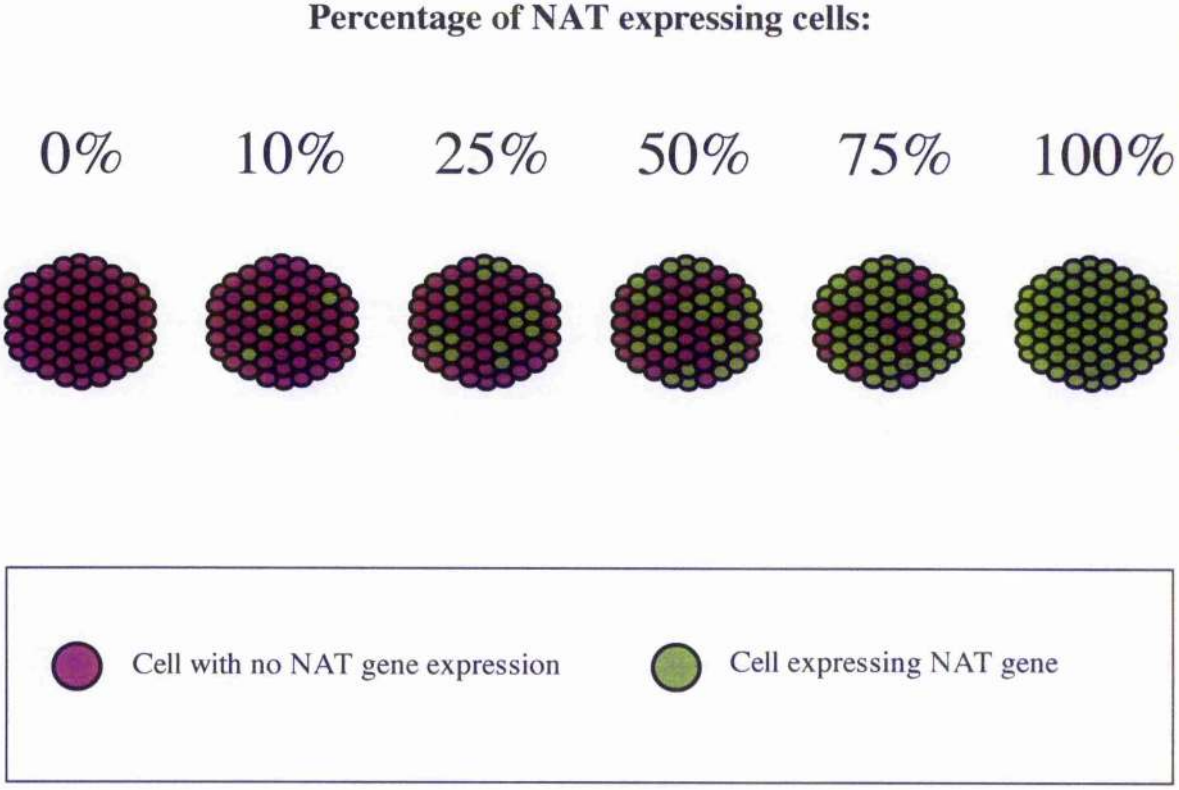

Figure 10-1: Multicellular mosaic spheroids

Multicellular mosaic spheroids are composed of variable percentages of two cell populations with different characteristics. In this case, one of the cell populations display no expression of the NAT gene, while the other is positive for NAT gene expression.

Establishing mosaic spheroids with a range of proportions of NAT-expressing cells would allow determination of sensitivity of scintigraphic analyses of these xenografts compared to the results of analyses of NAT gene expression by TaqMan RT-PCR.

Furthermore, a mosaic spheroid model would allow estimation of minimum requirement for NAT gene transfection to allow sterilisation by combinations of targeted radiotherapy and radiopotentiators.

10.3 The effect of topotecan pre-treatment on intracellular uptake of [^{131}I]MIBG

10.3.1 TPT-induced enhancement of [^{131}I]MIBG uptake in vitro

SK-N-BE(2c) and SHSY5Y cells tested immediately after removal of unincorporated TPT displayed a small, but insignificant increase in uptake of [^{131}I]MIBG. Significant enhancement of [^{131}I]MIBG uptake was observed 24h after removal of the drug (approximately 2-2.5 times the level observed in untreated controls), after which the increased accumulation of the radiopharmaceutical fell, and had returned to the levels observed in untreated cells 72h after removal of TPT (Chapter 3). However enhanced uptake did not correspond with an increase in bNAT gene expression *in vitro*.

Interestingly, increased uptake of [^{131}I]MIBG was also observed *in vitro* in TPT pretreated UVW/NAT cells, which contain an expression vector incorporating the bNAT gene under the control of a viral (RSV) promoter. Untreated and TPT treated UVW/NAT cells displayed negligible expression of the hNAT gene, and no increase in bNAT mRNA levels. This suggests that the enhancement of [^{131}I]MIBG uptake observed in this cell line was not due to an increased activation of either the endogenous hNAT gene promoter, or an alteration in RSV promoter-driven bNAT gene expression.

10.3.2 Drug-induced enhancement of [^{131}I]MIBG uptake in vivo

The *in vitro* results, reported in the previous section, suggested that, as pre-treatment with TPT enhanced intracellular concentration of [^{131}I]MIBG, this regimen would induce an increase in [^{131}I]MIBG-induced toxicity. However, while previous studies reported that a wide range of DNA-interacting drugs cause increases in uptake of radio-labelled MIBG, these increases were not found to be tumour specific. For example, following cisplatin pre-treatment, greater concentration of radio-labelled MIBG has been reported in a variety of normal organs [71, 158], suggesting that some non-target tissues may be adversely affected by combination therapy involving administration of chemotherapeutic drugs followed by [^{131}I]MIBG.

10.3.3 The effect of topotecan on the biodistribution of [^{131}I]MIBG

The concentration of [^{131}I]MIBG in SK-N-BE(2c) or UVW/NAT tumours was second only to that in adrenals. The influence of prior administration of topotecan on the biodistribution of [^{131}I]MIBG in tumour-bearing nude mice was examined. Pretreatment with topotecan had no effect on [^{131}I]MIBG accumulation by UVW/NAT tumours but induced a modest though insignificant increase in uptake by SK-N-BE(2c) tumours. Likewise, topotecan treatment induced greater accumulation of [^{131}I]MIBG in adrenals and heart in both groups of tumour-bearing mice. However, these increases were not significant.

The concentration of [^{131}I]MIBG was low in muscle, kidney, lung, thyroid and marrow, and in none of these nonsympathetically innervated tissues was there a significant difference in radiopharmaceutical uptake after topotecan administration.

10.3.4 Assessment of marrow toxicity

The bone marrow is the dose limiting tissue in neuroblastoma patients treated with [^{131}I]MIBG, and toxicity is manifest by prolonged thrombocytopenia [179]. Furthermore, topotecan is also myelotoxic [126]. Encouragingly, TPT did not increase the concentration of activity in the bone marrow of experimental animals. Furthermore, while therapeutically effective combinations of topotecan and [^{131}I]MIBG induced a reduction of platelet numbers and a decrease in the clonogenic capacity of CFU-A transiently-engrafting stem cells in SK-N-BE(2c) tumour-bearing mice, these indices of marrow integrity returned to normal levels two weeks after treatment.

This suggests that combined therapy involving these agents will not increase adverse reactions in a therapeutic setting.

10.4 The effect of topotecan on expression of the noradrenaline transporter gene

The effects on NAT gene expression of other DNA interacting agents, as shown in Table 3-1, have been previously reported. Each has been shown to cause an upregulation of mRNA signal by semi-quantitative RT-PCR [154, 157] and by Northern blotting [158]. In this study, real time RT-PCR showed that there was no significant upregulation of NAT gene expression in SK-N-BE(2c) and UVW/NAT cells following treatment with TPT.

It is possible that alternatively spliced, or mutant forms, of NAT mRNA could be involved, which allow production of functional NAT protein, but are undetectable by the PCR primers employed in this study.

Alternatively, factors other than increased NAT gene expression may be responsible for increased [^{131}I]MIBG uptake. Expression of the NAT gene product may be partially controlled at the post-transcriptional or post-translational stages by an as yet undiscovered pathway. This would lead to alterations in the cellular concentration of functional NAT protein, without affecting gene transcription. Development of assay for NAT protein concentration (eg. Western blot) would help to resolve this issue.

Furthermore, monoamine transporters other than NAT may be partly responsible for the accumulation of [^{131}I]MIBG by tumour cells. Although the principal mechanism of cellular uptake of [^{131}I]MIBG involves the NAT protein, the possibility of tumour concentration via vesicular or cell membrane-associated monoamine transporters cannot be discounted [202, 203].

It should also be noted that previous analyses of NAT gene product were based on densitometric quantitation of band intensities, whereas real time RT-PCR relies on standards of known concentration, allowing an exact quantitation of starting number of copies of the target sequence. It is possible, therefore, that previously reported increases in

band intensity in NAT positive samples, may reflect the limitations of the technology, rather than a genuine increase in NAT gene expression.

10.5 The effects of combinations of topotecan and [^{131}I]MIBG *in vitro* and *in vivo*

10.5.1 Supra-additive cytotoxicity in SK-N-BE(2c) and UVW/NAT cells in vitro

In many previous studies, synergistic cell killing *in vitro* by ionising radiation and Topo I inhibitors was reported in a wide range of human and animal cell lines, [85, 136-141]. Also, *in vivo* radiopotentiation by Topo I inhibitors has been demonstrated in xenografts of murine fibrosarcoma and MCa-4 mammary carcinoma [140, 142] and rhabdomyosarcoma [143].

While TPT and [^{131}I]MIBG have been combined in pilot studies being undertaken in the Netherlands, no preclinical studies have attempted to combine topotecan and [^{131}I]MIBG therapy. Therefore, the potential of TPT to potentiate this form of targeted radiotherapy was unresolved.

In vitro investigations of the interaction between topotecan and [^{131}I]MIBG in SK-N-BE(2c) and UVW/NAT cells by both isobologram and median-effect / combination-index analyses indicated that supra-additive toxicity in NAT expressing cells was achieved by combinations of these two agents. Radiopotentiation in SK-N-BE(2c) was observed at low toxicity levels following all three scheduled combinations. However, at higher toxicity levels (ie. > IC_{50}) combination treatment was less effective. UVW/NAT cells also exhibited supra-additive responses. However in this cell line radiopotentiation was observed at higher toxicity levels (ie. > IC_{50}), but were not as affected by doses lower doses of combination treatment (ie. < IC_{30}).

The contradictory effectiveness of varying doses of combinations of TPT and [^{131}I]MIBG to these two cell lines may reflect an underlying difference in their respective response to each agent. SK-N-BE(2c) cells were highly sensitive to low doses of TPT (90% survival at 1ng/ml; 10% survival at 5ng/ml (Figure 4-3). Thereafter a plateau, with

respect to clonogenic survival, was observed (ie. concentrations of TPT greater than 5ng/ml did not result in greater levels of toxicity). UVW/NAT were not as sensitive to low doses of the drug (90% survival at 1ng/ml; 45% survival at 5ng/ml), however a greater proportion of UVW/NAT were susceptible to treatment (ie. the plateau observed in UVW/NAT cells was approximately 2%, compared to ≈10% in SK-N-BE(2c) cells).

This plateau is in agreement, with previously reported effects of TPT [132] and of other Topo I inhibitors [137, 162], and is attributed to the S-phase specificity of topotecan-induced toxicity. In any population of cells, different sub-populations will be at different stages of the cell cycle. Cells in G_1 during treatment will be unaffected by topotecan exposure.

The results of cell cycle analysis reported in Chapter 8 confirmed that a higher percentage of SK-N-BE(2c) than UVW/NAT cells were in G_1 (75.13 ± 0.29%, compared to 62.56 ± 0.53%), while a higher proportion of UVW/NAT cells were undergoing DNA replication and mitosis (for SK-N-BE(2c) cells, S-phase and G_2/M proportions were 10.47 ± 0.25% and 11.79 ± 0.45% respectively; for UVW/NAT S-phase and G_2/M proportions were 12.26 ± 0.24% and 21.22 ± 0.64% respectively).

This suggests that, while SK-N-BE(2c) cells are more sensitive to topotecan-induced toxicity, a higher proportion of the cell population is in G_1. Consequently, a higher percentage of cells will be resistant to the drug. UVW/NAT cells are more resistant to topotecan-induced toxicity. However, more UVW/NAT cells are in S-phase, and a lower percentage are in G_1 during treatment. Therefore, a higher percentage of these cells will be affected by topotecan treatment.

Both SK-N-BE(2c) and UVW/NAT cells were sensitive to [^{131}I]MIBG. However the results of SCGE assays suggest that UVW/NAT cells exhibit more efficient DNA damage repair than SK-N-BE(2c) cells (Chapter 9).

These observations may explain the differing responses of UVW/NAT and SK-N-BE(2c) cells to topotecan/[^{131}I]MIBG combination therapy. Combining these agents resulted in supra-additive toxicity in SK-N-BE(2c) cells at low levels of toxicity, due to sensitivity to both agents and less efficient DNA repair. However, at higher toxicity levels the apparent infra-additive interaction may be due to the greater proportion of SK-N-BE(2c) cells in G_1 ($\approx$ 10%), which are not affected by topotecan treatment.

Combining topotecan and [^{131}I]MIBG in UVW/NAT cells resulted in an infra-additive interaction at low levels of toxicity, possibly due to higher resistance to TPT combined with more efficient DNA repair. However, higher doses of the two drugs (ie. > IC_{50}) resulted in supra-additive levels of kill, possibly due to an inability of DNA repair mechanisms to adequately deal with greater levels of damage, combined with a higher proportion of UVW/NAT cells treatable by higher doses of TPT (ie. $\approx$ 98% compared to $\approx$ 90% for SK-N-BE(2c) cells).

10.5.2 The effect on toxicity in vitro and in vivo of alternative scheduling of topotecan and [^{131}I]MIBG

The results of this study indicated that supra-additive levels of cytotoxicity were achieved *in vitro* in NAT expressing cells treated with combinations of TPT and [^{131}I]MIBG. Furthermore, TPT potentiated the therapeutic index of [^{131}I]MIBG targeted radiotherapy in NAT-expressing tumours *in vivo*.

Combination-index analyses suggested that administration of TPT prior to [^{131}I]MIBG (schedule [i]) was less effective than administration of TPT following or concurrently with [^{131}I]MIBG (schedule [ii] and schedule [iii] respectively). Furthermore, with respect to growth delay or cure of experimental tumours, exposure to TPT 24h before [^{131}I]MIBG (schedule [i] was less effective than administration of topotecan 24h after [^{131}I]MIBG (schedule [ii]), which was not as effective than simultaneous treatment with [^{131}I]MIBG and topotecan (schedule [iii]).

10.5.3 Cytotoxicity and TPT-induced enhancement of [^{131}I]MIBG uptake

SK-N-BE(2c) and UVW/NAT cells and xenografts treated with TPT subsequently exhibited an enhanced uptake of [^{131}I]MIBG (see Chapter 3). However, the efficacy of TPT administration of NAT expressing cells prior to [^{131}I]MIBG was less than TPT administration either following, or concurrently with [^{131}I]MIBG (Chapters 5, 6 & 7). This suggests that increased uptake of the radiopharmaceutical due to prior administration of TPT (and, presumably, increased [^{131}I]MIBG-induced toxicity) was not as important a factor for overall survival as increased disruption of DNA repair, observed in cells treated by combination schedules [ii] and [iii], as reported in Chapter 9.

10.6 The effects of topotecan and [^{131}I]MIBG on cellular mechanisms

10.6.1 The effect of scheduling of topotecan and [^{131}I]MIBG on cell cycle distribution

The results of cell cycle analyse reported in Chapter 8 demonstrated that administration of the less effective combination schedule (schedule [i]) resulted in a different cell cycle distribution than administration of schedules [ii] or [iii]. While previous studies were unable to find a clear link between cell cycle distribution and cytotoxicity [189, 190], it is tempting to theorise a possible link between these phenomena.

Administration of TPT as a single agent increased the percentages of cells in S-phase and G_2/M. If this was followed by [^{131}I]MIBG therapy, as in schedule [i], then, while the increased proportion of cells in G_2/M would be radiosensitive, the increased proportion of cells in S-phase would be more radioresistant than would be found in untreated cells, where the majority of cells are in G_1. While some of these cells will be in early G_1, and therefore exhibit radioresistance, others are will be in late G_1, and therefore exhibit radiosensitivity [186].

Administration of [^{131}I]MIBG before TPT, as in schedule [ii], will increase the proportion of cells in S-phase, and G_2/M. Cells in S-phase will be more sensitive to subsequent TPT treatment, through formation of double strand breaks by the fork collision model [85], and cells in G_2 have previously been reported to attempt repair of DNA double strand breaks (DSBs) [205, 206]. As a role for Topo I has been postulated in DNA damage repair [170-175], increased Topo I activity during G_2-associated DSB repair would increase sensitivity to TPT during this phase of the cell cycle.

Likewise, simultaneous administration of TPT and [^{131}I]MIBG, as in schedule [iii] will increase the proportion of cells in S-phase, which will increase TPT sensitivity but induce radioresistance. However, simultaneous scheduling will also increase the

proportion of cells in G_2/M, which will induce radiosensitivity and also possible TPT sensitivity through disruption of DNA repair.

10.6.2 The effect of scheduling of topotecan and [^{131}I]MIBG on DNA damage and repair

Treatment by either drug as a single agent, or by the less effective schedule resulted in a different response to DNA damage in cells assayed by single cell gel electrophoresis (SCGE), than treatment by schedules [ii] and [iii] (see Chapter 9). While administration of the two agents alone, or in any of the scheduled combinations resulted in significant amounts of DNA fragmentation in cells assayed immediately after treatment, cells assayed 24h after treatment exhibited levels of DNA fragmentation which were indistinguishable from those of untreated controls, following administration of TPT or [^{131}I]MIBG as single agents. Similar time dependency (ie extensive damage compared to untreated controls immediately after treatment and insignificant damage 24h later) also resulted from combination schedule [i].

However, administration of combination schedule [ii] or schedule [iii], resulted in significant levels of DNA fragmentation compared to untreated controls immediately after treatment, and significant DNA damage was also observed after 24h. This suggests that DNA repair pathways are not as efficient and greater long-term effects were achieved in cells treated by either schedules [ii], or schedule [iii]. Administration of combination schedule [i] was not as effective at disrupting DNA repair than either of the other two combination schedules.

These effects could be due to inhibition of DNA repair mechanisms [170-172], or TPT-induced Topo I cleavage activity [154]. These theories will be discussed in greater detail in Chapter 11.

10.7 Future work arising from the investigations of combinations of topotecan and [^{131}I]MIBG

10.7.1 Multiple administration of TPT to enhance supra-additivity of cell kill

Prior administration of TPT enhanced [^{131}I]MIBG uptake. Subsequent (or concurrent) administration of TPT resulted in reduced DNA repair. It is possible that multiple administrations of TPT could be used to combine these effects, resulting in greater levels of toxicity *in vitro* and *in vivo*. In this schedule, TPT would be administered prior to [^{131}I]MIBG to enhance cellular uptake, while a second administration of TPT concurrently with, or following the radiopharmaceutical would disrupt DNA damage repair.

10.7.2 Future work arising from investigations of the effects of topotecan and [^{131}I]MIBG on cellular mechanisms

The results of this study provide a useful insight into the effects of combinations of TPT and [^{131}I]MIBG on cellular mechanisms. However, further investigations will be required. For example, while less effective than schedules [ii] and [iii], administration of combination schedule [i] was capable of producing supra-additive levels of cytotoxicity *in vitro*, and caused effective growth delay of experimental tumours *in vivo*. This suggests that the time points examined in the study of DNA fragmentation and repair reported in Chapter 9 were not sufficient to adequately correlate long-term disruption of DNA repair, and either *in vitro* reduction in clongenicity or *in vivo* delay in xenograft tumour growth. Examination of DNA fragmentation at time points between 0h and 24h will be necessary

to discover the relative DNA repair efficiency in cells treated with either agent alone, and in cells treated by combination schedule [i].

Furthermore, the studies of cell cycle distribution and topoisomerase I activity described in Chapter 8 only investigated the effects of TPT and [^{131}I]MIBG immediately after treatment (ie. 0h), while the effects of combination therapy on DNA damage and repair described in Chapter 9 described the effects of the two agents at two time points; 0h and 24h after treatment. Therefore, just as examination of DNA fragmentation at time points between 0h and 24h will be necessary to investigate DNA repair efficiency, investigations into the longevity of altered cell cycle distribution due to administration of different schedules, and the extent of reduced Topo I catalytic activity following administration of TPT and/or [^{131}I]MIBG, at different time points after removal of the two drugs (0h to 24h), may help to elucidate the underlying mechanism of DNA damage repair inhibition.

Chapter 11

Discussion

II:

The role of topoisomerase I in the response to DNA damage

11.1 Introduction

Topoisomerase I activity is utilised during replication to prevent extreme stress to parent DNA, allowing the replication fork to proceed down the DNA strand, and preventing newly synthesised DNA becoming tangled in parent DNA [82, 83]. During transcription, transient unwinding of the DNA helix prevents RNA polymerase generating supercoiled tensions in template DNA [187]. Furthermore, a role for Topo I has been postulated in cellular pathways involved in the response to DNA damage. Several studies have suggested Topo I involvement in DNA damage repair [170-175].

This chapter describes the current understanding of cellular factors which affect topoisomerase I activity, how this can lead to an altered role for Topo I following DNA damage, and suggest possible approaches to the resolution of the underlying mechanism of TPT-induced radiopotentiation.

11.2 Factors which affect topoisomerase I activity: PARP-1 and p53

Poly(ADP-ribose) polymerase (PARP-1), is an enzyme involved in DNA repair [207, 208]. PARP-1 binds strongly to the sites of DNA damage, and activates DNA ligase III and DNA polymerase β by an indirect mechanism which involves binding to the base excision repair (BER) scaffold protein XRCC-1 (X-Ray Cross-Complementing-1) [161, 208-210]. PARP-1 also binds directly to Topo I, and induces increased formation of Topo I – DNA complexes [211].

PARP-1 is also responsible for the modification of the activity of a variety of proteins, including p53 and itself, by addition of poly(ADP-ribose) units [188, 209, 210], which alters the activity of the target protein [212]. PARP-1 is irreversibly degraded in cells undergoing apoptosis [213].

Boothman et al first reported a decrease in Topo I - mediated unwinding of supercoiled DNA following irradiation. They also reported that addition of PARP-1 inhibitors prevented this down-regulation of Topo I [161]. Down-regulation of Topo I enzymatic activity by PARP-1 was confirmed by Smith et al, who also reported that Topo I could form a complex with p53 which caused enhancement of Topo I - mediated unwinding [188].

11.3 Topoisomerase I activity and DNA damage

Following the formation of a number of different types of DNA lesions, (eg. single strand breaks, creation of apurinic sites, base-pair mismatches, etc) there is a down-regulation in Topo I catalytic activity in cells attempting DNA repair. This effect appears to be due to PARP-1-induced ADP-ribosylation, which occurs in the presence of the substrate Nicotinamide adenine dinucleotide (NAD+) [161, 188]. Therefore, PARP-1

ADP-ribosylates p53, preventing p53 enhancement of Topo I catalytic function [161], and also down-regulates Topo I catalytic activity by the same method.

However, PARP-1 is not only responsible for down-regulation in catalytic function, and can also induce increased formation of Topo I – DNA complexes. Therefore, with nicked DNA acting as a substrate for Topo I, there is a rapid sequestration of Topo I onto the sites of DNA lesions [170-172, 174, 211].

There is some evidence to suggest that a variety of DNA lesions, if located near a Topo I scissile site, can stimulate a Topo I-mediated cleavage reaction, either on the scissile strand, or on the opposite strand [214]. This would exacerbate the effects of the original lesion by causing the formation of additional single strand breaks (SSBs), irrepairable double strand breaks, (and also deleterious recombination events and covalent protein-DNA crosslinks).

Following DNA damage, if cells were undergoing repair, down-regulation of topoisomerase I catalytic activity by ADP-ribosylation, would help to prevent potentially hazardous Topo I-induced strand breaks on the scissile and non-scissile strand [161]. Therefore, any involvement that Topo I has in the repair of DNA damage would not involve its DNA cleavage / resealing activity. It may be that inactive Topo I may be helping to stabilise the site of damage until the DNA repair pathway becomes involved [174, 214].

Alternatively, it is possible that the creation of a complex between inactive Topo I and DNA at the site of damage may act as a marker for DNA repair enzymes [174, 175, 214]. See Figure 11-1.

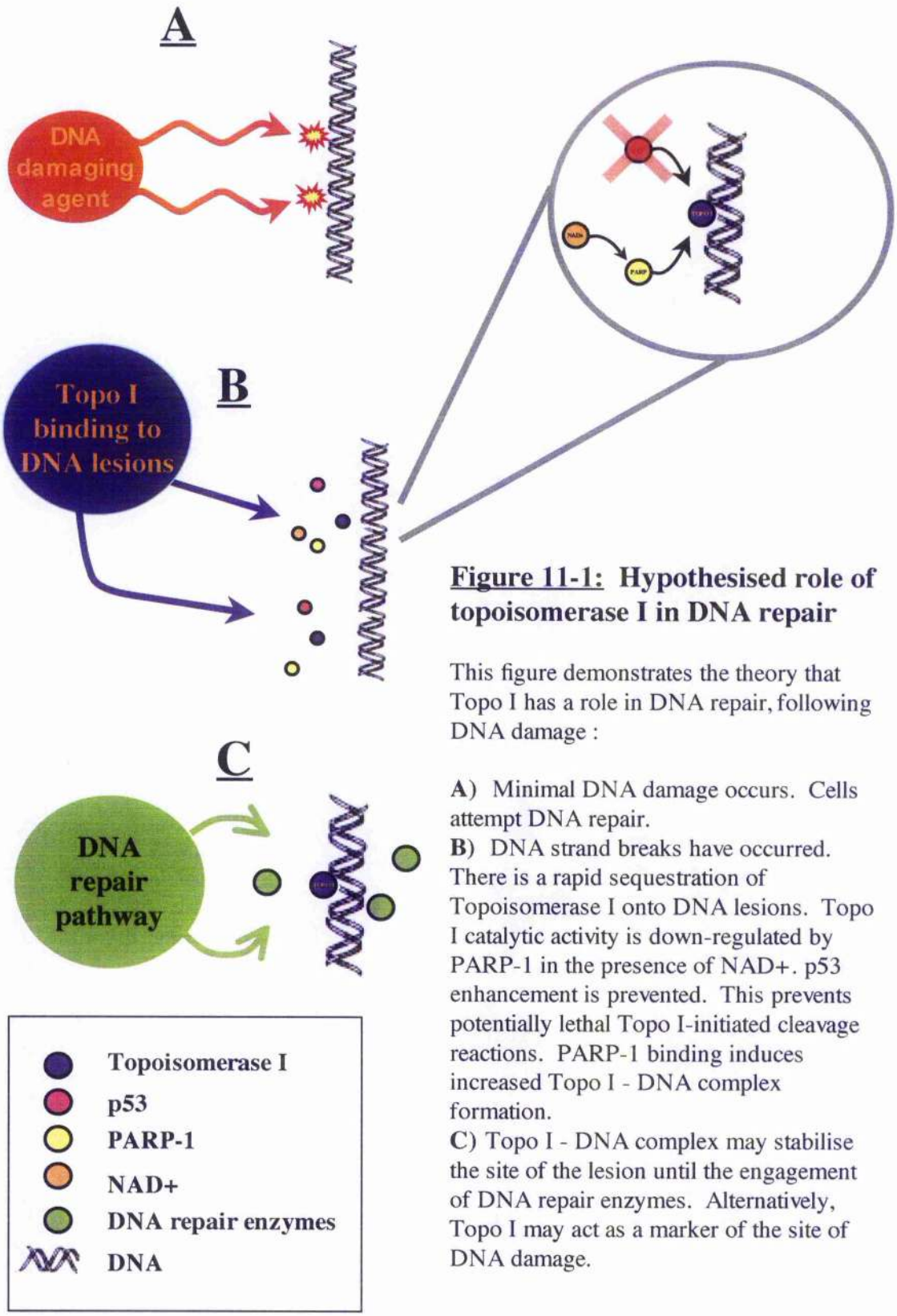

Figure 11-1: Hypothesised role of topoisomerase I in DNA repair

This figure demonstrates the theory that Topo I has a role in DNA repair, following DNA damage :

A) Minimal DNA damage occurs. Cells attempt DNA repair.
B) DNA strand breaks have occurred. There is a rapid sequestration of Topoisomerase I onto DNA lesions. Topo I catalytic activity is down-regulated by PARP-1 in the presence of NAD+. p53 enhancement is prevented. This prevents potentially lethal Topo I-initiated cleavage reactions. PARP-1 binding induces increased Topo I - DNA complex formation.
C) Topo I - DNA complex may stabilise the site of the lesion until the engagement of DNA repair enzymes. Alternatively, Topo I may act as a marker of the site of DNA damage.

11.4 Involvement of the camptothecins following DNA damage

The underlying mechanism of TPT radiopotentiation of cell death, is, at present, unknown. Most theories rely on the assumption that TPT-induced cell death follows the fork collision model [85]. Camptothecin analogues (such as TPT) stabilise the Topo I - DNA cleavable complex, preventing the religation step, and keeping Topo I irreversibly bound to DNA. During the next round of DNA replication, collision of the stabilised Topo I - DNA complex with the replication fork results in an irreversible double strand break, leading to cell cycle arrest and cell death. See Figure 11-2.

However, a more controversial theory suggests that the effect of TPT on Topo I may be more extreme. Boothman et al suggested that the radiopotentiation seen in cells treated with camptothecin analogues may be due to enhanced Topo I activity [161].

Due to their ability to initiate DNA strand breakage and ligation events, Topo I - DNA complexes are potentially dangerous to the cell. In normal circumstances, the interacellular levels of Topo I are kept relatively constant, and the levels and duration of Topo I - DNA complexes are strictly controlled [175, 215, 216]. In the alternative theory, topotecan, by increasing the longeivity of the Topo I - DNA complex increases the probability of unintended Topo I- mediated cleavage reactions [161, 175]. Topo I could then cleave the intact strand opposite the initial lesion, converting the radiation-induced SSB into a potentially lethal DSB [161, 214]. See Figure 11-2.

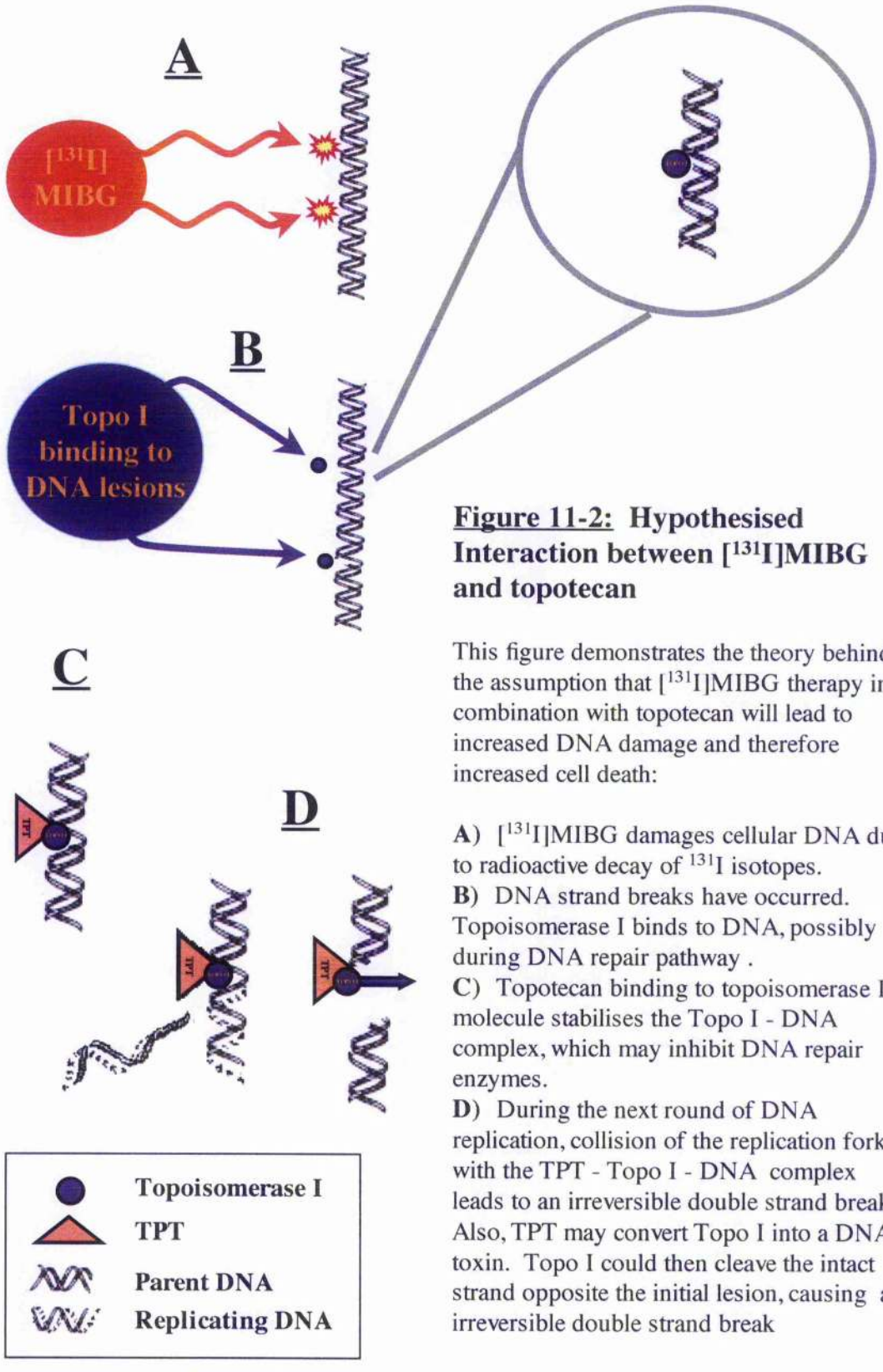

Figure 11-2: Hypothesised Interaction between [^{131}I]MIBG and topotecan

This figure demonstrates the theory behind the assumption that [^{131}I]MIBG therapy in combination with topotecan will lead to increased DNA damage and therefore increased cell death:

A) [^{131}I]MIBG damages cellular DNA due to radioactive decay of ^{131}I isotopes.
B) DNA strand breaks have occurred. Topoisomerase I binds to DNA, possibly during DNA repair pathway .
C) Topotecan binding to topoisomerase I molecule stabilises the Topo I - DNA complex, which may inhibit DNA repair enzymes.
D) During the next round of DNA replication, collision of the replication fork with the TPT - Topo I - DNA complex leads to an irreversible double strand break. Also, TPT may convert Topo I into a DNA toxin. Topo I could then cleave the intact strand opposite the initial lesion, causing an irreversible double strand break

11.5 Future work which may resolve the role of the camptothecins following DNA damage

An experimental study could be undertaken to resolve the underlying mechanism of TPT-induced radiopotentiation. Cells at different stages of the cell cycle, treated with combinations of TPT and radiation, would be tested by neutral comet assay, which only detects double strand breaks. If the classic theory is correct, DSBs should only be detectable in cells that have undergone S-phase.

However, if DSBs are inducible at other stages of the cell cycle, this would suggest that the alternative theory is correct. Optimisation of the timing of TPT administration would induce the maximum effect in the shortest time, in order to prevent cells going through the whole cell cycle before evaluation.

Chapter 12

Discussion

III:

Further avenues of research arising from this study, and final conclusions

12.1 Possible enhancement of supra-additive cytotoxicity caused by combinations of topotecan and [^{131}I]MIBG

The results of this study indicate that supra-additive levels of killing may be achieved in NAT expressing cells and xenografts treated with a combination of TPT and [^{131}I]MIBG. This chapter will describe the possibility of enhancing the effectiveness of this combination by introducing other drugs with the potential to induce synergy with TPT and/or [^{131}I]MIBG. The potential of radiosensitising agents other than TPT to enhance [^{131}I]MIBG therapy will also be discussed, as will the use of alternatives to ^{131}I as the choice of radionuclide in some therapeutic situations.

12.1.1 Potential of targeting cellular pathways to enhance topotecan-induced toxicity

In normal circumstances, the levels and duration of Topo I - DNA complexes are strictly controlled by several pathways [175, 215, 216]. Tyrosyl DNA phosphodiesterase (Tdp 1) catalyses the removal of the Topo I linked to 3'-DNA terminus by hydrolysing the covalent bond between the Topo I tyrosyl residue and the 3'-DNA phosphate [215]. Furthermore, TPT-stabilised Topo I – DNA complexes can be removed by Topo I ubiquitination, which flags the molecule for degradation by the 26S proteosome [216].

Therefore, it may be possible to enhance TPT-induced toxicity by disrupting these cellular pathways. Gene silencing of Tdp 1, by for example, the utilisation of RNAi technology, would prevent removal of the Topo I polypeptide by Tdp 1-induced hydrolysis. Likewise, a treatment regime incorporating the 26S proteosome inhibitor MG132 [217], would block the ubiquitin-induced degradation of Topo I.

12.2 Improving on [^{131}I]MIBG-derived regimens: Alternative radiosensitising agents

Optimisation of radiation damage induced in target cells can be obtained by rational combination of this treatment with radiosensitising agents. While the results of this study confirm radiopotentiation of [^{131}I]MIBG-induced toxicity by the topoisomerase I inhibitor topotecan, other agents with the potential to induce radiosensitisation could prove to be more beneficial.

12.2.1 Disulfiram (DS)

DS enhances cytotoxicity to cytotoxic drugs in cancer cells [218]. It counteracts the activity of the anti-apoptotic transcription factor NF-kB [219] NF-kB is activated by radiation, and tumour cells with increased NF-kB activity are resistant to chemo- and radiotherapy [220, 221]. However, the effectiveness of DS as a radiosensitiser of [^{131}I]MIBG targeted radiotherapy is unresolved.

12.2.2 PJ34

PJ34 is an inhibitor of PARP-1. It has previously been shown to be especially effective in enhancing cytotoxicity of low dose irradiation [222]. Therefore, PJ34 could also be an effective radiosensitiser of [^{131}I]MIBG-induced toxicity.

Furthermore, as PARP-1 is responsible for both down-regulation in Topo I catalytic activity in cells attempting DNA repair [161], and increased formation of Topo I – DNA complexes [211], investigations of treatment regimens including both PJ34 and TPT could help to resolve the contributions of these activities to TPT-induced radiopotentiation.

12.3 Choice of radionuclide: Alternatives to ^{131}I as a conjugate for MIBG

Agents other than topotecan have the potential to prove effective as radiosensitisers. Likewise, radionuclides other than ^{131}I may prove to be more effective in some situations. The goal of targeted radiotherapy is delivery of radiation to tumour cells with the sparing of normal tissue. However, in order to maximise the effectiveness of the therapeutic agent, and minimise normal tissue toxicity, the choice of radionuclide is important. Factors such as subcellular localisation of the targeting agent, size of the tumour mass, path length of radioisotope decay and linear energy transfer (LET - the measure of energy transferred per unit length of track) [223] should be taken into account.

While the focus of this study has been the β–emitter [^{131}I]MIBG, ^{131}I has a long path length and relatively low LET. Therefore, as tumour size decreases, the amount of energy absorbed by the tumour becomes progressively smaller, and more of the energy is deposited outside the target [224].

For this reason, ^{131}I may not be the optimal choice of radionuclide in all therapeutic situations. For NAT-expressing tumours, which have the potential to be treated by radiolabelled MIBG, establishing the most appropriate radionuclides whose decay particles vary with respect to LET and path length could improve the therapeutic efficacy of this targeting molecule (Table 12-1, Figure 12-1).

Radionuclide	Decay particle	Particle range	Half life	Current use
^{131}I	b	0.8mm	8 days	therapy
^{211}At	a	0.05mm	7 hours	therapy
^{123}I	Auger electron	~ 1-10nm	13.2 hours	imaging
^{125}I	Auger electron	~ 1-10nm	60.1 days	imaging

Table 12-1: Alternatives to ^{131}I as a conjugate for MIBG

Different radionuclides have different properties which may be more beneficial than ^{131}I in certain circumstances. See Figure 12-1.

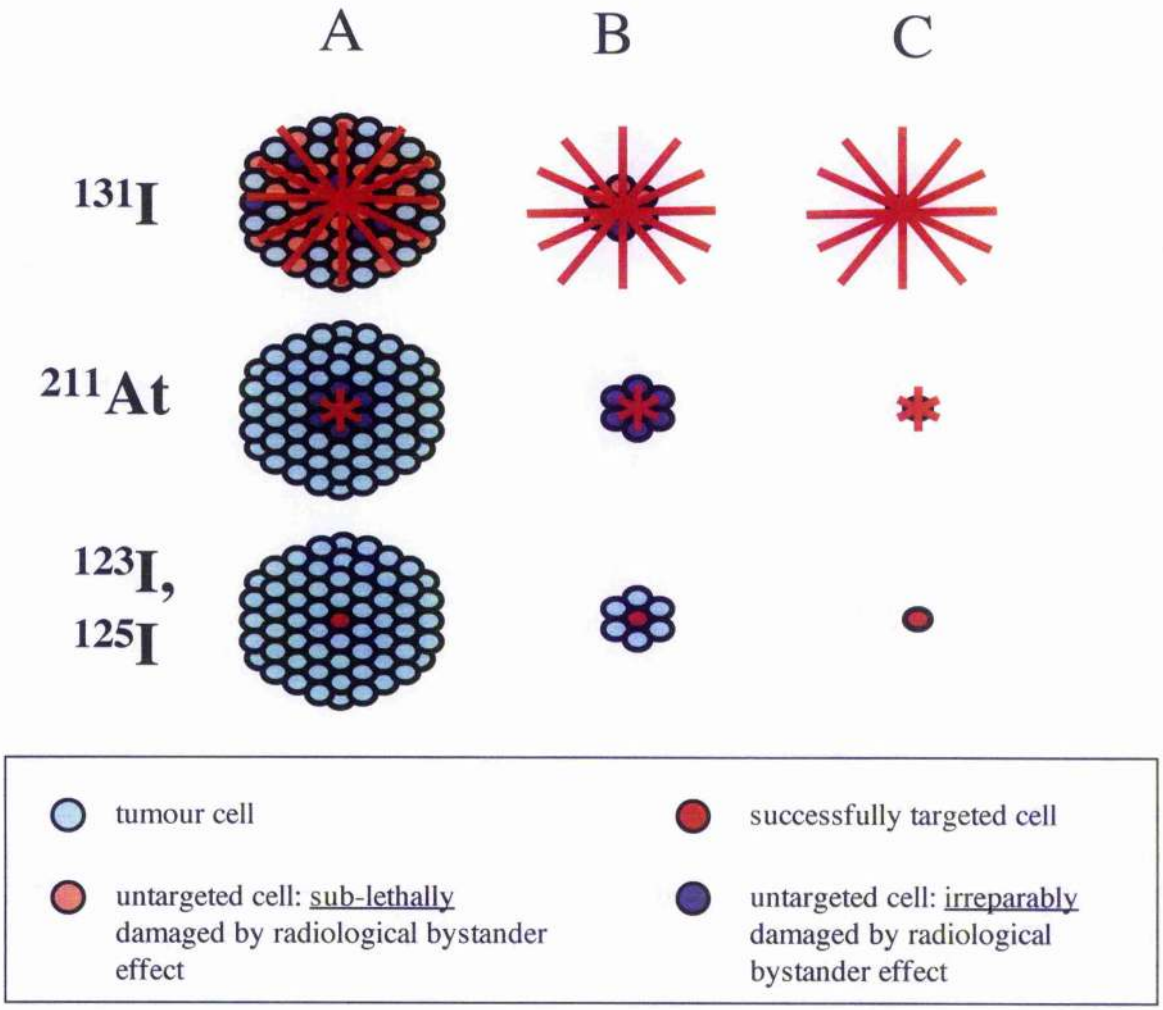

Figure 12-1: Relationship between particle range, radiological bystander effect and linear energy transfer

A) Large tumour masses: As ^{131}I has a longer particle length than ^{211}At, ^{123}I, or ^{125}I, the radiological bystander effect will cause damage to a greater number of cells.

B) Micometastases: In smaller tumours, ^{131}I will be less effective as the majority of the energy will be deposited outside the tumour mass. ^{211}At has a far greater LET, therefore, damage caused by ^{211}At to adjacent cells is more likely to be irreparable, leading to far greater toxicity in micometastases.

C) Circulating tumour cells: ^{123}I and ^{125}I have a very short range, but a very high LET, and are therefore only toxic to individual cells. They will be most effective against circulating tumour cells. The longer path lengths of ^{131}I and ^{211}At are more likely to cause damage to normal tissue.

12.3.1 [^{211}At]MABG

^{211}At, an α-emitting isotope of Astatine (At), is a radiohalogen that has potential as an alternative to radio-iodine in the treatment of neuroblastoma by noradrenaline analogues [20].

Astatine is found underneath iodine in group 7A of the periodic table, and has similar chemical properties [225]. Naturally occurring astatine is incredibly rare (less than 29 grams are present in the earth's crust), but synthetic At can be generated in a cyclotron by bombarding bismuth with α-particles [225].

^{211}At has a shorter particle range than ^{131}I (50μm for ^{211}At, compared to 800μm for ^{131}I). This means that [^{211}At]MABG therapy will affect fewer untargeted cells by the radiological bystander effect than [^{131}I]MIBG therapy.

However, ^{211}At has a very high LET compared to ^{131}I [226], therefore the damage caused by [^{211}At]MABG-induced radiological bystander effect is more likely to be lethal than damage caused by [^{131}I]MIBG therapy, resulting in a greater probability of irreparable damage, and, therefore, far superior toxicity in micometastases [20, 226] (Table 12-1; Figure 12-1).

12.3.2 [^{123}I]MIBG and [^{125}I]MIBG

It has previously been assumed that the effectiveness of Auger electron emitters such as ^{123}I and ^{125}I would be confined to molecules within reach of the nucleus [227, 228]. These atoms decay by electron capture and internal conversion, which results in the emission of extremely densely ionising radiation of very short range (1-10nm). Therefore, targeting agents which remain cytoplasmic, or membrane bound, would not be as effective if conjugated to Auger electron emitters than if conjugated to radionuclides with longer path lengths, such as β–emitters [227, 228].

However, it has previously been reported that [^{123}I]MIBG and [^{125}I]MIBG were more toxic to neuroblastoma cells than would be expected by cytoplasmic MIBG localisation [20], suggesting that these short range emitters would be well suited to the treatment of circulating tumour cells (Table 12-1; Figure 12-1). The effectiveness of ^{123}I and ^{125}I labelled MIBG may be explained by the recent identification of radiation-induced biological bystander effects [229-236], and it is possible that targeting molecules conjugated to short-range Auger emitters may be of greater therapeutic benefit than was previously believed.

12.4 Radiation-induced biological bystander effects (RIBBEs)

While the contribution to kill of neighbouring non-targeted cells by radioactive decay particles emanating from targeted cells is relatively well characterised [237, 238], the significance of radiation-induced biological bystander effects (RIBBEs) has only recently been perceived [229]. RIBBEs involve the cellular processing of the radiation insult into toxic metabolites. Therefore, translation of the physical radiation insult into biological signals or toxins, means that cytotoxicity is elicited by both direct DNA damage and also from RIBBEs. RIBBEs have been reported utilising high and low LET radiation delivered by focused microbeams and by transfer of media from irradiated to unirradiated cells [230-236] (Figure 12-2).

RIBBEs are a significant contributor to the total effects elicited in cells exposed to low dose and dose rate irradiation [239]. As this is a feature of targeted radionuclide therapy [240], the magnitude of RIBBEs may be pertinent to the success of this mode of treatment. The mechanisms and potency of these bystander effects, particularly those induced by radiopharmaceuticals, are, as yet, unresolved.

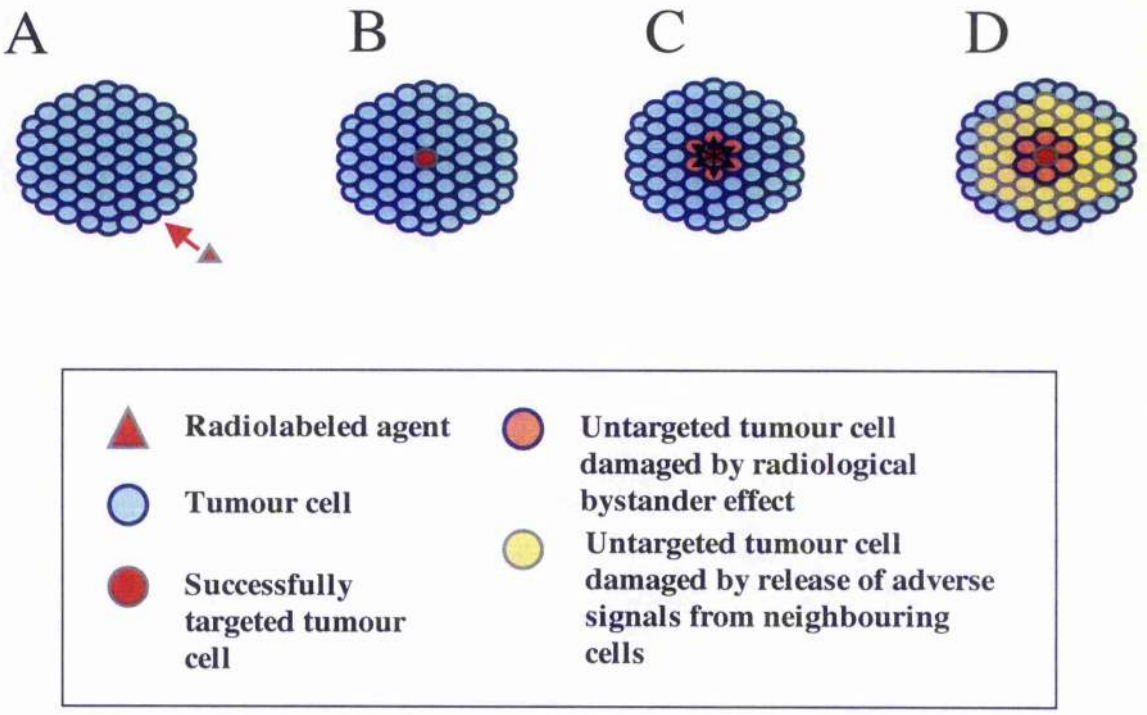

Figure 12-2: Radiation-induced biological bystander effect (RIBBE)

RIBBE involves the cellular processing of the radiation insult into toxic metabolites:

A) Tumour cells are targeted by a radiolabelled agent

B) Only a fraction of the tumour is successfully targeted. The majority remain unaffected.

C) Energy released by decay of the radioisotope emanates from the targeted portions of the tumour in three dimensions, causing damage to neighbouring cells that have not been successfully targeted.

D) Damaged cells release biological signals which in turn cause damage to neighbouring cells.

12.5 NAT gene therapy

12.5.1 Targeted radionuclide therapy for tumours with no radiotargetable feature

Most tumours do not possess a radiotargetable feature. However, the UVW/NAT cell line used in this study is derived from the human glioblastoma cell line UVW which was transfected with a pREP9 episomal expression vector containing a copy of the bovine NAT cDNA. This demonstrates that introduction of NAT transgenes into tumours with no radiotargetable feature can endow them with the capacity for uptake of radioiodinated MIBG.

Generally, mammalian transcriptional control elements are unsatisfactory for cancer gene therapy, due to low expression capacity and limited tumour specificity. A promising alternative means of restricting transgene expression to malignant cells is the exploitation of the telomerase activity of tumour cells [241-244], or the utilisation of radiation-inducible control elements [245, 246].

12.5.2 Tumour specific gene expression: Telomerase promoter elements

Telomeres are necessary for chromosome stability. In normal cells, there is a gradual loss of telomeric sequences during successive cell divisions, and in the absence of mechanisms to prevent telomere shortening, cells have a limited proliferative life span before entering senescence [247]. In immortal cells, including cancer cells, telomere length is maintained through the actions of a specialized reverse transcriptase, called telomerase. Telomerase activity is thought to be essential for immortalization of human cells *in vitro* and of cancer cells *in vivo*, and it is detectable in 85% of malignant tumors [248].

Telomerase activity depends upon the presence of both the RNA subunit (hTR) and the catalytic protein subunit (hTERT) [249]. It has previously been demonstrated that both hTR and hTERT promoters can induce high levels of NAT transgene transcription, enabling [^{131}I]MIBG- and [^{211}At]MABG-mediated host cell kill in a variety of tumour cell lines [237, 250-252].

12.5.3 Radiation-inducible control elements

Selective transgene expression may also be achieved by radiation-inducible control elements, such as the $p21^{WAF-1/CIP-1}$ promoter [245, 246]. The tumour growth suppressor $p21^{WAF1/CIP1}$ is a potent inhibitor of cyclin-dependent kinases, and enhanced protein levels are found in cells undergoing either p53-associated G_1 arrest or apoptosis following DNA damage [253]. It has been demonstrated that activation of the $p21^{WAF-1/CIP-1}$ promoter occurs following external beam irradiation and hypoxia in tumour xenografts, regardless of their p53 status. Furthermore the $p21^{WAF-1/CIP-1}$ promoter has low levels of activity in the absence of these stimuli in tumours, but not normal cells, suggesting a tumour specific mode of activation [246].

It should therefore be possible to utilise the $p21^{WAF-1/CIP-1}$ promoter to drive expression of NAT in tumours following activation by radiopharmaceuticals. In neuroblastoma cells, following introduction of a vector incorporating the NAT gene under the control of the $p21^{WAF-1/CIP-1}$ promoter, a priming dose of [^{131}I]MIBG is administered. This is accumulated specifically in the neuroblastoma cells, and results in stimulation of the $p21^{WAF-1/CIP-1}$ promoter, leading to enhanced NAT expression. Subsequent administration of high doses of [^{131}I]MIBG would therefore be more therapeutically effective.

For the treatment of other tumour types, without endogenous NAT gene expression, a priming dose of conformal external beam irradiation could be used to induce activation of the $p21^{WAF-1/CIP-1}$ promoter. However, while triggering the $p21^{WAF-1/CIP-1}$ promoter by external beam irradiation shows promise for treatment of discernable tumour masses, it is inappropriate for management of covert disease.

12.6 NAT gene therapy: Gene delivery

Selective NAT gene expression in malignant tissues, through the use of tumour specific, or radiation-inducible promoter elements suggests that these strategies could be of therapeutic benefit. However, in many cases, the efficacy of gene therapy has been hampered by inefficient gene delivery.

12.6.1 Viral vectors

Of the clinical trials of gene therapy carried out to date, 66% have concerned the treatment of cancer, and 70% have utilised viral vectors [254]. During infection of a cell, viruses use specific entry mechanisms to gain entry. This makes viruses attractive as vectors for gene therapy [10, 254]. However, the challenge of developing viral vectors lies in harnessing their targeting efficiency while abrogating their ability to cause infection and cell death. Recently, mutant viruses have been shown to be capable of delivering transgenes, allowing high levels of gene expression and selective replication in tumour cells [255].

Retroviruses were the first vectors used in gene therapy, and remain the most commonly used (28% of all trials). However, retroviruses have a relatively limited capacity to carry therapeutic genes, and the risk of insertional mutagenesis by retroviral integration into the chromosomes of target cells further limits the effectiveness of these vectors [254].

Adenoviruses are the second most commonly utilised viral vector (26% of all trials), while, to date, clinical trials involving herpes simplex viral (HSV) vectors have been limited (2.8% of all trials) [254]. Adenoviruses are attractive candidates for gene delivery due to their capacity for carrying large DNA loads and their high efficiency of

transduction, and recombinant HSV vectors have recently demonstrated efficient delivery and expression of transgenes [255]. Construction of recombinant adenoviral or HSV vectors could allow delivery of telomerase promoter- or $p21^{WAF-1/CIP-1}$ promoter-NAT transgene constructs.

12.6.2 Immunoliposomes

Non-viral delivery vehicles (cationic lipid/DNA complexes) have been utilised in 9.3% of gene therapy trials [254]. The tumour targeting of CCLs can be improved by coupling a monoclonal antibody (mAb) or its Fab fragment, directed to tumour-specific antigens, to their external surface.

This strategy has been described using mAbs directed against the neuroblastoma- and melanoma-specific antigen GD_2 [256-259]. Conjugation of CCLs to other tumour targeting mAbs would allow successful gene delivery specifically to malignant tissue [260-265]. See Table 12-2.

Antibody	Cell Target	References
81C6 (Anti- tenacin)	Extracellular matrix glycoprotein tenacin - Expressed in >95% brain malignancies	**[260, 261]**
Anti-GD_2	Disialoganglioside (GD_2) - Expressed on surface of neuroblastoma and melanoma tissue - Low expression in normal tissue	**[262, 263]**
Anti-CEA	GPI-anchored cell surface membrane protein CEA - Expressed in a wide variety of tumours - Antigen not present in normal cells	**[264, 265]**

Table 12-2: mABs or Fab fragments which may be coupled to CCLs

Tumour targeting of Coated Cationic liposomes (CCLs) can be improved by coupling a monoclonal antibody (mAb) or its Fab fragment, directed to tumour-specific antigens, to their external surface.

This would allow successful gene delivery specifically to malignant tissue.

12.7 The use of multicellular mosaic spheroids to determine transfection efficiencies

As described in Section 10.2.2, mosaic spheroids with a range of proportions of NAT-expressing cells would allow determination of sensitivity of scintigraphic analyses to the results of analyses of NAT gene expression. This model would also allow an estimation of minimum requirement for NAT gene transfection to allow tumour sterilisation by the administration of combinations of targeted radiotherapy (ie. [^{131}I]MIBG as used in this study, or [^{123}I]MIBG [^{125}I]MIBG or [^{211}At]MABG as described in section 12.3), and radiosensitising agents (ie. TPT as used in this study, or DS or PJ34 as described in section 12.2) following NAT gene therapy (Figure 10-1).

12.8 Conclusions

12.8.1 Development of a real-time RT-PCR assay for prediction of the uptake of [^{131}I]MIBG

Assays based on real-time PCR methodology may also facilitate the development of novel therapies designed to alter cellular function at the transcriptional level [71]. For example, several studies have indicated that a wide range of DNA-interacting agents cause an increase in the ability of neuroblastoma cells to actively uptake radio-labelled MIBG [154, 157-159], and, likewise, TPT induces increased accumulation of this radiopharmaceutical (see Chapter 3). Whilst TPT-induced enhancement of uptake did not correlate with an increase of NAT gene product, the molecular mechanisms involved have yet to be elucidated, and the assay described in Chapter 2 has the potential to allow quantitative analysis of the effects of these agents on NAT expression and enable the design of improved therapeutic schedules.

12.8.2 Cytotoxic interaction between topotecan and [^{131}I]MIBG

The results of this study indicate that supra-additive levels of killing may be achieved in NAT expressing cells and xenografts treated with a combination of TPT and [^{131}I]MIBG. Furthermore, combination treatment was well tolerated by experimental animals and caused negligible myelotoxicity.

However, the effectiveness of combinations of topotecan and [^{131}I]MIBG was dependent on the order of administration. Maximal TPT-induced radiosensitisation was induced by the administration of the drug concurrently with, or following [^{131}I]MIBG. Furthermore, while radiopotentiation may be linked to disruption of DNA repair, the exact mechanisms were outside the scope of this study, and remain unresolved. Nevertheless, the results of this study suggest that combinations of topotecan and [^{131}I]MIBG, produce encouraging results *in vitro* and *in vivo*.

If the synergy demonstrated in model systems between topotecan and [^{131}I]MIBG in the present study can be replicated in patients with neuroblastoma, there is potential for real therapeutic gain. Clinical studies of topotecan given simultaneously with, and subsequently to, [^{131}I]MIBG have commenced in the United Kingdom, and in Europe.

References

[1] Ackernecht EH
History and geography of the most important diseases. *Hufner, New York 1965*

[2] Cassileth BR
The evolution of oncology. *Perspect. Biol. Med 1983: 26, 362-374*

[3] Bagshawe KD
The history of targeted therapy for cancer
In: Targeted Therapy for Cancer
Ed. Syrigos KN, Harrington KJ
Oxford University Press 2003: 3-16

[4] Waters J, Cunningham D
Antisense therapy as a target modality
In: Targeted Therapy for Cancer
Ed. Syrigos KN, Harrington KJ
Oxford University Press 2003: 162-186

[5] Khan IM, Coulson JM
A novel method to stabilise antisesnse oligonucleotides against exonuclease degradation.
Nucl Acids res 1993: 21, 2957-2958

[6] Ichim TE, Li M, Qian H, Popov IA, Rycerz K, Zheng X, White D, Zhong R, Min W-P
RNA Interference: A Potent Tool for Gene-Specific Therapeutics. *American Journal of Transplantation 2004: 4(8), 1227-1236*

[7] El-Aneed, A
Current strategies in cancer gene therapy. *European Journal of Pharmacology 2004: 498, 1-8*

[8] Gregoriadis G
Homing of liposomes to target cells. *Biochem Soc Transact 1975: 3, 613-618*

[9] Leserman LD, Machy P, Barbet J
Cell specific drug transfer from liposome bearing monoclonal antibodies. *Nature 1981: 293, 226-228*

[10] Harrington KJ, Vile RG
Targeting of cancer gene therapy
In: Targeted Therapy for Cancer
Ed. Syrigos KN, Harrington KJ
Oxford University Press 2003: 111-154

[11] Pandha HS
Genetic immunotherapy for cancer
In: Targeted Therapy for Cancer
Ed. Syrigos KN, Harrington KJ
Oxford University Press 2003: 95-110

[12] Vaughan AT, Anderson P, Dykes PW, Chapman CE, Bradwell AR
Limitations to the killing of tumours using radiolabelled antibodies. *Brit. J. Radiol. 1987: 60, 567-572*

[13] Reisfeld RA, Sell S
Monoclonal antibodies and cancer therapy
UCL Symposium in Molecular and Cellular Biology
New Series Vol 27. AlanR Liss Inc, New York 1985: 207-257

[14] Bagshawe KD
Antibody directed enzymes revive anticancer prodrug concepts. *Br J Cancer 1987: 56(5), 531-532*

[15] Huber BE, Richards CA, Krenitsky TA
Retroviral-mediated gene therapy for the treatment of hepatocellular carcinoma: An innovative approach for cancer therapy. *Proc Natl Acad Sci, USA 1991: 88, 8039-8043*

[16] Porter A, Aref A, Chodounsky Z, et al
A global stategy for radiotherapy: a who consultation. *Clinical Oncology 1999: 11, 368-370*

[17] Mairs RJ, Boyd M
Targeting radiotherapy to cancer by gene transfer. *Journal of Biomedicine and Biotechnology 2003: 2, 102-109.*

[18] Mairs RJ, Cunningham SH, Boyd M, Carlin S
Applications of gene transfer to targeted radiotherapy. *Current Pharmaceutical Design 2000: 6, 1419-1432*

[19] Denning C, Pitts JD
Bystander effects of different enzyme-prodrug systems for cancer gene therapy depend on different pathways for intracellular transfer of toxic metabolites, a factor that will govern clinical choice of appropriate regimes. *Hum Gene Ther 1997: 8(15), 1825-1835*

[20] Cunningham SH, Mairs RJ, Wheldon TE, Welsh PC, Vaidynathan G Zalutsky MR
Toxicity to neuroblastoma cells and spheroids of benzylguanidine conjugated to radionuclides with short-range emissions. *Br J Cancer 1998: 77, 2061-2068*

[21] Simpson JK, Gaze MN
Current management of neuroblastoma. *The Oncologist 1998: 3(4), 253-262*

[22] Office of Population Census and Surveys.
Childhood cancer in Britain, incidence, survival and mortality. *London: HMSO 1982*

[23] Oppenheimer O, Alaminos M, Gerald WL
Genomic medecine and neuroblastoma. *Expert Review of Molecular Diagnostics 2003: 3(1), 39-54*

[24] Grovas A, Fremgen A, Rauck A, Ruymann FB, Hutchison CL, Winchester DP , Menck HR

The National Cancer Data Base report on patterns of childhood cancers in the United States. *Cancer 1997: 80, 2321-2332*

[25] Maris JM, Matthay KK
Molecular biology of neuroblastoma. *Journal of Clinical Oncology 1999: 7, 2264-2279*

[26] Seeger RC, Brodeur GM, Sather H, Dalton A, Siegel SE, Wong KY, Hammond D
Association of multiple copies of the N-*myc* oncogene with rapid progression of neuroblastoma. *N Engl J Med 1985: 313, 1111-1116*

[27] Matthay KK, Perez C, Seeger RC, Brodeur GM, Shimada H, Atkinson JB, Black CT, Gerbing R, Haase GM, Stram DO, Swift P, Lukens JN
Successful treatment of stage III neuroblastoma based on prospective biological staging: A childrens cancer group study. *J Clin Oncol 1998: 16, 1256-1264*

[28] Brodeur GM, Sekhon GS, Goldstein MN
Chromosomal abberations in human neuroblastomas. *Cancer 1997: 40, 2256-2263*

[29] Brodeur GM, Green AA, Hayes FA, Williams KJ, Williams DL, Tsiatis AA
Cytogenetic features of human neuroblastomas and cell lines. *Cancer Res 1981: 41, 4678-4686*

[30] Fong CT, Dracopoli NC, White PS, Merrill PT, Griffith RC, Housman DE, Brodeur GM
Loss of heterozygosity for the short arm of chromosome 1 in human neuroblastomas: Correlation with N-*myc* amplification. *Proc Natl Acad Sci USA 1989: 86, 3753-3757*

[31] Fong CT, White PS, Peterson K, Sapienza C, Cavenee WK, Kern SE, V ogelstein B, Cantor AB, Look AT, Brodeur GM
Loss of heterozygosity for chromosomes 1 or 14 defines subsets of advanced neuroblastomas. *Cancer Res 1992: 52, 1780-1785*

[32] White PS, Maris JM, Beltinger C, Sulman E, Marshall HN, Fujimori M, Kaufman BA, Biegel JA, Allen C, Hilliard C, Valentine MB, Look AT, Enomoto H, Sakiyama S, Brodeur GM
A region of consistent deletion in neuroblastoma maps within human chromosome 1p36.2-36.3. *Proc Natl Acad Sci USA 1995: 92, 5520-5524*

[33] Takita J, Hayashi Y, Kohno T, Shiseki M, Yamaguchi M, Hanada R, Yamamoto K, Yokota J
Allelotype of neuroblastoma. *Oncogene 1995: 11, 1829-1834*

[34] Maris JM, White PS, Beltinger C, Sulman EP, Castleberry RP, Shuster JJ, Look AT, Brodeur GM
Significance of chromosome 1p loss of heterozygosity in neuroblastma. *Cancer Res 1995: 55, 4664-4669*

[35] Gehring M, Berthold F, Edler L, Schwab M, Amler LC
The 1p deletion is not a reliable marker for the prognosis of patients with neuroblastoma. *Cancer Res 1995: 55, 5366-5369*

[36] Caron H, van Sluis P, de Kraker J, Bokkerink J, Egeler M, Laureys G, Slater R, Westerveld A, Versteeg R, Buys CHCM
Allelic loss of chromosome 1p as a predictor of unfavourable outcome in patients with neuroblastoma. *N Engl J Med 1996: 334, 225-230*

[37] Martinsson T, Sjoberg RM, Hedborg F, Kogner P
Deletion of chromosome 1p loci and microsatellite instability in neuroblastomas analysed with short-tandem repeat polymorphisms. *Cancer Res 1995: 55, 5681-5686*

[38] Mertens F, JohanssonB, Mitelman F
Chromosomal imbalance maps of malignant solid tumours: A cytogenetic survey of 3185 neoplasms. *Cancer Res 1997: 57, 2765-2780*

[39] Ejeskar K, Aburatani H, Abrahamsson J, Kogner P, Martinsson T

Loss of heterozygosity of 3p markers in neuroblastoma tumours inplicate a tumour-suppressor locus distal to the *FHIT* gene. *Br J Cancer 1998: 77, 1787-1791*

[**40**] Caron H, van Sluis P, Buschman R Pereira do Tanque R, Maes P, Beks L, De Kraker J, Voute PA, Vergnaud G, Westerveld A, Slater R, Versteeg R,
Allelic loss of the short arm of chromosome 4 in neuroblastoma suggests a novel tumour suppressor gene locus. *Hum Genet 1996: 97, 834-837*

[**41**] Meltzer SJ, O'Doherty SP, Frantz CN, Smolinski K, Yin J, Cantor AB, Liu J, Valentine M, Brodeur GM, Berg PE
Allelic imbalance on chromosome 5q predicts long-term survival in neuroblastoma. *Br J Cancer 1996: 74, 1855-1861*

[**42**] Takita J, Hayashi Y, Kohno T, Yamaguchi N, Hanada R, Yamamoto K, Yokota J
Deletion map of chromosome 9 and *p16* (CDKN2A) gene alterations in neuroblastoma. *Cancer Res 1997: 57, 907-912*

[**43**] Marshall B, Isidro G, Martins AG, Boavida MG
Loss of heterozygosity at chromosome 9p21 in primary neuroblastomas: Evidence for two deleted regions. *Cancer Genet Cytogenet 1997: 96, 134-139*

[**44**] Srivatsan ES, Ying KL, Seeger RC
Deletion of chromosome 11 and of 14q sequences in neuroblastoma. *Genes Chromosom Cancer 1993: 7, 32-37*

[**45**] Takayama H, Suzuki T, Mugishima H, Fujisawa T, Ookuni M, Scwab M, Gehring M, Nakamura Y, Sugimura T, Terada M, Yokota J
Deletion mapping of chromosomes 14q and 1p in human neuroblastoma. *Oncogene 1992: 7, 1185-1189*

[**46**] Reale MA, Reyes-Mugica M, Pierceall WE, Rubinstein MC, Hedrick L, Cohn SL, Nakagawara A, Brodeur GM, Fearon ER

Loss of *DCC* expression in neuroblastoma is associated with disease dissemination. *Clin Cancer Res 1996: 2, 1097-1102*

[47] Norris MD, Bordow SB, Haber PS, Marshall GM, Kavallaris M, Madafiglio J, Cohn SL, Salwen H, Schmidt ML, Hipfner DR, Cole SPC, Deeley RG, Haber M
Evidence that *MYC* N oncogene regulates *MRP* gene expression in neuroblastoma. *Eur J cancer 1997: 33, 1911-1916*

[48] Shafford EA, Rogers DW, Pritchard J
Advanced neuroblastoma: Improved response rate using a multiagent regimen (OPEC) including sequential cisplatin and VM-26. *J Clin Oncol 1984: 2, 742-747*

[49] Matthay KK, Sather HN, Seeger RC
Excellent outcome of stage II neuroblastoma is independent of residual disease and radiation therapy. *J Clin Oncol 1989: 7, 236-244*

[50] D'Angio GJ, Evans AE, Koop CE
Special pattern of widespread neuroblastoma with a favourable prognosis. *Lancet 1971: 1, 1046-1049*

[51] Matthay KK, Villablanca JG, Seeger RC, Stram DO, et al
Treatment of high-risk neuroblastoma with chemotherapy, radiotherapy, autologous bone marrow transplantation, and 13-*cis*-retinoic acid. *New England J Medicine 1999: 341, 1165-1173*

[52] Mastrangelo S, Tornesello A, Diociaiuti L, Pession A, Prete A, Rufini V, Tronconc L, Mastrangelo R
Treatment of advanced neuroblastoma: feasibility and therapeautic potential of a novel approach combining 131 I-MIBG and multiple drug chemotherapy. *British Journal of Cancer 2001: 84(4), 460-464*

[53] Davidoff AM, Leary MA, Ng CYC, Brown P, Leary MA, Spurbeck WW, Zhou J, Horwitz E, Vanin EF, Nienhuis AW

Gene therapy-mediated expression by tumor cells of the angiogenesis inhibitor flk-1 results in inhibition of neuroblastoma growth in-vivo. *Journal of Pediatric Surgery 2001: 36(1), 30-36*

[54] Cho H-S, Jun Y-S, Park CY, Lyu CJ, Kim BS, Kim K-Y
Retroviral-mediated IL-2 gene transfer into murine neuroblastoma. *Yonsei Medical Journal 2000: 41(1), 76-81*

[55] Meck MM, Wierdl M, Wagner, Burger RA, Guichard SM, Krull EJ, Harris LC, Potter PM, Danks MK
A virus-directed enzyme prodrug therapy approach to purging neuroblastoma cells from hematopoietic cells using adenovirus encoding rabit carboxylesterase and CPT-11. *Cancer Research 2001: 61(13), 5083-5089*

[56] Tanabe Y, Ito S, Nagae I
Stealth liposomal doxorubicin, target therapy for neuroblastoma. *Zasshi/Tokyo Ika Daigaku 2000: 58(4), 481-493*

[57] Calzolari P, Prete A, Paolucci P, Paolucci G
Liposomes for high dose chemotherapy. *Clinical Chemistry & Enzymology Communications 1990: 2(4-6), 359-362*

[58] Kamio Y, Kato H, Kishikawa T, Toda T, Sasaki S, Ito J, Kato T, Tanaka R
Enhancement of both intracellular uptake and antitumor action of cisplatinum on human neuroblastoma cells by encapsulation in liposomes. *Japanese Journal of Cancer Research 1989: 80(8), 787-793*

[59] Cheung N-KV, Kushner BH, Kramer K
Monoclonal antibody-based therapy of neurobloastoma. *Hematology-Oncology clinics of North America 2001: 15(5), 853-866*

[60] Hoefnagel CA, Rutgers M, Buitenhuis CKM Smets LA, de Kraker J, Meli M, Carrel F, Amstutz H, Schubiger PA, Novak-Hofer I

A comparison of targeting of neuroblastoma with mIBG and anti L1-CAM antibody mAb chCE7: therapeutic efficacy in a neuroblastoma xenograft model and imaging of neuroblastoma patients. *European Journal of Nuclear medicine 2001: 28(3), 359-368*

[61] Jacque S Jr, Tobes MC, Sissons JC, Baker JA, Wieland DM
Comparison of the sodium dependence of uptake of meta-iodo-benzylguanidine and norepenephrine into cultured bovine adrenomedullary cells. *Mol Pharmacology 1984: 26, 539-546*

[62] Mairs RJ, Livingstone AL, Gaze MN, Wheldon TE, Barrett A
Prediction of accumulation of ^{131}I-meta-iodo-benzylguanidine in neuroblastoma cell lines by means of reverse transcription and polymerase chain reaction. *Br J Cancer 1994: 70, 97-101*

[63] Staalman CR, Hoefnagel CA.
Imaging of Neuroblastoma and Metastasis.
In: Neuroblastoma
Ed: Brodeur GM, Sawada T, Tsuchida Y, Voûte PA
Elsevier Science B.V. 2000: 303-32

[64] Habrand JL, D'Angio GJ.
Radiotherapy in Neuroblastoma
In: Neuroblastoma
Ed: Brodeur GM, Sawada T, Tsuchida Y, Voûte PA
Elsevier Science B.V. 2000: 479-496

[65] Garaventa A, Guerra P, Arrighini A, Bertolazzi M, Bestagno M, De Bernardi B, Lanino E, Villavecchia GP, Claudiani F
Treatment of advanced neuroblastoma with [^{131}I] metaiodobenzylguanidine. *Cancer 1991: 67, 922-928*

[66] Voute PA, Hoefnagel CA, de Kraker J, Valdes Olmos R, Bakker DJ, van de Kliej AJ

Results in treatment with [^{131}I] metaiodobenzylguanidine in patients with neuroblastoma. Future prospects of zetotherapy
In: Advances in Neuroblastoma Research, 3rd edition,
New York: Wiley-Liss 1991: 439-445

[67] Lashford LS, Lewis IJ, Fielding SL
Phase I/II study of Iodine-131-metaiodobenzylguanidine in chemoresistant neuroblastoma: A United Kingdom Children's Cancer Study Group Investigation. *J Clin Oncol 1992: 10, 1889-1896*

[68] Castellani MR, Chiti A, Seregni E, Bombardieri E.
Role of 131I-metaiodobenzylguanidine (MIBG) in the treatment of neuroendocrine tumours: Experience of the National Cancer Institute of Milan. *Quarterly Journal of Nuclear Medicine 2000: 44(1), 77-87*

[69] Garaventa A, Bellagamba O, Lo Piccolo MS, Milanaccio C, Lanino E, Bertolazzi L, Villavecchia GP, Cabria M, Scopinaro G, Claudiani F, De Bernardi B.
^{131}I-metaiodobenzylguanidine (^{131}I-MIBG) therapy for residual neuroblastoma: A mono-institutional experience with 43 patients. *British Journal of Cancer 1999: 81(8), 1378-1384*

[70] Matthay KK, DeSantes K, Hasegawa B, Huberly J, Hattner RS, Ablin A, Reynolds CP, Seeger RC, Weinberg VK, Price D
Phase I dose escalation of ^{131}I-metaiodobenzylguanidine with autologous bone marrow support in refractory neuroblastoma. *Journal of Clinical Oncology 1998: 16(1), 229-236*

[71] Mairs RJ
Neuroblastoma therapy using radiolabelled [^{131}I] metaiodobenzylguanidine ([^{131}I]MIBG) in combination with other agents. *Eur J Cancer1999: 35, 1171-1173*

[72] Brans B, Monsieurs M, Laureys G, Kaufman J-M, Thierens H, Dierckx RA.

Thyroidal uptake and radiation dose after repetitive I-131-MIBG treatments: Influence of potassium iodide for thyroid blocking. *Medical & Pediatric Oncology 2002: 38(1), 41-46*

[73] Van Santen HM, De Kraker J, Van Eck BLF, De Vijlder JJM, Vulsma T.
High incidence of thyroid dysfunction despite prophylaxis with potassium iodide during ^{131}I-meta-iodobenzylguanidine treatment in children with neuroblastoma. *Cancer 2002: 94(7), 2081-2089*

[74] Voute PA, van de Kleij AJ, de Kraker J, Hoefnagel CA, Tiel-Van Buul MMC, Van Gennip H
Clinical experience with radiation enhancement by hyperbaric oxygen in children with recurrent neuroblastoma stage IV. *Eur J Cancer 1995: 31(4), 596-600*

[75] Stankova J, Kavan P, Krizova H, Hermanska E, Dosel P, Sazel M.
^{131}I-meta-iodobenzylguanidine in the treatment of the high risk neuroblastoma patients - Experiences from the Department of Pediatric Oncology in Faculty Hospital Motol in Prague. *Casopis Lekaru Ceskych 2001: 140(1), 13-17*

[76] van Hasselt EJ, Heij HA, de Kraker J, Vos A, Voute PA
Pretreatment with [^{131}I] meta-iodobenzylguanidine and surgical resection of advanced neuroblastoma. *Eur J Pediat Surg 1996: 6, 155-158*

[77] Yanik GA, Levine JE, Matthay KK, Sisson JC, Shulkin BL, Shapiro B, Hubers D, Spalding S, Braun T, Ferrara JLM, Hutchinson RJ.
Pilot study of Iodine-131-metaiodobenzylguanidine in combination with myeloablative chemotherapy and autologous stem-cell support for the treatment of neuroblastoma. *Journal of Clinical Oncology 2002: 20(8), 2142-2149*

[78] Miano M, Garaventa A, Pizzitola MR, Lo Piccolo MS, Dallorso S, Villavecchia GP, Bertolazzi C, Cabria M, De Bernardi B.

Megatherapy combining I^{131} metaiodobenzylguanidine and high-dose chemotherapy with haematopoietic progenitor cell rescue for neuroblastoma. *Bone Marrow Transplantation 2001: 27(6), 571-574*

[79] Sari O, Ugur O, Emir S, Akyuz C.
Combined use of chemotherapy and ^{131}I-metaiodobenzylguanidine in the treatment of advanced-stage neuroblastoma. *Turkish Journal of Pediatrics 2001: 43(1), 29-33*

[80] Klingebiel T, Bader P, Bares R, Beck J, Hero B, Jurgens H, Lang P, Niethammer D, Rath B, Handgretinger R
Treatment of neuroblastoma stage 4 with ^{131} I-meta-iodo-benzylguanidine, high-dose chemotherapy and immunotherapy. *European Journal of Cancer 1998: 34(9), 1398-1402*

[81] Gaze MN, Wheldon TE, O'Donoghue JA, Hilditch TE, McNee SG, Simpson E, Barrett A.
Multi-modality megatherapy with [^{131}I]metaiodobenzylguanidine, high dose melphalan and total body irradiation with bone marrow rescue: Feasibility study of a new strategy for advanced neuroblastoma. *European Journal of Cancer 1995: 31(2), 252-256*

[82] Champoux JJ
DNA topoisomerases: Structure, function and mechanism. *Annu Rev Biochem 2001: 70, 369-413*

[83] Rothenberg ML
Topoisomerase I inhibitors: Review and update. *Annals of Oncology 1997: 8, 837-855*

[84] Voigt W, Matsui S, Yin MB, Burhans WC, Minderman H, Rustum YM
Topoisomerase I inhibitor SN-38 can induce DNA damage and chromosomal aberrations independent from DNA synthesis. *Anticancer Research 1998: 18(5A), 3499-3505*

[85] Chen AY, Choy H, Rothenberg ML
DNA Topoisomerase I – targeting drugs as radiosensitizers. *Oncology 1999: 13, 39-46*

[**86**] Gellert M
DNA topoisomerases. *Annu Rev Biochem 1981: 50, 879-910*

[**87**] Wang JC
DNA topoisomerases. *Annu Rev Biochem 1996: 65, 635-692*

[**88**] Eng WK, Faucette L, Johnson RK, Sternglanz R
Evidence that DNA topoisomerase I is necessary for the cytotoxic effects of camptothecin. *Mol Pharmacol 1988: 34, 755-760*

[**89**] Robert F, Soong SJ, Wheeler RH
A phase II study of topotecan in patients with recurrent head-and-neck cancer. *Am J Clin Oncol 1997: 20, 298-302*

[**90**] Kim H-R, Yang S-H, Jeong E-T,
Clinical study of topotecan as second-line treatment in small cell lung cancer. *Tuberculosis & Respiratory Diseases 2002: 52(3), 230-240*

[**91**] Brown III JV, Peters III WA, Rettenmaier MA, Graham CL, Smith MR, Drescher CW, Micha JP
Three-consecutive-day topotecan is an active regimen for recurrent epithelial ovarian cancer. *Gynecologic Oncology 2003: 88(2), 136-140*

[**92**] Puls LE, Hunter JE, Crane MM,
Effect of topotecan infusion duration on hematologic toxicity in recurrent ovarian carcinoma. *Medical Oncology 2002: 19(1), 25-33.*

[**93**] Gore M, Oza A, Rustin G, Malfetano J, Calvert H, Clarke-Pearson D, Carmichael J, Ross G, Beckman RA, Fields SZ
A randomised trial of oral versus intravenous topotecan in patients with relapsed epithelial ovarian cancer. *European Journal of Cancer 2002: 38(1), 57-63*

[**94**] Oberhoff C, Kieback DG, Wurstlein R, Deertz H, Schouli J, Van Soest C, Hilfrich J, Mesrogli M, Von Minckwitz G, Staab HJ, Schindler AE
Topotecan chemotherapy in patients with breast cancer and brain metastases: Results of a pilot study. *Onkologie 2001: 24(3), 256-260*

[**95**] Levine EG, Cirrincione CT, Szatrowski TP, Canellos G, Norton L, Henderson IC
Phase II trial of topotecan in advanced breast cancer. A cancer and leukemia group B study. *American J Clin Oncol-Cancer Clinical Trials 1999: 22(3), 218-222*

[**96**] Macdonald JS, Jacobson JL, Ketchel SJ, Weiss GG, Taylor S, Mils G, Kuebler JP, Rivkin S, Conrad M
A phase II trial of topotecan in esophageal carcinoma: A Southwest Oncology Group study (SWOG 9339). *Investigational New Drugs 2000: 18(2), 199-202*

[**97**] Klein CE, Tangen CM, Braun TJ, Hussain MHA, Peereboom DM, Nichols CR, Rivkin SE, Dakhil SR, Crawford ED
SWOG-9510: Evaluation of topotecan in hormone refactory prostate cancer: a Southwest Oncology group study. *Prostate 2002: 52(4) 264-268*

[**98**] Saylors RL, Stine KC, Sullivan J, Kepner JL, Wall DA, Bernstein ML, Harris MB, Hayashi R, Vietti TJ
Cyclophosphamide plus topotecan in children with recurrent or refractory solid tumors: A Pediatric Oncology Group phase II study. *J Clin Oncol 2001: 19(15), 3463-3469*

[**99**] West W, Birch R, Schnell F, Hainsworth J, Tongol J, Campos L
Phase I study of paclitaxel and topotecan for the first-line treatment of extensive-stage small cell lung cancer. *Oncologist 2003: 8(1), 76-82*

[**100**] Joppert MG, Garfield DH, Gregurich MA, Nemunaitis JJ, Marsland TA, Khandelwal P, Asmar L
A phase II multicenter study of combined topotecan and gemcitabine as first line chemotherapy for advanced non-small cell lung cancer. *Lung Cancer 2003: 39(2), 215-219*

[**101**] Guarino MJ, Schneider CJ, Grubbs SS, Biggs DD, Himelstein AL, Hogaboom K, Tilak S
A dose-escalation study of weekly topotecan, cisplatin, and gemcitabine front-line therapy in patients with inoperable non-small cell lung cancer. *Oncologist 2002: 7(6), 509-515*

[**102**] Ardizzoni A, Manegold C, Debruyne C, Gaafar R, Buchholz E, Smit EF, Lianes P, Ten Velde G, Bosquee L, Legrand C, Neumaier C, King K, Giaccone G
European Organization for Research and Treatment of Cancer (EORTC) 08957 phase II study of topotecan in combination with cisplatin as second-line treatment of refractory and sensitive small cell lung cancer. *Clinical Cancer Research 2003: 9(11), 143-150*

[**103**] Mok TSK, Wong H, Zee B, Yu KH, Leung TWT, Lee TW, Yim A, Chan ATC, Yeo W, Chak K, Johnson P
A phase I-II study of sequential administration of topotecan and oral etoposide (toposiomerase I and II inhibitors) in the treatment of patients with small cell lung carcinoma. *Cancer 2002: 95(7), 1511-1519*

[**104**] Mavroudis D, Pavlakou G, Blazoyiannakis G, Veslemes M, Apostolopoulou F, Kouroussis Ch, Kakolyris S, Agelaki S, Androulakis N, Vardakis N, Magkanas E, Samonis G, Georgoulias V
Sequential administration of cisplatin-etoposide followed by topotecan in patients with extensive stage small cell lung cancer. A multicenter phase II study. *Lung Cancer 2003: 39(1), 71-76*

[**105**] Seiden MV, Ng S-W, Supko JG, Ryan DP, Clark JW, Lynch T, Huang K-C, Kwiatkowski D, Skarin A, Eder Jr JP
A phase I clinical trial of sequentially administered doxorubicin and topotecan in refractory solid tumors. *Clinical Cancer Research 2002: 8(3), 691-697*

[**106**] Korfel A, Oehm C, Von Pawel J, Keppler U, Depermann M, Kaubitsch S, Thiel E

Response to topotecan of symptomatic brain metastases of small-cell lung cancer also after whole-brain irradiation: A multicentre phase II study. *European Journal of Cancer 2002: 38(13), 1724-1729*

[**107**] Rinaldi DA, Lormand NA, Brierre JE, Cole JL, Barnes BC, Mills G, Yadlapati S, Fontenot MF, Buller EJ, Rainey JM
A phase II trial of topotecan and gemcitabine in patients with previously treated, advanced nonsmall cell lung carcinoma. *Cancer 2002: 95(6) 1274-1278*

[**108**] Homesley H, Benigno B, Williams J, Vaccarello L.
A phase I study of weekly topotecan and paclitaxel in previously treated epithelial ovarian carcinoma patients. *Gynecologic Oncology 2002 87(2), 171-177*

[**109**] Schoemaker NE, Herben VMM, De Jong LA, Van Waardenburg RCAM, Pluim D, Ten Bokkel Huinink WW, Beijnen JH, Schellens JHM
Topoisomerase I levels in white blood cells of patients with ovarian cancer treated with paclitaxel-cisplatin-topotecan in a phase I study. *Anti-Cancer Drugs 2002: 13(1), 87-91*

[**110**] Ferrari S, Rovati B, Cucca L, Scarabelli C, Presti M, Beccaria C, Collova E, Porta C, Danova M
Impact of topotecan-based chemotherapy on the immune system of advanced ovarian cancer patients: An immunophenotypic study. *Oncol Rep 2002: 9(5) 1107-1113*

[**111**] Sehouli J, Stengel D, Oskay G, Camara O, Hindenburg H-J, Klare P, Blohmer J, Heinrich G, Elling D, Ledwon P, Lichtenegger W
A phase II study of topotecan plus gemcitabine in the treatment of patients with relapsed ovarian cancer after failure of first-line chemotherapy. *Ann Oncol. 2002: 13(11), 1749-1755*

[**112**] Ryan CW, Fleming GF, Janisch L, Ratain MJ.
A phase I study of liposomal doxorubicin (Doxil) with topotecan. *Am J Clin Oncol-Cancer Clinical Trials 2000: 23(3), 297-300*

[113] Mainwaring MG, Rimsza LM, Chen SF, Gomez SP, Weeks FW, Reddy V, Lynch J, May WS, Kahn S, Moreb J, Leather H, Braylan R, Rowe TC, Fieniewicz KJ, Wingard JR
Treatment of refactory acute leukemia with timed sequential chemotherapy using topotecan followed by etoposide + mitoxantrone (T-EM) and correlation with topoisomerase II levels. *Leuk Lymphoma 2002: 43(5) 989-999*

[114] Cortes J, Kantarjian H, Albitar M, Thomas D, Faderl S, Koller C, Garcia-Manero G, Giles F, Andreeff M, O'Brien S, Keating M, Estey E
A randomized trial of liposomal daunorubicin and cytarabine versus liposomal daunorubicin and topotecan with or without thalidomide as initial therapy for patients with poor prognosis acute myelogenous leukemia or myelodysplastic syndrome. *Cancer 2003: 97(5), 1234-1241*

[115] Estey EH, Thall PF, Cortes JE, Giles FJ, O'Brien S, Pierce SA, Wang X, Kantarjian HM, Beran M
Comparison of idarubicin + ara-C-, fludarabine + ara-C-, and topotecan + ara-C-based regimens in treatment of newly diagnosed acute myeloid leukemia, refractory anemia with excess blasts in transformation, or refractory anemia with excess blasts. *Blood 2001: 98(13), 3575-3583*

[116] Dunton CJ, King SA, Neufeld J, Tolosa J, Perez G, Avila A, Underhill K
Phase I study of topotecan and radiation therapy in advanced cervical cancer. *Gynecologic Oncology 2002: 85(1), 185-187*

[117] Fiorica J, Holloway R, Ndubisi B, Orr J, Grendys E, Boothby R, DeCesare S, LaPolla J, Hoffman M, Patel J
Phase II trial of topotecan and cisplatin in persistent or recurrent squamous and nonsquamous carcinomas of the cervix. *Gynecologic Oncology 2002: 85(1), 89-94*

[118] Crump M, Couban S, Meyer R, Rudinskas L, Zanke B, Gluck S, Maksymiuk A, Hoskins P, Matthews S, Eisenhauer E

Phase II study of sequential topotecan and etoposide in patients with intermediate grade non-Hodgkin's lymphoma: A National Cancer Institute of Canada Clinical Trials Group study. *Leukemia & Lymphoma 2002: Vol 43(8), 1581-1587*

[119] Fisher B, Won M, Macdonald D, Johnson DW, Roa W
Phase II study of topotecan plus cranial radiation for glioblastoma multiforme: Results of Radiation Therapy Oncology Group 9513. *International Journal of Radiation Oncology, Biology, Physics 2002: Vol 53(4), 980-986*

[120] Gross MW, Altscher R, Brandtner M
Acute toxicity and changes in quality of life during a combined radio-chemotherapy of glioblastomas with topotecan (Hycamtin). *Strahlenther Onkol 2001: 177(12), 656-661*

[121] Grabenbauer GG, Anders K, Fietkau RJ, Klautke G, Feldmann HJ, Weiser S, Staab H-J, Krauseneck P, Sauer R
Prolonged infusional topotecan and accelerated hyperfractionated 3d-conformal radiation in patients with newly diagnosed glioblastoma - A phase I study. *Journal of Neuro-Oncology 2002: 60(3), 269-275*

[122] Burch PA, Bernath AM, Cascino TL, Scheithauer BW, Novotny P, Nair S, Buckner JC, Pfiefle DM, Kugler JW, Tschetter LK
A North Central Cancer Treatment Group phase II trial of topotecan in relapsed gliomas. *Investigational New Drugs 2000: 18(3), 275-280*

[123] Bomgaars L, Berg SL, Blaney SM,
The development of camptothecin analogs in childhood cancers. *Oncologist 2001: 6(6) 506-516*

[124] Vassal G, Pondarre C, Cappelli C, Terrier-Lacombe MJ, Boland I, Morizet J, Benard J, Venuat AM, Ardouin P, Hartmann O, Gouyette A
DNA-topoisomerase I, a new target for the treatment of neuroblastoma. *Eur J Cancer 1997: 33, 2011-2015*

[125] Zamboni WC, Stewart CF, Thompson J, Santana VM, Cheshire PJ, Richmond LB, Luo X, Poquette C, Houghton JA, Houghton PJ
Relationship between topotecan systemic exposure and tumor response in human neuroblastoma xenografts. *J Natl Cancer Inst 1998: 90, 505-511*

[126] Kramer K, Kushner BH, Cheung N-KV.
Oral topotecan for refractory and relapsed neuroblastoma: A retrospective analysis. *J Ped Hematol Oncol 2003: 25, 601-605.*

[127] Pratt CB, Stewart C, Santana VM, Bowman L, Furman W, Ochs Marina JN, Kuttesch JF, Heideman R, Sandlund JT, Avery L, Meyer WH
Phase I Study of Topotecan for Pediatric Patients with Malignant Solid Tumors. *J Clin Oncol 1994: 12, 539-543*

[128] Tubergen DG, Stewart CF, Pratt CB, Zamboni WC, Winick N, Santana VM, Dryer ZA, Kurtzberg J, Bell JB, Grier H, Vietti TJ.
Phase I trial and pharmacokinetic (pk) and pharmacodynamics (pd) study of topotecan using a five-day course in children with refractory solid tumors: A Pediatric Oncology Group study. *J Ped Hematol Oncol 1996: 18, 352-361*

[129] Langler A, Christaras A, Abshagen K, Krauth K, Hero B, Berthold F.
Topotecan in the treatment of refractory neuroblastoma and other malignant tumors in childhood - A phase-II-study. *Klinische Padiatrie 2002: 214(4), 153-156.*

[130] Perez Martinez A, Contra T, Scaglione C, Diaz Perez MA, Madero Lopez L,
Topotecan for pediatric patients with resistant and recurrent solid tumors. *Anales de Pediatria 2003: 59(2), 143-148*

[131] Bowers DC, Aquino VM, Leavey PJ, Bash RO, Journeycake JM, Tomlinson G, Mulne AF, Haynes HJ, Winick NJ
Phase I study of oral cyclophosphamide and oral topotecan for children with recurrent or refractory solid tumors. *Pediatric Blood & Cancer 2004: 42(1), 93-98)*

[132] Donfrancesco A, Jenkner A, Castellano A, Ilari I, Milano GM, De Sio L, Cozza R, Fidani P, Deb G, De Laurentis C, Inserra A Dominici C.
Ifosfamide/carboplatin/etoposide (ICE) as front-line, topotecan/ cyclophosphamide as second-line and oral temozolomide as third-line treatment for advanced neuroblastoma over one year of age. *Acta Paediatrica, International Journal of Paediatrics 2004: 93(445), 6-11.*

[133] Kushner BH, Cheung N-KV, Kramer K, Dunkel IJ, Calleja E, Boulad F.
Topotecan combined with myeloablative doses of thiotepa and carboplatin for neuroblastoma, brain tumors, and other poor-risk solid tumors in children and young adults. *Bone Marrow Transplantation 2001: 28(6), 551-556.*

[134] Garaventa A, Luksch R, Biasotti S, Severi G, Pizzitola MR, Viscardi E, Prete A, Mastrangelo S, Podda M, Haupt R, De Bernardi B
A phase II study of topotecan with vincristine and doxorubicin in children with recurrent/refractory neuroblastoma. *Cancer 2003: 98(11), 2488-2494*

[135] Kushner BH, Kramer K, Modak S, Cheung N-KV
Camptothecin analogs (irinotecan or topotecan) plus high-dose cyclophosphamide as preparative regimens for antibody-based immunotherapy in resistant neuroblastoma. *Clinical Cancer Research 2004: 10(11), 84-87*

[136] Mattern MR, Hofmann GA, McCabe FL, Johnson RK
Synergistic cell killing by ionizing radiation and topoisomerase I inhibitor topotecan (SK&F 104864). *Cancer Research 1991: 51, 5813-5816*

[137] Hennequin C, Giocanti N, Balosso J Favaudon V
Interaction of ionising radiation with the topoisomerase I poison camptothecin in growing V-79 and HeLa cells. *Cancer Research 1994: 54, 1720-1728*

[138] Kohara H, Tabata M, Kiura K, Ueoka H, Kawata K, Chikamori M, Aoe K, Chikamori K, Matsushita A, Harada M

Synergistic effects of topoisomerase I inhibitor, 7-ethyl-10-hydroxycamptothecin, and irradiation in a cisplatin-resistant human small cell lung cancer cell line. *Clinical Cancer research 2002: 8, 287-292*

[139] Marchesini R, Colombo A, Caserini C, Perego P, Supino R, Capranico G, Tronconi M, Zunino F
Interaction of ionizing radiation with TPT in two human cell lines. *Int J Cancer 1996: 66, 342-346*

[140] Boscia RE, Korbut T, Holden SA Ara G, Teicher BA
Interaction of topoisomerase I inhibitors with radiation in *cis*-diaminedichloroplatinum(II) - sensitive and - resistant cells *in vitro* and in the FSAIIC fibrosarcoma *in vivo*. *In J Cancer 1993: 53, 118-123*

[141] Lamond JP, Wang M, Kinsella TJ and Boothman DA
Concentration and timing dependence enhancement between topotecan, a topoisomerase I inhibitor and ionising radiation. *Int J Radiat Oncol Biol Physol 1996: 36, 361-368*

[142] Kirichenko AV, Rich TA, Newman RA, Travis EL
Potentiation of mirine MCa-4 carcinoma radioresponse by 9-amino-20(S)-camptothecin. *Cancer research 1997: 57, 1929-1933*

[143] Chastagner P, Merlin JL, Marchal C, Hoffstetter S, Barberi-heyob M, Vassal G, Duprez A
In vivo potentiation of radiation response by topotecan in human rhabdomyosarcoma xenografted into nude mice. *Clinical Cancer research 2000: 6, 3327-3333*

[144] Hoefnagel CA
Nuclear medicine therapy of neuroblastoma. *Quart. J. Nucl. Med 1999: 43, 336-343*

[145] Bieche I, Olivi M, Champeme MH, Vidaud D, Lidereau R, Vidaud M

Novel approach to quantitative polymerase chain reaction using real-time detection: application to the detection of gene amplification in breast cancer. *Int. J. Cancer 1998: 78, 661-666*

[146] Holland PM, Abramson RD, Watson R, Gelfland DH
Detection of specific polymerase chain reaction product by utilising the 5' to 3' exonuclease activity of *Thermus aquaticus* DNA polymerase. *Proc. Nat. Acad. Sci 1991: 88, 7276-7280*

[147] Biedler JL, Helson L, Spengler BA
Morphology and growth, tumorigenicity, and cytogenetics of human neuroblastoma cells in continuous culture. *Cancer Res 1973: 33, 2643-2652*

[148] Tumilowicz, JJ Nichols, WW Cholon JJ, Greene AE
Definition of a continuous human cell line derived from neuroblastoma. *Cancer Res 1970: 30, 2110-2118*

[149] Soule HD, Vazguez J, Long A, Albert S, Brennan M
A human cell line from a pleural effusion derived from a breast carcinoma. *J. Natl. Cancer Inst. 1973: 51, 1409-1416*

[150] Ross G
Cellular and molecular studies on the mechanistic basis of clinical radioresistance in human glioma. *PhD thesis, University of Glasgow, 1992.*

[151] Frame MC. Freshney RI. Vaughan PFT. et al
Interrelationship between differentiation and malignancy-associated properties in glioma. *Br J Cancer 1984: 49(3), 269-280*

[152] Boyd M, Cunningham SH, Brown MM, Mairs RJ, Wheldon TE
Noradrenaline tranporter gene transfer for radiation cell kill by ^{131}I- meta-iodobenzylguanidine. *Gene Therapy 1999: 6, 1147-1152*

[153] Carlin S, Mairs RJ, McCluskey AG, Tweddle DA, Sprigg A, Estlin C, Board J, George RE, Ellershaw C, Pearson ADJ, Lunec J, Montaldo PG, Ponzoni M, van Eck-Smit BL, Hoefnagel CA, van den Brug MD, Tytgat GAM, Caron HN
Development of a real-time polymerase chain reaction assay for prediction of the uptake of [^{131}I]meta-iodobenzylguanidine by neuroblastoma tumours. *Clinical Cancer Research 2003: 9(9), 3338-3344*

[154] Armour A, Cunningham SH, Gaze MN, Wheldon TE, Mairs RJ
The effect of cisplatin pretreatment on the accumulation of MIBG by neuroblastoma cells in vitro. *Brit. J. Cancer 1997: 75, 470-476*

[155] Quantitation of DNA and RNA with fluorescence spectroscopy
In: Current Protocols in Molecular Biology
Ed. Ausubel FM, Brent R, Kingston RE, Moore DD, Seidman JG, Struhl K
John Wiley & Son Inc. 2001: A.3D.2

[156] Basic constants, units and conversion factors
In: CRC Handbook of Chemistry & Physics, 73rd Edition
Ed. Lide DR
CRC Press Inc. 1992: 1.1-1.6

[157] Montaldo PG, Raffaghello L, Guaraccia F, Pistoia V, Garaventa A, Ponzoni M
Increase of meta-iodobenzylguanidine Uptake and Intracellular Half-life during Differentiation of Human Neuroblastoma cells. *Int J Cancer 1996: 67, 95-100*

[158] Meco D, Lasorella A, Riccardi A, Servidei T, Mastangelo R, Riccardi R
Influence of Cisplatin and Doxorubicin on ^{125}I-meta-iodobenzylguanidine Uptake in Human neuroblastoma Cell Lines. *Eur J Cancer 1999: 35, 1227-1234*

[159] Smets LA, Jannsen M, Rutgers M, Ritzen K, Buitenhuis C
Pharmacokinetics and Intracellular Distribution of the Tumour-targetted Radiopharmaceutical m-iodo-benzylguanidine in SK-N-SH Neuroblastomas and PC-12 Phaochromocytoma cells. *Int J Cancer 1991: 48, 609-615*

[160] Biedler JL, Helson L, Spengler BA
Multiple neurotransmitter synthesis by human neuroblastoma cell lines and clones. *Cancer Res 1978: 38, 3751-3757*

[161] Boothman DA, Fukunaga N, Wang M
Down-regulation of topisomerase I in mammalian cells following ionizing radiation. *Cancer Research 1994: 54, 4618-4626*

[162] Keshelava N, Groshen S, Reynolds P
Cross-resistance of topoisomerase I and II inhibitors in neuroblastoma cell lines. *Cancer Chemother Pharmacol 2000: 45, 1-8*

[163] Greco WR, Bravo G, Parsons JC
The search for synergy: A critical review from a response surface perspective. *Pharmacological Reviews 1995: 47(2), 331-385*

[164] Steel GG, Peckham MJ
Exploitable mechanisms in combined radiotherapy-chemotherapy: The concept of additivity. *Int J Radiat Oncol Biol Physol 1979: 5, 85-91*

[165] Berenbaum M
What is synergy? *Pharmacol Rev 1989: 41, 93-141*

[166] Chou TC, Talalay P.
Quantitative analysis of dose-effect relationships: the combined effects of multiple drugs or enzyme inhibitors. *Adv. Enzyme Regul., 22: 27-55, 1984.*

[167] Chou TC
The median-effect principle and the combination index for quantitation of synergism and anatagonism
In: Synergism and Anatagonism in Chemotherapy
Ed: Chou TC, Rideout DC

New York Academic Press, 1991: 61-102

[168] Jagdev SP, Coleman RE, Shipman RM, Rostami-H A, Croucher PI
The bisphosphate, zoledronic acid, induces apoptosis of breast cancer cells: evidence for synergy with paclitaxel. *Br J Cancer 2001: 84(8) 1126-1134*

[169] Wahl AF, Donaldson KL, Mixan BJ, Trail PA, Siegall CB
Selective tumor sensitisation to taxanes with the mAb-grug conjugate CBR96-doxorubicin. *Int J Cancer 2001: 93, 590-600*

[170] Boothman DA, Trask DK, Pardee AB
Inhibition of potentially lethal DNA damage repair in human tumour cells by ß-lapachone, an activator of of topoisomerase I. *Cancer Research 1989: 49, 605-12*

[171] Boothman DA, Pardee AB
Inhibition of radiation-induced neoplastic transformation by ß-lapachone. *Proc. Natl. Acad. Sci. USA 1989: 86, 4963-67*

[172] Boothman DA, Wang M, Scea RA, Burrows HL, Strickfaden S, Owens JK
Posttreatment exposure to camptothecin enhances the lethal effects of X-rays on radioresistant human malignant melanoma cells. *Int J Radiat Oncol Biol Physol 1992: 24, 939-48*

[173] Cortes F, Pastor N
Ionising radiation damage repair: a role for topoisomerases? *Mutagenesis 2001: 16(4), 365-68*

[174] Thielmann HW, Popanda O, Staab H-J
Subnuclear distribution of DNA topoisomerase I and Bax protein in normal and Xeroderma pigmentosum fibroblasts after irradiation with UV light and γ rays or treatment with topotecan. *J Clin Res Oncol 1999: 125, 193-208*

[175] Larsen AK, Gobert C

DNA topoisomerase I in oncology: Dr. Jekyll or Mr. Hyde? *Pathology Oncology Research 1999: 5(3), 171-78*

[**176**] Chou TC
Synergy determination issues. *Journal of Virology 2002: 76(20), 10577-10578*

[**177**] Rutgers M, Buitenhuis CKM, Hoefnagel CA, Voute PA, Smets LA.
Targeting of meta-iodobenzylguanidine to SK-N-SH human neuroblastoma xenografts: tissue distribution, metabolism and therapeutic efficacy. *Int J Cancer 2000: 87, 412-422.*

[**178**] Morton DB, Griffiths PHM.
Endpoints in animal study protocols. *Vet Record 1985: 116, 431-43.*

[**179**] Dubois SG, Messina J, Maris JM, Huberty J, Glidden DV, Veatch J, Charron M, Hawkins R, Matthay KK
Hematologic toxicity of high-dose iodine-131-metaiodobenzylguanidine therapy for advanced neuroblastoma. *J Clin Oncol 2004: 22, 2452-2460.*

[**180**] Workman P, Twentyman P, Balkwill F, Balmain A, Chaplin D, Double J, Embleton J, Newell D, Raymond R, Stables J, Stephens T, Wallace J, Navaratnam V,
United Kingdom Co-ordinating Committee on Cancer Research (UKCCCR) Guidelines for the Welfare of Animals in Experimental Neoplasia (Second Edition). *British Journal of Cancer 1998: 77(1), 1-10*

[**181**] Gaze MN, Hamilton TG, Mairs RJ. Pharmacokinetics and efficacy of 131I-meta-iodo-benzyl guanidine in two neuroblastoma xenografts. *Br J Radiol 1994: 67, 573-578.*

[**182**] Boyd M, Ross S, Owens J, Hunter D, Babich J, Zalutsky MR, Hamilton TG, Bell S, Mairs RJ
Preclinical evalaution of no-carrier-added [^{131}I]meta-iodobenzyl guanidine, for the treatment of tumours transfected with the noradrenaline transporter gene. *Lett Drug Des Disc 2004: 1, 50-57.*

[183] Thompson J, George EO, Poquette CA, Cheshire PJ, Richmond LB, De Graaf SSN, Ma M, Stewart CF, Houghton PJ. Synergy of topotecan in combination with vincristine for treatment of pediatric solid tumor xenografts. *Clin Cancer Res 1999: 5, 3617-3631.*

[184] Graham GJ, Wright EG
Haemopoietic stem cells: Their heterogeneity and regulation. *Int J Exp Pathol 1997: 78, 197-218*

[185] Graham GJ, Freshney MG
CFU-A assay for measurement of the anti-proliferative effects of chemokines on murine early haemopoietic progenitors.
In: Chemokine Protocols.
Ed. Proudfoot AEI, Wells TNC, Power CA.
Totwa, NJ: Humana Press Inc. 2000: 179-189.

[186] Hall EJ
Radiosensitivity and cell age in the mitotic cycle
In: Radiobiology for the radiologist, 4th Edition
JB Lippincott company, Philadelphia, 1994: 91-105

[187] Champoux JJ, Aronoff R
The effects of camptothecin on the reaction and specificity of the wheat germ type I topoisomerase. *J Biol Chem 1989: 264, 1010-1015*

[188] Smith HM. Grosovsky AJ.
PolyADP-ribose-mediated regulation of p53 complexed with topoisomerase I following ionizing radiation. *Carcinogenesis 1999: 20(8), 1439-1443*

[189] Goldwasser F, Shimizu T, Jackman J, Hoki Y, O'Connor PM. Kohn KW, Pommier Y
Correlations between S and G_2 arrest and the cytotoxicity of campothecin in human carcinoma cells. *Cancer research 1996: 56, 4430-4437*

[**190**] Del Bino G, Skierski JS, Darzynkiewicz Z
Diverse effects of camptothecin, an inhibitor of topoisomerase I on the cell cycle of lymphocytic (L1210, MOLT-4) and myelogenous (HL-60, KG1) leukemic cells. *Cancer research 1990: 50, 5746-5750*

[**191**] McDonald AC, Brown R
Induction of p53-dependent and p53-independent cellular responses by topoisomerase I inhibitors. *British Journal of Cancer 1998: 78(6), 745-751*

[**192**] Rojas E, Lopez MC, Valverde M
Single cell gel electrophoresis assay: methodology and applications. *Journal of Chromotography B 1999: 772, 225-254*

[**193**] Morris EJ, Dreixler JC, Cheng KY, Wilson PM, Gin RM, Geller HM.
An Optimization of Single Cell Gel Electrophoresis (SCGE) for Quantitative Analysis of Neuronal DNA Damage. *Biotechniques 1999: 26(2), 282-289*

[**194**] SISA (Simple Interactive Statistical Analysis) website: http://home.clara.net/sisa/

[**195**] VassarStats: Statistical computation website:
http://faculty.vassar.edu/lowry/VassarStats.html

[**196**] Olive PL, Banath JP, and Durand RE
Detection of Etoposide Resistance by measuring DNA damage in individual Chinese Hamster cells. *J. Natl Cancer Inst 1990: 82(9), 779-783*

[**197**] Olive PL, Banath JP, and Durand RE
Heterogeneity in Radiation-induced DNA damage and repair in tumour and normal cells measured using the "comet" assay. *Radiat Res 1990: 122(1), 86-94*

[**198**] Tabachnick BG, Fidell LS.
Using Multivariate Statistics, 2nd Edition.
Harper & Row Publishers, New York 1996: 72

[**199**] Burchill SA, Selby PJ
Molecular detection of low-level disease in patients with cancer. *J. Pathol 2000: 190, 6-14*

[**200**] Wang Y, Einhorn P, Triche TJ, Seeger RC, Reynolds CP
Expression of protein gene product 9.5 and tyrosine hydroxylase in childhood small round cell tumors. *Clin. Cancer Res 2000: 6, 551-518*

[**201**] Lo Piccolo MS, Cheung NKV, Cheung IY
GD2 synthase: A new molecular marker for detecting neuroblastoma. *Cancer 2001: 92, 924-931*

[**202**] Tytgat GAM, Cornelissen J, Van den Brug M, Van Kuilenburg ABP, Voute PA, Van der Kleij AJ, Van Gennip AH
HBO and the uptake and retention of [^{125}I]MIBG in human platelets and two neuroendocrine cell lines. *Anticancer Research 1997: 17(2A), 1209-1212*

[**203**] Tytgat GAM, Van den Brug M, Voute PA, Smets LA, Rutgers M
Human megakaryocytes cultured *in vitro* accumulate serotonin but not meta-iodobenzylguanidine whereas platelets concentrate both. *Exp. Hematol 2002: 30, 555-563*

[**204**] Boyd M, Mairs SC, Stevenson K, Livingstone A, Clark AM, Ross SC, Mairs RJ
Transfectant mosaic spheroids: a new model for the evaluation of bystander effects in experimental gene therapy. *J. Gene Medicine 2002: 4, 1–10*

[**205**] Kruger I, Rothkamm K, Lobrich M
Enhanced fidelity for rejoining radiation-induced DNA double-strand breaks in the G_2 phase of Chinese hamster ovary cells. *Nucleic Acids Research, 2004: 32(9), 2677-2684*

[**206**] Golding SE, Rosenberg E, Khalil A, McEwen A, Holmes M, Neill S, Povirk LF, Valerie K
Double strand break repair by homologous recombination is regulated by cell cycle-

independent signaling via ATM in human glioma cells. *Journal of Biological Chemistry 2004: 279(15) 15402–15410*

[**207**] Pieper A, Verma A, Zhang J, Snyder S
Poly(ADP-ribose) polymerase, nitric oxide and cell death. *Trends Pharmacol Sci 1999: 20, 171–181*

[**208**] Oliver FJ, Menissier-de Murcia J, de Murcia G
Poly(ADP-ribose) polymerase in the cellular response to DNA damage, apoptosis, and disease. *Am J Hum Genet 1999: 64, 1282–1288*

[**209**] Herceg Z, Wang Z-Q
Functions of poly(ADP-ribose) polymerase (PARP) in DNA repair, genomic integrity and cell death. *Mutation Research 2001: 477, 97–110*

[**210**] Virag L, Szabo C
The therapeutic potential of poly(ADP-ribose) polymerase inhibitors. *Pharmacological Reviews 2002: 54(3) 375-429*

[**211**] Bauer PI, Chen H-J, Kenesi E, Kenessey I, Buki KG, Kirsten E, Hakam A, Hwang JI, Kun E
Molecular interactions between poly(ADP-ribose) polymerase (PARP I) and topoisomerase I (Topo I): Identification of topology of binding. *FEBS Letters 2001: 506(3), 239-242)*

[**212**] Shishido K, Noguchi N, Ando T
Correlation of enzyme-induced cleavage sites on negatively superhelical DNA between prokaryotic topoisomease I and S1 nuclease. *Biochem Biophys Acta 1983: 740, 108-117*

[**213**] Kaufmann SH, Desnoyers S, Ottaviano Y, Davidson NE, Poirier GG
Specific proteolytic cleavage of poly(ADP-ribose) polymerase: an early marker of chemotherapy-induced apoptosis. *Cancer Res 1993: 53, 3976-3985*

[**214**] Kingma PS, Osheroff N
The response of eukaryotic topoisomerases to DNA damage. *Biochemica et Biophisica Acta 1998: 1400, 223-232*

[**215**] Plo I, Liao Z-Y, Barcelo JM, Kolhagen G, Caldecott KW, Weinfeld M, Pommier Y
Association of XRCC 1 and tyrosyl DNA phosphodiesterase (Tdp 1) for the repair of topoisomerase I-mediated DNA lesions. *DNA repair 2003: 2, 1087-1100*

[**216**] Desai SD, Liu LF, Vasquez-Abad D, D'Arpa P
Ubiquitin-dependent destruction of topoisomerase I is stimulated by the antitumour drug camptothecin. *Journal of Biological Chemistry 1997: 272(39), 25159-24164*

[**217**] Mao Y, Muller MT
Down modulation of topoisomerase I affects DNA repair efficiency. *DNA repair 2003: 2, 1115-1126*

[**218**] Evans RG, Engel C, Wheatley C, Nielsen J
Modification of the sensitivity of repair of potentially lethal damage by diethyldithiocarbamate during and following exposure of plateau-phase cultures of mammalian cells to radiation and cis-diamminedichloroplatinum(ii). *Cancer Res 1982: 42, 3074-3078.*

[**219**] Barkett M, Gilmore TD
Control of apoptosis by Rel/NF-kappaB transcription factors. *Oncogene 1999: 18, 6910-6924.*

[**220**] Baldwin AS
Control of oncogenesis and cancer therapy resistance by the transcription factor NF-kappaB. *J Clin Invest 2001: 107, 241-246.*

[**221**] Yamamoto Y, Gaynor RB
Therapeutic potential of inhibition of the NF-kappaB pathway in the treatment of inflammation and cancer. *J Clin Invest 2001: 107, 135-142.*

[**222**] Shall S, de Murcia G
Poly(ADP-ribose)polymerase-1: What have we learned from the deficient mouse model? *Mutat Res 2000: 460, 1-15.*

[**223**] Hall EJ
Linear energy transfer and relative biological effectiveness
In: Radiobiology for the radiologist, 4th Edition
JB Lippincott company, Philadelphia, 1994: 153-164

[**224**] Humm JL
Dosimetric aspects of radiolabelled antibodies for tumour therapy. *J Nucl Med 1986: 27, 1490-1497*

[**225**] Properties of the elements and inorganic compounds
In: CRC Handbook of Chemistry & Physics, 73rd Edition
Ed. Lide DR
CRC Press Inc. 1992: 4.1-4.34

[**226**] Strickland DK, Vaidyanathan G, Zalutsky MR
Cytotoxicity of α-particle-emitting *m*-[^{211}At] astatobenzulguanidine on human neuroblastoma cells. *Cancer Research 1994: 54, 5414-5419*

[**227**] Kassis AI, Fayad F, Kinsey BM, Sastry KSR, Taube RA, Adelstein SJ
Radiotoxicity of ^{125}I in mammalian cells. *Radiat. Res 1987: 111, 305-318*

[**228**] Gaze MN, Huxham IM, Mairs RJ, Barrett A
Intracellular localisation of metaiodobenzylguanidine in human neuroblastoma cells by electron spectroscopic imaging. *Int J Cancer 1991: 47, 875-880*

[**229**] Mothersill CE, Moriarty MD, Seymour CB
Radiotherapy and the potential exploitation of bystander effects. *Int J Radiation Oncol Biol Phys 2004: 58, 575-579.*

[**230**] Mothersill C, Seymore CB
Radiation induced bystander effects: past history and future directions. *Radiation Res 2001: 155, 759-767.*

[**231**] Little JB, Azzam EI, de Toledo SM, Nagasawa H
Bystander effects:intercellular transmission of radiation damage signals. *Radiat Prot Dosimetry 2002: 99, 159-162.*

[**232**] Mothersill C, Seymour CB
Medium from irradiated human epithelial cells but not human fibroblasts reduces the clonogenic survival of unirradiated cells. *Int J Radiat Biol 1997: 71, 421-427.*

[**233**] Mothersill C, Seymour CB
Cell-cell contact during g-irradiation is not required to induce a bystander effect in normal human keratinocytes: Evidence for release of a survivial controlling signal into the medium. *Radiat Res 1998: 149, 256-262.*

[**234**] Nagasaw H, Little JB
Induction of sister chromatid exchanges by extremely low doses of alpha-particles. *Cancer Res 1992: 52, 6394-6396.*

[**235**] Zhou HN, Randers-Pehrson G, Hei TK
Studies of bystander mutagenic response using a charged particle microbeam. *Radiat Res 2000: 153, 234-235.*

[**236**] Prise K, Folkard M, Michael BD
Bystander responses induced by low LET radiation. *Oncogene 2003: 22, 7043-7049.*

[**237**] Boyd M, Mairs RJ, Keith WN, Ross SC, Welsh P, Akabani G, Owens J, Vaidyanathan G, Carruthers R, Dorrens J, Zalutsky MR

An efficient targeted radiotherapy / gene therapy strategy utilising human telomerase promoters and radioastatine and harnessing radiation mediated bystander effects. *J Gene Med 2004: 6, 937-947.*

[238] Boyd M, Mairs SC, Stevenson K, Livingstone A, Clark A-M, Ross SC, Mairs RJ
Transfectant Mosaic Spheroids: a new model for evaluation of targeted radiotherapy and experimental gene therapy. *J Gene Med 2002: 4, 567-576.*

[239] Seymour CB, Mothersill C
Relative contribution of bystander and targeted cell lilling to the low-Dose region of the radiation dose-response curve. *Radiat Res 2000: 153, 508-511.*

[240] Carlsson J, Aronsson EF, Hietala S-O, Stigbrand T, Tennvall J (2003).
Tumour therapy with radionuclides: assessment of progress and problems. *Radiother and Oncol 2003: 66, 107-117.*

[241] Kim NW, Piatyszek MA, Prowse KR, Harley CB, West MD, Ho PL, Coviello GM, Wright WE, Weinrich SL, Shay JW
Specific association of human telomerase activity with immortal cells and cancer. *Science 1994: 266, 2011-2015.*

[242] Shay JW, Bacchetti SA
Survey of telomerase activity in human cancer. *Eur J Cancer 1997: 33, 787-791.*

[243] Holt SE, Shay JW
Role of telomerase in cellular proliferation and cancer. *J Cell Physiol 1999: 180, 10-18.*

[244] Keith WN, Evans TRJ, Glasspool RM (2001).
Telomerase and cancer: time to move from a promising target to a clinical reality. *J Pathol 2001: 195, 404-414.*

[245] Worthington J, Robson T, O'Keeffe M, Hirst DG (2002).

Tumour cell radiosensitisation using constitutive (CMV) and radiation inducible (WAF-1) promoters to drive the iNOS gene: a novel suicide gene therapy. *Gene Therapy 2002: 9, 263-269.*

[246] Worthington J, McCarthy HO, Barrett E, Adams C, Robson T, Hirst DG
Use of the radiation inducible WAF1 promoter to drive iNOS gene therapy as a novel anti-cancer treatment. *J Gene Med 2004: 6, 673-680.*

[247] Holt SE, Shay J W
Role of of telomerase in cellular proliferation and cancer. *J Cell Physiol 1999: 180, 10–18*

[248] Shay JW, Bacchetti S
A survey of telomerase activity in human cancer. *Eur J Cancer 1997: 33, 787–791*

[249] Shay JW, Zou Y, Hiyama E, Wright WE
Telomerase and cancer. *Hum Molec Genet 2001: 10, 677-685.*

[250] Cunningham SH, Boyd M, Brown MM, Carlin S, McCluskey A, Livingstone A, Mairs RJ, Wheldon TE
A gene therapy approach to enhance targeted radiotherapy of neuroblastoma. *Med Paed Oncol 2000: 35, 708-711*

[251] Fullerton NE, Mairs RJ, Kirk D, Keith WN, Carruthers R, McCluskey AG, Brown MM, Wilson L, Boyd M
Application or targeted radiotherapy/gene therapy to bladder cancer cell lines. *European Urology 2004: in Press*

[252] Fullerton NE, Boyd M, Mairs RJ, Keith WN, Alderwish O, Brown MM, Livingstone A, Kirk D
Combining a targeted radiotherapy and gene therapy approach for adenocarcinoma of prostate. *Prostate Cancer and Prostatic Disease 2004: In press*

[253] El-Deiry WS, Harper JW, O'Connor PM, Velculescu VE, Canman CE, Jackman J, Pietenpol JA, Burrell M, Hill DE, Wang Y
WAF1/CIP1 is induced in p53-mediated G1 arrest and apoptosis. *Cancer Res 1994: 54, 1169–1174*

[254] Edelstein ML, Abedi MR, Wixon J, Edelstein RM
Gene therapy clinical trials worldwide 1989-2004: an overview. *J Gene Med 2004: 6, 597-602.*

[255] Boyd M, Spenning HS, Mairs RJ
Radiation and gene therapy: Rays of hope for the new millennium. *Current Gene Therapy 2003: 3, 319-339*

[256] Pagnan G Stuart DD, Pastorino F, Raffaghello L, Montaldo PG, Allen TM, Calabretta B, Ponzoni M
Delivery of c-myb antisense oligodeoxynucleotides to human neuroblastoma cells via disialoganglioside GD2-targeted immunoliposomes: antitumor effects. *J Natl Canc Inst 2000: 92, 253-261*

[257] Pastorino F, Stuart D, Ponzoni M, Allen TM
Targeted delivery of antisense oligonucleotides in cancer. *J Controlled Release 2001: 74, 69-75.*

[258] Pastorino F Brignole C, Marimpietri D, Sapra P, Moase EH, Allen TM, Ponzoni M.
Doxorubicin-loaded Fab' fragments of anti-disialoganglioside immunoliposomes selectively inhibit the growth and dissemination of human neuroblastoma in nude mice. *Cancer Res 2003: 63, 86-92.*

[259] Raffaghello L, Pagnan G, Pastorino F, Cosimo E, Brignole C, Marimpietri D, Montaldo PG, Gambini C, Allen TM, Bogenmann E, Ponzoni M
In vitro and in vivo antitumor activity of liposomal fenretinide targeted to human neuroblastoma. *Int J Cancer 2003: 104, 559-567.*

[**260**] Zalutsky MR, McLendon RE, Garg PK, Archer GE, Schuster JM, Bigner DB (1994). Radioimmunotherapy of neoplastic meningitis in rats using an -particle-emitting immunoconjugate. *Cancer Res 1994: 54, 4719-4725*

[**261**] Akabani G, Reist CJ, Cokgor I, Friedman AH, Friedman HS, Coleman RE, Zhao XG, Bigner DD, Zalutsky MR
Dosimetry of 131I-labeled 81C6 monoclonal antibody administered into surgically created resection cavities in patients with malignant brain tumors. *J Nucl Med 1999: 40, 631-638*

[**262**] Schilz G, Cheresh DA, Vark NM, Yu A, Staffileno LK, Reisfeld RA
Detection of ganglioside GD2 in tumour tissues and sera of neuroblastoma patients. *Cancer Res 1984: 44, 5914-5920.*

[**263**] Pagnan G, Montaldo PG, Pastorino F, Raffaghello L, Krichmeier M, Allen TM
GD2-mediated melanoma cell targeting and cytotoxicity of liposome-entrapped fenretinide. *Int J Cancer 1999: 81, 268-274.*

[**264**] Boehm MK, Perkins SJ
Structural models for carcinoembryonic antigen and its complex with the single chain Fv antibody molecule MFE23. *FEBS Lett 2000: 475, 11-16.*

[**265**] Hammarstrom S
The carcinoembryonic antigen (CEA) family: structures, suggested functions and expression in normal and malignant tissues. *Cancer Biol 1999: 9, 67-81.*